WOJSKOWA AKADEMIA TECHNICZNA
im. Jarosława Dąbrowskiego
WYDZIAŁ MECHATRONIKI, UZBROJENIA I LOTNICTWA

ROZPRAWA DOKTORSKA

Aerostrukturalna optymalizacja wirnika nośnego śmigłowca z uwzględnieniem ograniczeń masowych i wytrzymałościowych

mgr inż. Jakub KOCJAN

Promotor: **dr hab. inż. Stanisław KACHEL, prof. WAT**
Promotor pomocniczy: **ppłk dr. inż. Robert ROGÓLSKI**

Warszawa 2025 r.

(strona celowo zostawiona pusta)

Spis treści

Streszczenie

W związku z planowanym rozwojem konstrukcji śmigłowców wojskowych w ramach Sojuszu Północnoatlantyckiego, w ramach programu NGRC (*Next Generation Rotorcraft Capability*), rozpisanego przez NSPA (*NATO Support and Procurement Agency*) w 2021, w Wojskowej Akademii Technicznej podjęto badania mające na celu uzyskanie zdolności do projektowania nowoczesnych wiropłatów odpowiadających wymaganiom operacyjno-technicznym przewidywanym do osiągniecia na lata 2030-2050.

Badania poprzedzone zostały analizą charakterystyk taktyczno-technicznych istniejących konstrukcji śmigłowcowych. W ramach analizy dokonano porównania niemal wszystkich obecnie eksploatowanych wiropłatów. Śmigłowce zostały porównane zarówno pod kątem ich parametrów wymiarowych, jak i osiągowych. Porównawczo zestawiono również wskaźniki odnoszące się do przeznaczenia oraz maksymalnej masy startowej. Do porównania konstrukcji wykorzystano zarówno parametry geometryczne (bezwzględne wymiary zewnętrzne), jak i odpowiednie współczynniki bezwymiarowe. Współczynniki te umożliwiają porównanie osiągów konstrukcji różniących się pod względem geometrycznym, lecz przeznaczonych do realizacji podobnych zadań. Wyniki analizy porównawczej umożliwiają określenie potencjalnych kierunków rozwoju konstrukcji oraz wskazanie deficytów projektowych, które niniejsza praca może wypełnić.

Parametry wyodrębnione w ramach analizy konstrukcji są podstawą do określenia modelu matematycznego optymalizacji wielokryterialnej wirnika nośnego. W pracy przedstawiono proces formułowania modelu matematycznego optymalizacji. Zaproponowano postać funkcjonału optymalizacji wielokryterialnej, zmienne decyzyjne, ograniczenia oraz parametry projektowe traktowane jako niezmienne. W dalszej fazie badań zaprezentowano metodę wyznaczania ekstremalnych wartości funkcjonału poprzez użycie metody systematycznego przeszukiwania z wykorzystaniem technik komputerowych.

Podstawą do analizy numerycznej zagadnienia jest przygotowanie parametrycznego modelu pojedynczej łopaty wirnika nośnego. Parametryzacja geometrii łopaty jest realizowana z wykorzystaniem środowiskowego języka programowania GRIP (*Graphics Interactive Programming*). Dzięki użyciu tego języka możliwe jest skryptowe programowanie obiektów geometrycznych z jednoczesną deklaracją parametrów masowych takich jak środek ciężkości, czy momenty bezwładności. Równolegle z wykorzystaniem metod komputerowych wykonywane są obliczenia analityczne, które pozwalają na wyliczenie trymowania łopat wirnika nośnego tj. określenia funkcji zmiany kątów skoku ogólnego i okresowego

w zależności od azymutalnego położenia łopat. Otrzymane wyniki służą typowaniu pożądanych parametrów symulacji, jak również wygenerowaniu modeli parametrycznych wirnika nośnego wraz z odpowiednimi domenami płynowymi oraz ich strukturą wewnętrzną.

W kolejnej fazie badań zrealizowano analizy numeryczne obejmujące:

- analizę zagadnienia stacjonarnego dla jednej łopaty wirnika z opływem symulowanym dla warunków ruchu obrotowego,
- analizę n-łopatowego wirnika z odwzorowaniem zarówno ruchu obrotowego wirnika jak i ruchu postępowego śmigłowca; dodatkowo uwzględniono zmianę skoku okresowego łopat.

Do przygotowania symulacji wykorzystano zapisy parametrów lotu rzeczywistego śmigłowca oraz posłużono się modelem geometrycznym jego łopat. Porównanie wyników obliczeń z rzeczywistymi osiągami śmigłowca potwierdziło wiarygodność zastosowanej metody.

W następnym etapie przeprowadzono analizy wytrzymałościowe łopaty wirnika nośnego wykonując stosowne obliczenia analityczne oraz analizy numeryczne MES. Zaprezentowano sposób wstępnej optymalizacji struktury z wykorzystaniem języka GRIP. Do zadania obciążeń wykorzystano rozkład sił będący wynikiem symulacji CFD z poprzedniego etapu.

W kolejnej fazie badań modelowych dokonano powiązania obliczeń numerycznych poprzez zastosowanie metody FSI (*Fluid-Structure Interaction*). Wyniki analiz CFD były transferowane do modelu strukturalnego. Następnie odkształcenia spowodowane obciążeniami były zwrotnie przekazywane do modelu CFD i uwzględniane w modyfikacji siatki obliczeniowej. Proces realizowany był iteracyjnie w określonych krokach czasowych. Odwzorowano w ten sposób wpływ odkształceń łopat wirnika na generowaną siłę nośną.

Modele aproksymujące własności aerodynamiczne i strukturalne wirnika nośnego wykorzystane zostają potem do optymalizacji wielokryterialnego funkcjonału. Parametry zmienne w symulacji są jednocześnie zmiennymi decyzyjnymi. Algorytm uruchamiany jest iteracyjne do momentu uzyskania zbioru rozwiązań optymalnych. Ostatecznie wybierane są rozwiązania najbardziej użyteczne zgodnie z narzuconą funkcją preferencji.

W podsumowaniu wskazano na przydatność i oryginalność metody w zastosowaniu do projektowania wirnika śmigłowca. Wykazano, że otrzymane wyniki obliczeń analitycznych i komputerowych są wiarygodne i mają zastosowanie w kontekście poszukiwania nowych rozwiązań projektowych. Modele geometryczne mogą zostać wykorzystane w dalszych etapach projektowania i posłużyć jako baza dla kolejnych etapów rozwojowych. Podkreślono także aspekt oryginalności metody ze względu na sposób realizacji zadania przy jednoczesnej redukcji czasu obliczeń wskutek rozdzielenia symulacji na dwa etapy. Wskazano również dalsze możliwe kierunki rozwoju i możliwości aplikacyjnego wykorzystania wyników.

Abstract

Due to the planned development of military helicopter designs within NATO's Next Generation Rotorcraft Capability (NGRC) program, announced by NATO Support and Procurement Agency (NSPA) in 2021, the Military University of Technology has undertaken research to develop capabilities for designing modern rotorcraft that meet the program's future requirements to be achieved in years 2030–2050.

The research is preceded by an analysis of existing helicopter designs. As part of the analysis, nearly all currently operated rotorcraft were compared in terms of their geometric and performance parameters. A classification was also made based on the intended use of the helicopter and its maximum take-off weight. Both absolute geometric dimensions and appropriate dimensionless coefficients were used for the comparison. These coefficients allow for comparing performance across geometrically different designs intended for similar missions. The results help to identify development directions and technological gaps which seems to be crucial in the context of this study.

The parameters identified during the structural analysis form the basis for defining a mathematical model for multi-criteria optimization of the main rotor. The study describes the development of this mathematical optimization model. It presents the multi-criteria optimization functional, decision variables, constraints, and parameters. This paper outlines a method for solving the functional using a search technique supported by computer-based methods.

The basis for the computational analysis is the development of a parametric model of the main rotor blade. The parameterization is carried out using the GRIP (*Graphics Interactive Programming*) programming language, which enables creating CAD objects along with simultaneous declaration of mass parameters such as center of mass and moments of inertia. In parallel, analytical calculations are performed to determine collective and cyclic pitch angles. The results are used to define simulation parameters and to generate parametric models of the main rotor, including appropriate fluid domains and internal structure.

In the next stage of the research, the following numerical fluid dynamics analysis was conducted:

- steady-state simulation for a single main rotor blade with simulated airflow,
- multi-dimensional simulation for the full rotor, including the forward motion of the helicopter and the rotational movement of the rotor around its axis, as well as variations in the cyclic pitch of the blades.

Real flight data from the helicopter and a blade model were used for preparing simulation. The results confirmed the reliability of the applied method.

In the next stage, strength analyses of the main rotor blade were carried out using both analytical calculations and numerical FEM analysis. A method for preliminary structural optimization was presented using the GRIP programming language and its implemented functions for CAD model inertia analysis. The load conditions were defined based on the force distribution obtained from the CFD simulations conducted in the previous phase.

In the next stage of undertaken researches, numerical calculations were coupled using the FSI (Fluid-Structure Interaction) method. The results of the CFD analyses were transferred to the structural model, and the deformations caused by the loads were then fed back into the CFD model which was considered by modifying the computational mesh. This process was repeated at each time step, simulating the rotor's operation while accounting for the impact of structural deformations on the generated aerodynamic force.

The above method was organized into a complex algorithm aimed at solving the optimization functional defined in the analysis stage. The variable parameters in the simulation also serve as decision variables established during this analysis. The algorithm is executed iteratively until a set of solutions is found that satisfies the initially defined optimization goal. The designer then makes decisions in accordance with a specified preference function.

The summary presents proof of the usefulness and novelty of the method in designing the main rotor of a helicopter. It has been demonstrated that both the obtained results, in the form of finalized models and analytical outcomes, provide a basis for the subsequent stages of the design process. The summary also highlights the novelty of the method in terms of optimization of the process itself and the minimization of computation time by implementation of a two-stage simulation. Furthermore, possible directions for further development and applications of collected results are indicated.

1. Wykaz publikacji stanowiących podstawę rozprawy doktorskiej

Tabela 1. Wykaz publikacji naukowych

Oznaczenie w tekście	Dane bibliograficzne	Punkty wg wykazu czasopism naukowych Ministra Nauki	Udział doktoranta
A1	Kachel S., Rogólski R., **Kocjan J.,** *Review of Modern Helicopter Constructions and an Outline of Rotorcraft Design Parameters*. Problems of Mechatronics. Armament, Aviation, Safety Engineering 2021; 12 (3): 27-52.	40	75%
A2	**Kocjan J**., Kachel S., Rogólski R., *Helicopter Main Rotor Blade Parametric Design for a Preliminary Aerodynamic Analysis Supported by CFD or Panel Method.* MDPI Materials 2022, 15, 4275.	140	75%
A3	**Kocjan J**., Kachel S., Rogólski, R., *Helicopter main rotor CFD analysis for different flight conditions using parametric blade model as an application for multidisciplinary optimization.* Journal of Theoretical and Applied Mechanics 2023;61(4):793-805	70	75%
A4	**Kocjan J**., Kachel S., Rogólski R., *Helicopter main rotor FSI analysis using parametric blade model as an application for multidisciplinary optimization.* Journal of Physics: Conf. Ser. 2716(1):012031	40	75%
A5	**Kocjan J.,** Rogólski R., *Parametric structure optimization of a main rotor blade as an application for FSI analysis in main rotor optimization process.* Aircraft Engeering and Aerospace Technology, vol. 96, 2024.	70	80%
A6	**Kocjan J.,** Rogólski, R., *Aerostructural helicopter main rotor optimization considering mass and strength limitations.* International Review of Aerospace Engineering, Vol. 18, no 2, 2025.	100	80%

2. Uzasadnienie podjęcia tematyki badawczej

Długoterminowa analiza śmigłowców wojskowych eksploatowanych w krajach NATO wykazuje, że w latach 2030-2050 większość wojskowych wiropłatów (zarówno produkcji zachodniej, jak i rosyjskiej) jest przewidziana do wycofania ze służby ze względu na zakończenie docelowej normy eksploatacji. W konsekwencji, w 2021 roku NSPA (*NATO Support and Procurement Agency*) ogłosiło wymagania dla wspólnego śmigłowca nowej generacji NGRC (*Next Generation Rotorcraft Capability*), którego wdrożenie planowane jest na drugą połowę następnej dekady. Pożądane zdolności przyszłościowego śmigłowca znacznie przewyższają możliwości aktualnie istniejących konstrukcji. W swoich założeniach NSPA zakłada, że śmigłowiec powinien charakteryzować się następującymi możliwościami operacyjnymi i osiągowymi:

- maksymalna prędkość dochodząca do 400 km/h,
- tankowanie w powietrzu,
- opcja użytkowania w trybie bezzałogowym,
- minimum 2,5 tony udźwigu,
- duży przedział transportowy,

W zakresie dodatkowo pożądanych własności formułowane są następujące oczekiwania:

- możliwości integracji szerokiej gamy uzbrojenia,
- możliwości współdziałania z okrętami,
- możliwości aplikacji napędu hybrydowego,
- zdolności w zakresie walki radioelektronicznej,
- zdolności w zakresie realizacji zadań poszukiwawczo-ratowniczych,
- zdolności w zakresie zwalczania okrętów podwodnych.

Uwzględniając oczekiwania NSPA co do możliwości osiągowych poszukiwanej konstrukcji, zwłaszcza w zakresie udźwigu i osiąganych prędkości, należy podkreślić, że parametry te zależą głównie od doskonałości konstrukcji płatowcowej i wirnika nośnego. Powyższe uzyskuje się maksymalizując osiągi przy jednoczesnej minimalizacji masy, co realizowane jest dzięki zastosowaniu udoskonalonych lub nowych rozwiązań konstrukcyjnych, a także nowoczesnych materiałów oraz technologii produkcji. Oznacza to, że rozwiązania konstrukcyjne pozwalające na osiągnięcie nowych możliwości albo nie zostały jeszcze opracowane, albo wymagają dalszych prac projektowo-badawczych.

Istniejąca luka technologiczna jest podstawą do badań nad optymalizacją konstrukcji elementów nośnych wiropłatów pod kątem maksymalizacji ich osiągów przy jednoczesnej minimalizacji parametrów masowych, co powinno prowadzić do oszczędności w kontekście przewidywanych kosztów eksploatacji.

Inwazja Federacji Rosyjskiej na Ukrainę i trwający w wyniku tego konflikt zrewidował wykorzystanie śmigłowców na współczesnym polu walki. Dla przyszłego teatru bojowych operacji lotniczych istotne będą wymagania wynikające z nowoczesnych technologii i ekstremalnych możliwości operacyjnych. W przypadku lotnictwa śmigłowcowego ważnymi aspektami są nie tylko najnowsze rozwiązania elektroniczne wspierające możliwości nawigacyjne, rozpoznawcze, łącznościowe, uderzeniowe, ale również parametry konstrukcji, zapewniające wypełnienie docelowych wymagań taktyczno-operacyjnych. Te właśnie wymagania determinują kształt i osiągi przyszłościowych wiropłatów. Sformułowane w prognozach operacyjnych i założeniach projektowych wymagania kształtują podstawowe charakterystyki projektowo-osiągowe, takie jak: udźwig, zasięg, wymiary, zakresy prędkości i wysokości lotu dla różnych reżimów misyjnych. Ich wartości są dodatkowo uwarunkowane przyjętym układem aerodynamicznym oraz możliwościami osiągowymi zespołu napędowego.

Na potwierdzenie powyższego można zauważyć, że wiele krajów, w kooperacji z producentami śmigłowców, poszukuje coraz to lepszych rozwiązań w dziedzinie statków powietrznych, umożliwiających pionowy start i lądowanie. Również w Wojskowej Akademii Technicznej, w ramach projektów badawczych ukierunkowanych na poszukiwanie nowych metod i rozwiązań w dziedzinie optymalizacji konstrukcji prowadzone są badania, których celem jest uzyskanie nowych możliwości projektowania i doskonalenia wiropłatów. Niniejsza praca doktorska stanowi rezultat wysiłków autorskich w obszarze działań wpisujących się w intensywny rozwój lotnictwa śmigłowcowego.

3. Analiza konstrukcji śmigłowców i cel badań

3.1. Analiza istniejących konstrukcji śmigłowcowych

Biorąc pod uwagę wymagania stawiane wiropłatom, jak również konieczność opracowania nowych możliwości rozwoju konstrukcji śmigłowcowych, w ramach realizacji pracy badawczej dokonano analizy aktualnie eksploatowanych śmigłowców pod kątem parametrów pozwalających na obiektywną ocenę jakości i wskazanie priorytetowych kierunków rozwoju. Przeprowadzona analiza umożliwiła opracowanie bazy danych, przydatnej w procesie projektowania nowych obiektów. Podział konstrukcji dostosowano do wymagań EASA (*European Union Aviation Safety Agency*) dla statków powietrznych cywilnych oraz EDA (*European Defence Agency*) dla statkowych powietrznych wojskowych, w konsekwencji czego rozważania pozostają w zgodności z aktualnie obowiązującymi kanonami prawa lotniczego.

Śmigłowce poddane analizie podzielono ze względu na przewidywany profil realizowanych zadań. Zestawione informacje mogą być docelowo użyteczne w procesie projektowania wstępnego. W kontekście zadania NGRC wykonana analiza stanowi podstawę do przygotowania koncepcji i określenia możliwych kierunków rozwoju, które spełnią wymagania nowoczesnego pola walki.

Głównym wnioskiem płynącym z analizy jest fakt, że parametry wirnika nośnego determinują osiągi śmigłowca. Kolejne etapy projektowania wstępnego oparte na wyliczeniach wirnika nośnego bazują na tychże kalkulacjach. Zwiększenie sprawności wirnika w toku działań programowo-symulacyjnych pozwali na uzyskanie korzystniejszych wskaźników użytkowych, istotnych z punktu widzenia potrzeb operacyjnych.

Analizując dostępne konstrukcje wirników nośnych określono zbiór parametrów konstrukcyjnych w znacznym stopniu determinujących własności osiągowe śmigłowców:

- R- promień łopaty wirnika nośnego;
- v_{tip} - prędkość końcówki łopaty;
- Ω - prędkość kątowa wirnika nośnego;
- b - liczba łopat wirnika;
- $c(r)$ - cięciwa łopaty (zwykle zmienna wzdłuż współrzędnej bieżącej r);
- $\vartheta(r)$ – kąt skręcenia łopaty (zmienny wzdłuż współrzędnej bieżącej r);
- d – grubość profilu lotniczego łopaty,
- a – nachylenie charakterystyki współczynnika siły nośnej na profilu.

W celu porównania ze sobą możliwości osiągowych różnych śmigłowców powyższe parametry wykorzystywane są do określenia bezwymiarowych współczynników w odniesieniu do maksymalnej masy startowej (MTOW). Wyniki przeprowadzonej statystycznej analizy wskazanych parametrów projektowych oraz ich porównanie przedstawiono w artykule [A1].

Charakterystycznymi parametrami określającymi możliwości konstrukcji są min.: obciążenie powierzchni nośnej oraz obciążenie mocy. Definiuje się je w sposób następujący:

- obciążenie powierzchni nośnej (tarczy wirnika): $p = \frac{MTOW}{\pi R^2}$ [kg/m^2]
- obciążenie mocy: $q = \frac{MTOW}{N_{PU}}$ [kg/HP]

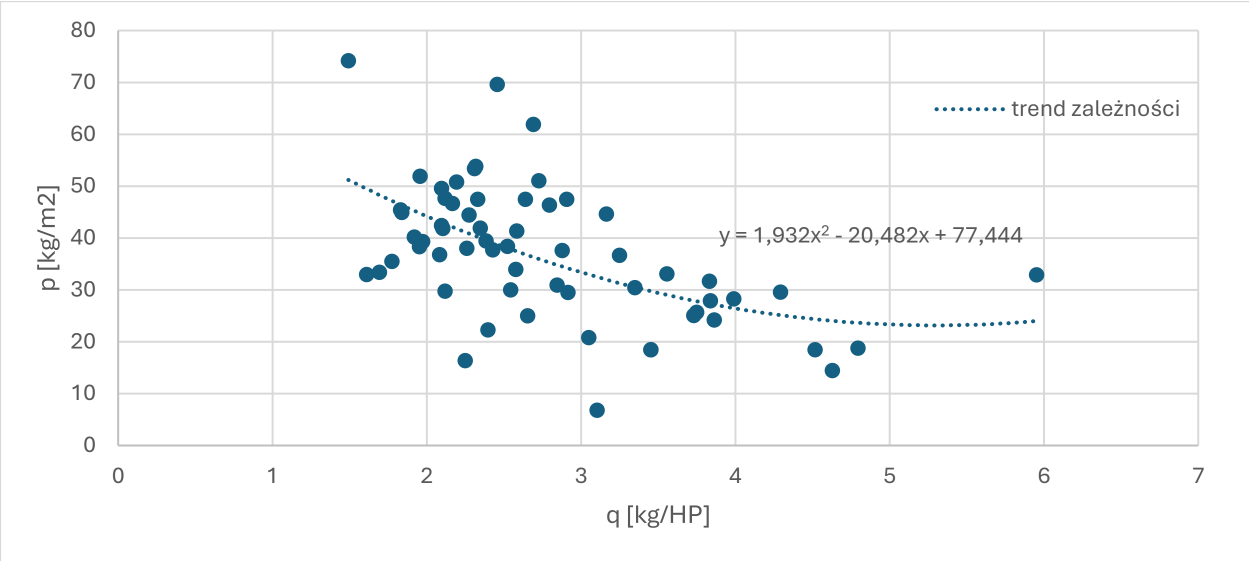

Rys. 1. Zależność obciążenia mocy od wielkości obciążenia powierzchni nośnej

Analizując zależność przedstawioną na rys. 1 widać wyraźnie, że wraz ze wzrostem obciążenia powierzchni nośnej maleje obciążenie zespołu napędowego. Jest to związane z geometrią wirnika nośnego i fizycznymi ograniczeniami długości łopat. Wzrost średnicy w bezpośredni sposób określa dostępną powierzchnię nośną, a tym samym siłę nośną wytwarzaną przez łopatę. Jednocześnie, wraz ze wzrostem promienia zwiększa się prędkość przepływu na końcówce łopaty wynikająca z sumy prędkości ruchu obrotowego wirnika i ruchu postępowego śmigłowca. Powoduje to ograniczenie w możliwości konstruowania wirnika, wynikające z możliwości lokalnego przekroczenia prędkości dźwięku. Wraz ze wzrostem maksymalnej masy startowej konieczne jest zastosowanie konfiguracji geometrycznej wirnika, która umożliwiałaby uzyskanie lepszych osiągów przy zachowanym promieniu, co pociąga konieczność zastosowania zespołu napędowego o wyższej mocy. Wzrost produktywnej powierzchni aerodynamicznej w obrębie tarczy wirnika możliwy jest w efekcie zwiększenia liczby łopat lub ich cięciwy. Parametrem, który określa stosunek całkowitej powierzchni nośnej łopat do powierzchni kołowej dysku wirnikowego określany jest jako tzw. współczynnik wypełnienia. Zależność opisana jest wzorem:

$$\sigma = \frac{zc}{\pi R}$$

gdzie *z* to liczba łopat, *c* to cięciwa łopaty, a *R* to promień wirnika.

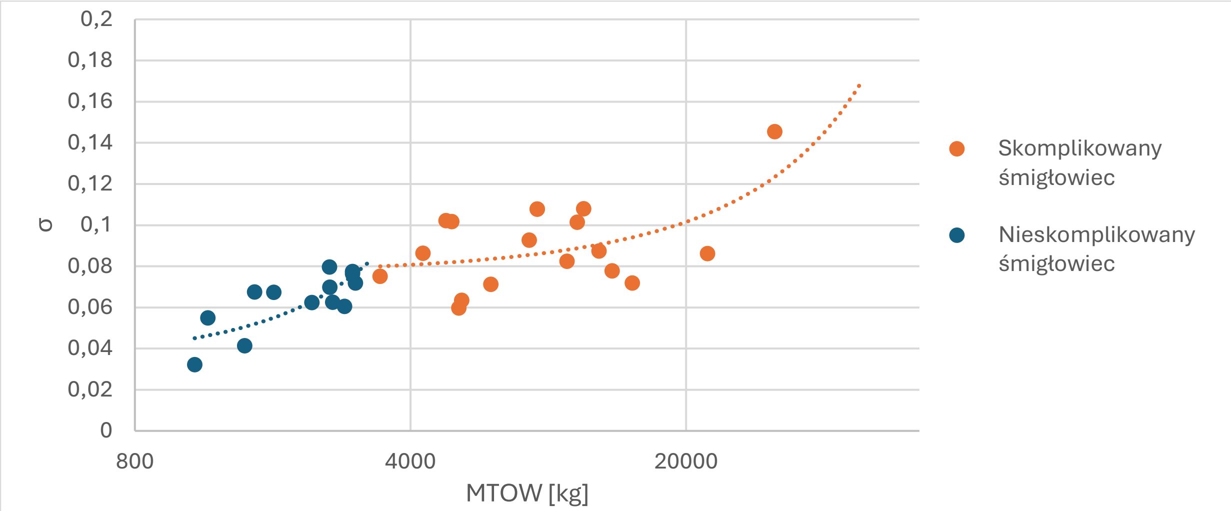

Rys. 2. Zależność współczynnika wypełnienia od maksymalnej masy startowej

Na rysunku nr 2 przedstawiono statystyczną charakterystykę zależności współczynnika wypełnienia od maksymalnej masy startowej z uwzględnieniem podziału na kategorie projektowe śmigłowca. Można zauważyć, że wraz z osiąganiem coraz wyższej masy startowej wzrasta współczynnik wypełnienia. Zmiana wartości współczynnika pozwala na ocenę zmiany doskonałości konstrukcji, przy założeniu zachowania stałych innych parametrów konstrukcji śmigłowca, a także przy jednoczesnym utrzymaniu stałej maksymalnej masy startowej. Spadek wartości współczynnika (przy stałej MTOW), czyli zmniejszenie powierzchni nośnej łopat wirnika w stosunku całkowitej powierzchni wirowania, pozwala na wyciągnięcie wniosków o zwiększeniu zdolności łopat do generowania sił potrzebnych do realizacji misji, co przekłada się na jej zwiększoną doskonałość przy jednoczesnym obniżeniu masy elementów nośnych.

Powyższe współczynniki przedstawiono jako najważniejsze przykłady z punktu widzenia prowadzonych badań porównawczych. Całość analizy została opublikowana w artykule [A1], a także zaprezentowana na konferencjach [g, h]. Opisane parametry pozwalają porównać możliwości istniejących konstrukcji, a także mogą posłużyć do oceny wyników badań mających na celu poprawienie aerodynamiki wirnika nośnego.

Na podstawie analizy statystycznej i oceny parametrów można wysunąć wniosek, że istnieją jeszcze kierunki rozwoju konstrukcji śmigłowcowych, które niosą perspektywę uzyskania lepszych efektów. Jednym z nich jest nurt doskonalenia aerodynamiki i konstrukcji elementów nośnych, czyli łopat wirnika nośnego. Pomimo istniejących fizycznych ograniczeń możliwe jest poszukiwanie nowatorskich rozwiązań z zastosowaniem oryginalnych kształtów bryły oraz nowoczesnych materiałów i technologii.

3.2. Wskazanie możliwych ścieżek rozwoju

W wyniku przeprowadzonej analizy dokonano ewaluacji prowadzonych na świecie badań i wskazano możliwe ścieżki rozwoju nowoczesnych konstrukcji śmigłowcowych. Z jednej strony aktualnie trwające badania zmierzają ku rozwiązaniom nietypowym, aerodynamicznie niekonwencjonalnym, natomiast z drugiej strony ustawicznie doskonalone są konstrukcje klasyczne budowane w oparciu o tradycyjny układ Sikorskiego.

W przypadku nurtu poszukującego nowych rozwiązań w dziedzinie budowy wiropłatów, wśród środowisk akademickich, producentów i wiodących armii, główną propozycją jest projekt konstrukcji wiropłata współosiowego z zastosowaniem śmigła pchającego, bądź też jednoosiowego z zastosowaniem dwóch równoległych śmigieł. Jednym z takich działań jest realizacja programu FARA (*Future Attack Reconnaissance Aircraft*). W ramach programu FARA Siły Zbrojne Stanów Zjednoczonych poszukują nowych rozwiązań technologicznych. W projekcie zaproponowano dwie zaawansowane konstrukcje, które łączą w sobie kluczowe cechy śmigłowców: wysoką manewrowość, zdolność do pionowego startu i lądowania w trudnym terenie, a także możliwość osiągania relatywnie wyższych prędkości lotu. Obecnie, w fazie testów badawczych znajdują się dwa modele: Boeing Defiant X oraz Sikorsky Raider X. Przykładową konstrukcję zaprezentowano na rys. 3.

Rys. 3. Boeing Defiant X, źródło materiały promocyjne Boeing

Drugim nurtem badań jest rozwój śmigłowców z zastosowaniem klasycznego układu aerodynamicznego, czyli tzw. „układu Sikorskiego" – z jednym wirnikiem nośnym i bocznym śmigłem ogonowym, którego zadaniem jest równoważenie momentu reakcyjnego wirnika głównego. W przypadku tego układu wirnik nośny pełni podstawową rolę zarówno jako źródło siły nośnej, jak i ciągu. Jego konstrukcja w znacznym stopniu wpływa na kluczowe parametry osiągowe śmigłowca, takie jak prędkość maksymalna, prędkość wznoszenia, udźwig czy maksymalna masa startowa. W związku z tym, przemysł oraz instytucje badawcze nieustannie prowadzą prace nad doskonaleniem technologii wirników nośnych, dążąc do poprawy ich wydajności. Przykład wirnika o zoptymalizowanym numerycznie kształcie przedstawia rys. 4, na którym zaprezentowano śmigłowiec H160M firmy Airbus.

Rys. 4. Śmigłowiec Airbus H160M , źródło materiały promocyjne Airbus

Biorąc pod uwagę doświadczenia osobiste oraz posiadaną wiedzę, a także potencjał WAT podjęto badania w nurcie rozwoju istniejących konstrukcji. Wykorzystano do tego model badawczy odwzorowujący własności aerodynamiczne popularnego polskiego śmigłowca W-3 Sokół. W modelowaniu uwzględniono budowę łopaty przedmiotowego śmigłowca, jej cechy geometryczne i konstrukcyjne. W ramach przeprowadzonych symulacji analizie poddane zostały możliwości osiągowe w różnych warunkach lotu ze względu na prędkość postępową, wysokość oraz prędkość kątową ruchu obrotowego wirnika.

3.3. Określenie innowacyjności prowadzonych badań

Analizując aktualnie realizowane badania w zakresie rozwoju śmigłowców o klasycznym układzie aerodynamicznym można wskazać pewne obszary, w których zastosowanie nowoczesnych metod komputerowych pozwala na przeprowadzenie optymalizacji konstrukcji. Jednocześnie wskazać można kierunki wdrażania nowych innowacyjnych rozwiązań.

Podstawową cechą determinującą generowanie siły nośnej wirnika jest geometria jego łopat. To właśnie kształt i wymiary łopaty decydują o właściwościach aerodynamicznych. Dzięki nowoczesnym metodom projektowania możliwe jest opracowanie łopat o optymalnym kształcie, które przewyższają parametrami aerodynamicznymi konstrukcje zaprojektowane w sposób klasyczny. Jednak w tym celu konieczne jest opracowanie metody uwzględniającej liczne kryteria, zmienne oraz ograniczenia. Aktualnie rozwijane metody zostały opisane w artykułach [A1, A2]. Jednym z przykładów dokonanej optymalizacji łopaty wirnika śmigłowca AH-64A jest praca zaprezentowana podczas 47. Forum Wiropłatowego. Przedstawiono tam technikę połączonych symulacji CFD (*Computer Fluid Dynamics*) z wykorzystaniem wcześniej przygotowanego solvera, który poszukuje kształtu zapewniającego stateczność pracy. Innym przykładem jest zastosowanie modeli zastępczych Co-Kriging opartych na dwóch poziomach dokładności odwzorowania. Osobnym zagadnieniem jest poprawa osiągów poprzez optymalizację i dobór odpowiedniego profilu lotniczego. Oprócz kryteriów osiągowych, analizowane są również inne właściwości mające wpływ na efektywność wykonywania zadań. Jednym z istotnych kierunków rozwoju jest zmniejszanie wibracji w kabinie załogi poprzez udoskonalanie wirnika nośnego będącego zasadniczym źródłem drgań. Choć działania te nie zwiększają bezpośrednio osiągów śmigłowca, znacząco wpływają na wydłużenie żywotności konstrukcji zmniejszając ograniczenia resursowe płatowca i jego podzespołów.

Dodatkową korzyścią jest poprawa komfortu załogi, co przekłada się na wydajność i skuteczność realizacji misji. Wyższy komfort pracy umożliwia załodze dłuższe operowanie w niekorzystnych warunkach. W przypadku śmigłowców wojskowych, gdzie czas trwania misji często jest trudny do przewidzenia, lepsze warunki pracy pozytywnie wpływają na precyzję oraz efektywność długotrwałych działań operacyjnych.

Osobnym, lecz równie istotnym zagadnieniem w procesie optymalizacji kształtu łopaty wirnika jest projektowanie jej końcówki. Kształt końcówki znacząco wpływa na parametry osiągowe, ponieważ umożliwia przekraczanie ograniczeń fizycznych charakterystycznych dla klasycznych łopat o końcówkach prostokątnych lub trapezowych. Innowacyjne rozwiązania w tej dziedzinie pozwalają na poprawę wydajności aerodynamicznej, redukcję oporu i hałasu, a także zwiększenie efektywności wirnika w różnych warunkach operacyjnych. Zastosowanie końcówek o zoptymalizowanym kształcie pozwala na osiągnięcie wyższych prędkości obrotowych wirnika. Dzięki takiemu rozwiązaniu możliwe jest przeniesienie krytycznej liczby Macha (wynikającej z sumy prędkości obrotowej wirnika i prędkości postępowej) na wyższe zakresy prędkości. W konsekwencji, wirnik może efektywnie działać w bardziej wymagających warunkach aerodynamicznych, przy zapewnieniu wymaganych osiągów oraz nieprzekraczaniu krytycznej prędkości opływu.

W przedstawionych kierunkach rozwoju główny nacisk położony jest na dobór kształtu łopat zapewniający znaczącą poprawę osiągów. Wśród analizowanych publikacji i wystąpień naukowych niewiele jest prac poświęconych zagadnieniom optymalizacji osiągów z jednoczesnym doborem optymalnej struktury wytrzymałościowej.

Powyższe analizy zaprezentowane zostały szczegółowo w publikacjach [A1-A6].

3.4. Określenie celu prowadzonych badań w kontekście przyjętej tezy

Ze względu na złożoność problemu, w celu zaprojektowania konstrukcji o możliwie najlepszych parametrach, do problemu modelowania wirnika nośnego zastosowano podejście analogiczne do rozwiązywania zadania optymalizacji wielokryterialnej, przy czym wykorzystano nowoczesne metody programowe.

Efektem przeprowadzonych badań będzie wypracowanie metody pozwalającej na zaprojektowanie wirnika nośnego o cechach najlepszych dla zadanych zmiennych decyzyjnych oraz określonej funkcji celu. Zadanie zostanie zrealizowane z wykorzystaniem nowoczesnych metod projektowania takich jak CAD (*Computer Aided Design*), CFD (*Computational Fluid Dynamics*) czy FSI (*Fluid-Structure Interaction*). Pozwoli to na uzyskanie zdolności do szybkiego opracowania geometrii i oceny modelowanej konstrukcji lotniczej już na etapie projektu wstępnego.

Wpisuje się to w potrzebę poszukiwania nowych rozwiązań w ramach programu wspólnego śmigłowca nowej generacji NGRC. Jednocześnie, według najlepszej wiedzy autora, w aktualnych publikacjach odnoszących się do symulacyjnych badań konstrukcji śmigłowcowych nie ma zbyt wielu rozwiązań z zakresu wielokryterialnej optymalizacji z efektami projektowania parametrycznego w powiązaniu z analizami numerycznymi typu FSI.

W konsekwencji multidyscyplinarnego podejścia do procesu poszukiwania optymalnego rozwiązania konstrukcyjnego wirnika śmigłowca zaproponowana została następująca teza pracy:

„zastosowanie zalgorytmizowanego procesu optymalizacji wielokryterialnej bazującej na nowoczesnych narzędziach programowych umożliwi zamodelowanie wirnika nośnego śmigłowca o własnościach aerodynamicznych i osiągowych znacznie lepszych w stosunku do konstrukcji projektowanej metodami klasycznymi nie uwzględniającymi algorytmicznej priorytetyzacji zadań."

4. Analiza matematycznego podejścia do procesu optymalizacji

Rozwój procesów optymalizacji przy użyciu nowoczesnych narzędzi komputerowych wymaga w pierwszej kolejności określenia ich podstaw matematycznych. Kompletną analizę matematyczną rozwiniętą w kontekście parametryzacji oraz optymalizacji konstrukcji opisano w artykule [A6]. W pracy przedstawiono proces budowania matematycznego modelu optymalizacyjnego dla charakterystycznych parametrów konstrukcyjnych wirnika. Matematyczny model odwzorowuje rzeczywisty problem inżynierski. Określenie ograniczeń i warunków brzegowych pozwala na dalszym etapie wprowadzić je również do poszukiwania rozwiązań numerycznych, ponieważ w stosowaniu metod komputerowych istnieje spore ryzyko otrzymania wyników niespójnych z rzeczywistością. Zaproponowany model pozwoli ocenić, czy przyjęty tok postępowania jest właściwy a otrzymane wyniki znajdą się w zbiorze rozwiązań akceptowalnych. W ramach modelu zaproponowano zbiór zmiennych decyzyjnych i niezależnych parametrów opisujących konstrukcję, zbiór ograniczeń i w ostatnim kroku funkcję celu, która jest matematycznym zapisem kryterium optymalizacji.

Zadanie optymalizacyjne polegało na znalezieniu rozwiązania satysfakcjonującego dla kilku ustalonych kryteriów. W konsekwencji w przypadku przedstawianych badań możemy mówić o optymalizacji wielokryterialnej. W tym przypadku formułowany jest funkcjonał złożony z kilku osobnych funkcji cząstkowych. Zadaniem projektanta jest spełnienie wszystkich przyjętych kryteriów i wytypowanie rozwiązania najlepszego, pomimo, że przyjęte do optymalizacji kryteria są często rozbieżne.

Rozwiązanie problemu optymalizacji wymaga określenia zbioru rozwiązań dopuszczalnych i przyjęcia uzasadnionego sposobu ich oceny. Zbiór rozwiązań różni się stopniem kompromisowości pomiędzy wyborem poszczególnych kryteriów. Z inżynierskiego punktu widzenia, rozwiązanie czysto matematyczne problemu często nie przynosi oczekiwanych rezultatów. Projektant musi wesprzeć się jedną z technik poszukiwania metody i podejmowania decyzji, aby wybrać rozwiązanie matematycznie optymalne i jednocześnie inżyniersko użyteczne.

Proces optymalizacji wielokryterialnej w zastosowaniu inżynierskim musi charakteryzować się kilkoma istotnymi cechami, takimi jak:

- zastosowanie schematycznego podejścia do rozwiązania;
- wykorzystanie dyskretnego zbioru zmiennych decyzyjnych, pozwalających na uzyskanie rzeczywistego rozwiązania dającego się zastosować w konstrukcji;

- wykorzystanie wielokryterialnej oceny rozwiązań dopuszczalnych przy zastosowaniu wcześniej przyjętej metody oceny i podejmowania decyzji.

W przypadku prezentowanych badań proces optymalizacji został przeprowadzony z wykorzystaniem nowoczesnych metod projektowania. W konsekwencji, przyjęty model matematyczny daje możliwość porównywania rozwiązań ze względu na ich wpływ na poprawę pożądanych parametrów osiągowych i możliwość przyjęcia kryteriów wyboru odpowiadających cechom użyteczności wyznaczonego rozwiązania.

W tym celu stosowany jest następujący tryb postępowania:

- normalizacja cząstkowych funkcji celu,
- skalaryzacja znormalizowanych funkcji celu z wykorzystaniem współczynników wagowych,
- określenie warunków kompromisowych,
- określenie funkcji preferencji,
- wybór podzbioru rozwiązań preferowanych,
- podjęcie decyzji zgodnie z założonymi preferencjami projektanta.

Stosując opisaną wyżej procedurę opracowano matematyczny model optymalizacji wirnika nośnego śmigłowca. Parametry konstrukcyjne (inżynierskie) zostały przypisane do konkretnych elementów modelu. Dla zadania modelowej optymalizacji przyjęte zostały następujące atrybuty:

1. Zmienne decyzyjne:
   a) c – cięciwa łopaty wirnika nośnego,
   b) R – promień zewnętrzny tarczy wirnika nośnego,
   c) h – wysokość dźwigara łopaty wirnika nośnego,
   d) d – szerokość wypełniacza ulowego.
2. Parametery stałe:
   a) stałe materiałowe,
   b) profil aerodynamiczny,
   c) prędkość obrotowa wirnika nośnego,
   d) warunki lotu (wysokość, prędkość postępowa).
3. Ograniczenia:
   a) warunek wytrzymałościowy związany z nieprzekraczalnością poziomu naprężeń dopuszczalnych: $\sigma_{dop} > \sigma(h, d)$;

b) warunki geometryczne dla wartości wymiarowych: $R_{max} > R > 0$, $c_{max} > c > 0$, $h_{max} > h > 0$, $d_{max} > d > 0$; (wartości maksymalne to maksymalne wartości dla istniejących konstrukcji o podobnym przeznaczeniu)

c) warunek nieprzekraczalności przemieszczeń w związku z aerosprężystą odkształcalnością konstrukcji: $\delta_{max} > \delta;$;

d) ograniczenie maksymalnego kąta nastawienia łopaty: $\theta < \theta_{max}.$

4. Potencjalne cząstkowe funkcje celu:

a) Kryterium maksymalizacji ciągu aerodynamicznego: $T(c, R) \geq MTOW(h, d)$;

b) Kryterium wypełnienia wirnika nośnego: $\sigma(R, c) \rightarrow max$;

c) Kryterium masy łopaty: $m(h, d) \rightarrow min$;

Uwzględniając powyższe funkcje celu zaproponowano wielokryterialny funkcjonał, który w ramach prowadzonej optymalizacji będzie minimalizowany. Kryterium maksymalizacji ciągu zostało zapisane w formie odwrotnej, aby zapewnić zgodność jednoczesność minimalizacji obu kryteriów cząstkowych. Wzrost współczynnika wypełnienia przekłada się na maksymalizacje ciągu, dlatego współczynnik wypełnienia jest funkcją uwikłaną w zależność ciągu. Stosując skalaryzację i normalizację cząstkowych funkcji celu, jako matematyczny model podlegający optymalizacji zaproponowano funkcjonał następującej postaci:

$$\tilde{\mathrm{F}}(c, R, h, d) = w_1 \frac{1}{\tilde{\mathrm{T}}}\big(\sigma(c, R)\big) + w_2 \tilde{\mathrm{m}}(h, d) \rightarrow min$$

gdzie odpowiednio:

- w_1 – waga kryterium osiągów zależna od profilu misji i docelowej konfiguracji śmigłowca,
- w_2 – waga kryterium masy również zależna od profilu misji i konfiguracji śmigłowca,
- $\tilde{T}$ – znormalizowana funkcja ciągu - $\tilde{T} = \frac{T(\sigma(c,R))}{T_{ref}}$;
- $\tilde{m}$ – znormalizowana funkcja masy – $\tilde{m} = \frac{\tilde{m}(h,d)}{m_{ref}}$;
- T_{ref}, m_{ref} – oznacza wartość referencyjną danej wielkości przyjmowaną jako wartość średnia na podstawie danych statystycznych dla danego typu śmigłowca i typowego profilu misji.

W celu rozwiązania problemu i otrzymania projektu konstrukcji, który spełnia wymagania projektanta, należy wybrać odpowiednią metodę poszukiwania rozwiązania optymalnego. W rozwiązaniach inżynierskich, gdzie celem jest znalezienie wariantów, które nie tylko spełniają preferencje inżyniera, ale także są technologicznie wykonalne, powszechnie stosuje się metody optymalizacji dyskretnej. Łączenie metod komputerowych z obliczeniami analitycznymi prowadzi do zaproponowania metody przeszukiwania przestrzeni stanów z lokalnym poszukiwaniem rozwiązań. Początkowe rozwiązanie bazuje na istniejącej konstrukcji łopaty śmigłowca lub jest wstępnie generowane na podstawie założeń analitycznych i potencjalnie akceptowalnych wariantów modelowych.

W ramach poszukiwania rozwiązania problemu opisanego w sposób matematyczny, z wykorzystaniem nowoczesnych metod komputerowych, zaproponowano algorytm wiążący środowiska CAD/CAE/CFD, który wyznacza rozwiązanie optymalne przy jednoczesnym zapewnieniu akceptowalnych wyników analiz wytrzymałościowych i aerodynamicznych. Użytecznym efektem dodatkowym będzie gotowy model strukturalny możliwy do zastosowania w kolejnych etapach projektowania śmigłowca. Schemat blokowy algorytmu przedstawiono na rys. 5. W ramach publikacji przedstawiających kolejne etapy prac został on omówiony w artykułach [A4-A6]. Jednocześnie opisana procedura optymalizacyjna została zaprezentowana na konferencji [a].

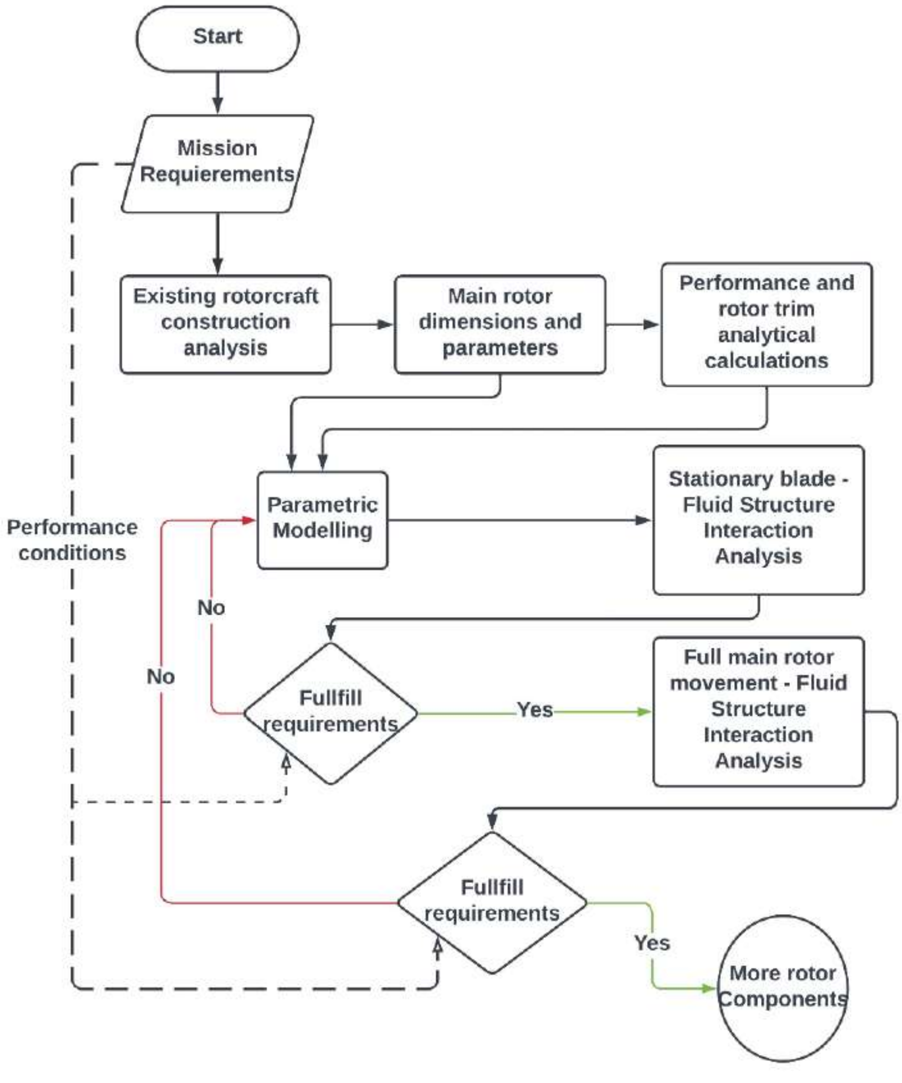

Rys. 5. Algorytm aerodynamiczno-strukturalnej optymalizacji wirnika nośnego śmigłowca

Realizacja algorytmu odbywa się poprzez wykorzystanie parametrów istniejących konstrukcji i wyznaczenie wstępnych założeń do projektu wirnika. Na tym etapie zostają określone również warunki lotu, dla których będą odbywały się obliczenia. W wyniku obliczeń analitycznych realizowanych metodami komputerowymi generowany jest parametryczny model, który następnie zostaje poddany analizom FSI w dwóch krokach. W pierwszym kroku, mniej kosztownym czasowo, oceniana jest w stacjonarnym opływie jedna łopata wirnika. Po pozytywnej ocenie rezultatów i spełnieniu kryteriów optymalizacji, zostaje utworzony całościowy model parametryczny – model wirnika uwzględniający pełną ilość łopat i ustawienie kątowe przekrojów profilowych w przestrzeni. Tym razem model jest poddany symulacji uwzględniającej ruch obrotowy wokół osi wirnika i zmianę kąta skoku ogólnego oraz okresowego wraz ze zmianą azymutalnego położenia łopaty w czasie. Po każdym kroku wyniki poddawane są analizie i oceniane pod kątem spełniania wymagań projektowych. W przypadku negatywnej oceny parametry konstrukcyjne są modyfikowane, a analizy przeprowadzane ponownie dla nowej geometrii łopaty.

5. Parametryczne przygotowanie modeli do obliczeń numerycznych dynamiki płynów

W celu wykonania parametrycznego modelu łopaty, a następnie właściwego zamodelowania wirnika nośnego i odwzorowania jego pracy w środowiskach komputerowych konieczna jest analiza matematycznego podejścia do jego pracy i zrozumienia zjawisk zachodzących w różnych wariantach wykonywanych operacji.

W pierwszym kroku, aby zrozumieć i opisać pracę wirnika nośnego należy rozważyć charakter pracy łopat w trakcie zawisu. W artykule [A2] scharakteryzowano siły powstające na łopatach w trakcie wykonywania zawisu i opisano w jaki sposób wyznaczać skok łopat wirnika nośnego w celu osiągnięcia wymaganego ciągu. Obliczanie wymaganej siły nośnej odbywa poprzez wykorzystanie teorii elementu łopaty. Geometrię opływu profilu łopatowego oraz siły występujące na elemencie łopaty przedstawiono na rys. 6.

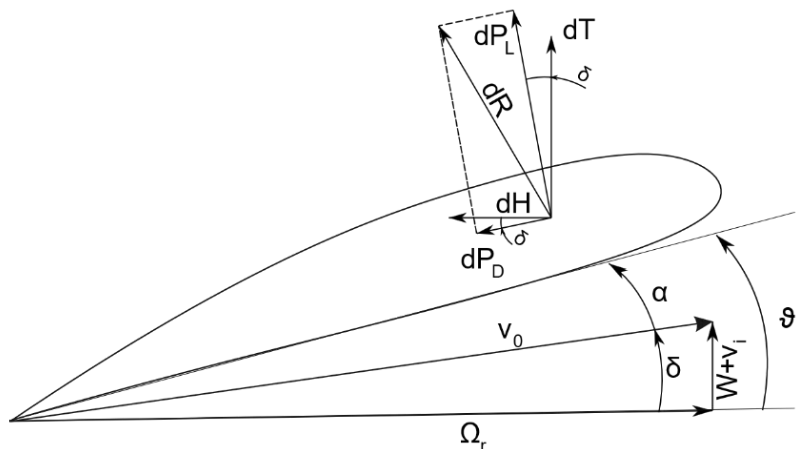

Rys. 6. Siły występujące na elemencie łopaty z oznaczeniem charakterystycznych kątów określanych w płaszczyźnie przekroju profilowego

Korzystając z przywołanej wyżej teorii w ramach algorytmu optymalizacyjnego, przygotowany został program w środowisku MATLAB, który poprzez iteracyjne obliczenia wyznacza kąt nastawienia łopaty dla stanu zawisu śmigłowca:

$$\theta(\psi) = \theta_0 - A_1 \cos(\psi) - B_1 \sin(\psi)$$

gdzie zastosowane parametry geometryczne to odpowiednio:

- $\theta(\psi)$ – kąt nastawienia łopaty w zależności od położenia azymutalnego ψ;
- θ_0 – kąt skoku ogólnego wirnika nośnego,
- A_1 – kąt skoku okresowego sterowania poprzecznego;
- B_1 – kąt skoku okresowego sterowania podłużnego.

Obliczone kąty są następnie wykorzystane do przygotowania modeli parametrycznych uwzględniających odpowiednie ustawienie łopaty. W rezultacie generowany jest model łopaty wirnika przeznaczony do analiz dynamiki płynów. Model został całkowicie sparametryzowany – generowanie geometrii odbywa się automatycznie we wcześniej przygotowanym programie, poprzez zadanie wartości parametrów takich jak promień, cięciwa (w funkcji długości łopaty), kąt skręcenia oraz kształt profilu (parametry określające zewnętrzny kontur profilu oraz początkowe kąty nastawienia).

Proces parametryzacji na każdym etapie badań realizowany jest z wykorzystaniem języka Siemens NX Open GRIP. Jest to język programowania umożliwiający generowanie modeli CAD za pomocą przygotowanego wcześniej kodu, z wykonywaniem zaawansowanych, niestandardowych operacji geometrycznych, bardziej efektywnie niż miałoby to miejsce w trybie interaktywnym, czyli z poziomu interfejsu użytkownika. Język GRIP pozwala na przygotowanie programu w którym za pomocą pojawiających się okien użytkownik może wprowadzić ustalone parametry. Dodatkowo, możliwe jest wczytywanie danych zawartych w przygotowanych wcześniej plikach, jak również wykonywanie operacji matematycznych pozwalających na wyliczenia wymiarów i obciążeń w trakcie generowania modelu geometrii. W konsekwencji, opracowany program do generowania łopaty wirnika nośnego umożliwia zmianę parametrów łopaty bez konieczności powtarzania procesu interaktywnego. Kluczowe parametry mogą być łatwo dostosowywane w celu wygenerowania modelu o nowych właściwościach. Przykładowy model z zaznaczeniem krzywych definicyjnych parametrycznie zadeklarowanych w określonych przekrojach łopaty przedstawia rys. 7.

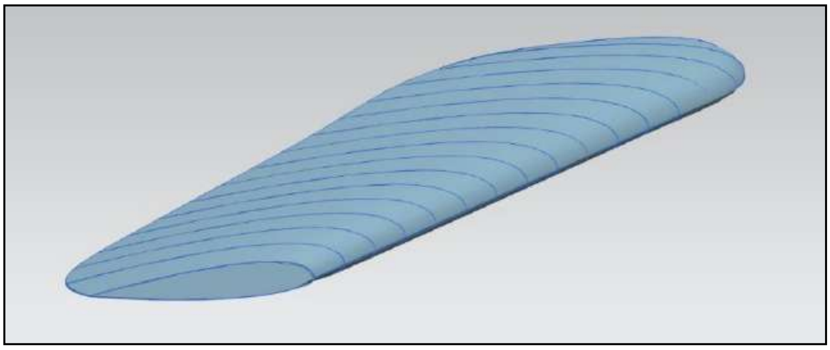

Rys. 7. Parametryczny model łopaty z zaznaczeniem definicyjnych krzywych profilowych

Model geometrii łopaty został rozwinięty o sparametryzowaną domenę płynową, dzięki czemu wynikowy plik z zadanym kształtem jest gotowy do implementacji do wybranego środowiska CFD. Na etapie badań opisanym w artykule [A2] analizowano pracę wirnika w warunkach zawisu. Jednocześnie wyniki badań zostały zaprezentowane na konferencjach [f] oraz [e].

W pierwszym kroku modelowana jest domena dla obliczeń numerycznych jednej łopaty przy warunkach opływu zadanych funkcją. Przygotowany program generuje domenę półcylindryczną z ćwierć-sferycznym wlotem wycinkowego opływu. W objętości domenowej zostaje wycięta geometria łopaty zgodnie z metodyką przygotowywania modeli do badań CFD. W ramach tego etapu przygotowano również domenę do badań dowolnego n-łopatowego wirnika nośnego. Objętości generowane są proporcjonalnie do wymiarów łopaty wirnika nośnego. Dla warunków zawisu główna objętość płynowa przeznaczona na symulację otaczającego opływu zostaje zamodelowana wewnątrz wydzielonego cylindra. Objętość lokalna wirnika, służąca do zagęszczenia siatki również jest modelowana jako cylinder. Jednocześnie w celu modelowania zmiany kąta skoku okresowego każdej łopacie przyporządkowany zostaje odrębny fragment lokalnej objętości cylindrycznej. Przykładowe modele zaprezentowano na rys. 8.

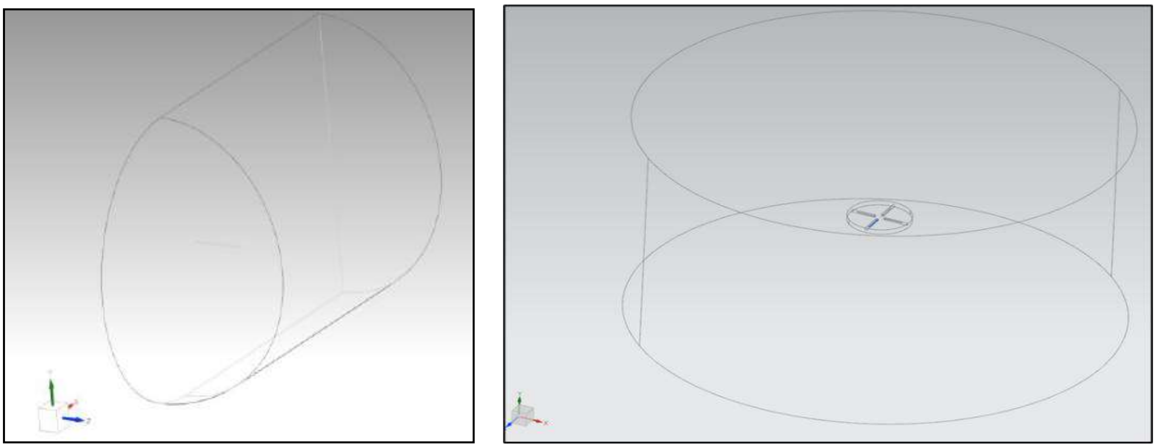

Rys. 8. Domeny płynowe wydzielone do symulacji w środowisku CFD:
a) jedna łopata z wycinkowym opływem, b) domena walcowa n-łopatowego kompletnego wirnika.

W ramach omawianego kroku badań dokonano oceny rozwiązań przeznaczonych do analiz aerodynamicznych w celu doboru oprogramowania najkorzystniejszego z punktu widzenia otrzymywanych wyników, ale również czasu wykonywanych obliczeń. Przedstawione wyżej modele CAD z sukcesem zaimplementowano do oprogramowania przeznaczonego do analiz panelowych oraz do zaawansowanego środowiska CFD. Model wirnika nośnego i jego łopaty bazuje na istniejącej konstrukcji, co pozwala to na ewaluację metody i porównanie wyników z rzeczywistymi osiągami. W obu programach zrealizowano obliczenia dla wariantu jednej łopaty i n-łopatowego wirnika. W przypadku symulacji jednej łopaty i jej opływu osiągnięto zadowalające wyniki w obu metodach. Natomiast w przypadku modelowania wirnika i jego ruchu obrotowego jedynie wyniki z analiz CFD były zgodne z oczekiwanymi tj. rzeczywistymi osiągami. Czas realizacji analiz wykonanych za pomocą metod panelowych był niższy w obu przypadkach, jednak znacząco niższy jedynie w przypadku symulacji całego wirnika.

W konsekwencji do prowadzenia dalszych badań i implementacji rozwiązań w algorytmie optymalizacyjnym wybrano analizy CFD, z podziałem na dwa etapy ewaluacji tzn. jednej łopaty z symulowanym opływem wycinkowej objętości płynu oraz pełnej symulacji wirnika nośnego w pełnej domenie walcowej. Pozwala to na przeprowadzenie w pierwszym kroku znacznie mniej czasochłonnej symulacji i ocenę przyjętej geometrii łopaty pod kątem otrzymywanych osiągów, a dopiero w kolejnym kroku, podczas symulacji pracy całego wirnika, ocenę jego zdolności jako kompletnego zespołu. Podejście takie zastosowano także w kolejnych etapach badań, gdzie badania CFD zostaną sprzężone z analizami MES.

Następny krok budowania modelu parametrycznego i jego wykorzystania do analiz numerycznych został opisany i opublikowany w artykule [A3]. W celu prawidłowego zbadania warunków pracy wirnika i określenia maksymalnych występujących obciążeń, konieczne jest odwzorowanie w symulacjach wszystkich możliwych faz lotu. W konsekwencji rozwinięto opisane wyżej rozwiązania o obliczenia i symulacji warunków lotu postępowego. W przywołanej publikacji szeroko opisano wykorzystany aparat matematyczny. Wyniki obliczeń programu są podstawą do rozwinięcia modelu parametrycznego i utworzenia geometrii wirnika nośnego wraz z odpowiednimi objętościami płynowymi. Do wcześniejszego programu generującego model parametryczny zostaje dodana możliwość wytworzenia wirnika wraz z geometrią przygotowaną pod kątem analizy lotu postępowego. Rozwinięty model CAD jest zbudowany w następujący sposób: główna objętość płynowa, przeznaczona na symulację otaczającego powietrza zamodelowana została w postaci prostopadłościanu. Wewnątrz lokalna objętość wirnika, wykorzystywana do zagęszczenia siatki obliczeniowej, modelowana jest w postaci cylindra. Jednocześnie każda łopata posiada własną objętość cylindryczną, co umożliwia jej swobodny obrót wokół własnej osi. Takie podejście pozwala na precyzyjne odwzorowanie dynamiki ruchu wirnika i dokładniejsze modelowanie zjawisk aerodynamicznych zachodzących w jego otoczeniu. Przykładową geometrię, będącą efektem działania przygotowanego algorytmu, zaprezentowano na rys. 9.

Domeny generowane są proporcjonalnie do zadanych wymiarów wirnika. Uwzględniają one uwarunkowania programów do numerycznej analizy dynamiki płynów pozwalając w pierwszej kolejności na wygenerowanie jakościowo dobrej siatki obliczeniowej. Prawidłowo wykonana siatka pozwala wykluczyć nieprawidłowości wyników spowodowane niewłaściwym doborem wymiarów domeny płynowej.

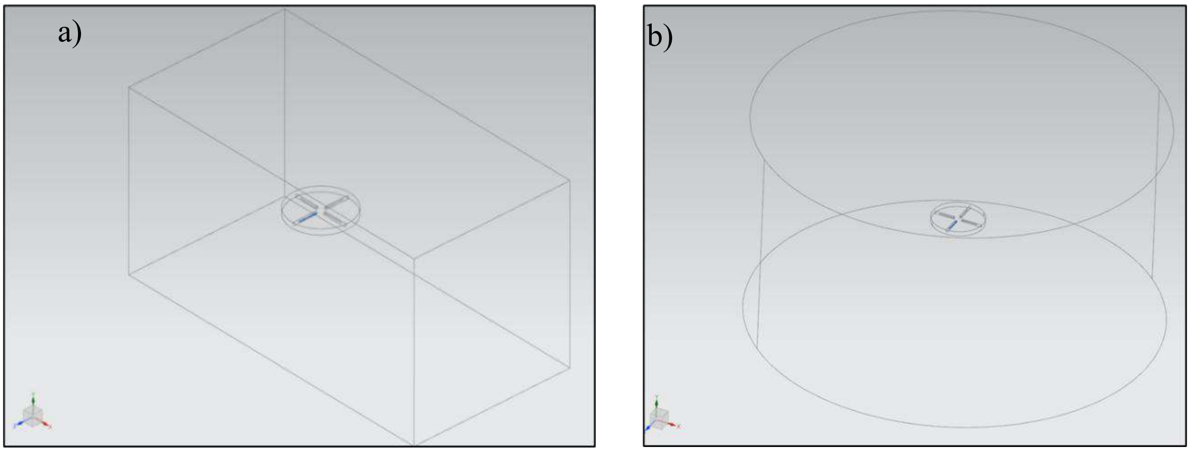

Rys. 9. Domeny płynowe do analizy różnych faz lotu: a) lot postępowy, b) zawis.

Podobnie, jak w przypadku analizy wirnika w zawisie, tak również w tym przypadku, dokonano ewaluacji modelu poprzez zastosowanie geometrii istniejącego śmigłowca w obliczeniach CFD i odwzorowanie warunków jego pracy w oparciu o dane z rejestratora parametrów lotu. W pracy szczegółowo przedstawiono sposób budowania siatki obliczeniowej, tak aby możliwa była symulacja warunków lotu śmigłowca i odwzorowanie ruchu łopat wraz ze zmianą ich azymutalnego położenia. W kolejnym kroku opracowanej symulacji określono uniwersalne warunki brzegowe, tak aby możliwe było wykonanie symulacji dla różnych wariantów lotu i konfiguracji wirnika. Poprzez określenie warunków brzegowych możliwe jest zamodelowanie opływu wirnika w locie postępowym i jednocześnie zadanie ruchu obrotowego wraz ze zmianą skoku w zależności od położenia azymutalnego łopat.

Uniwersalne dla obliczeń numerycznych warunki brzegowe zadano w następujący sposób. Badane powierzchnie nośne (powierzchnie łopat wirnika - granice wyciętych przestrzeni z cylindrycznej domeny płynowej) zostają oznaczone kolejno numerami łopat. Z tych powierzchni program będzie odczytywał wartości powstających sił. Łopaty zostają wycięte w przestrzeniach, których powierzchnie zewnętrzne stanowią powierzchnie wymiany danych z kolejną objętością odpowiadającą za modelowanie opływu całego wirnika. Zadaniem dodatkowej objętości wprowadzonej w postaci płaskiego cylindra jest odwzorowanie ruchu obrotowego wokół osi wirnika. Warunki brzegowy tejże domeny zadano na powierzchniach kontaktu z wewnętrznymi cylindrami łopat, jak również na powierzchniach kontaktu i wymiany danych z ogólną objętością płynową, w której symulowany jest ruch postępowy śmigłowca. Cała domena przepływu została zamodelowana jako prostopadłościan o wymiarach odpowiadających określonym wielokrotnościom średnicy wirnika, zgodnie z założeniami środowiska do obliczeń CFD. Na prawie wszystkich (poza jedną) powierzchniach zewnętrznych prostopadłościanu zostały zadany kierunek oraz prędkość lotu. Tylna ściana bryły znajdująca się za wirnikiem (patrząc w kierunku lotu) jest wylotem strumienia opływającego wirnik. Warunki brzegowe symulacji zadane dla parametrycznego modelu obliczeniowego zaprezentowano na rys.10.

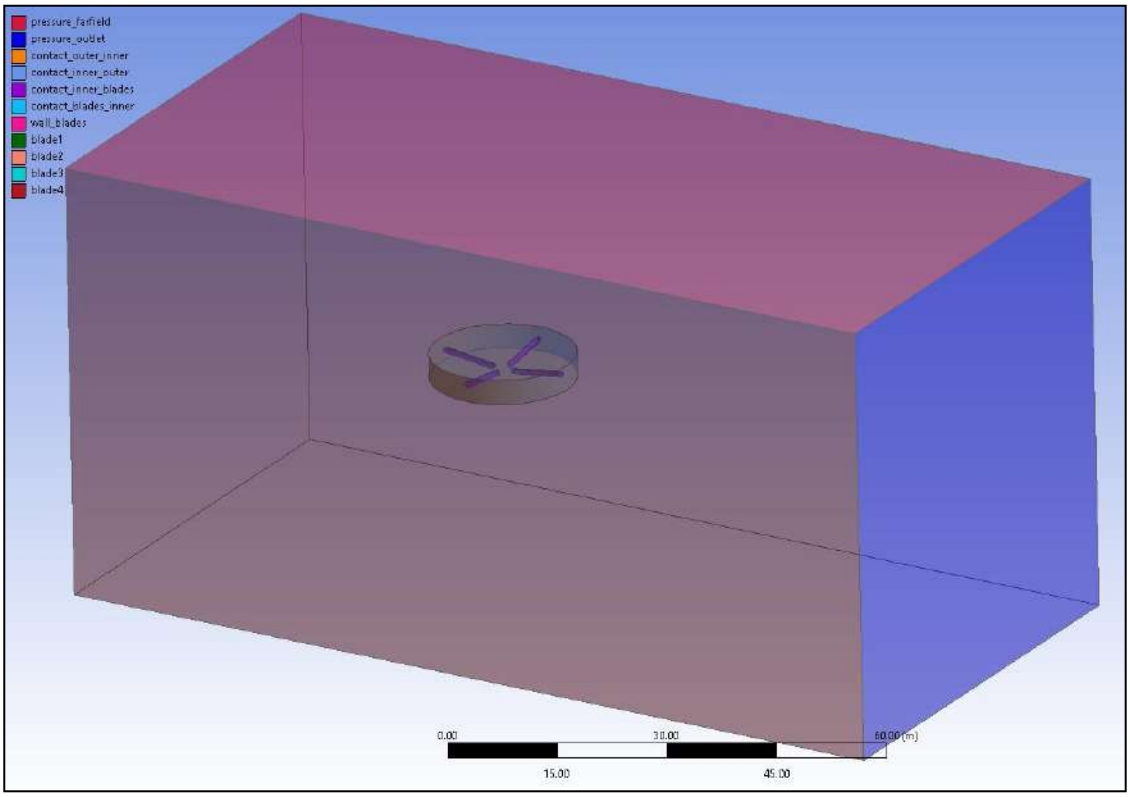

Rys. 10. Warunki brzegowe do symulacji CFD dla wydzielonej domeny opływu wirnika śmigłowca w ruchu postępowym

Bazując na istniejącej geometrii śmigłowca przeprowadzono opisany wyżej proces w celu oceny przyjętej metody. Wyliczono katy nastawienia łopat w locie postępowym dla pięciu wariantów symulacji. Kompletne zestawienie parametrów kątowych uwzględnianych w analizach CFD prezentuje Tabela nr 2.

Tabela 2**.** Kąty nastawienia łopat oraz kąt pochylenia tarczy wirnika

Wariant	**Skok ogólny [deg]**	**B1 [deg]**	**A1 [deg]**	**Kąt nachylenia tarczy wirnika [deg]**
1	11.12	3.46	-3.72	10.75
2	11.52	5.26	-4.87	10.71
3	8.31	2.52	-3.45	7.44
4	9.85	5.48	-5.48	7.43
5	9.48	3.1	-4.38	7.83

Wyliczone ustawienie wirnika posłużyło do wykonania obliczeń numerycznych dynamiki płynów Dla oczekiwanych wartości ciągu wirnika (zawsze równoważnych ciężarowi śmigłowca) każdy z wariantów geometrii modelowej poddano badaniu. W ramach wariantowania sprawdzano również inne możliwe warianty geometrii łopaty. Wyniki obliczeń zestawiono w Tabeli nr 3.

Tabela 3. Wyniki aerodynamicznej symulacji CFD w konfrontacji z wynikami obliczeń analitycznych

Obliczenia analityczne						**Symulacja CFD**	
Wariant	**Ciężar [N]**	**Promień WN [m]**	**Cięciwa łopaty [m]**	**Prędkość lotu [km/h]**	**Siła oporu [N]**	**Siła nośna [N]**	**Siła oporu [N]**
1	62784	7.85	0.3	100	1276	61706	1256
2	62784	7.85	0.3	150	2870	63708.25	2982
3	62784	7.85	0.44	100	1276	61537	1139
4	62784	7.85	0.44	200	5098	62625	5132
5	62784	7	0.6	100	1276	66850	1295

Wynikiem symulacji jest również rozkład ciśnienia na powierzchni łopat, który na późniejszym etapie zostanie przeniesiony jako obciążenie do obliczeń strukturalnych. Przykładowe rozkłady ciśnienia na wirujących łopatach zaprezentowano na rys. 11.

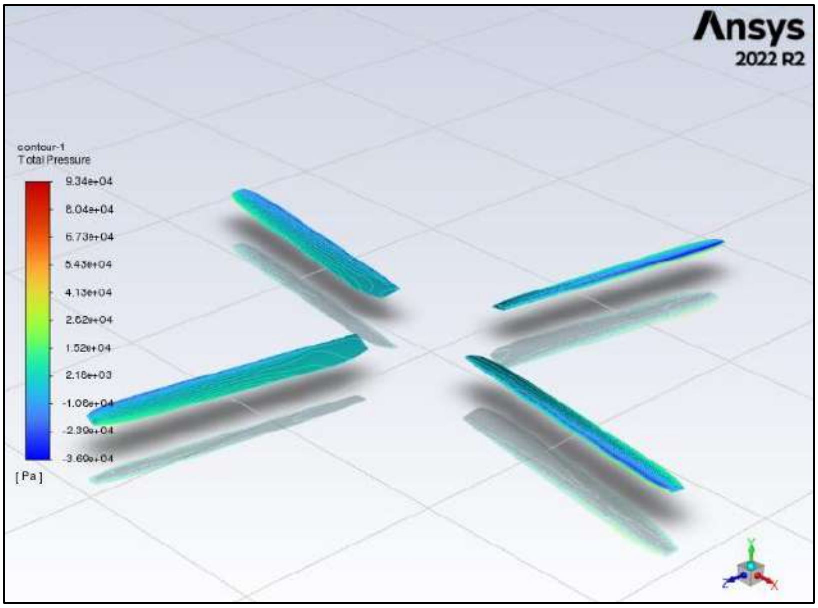

Rys. 11. Przykładowy wynik rozkładu ciśnienia na powierzchni łopat wirnika nośnego

Otrzymane wyniki były zgodne z obliczeniami analitycznymi, jak również z parametrami osiągowymi rzeczywistego śmigłowca. W ramach omawianych etapów badań udowodniono gotowość modelu parametrycznego i konfiguracji środowiska CFD do zastosowania w ramach zaproponowanego w pracy badawczej algorytmu. Wyniki symulacji i analizy sił powstających na wirniku będą miały zastosowanie w symulacji FSI. Rezultatem tego etapu były wspomniane wyżej artykuły [A2, A3]. Jednocześnie wyniki badań zaprezentowano na konferencji [f].

6. Przygotowanie analiz strukturalnych

W celu przeprowadzenia wielokryterialnej optymalizacji uwzględniającej zarówno parametry osiągowe jak i masowo-wytrzymałościowe konieczne jest przygotowanie modelu strukturalnego wirnika. Na tym etapie badań budowa modelu została poparta analitycznymi obliczeniami obciążeń, które następnie są wykorzystywane do wstępnego oszacowania wymiarów projektowanej struktury. Model generowany jest za pomocą skryptu programowego w języku GRIP z uwzględnieniem dodatkowego programu, który wyznacza momenty bezwładności profilu i iteracyjnie zmienia jego wymiary. Wyniki z poszczególnych etapów obliczeniowych dotyczących aerodynamiki, sztywności i drgań własnych łopat korygowane są poprzez pętlę, która umożliwia przeprowadzenie wstępnej optymalizacji struktury wewnętrznej przed zasadniczymi analizami typu FSI. Schemat blokowy algorytmu generowania modeli do sprzężonej analizy FSI zademonstrowano na rys. 12.

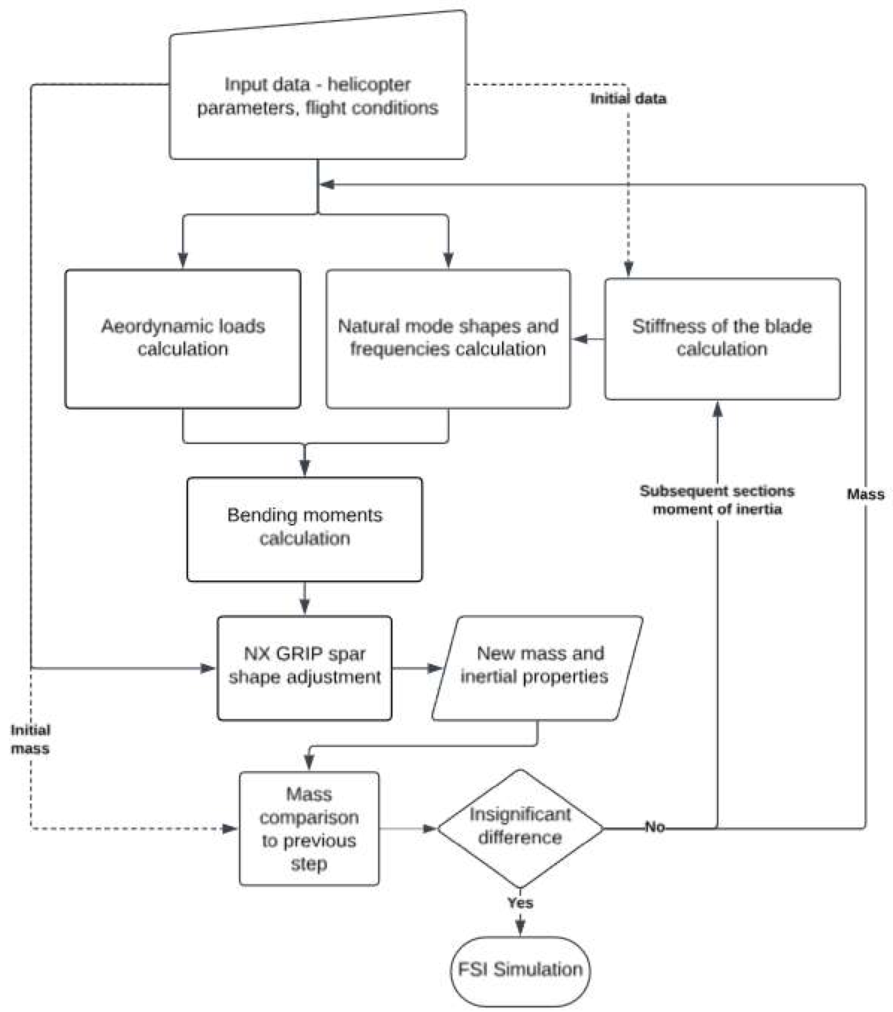

Rys. 12. Schemat blokowy generowania modeli wirnika w zastosowaniu do ostatecznej symulacji FSI

W pierwszym kroku na podstawie danych wejściowych dotyczących kształtu łopat, zastosowanych materiałów, a także projektowanych warunków lotu, realizowane są obliczenia analityczne przy wykorzystaniu własnych programów w środowisku MATLAB. Posługując się przygotowanym we wcześniejszym etapie programem do obliczeń ciągu wirnika z uwzględnieniem zmian kątów skoku ogólnego i okresowego, wyznaczany jest rozkład obciążeń aerodynamicznych w zależności od azymutu i promienia. Funkcja rozkładu sił aerodynamicznych działających na łopatę będzie wykorzystywana do wyliczenia momentów gnących. Przykładowy rozkład obciążenia aerodynamicznego tarczy nośnej wirnika oraz pojedynczej łopaty przedstawiony jest na rysunkach 13 i 14.

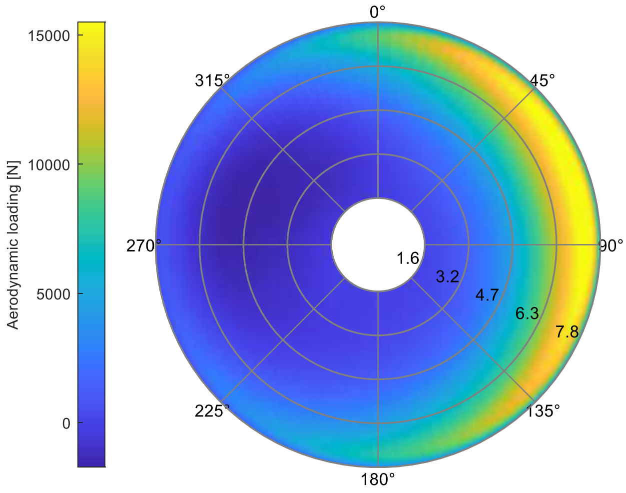

Rys. 13. Rozkład siły aerodynamicznej na powierzchni wirnika nośnego dla współczynnika prędkości 0.1

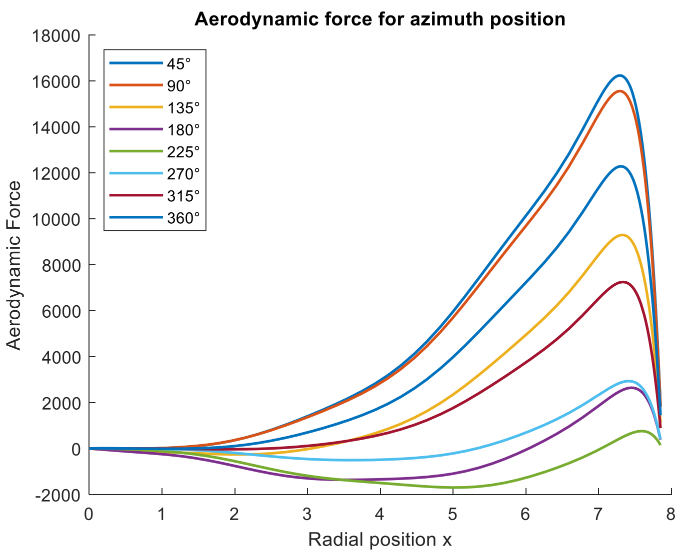

Rys. 14. Rozkład siły aerodynamicznej wzdłuż łopat w zależności od ich położenia azymutalnego dla współczynnika prędkości 0.1

W procesie równoległym do obliczeń aerodynamicznych wyznaczane są częstości drgań własnych łopaty. Wykorzystywane do tego są dane bezwładnościowe z analizy masowej modelu CAD. Biorąc pod uwagę własności zastosowanego materiału dla poszczególnych elementów konstrukcji przy wykorzystaniu metody energetycznej określane są kolejne postacie i częstości drgań własnych. Rozwiązanie matematyczne problemu zostało zrealizowane z wykorzystaniem środowiska MATLAB. W tym celu równanie energetyczne wirującej belki przekształcono do postaci macierzy. Wykorzystano w tym celu rozwinięcie funkcji w szeregi Fouriera. Wyznaczniki wyliczone z utworzonej macierzy współczynników są wartościami kolejnych częstotliwości drgań własnych. Wyniki w celu uproszczenia dalszych obliczeń został znormalizowane względem liczby π. Szczegółowy opis zastosowanej metody został zamieszczony w artykule [A5]. Przykładowe funkcje postaciowe oraz częstości kolejnych drgań własnych ω_i zostały zaprezentowane na rys. 15.

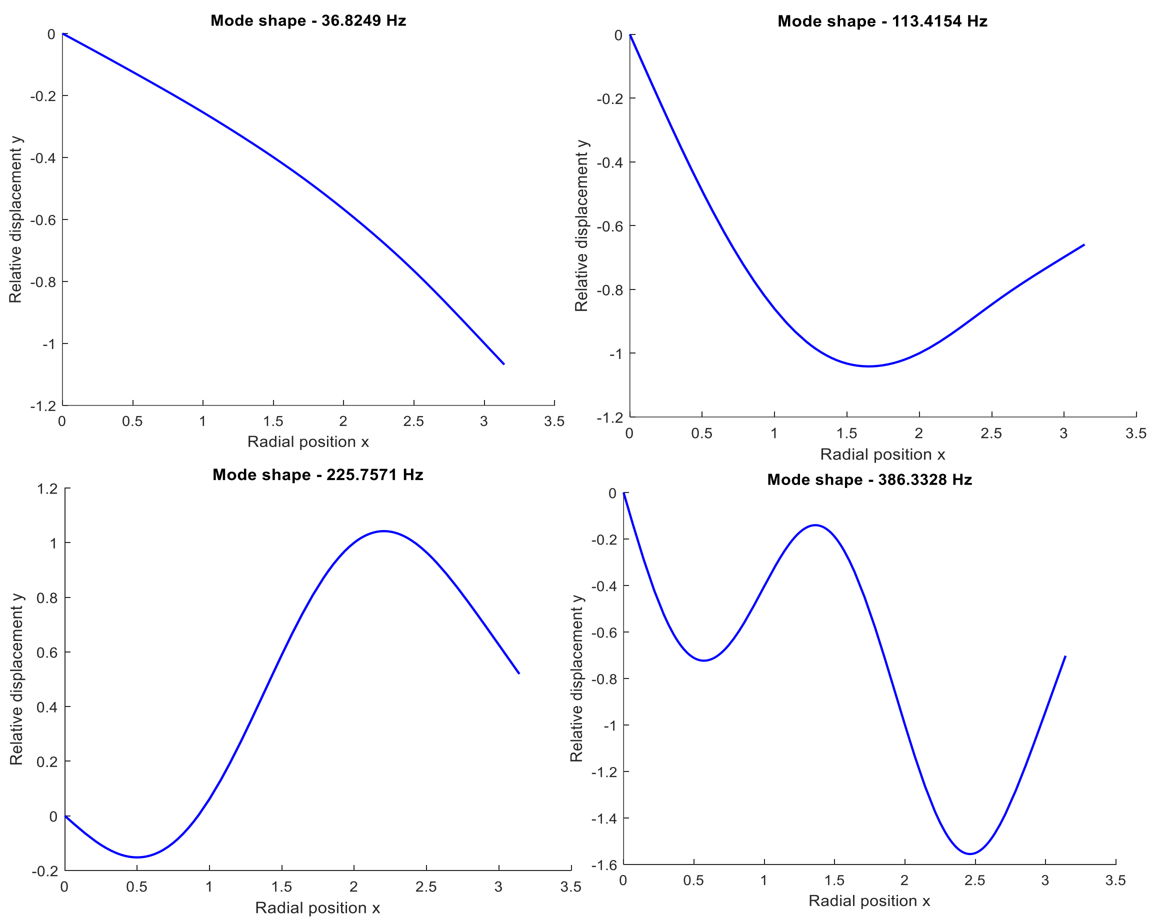

Rys. 15. Funkcje odwzorowujące kolejne postacie drgań własnych pojedynczej łopaty

Jak pokazano na rys. 12 wyniki dwóch równolegle realizowanych operacji są danymi wsadowymi do wyliczenia momentu gnącego działającego na łopatę w zależności od jej azymutalnego położenia. Moment gnący wyznaczany jest dla 3 pierwszych harmonicznych, a następnie sumowany jako wypadkowy moment całkowity. Przykładowe rozkłady momentu gnącego wzdłuż łopat przedstawione zostały na rys. 16.

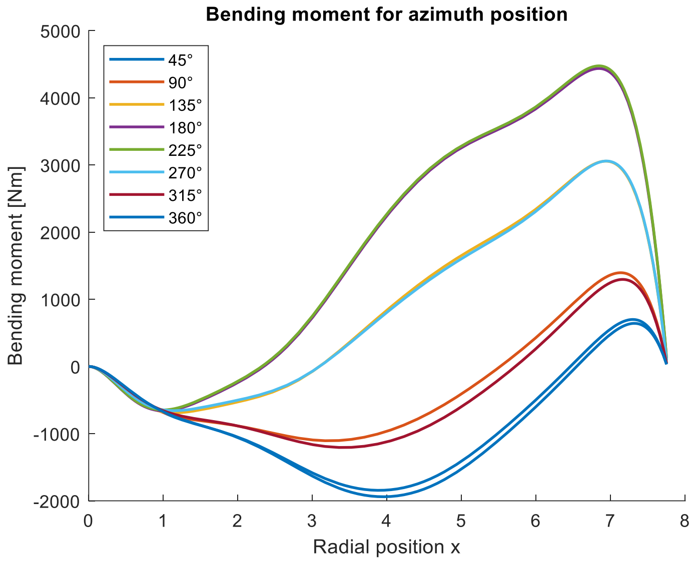

Rys. 16. Rozkłady momentu gnącego wzdłuż łopaty wirnika nośnego w zależności od jej azymutu

Program generuje wartości momentu gnącego dla ustalonej przez użytkownika liczby przekrojów. Wyliczone wartości są eksportowane do zewnętrznego pliku.

Następnie przy wykorzystaniu języka programowania GRIP tworzony jest parametryczny model geometrii przeznaczony do obliczeń numerycznych obciążeń i odkształceń występujących w łopacie. Program generuje wstępną geometrię zewnętrzną i wewnętrzną. Importuje wyliczone wcześniej wartości momentów gnących i we wskazanych przekrojach poprzecznych łopaty wyznacza naprężenia. Dedykowane komendy języka GRIP sterują obliczeniami geometrycznych momentów bezwładności we wskazanych przekrojach łopaty.

Program za każdym razem sprawdza warunek wytrzymałościowy nieprzekraczalności dopuszczalnych naprężeń normalnych od zginania (dla zadanego materiału konstrukcyjnego). Iteracyjnie dobierane są wymiary wysokości dźwigara i szerokości wypełniacza komórkowego, tak aby utrzymać bezpieczny poziom wytężenia struktury przy możliwie minimalnej wielkości przekroju. W każdej iteracji uwzględniana jest zmiana wymiarów przekroju, a tym samym zmiana momentu bezwładności. Łopata poddawana jest obliczeniom uwzględniającym zmienność momentów gnących determinowanych przez rozkłady obciążeń aerodynamicznych i masowych. Pętla kończy się w momencie uzyskania znikomych zmian masy łopaty w wyniku kolejnych iteracji. Przykład modelu struktury łopatowej zoptymalizowanego pod względem wytrzymałościowym pokazano na rys. 17.

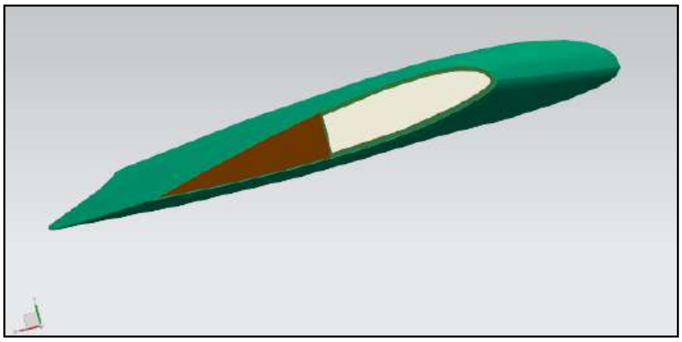

Rys. 17. Model CAD łopaty wirnika nośnego

Dostosowany do warunków wytrzymałościowych model geometryczny zostaje zaimportowana do programu Simcenter STAR-CCM+ na potrzeby przeprowadzenia symulacji modelowych FSI. Na bazie modelu wygenerowana zostaje siatka elementowa do analiz strukturalnych MES. Dynamicznie zmienne obciążenia łopat zostają zaimportowane w postaci rozkładów ciśnienia wyznaczanych z obliczeń CFD. Na tym etapie badań model podlegał ewaluacji poprzez jednokierunkową analizę FSI. Przykładowe wyniki naprężeń w strukturze dźwigara zaprezentowano na rys. 18.

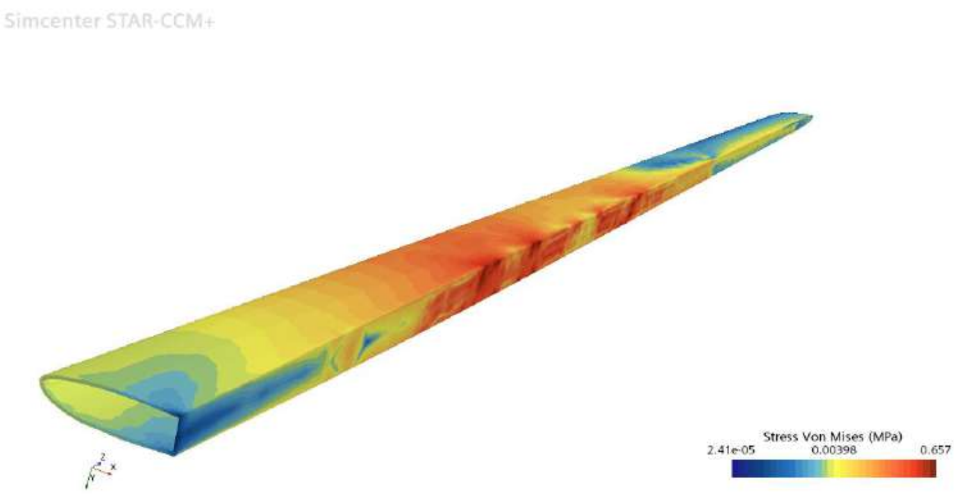

Rys. 18. Naprężenia w modelu MES dźwigara łopaty

Symulacje przeprowadzone zostały na modelu odpowiadającym rzeczywistej geometrii łopaty śmigłowca fabrycznego. Dobierając własności struktury modelowej uwzględniono dane rzeczywistych materiałów konstrukcyjnych (szczegółowe dane zostały omówione w artykule [A5]). Maksymalne wartości naprężeń numerycznych w strefach ich kumulacji (krawędzie w środkowej części ścianki dźwigarowej) nie przekraczały poziomów wartości dopuszczalnych, co potwierdziło poprawność przyjętej struktury modelowej.

Na tym etapie dokonano również analizy danych z pokładowego rejestratora parametrów lotu śmigłowca wojskowego. Wykorzystanie zapisów rzeczywistych pozwala lepiej zrozumieć dynamiczną pracę konstrukcji w zależności od wykonywanej misji. Wartości maksymalnie występujących przeciążeń, a także profil lotu ze zmianą wysokości i prędkości wykorzystywane są do oceny krytycznych faz lotu w których należy dokonać ewaluacji konstrukcji. Przykład zapisu jednej godziny lotu przedstawia rys. 19.

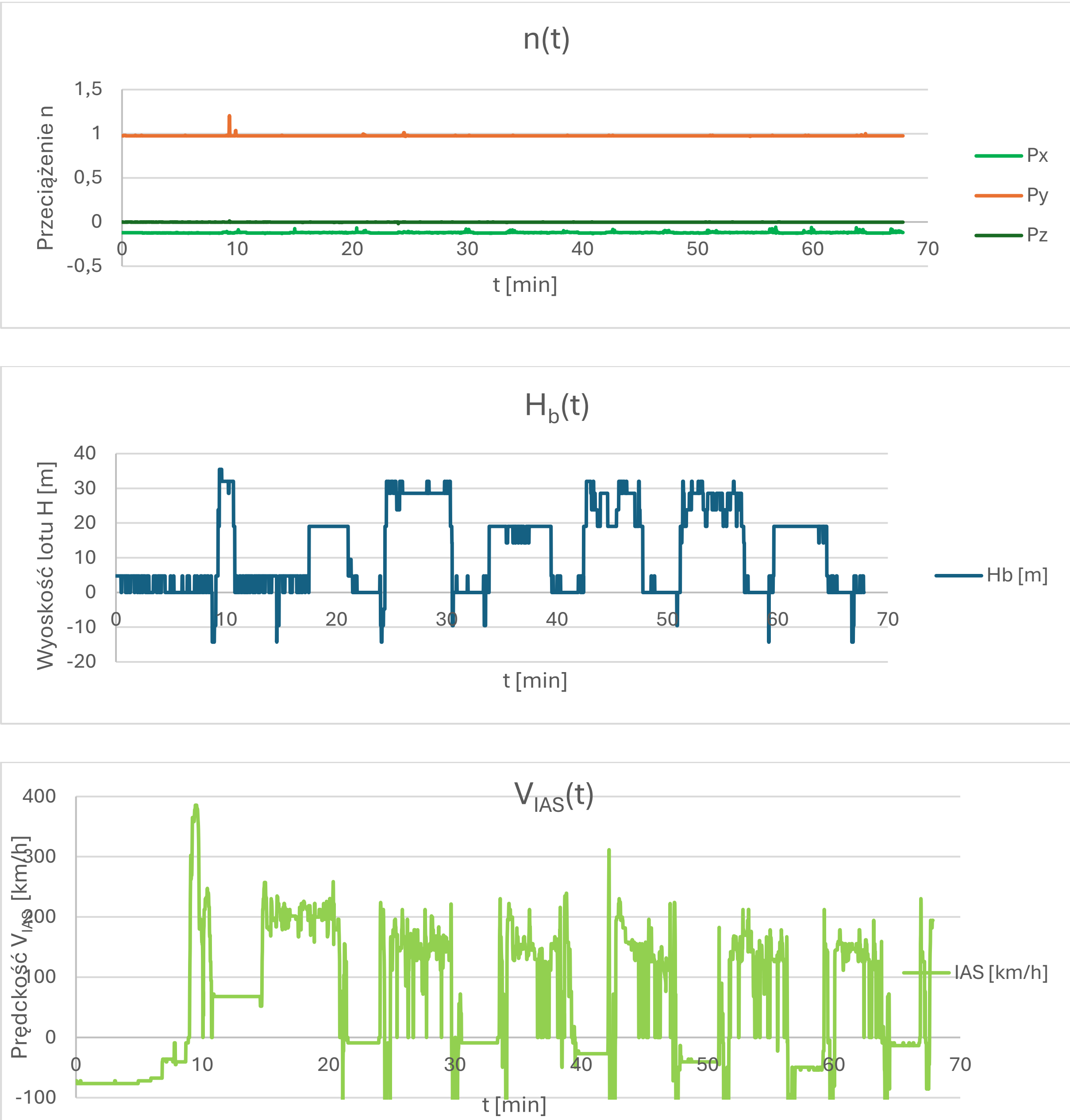

Rys. 19. Zapisy zmian zarejestrowanych parametrów lotu w czasie trwania misji:
a) przeciążeń n(t), b) wysokości barometrycznej $H_b(t)$, c) prędkości przyrządowej $V_{IAS}(t)$

Całość analiz oraz wyniki uzyskane w ramach przedstawionego etapu badań opublikowano w artykułach [A4, A5], które są podstawą niniejszej dysertacji. Jednocześnie wyniki przedmiotowego etapu zaprezentowano na konferencjach [c], [b] oraz [d].

7. Powiązanie modeli i przeprowadzenie multidyscyplinarnej optymalizacji

W ostatnim etapie badań następuje integracja wcześniej przygotowanych i wstępnie sprawdzonych elementów algorytmu zgodnie z ogólnym schematem procesowym przedstawionym na rys. 5. Ten etap prac został opisany w artykule [A6].

7.1. Algorytm multidyscyplinarnej optymalizacji

Zadania przewidziane w zalgorytmizowanym cyklu optymalizacji realizowane są w następujący niżej opisany sposób.

1. W pierwszym kroku ustalane są warunki misji. W zależności od przeznaczenia śmigłowca determinowane są pożądane parametry operacyjne i ich oczekiwane wartości. Do parametrów operacyjnych zaliczamy m.in. udźwig, długotrwałość lotu, zasięg, prędkość przelotową, maksymalną masę startową. Na tym etapie określany jest przewidywany profil lotu oraz rodzaje realizowanych zadań. Przekłada się to na wielkości przeciążeń, którym podlega konstrukcja i które muszą zostać uwzględnione w obciążeniach obliczeniowych. W końcowym etapie procesu opisane wyżej parametry posłużą również do oceny uzyskanych wyników numerycznych. Spełnienie lub poprawa wymaganych zdolności będzie podstawą do uznania przeprowadzonej optymalizacji za skuteczną. W razie negatywnej oceny i braku oczekiwanych zdolności śmigłowca, przedmiotowe wielkości zostaną wykorzystane do wytyczenia kierunku poprawy osiągów poprzez dostosowanie parametrów konstrukcyjnych podlegających optymalizacji.
2. W drugim kroku przeprowadzana jest ocena pożądanych parametrów misyjnych względem parametrów referencyjnych przypisywanych aktualnie istniejącym konstrukcjom. Ocena dokonywana jest z wykorzystaniem parametrów bezwzględnych (fizycznych), jak również z wykorzystaniem bezwymiarowych współczynników. Trendy wyznaczane dla danej grupy śmigłowców wojskowych pozwalają wskazać możliwe kierunki poprawy osiągów względem ich aktualnych poziomów. Pozwala to na wybranie parametrów fizycznych, które będą podlegały optymalizacji. Na tym etapie zostaje określony funkcjonał optymalizacji wielokryterialnej, który będzie analizowany w oparciu o metodę systematycznego przeszukiwania przestrzeni zmiennych projektowych.
3. Wyniki analizy trendów i porównania poszczególnych parametrów pozwalają przygotować zestaw pierwszych wartości parametrów konstrukcji właściwych do uzyskania pożądanych osiągów. Posłużą one do dalszych obliczeń i trymowania

wirnika, a także do rozwijania parametrycznego modelu geometrii CAD, który będzie podlegał przekształceniu wskutek przeprowadzonego procesu.

4. Niezbędne osiągi oraz warunki trymowania wirnika wyliczane są z wykorzystaniem analitycznego modelu, który został opisany w przywołanych wyżej artykułach. Kalkulacje wykonywane są w oparciu o środowisko MATLAB. Otrzymanymi wynikami są wartości ciągu wraz z ustawieniem kątowym łopat. Ustawienia łopat są wykorzystywane w kolejnym etapie do przygotowania symulacji pracy wirnika nośnego śmigłowca.
5. Najważniejszym etapem realizowanego procesu jest przygotowanie modelu parametrycznego wirnika. Parametryczne modele CAD zostają wygenerowane w taki sposób, aby możliwe było ich zastosowanie w środowiskach CFD i MES. Równocześnie, następuje utworzenie modelu kształtu zewnętrznego wraz z dostosowanymi domenami płynowymi oraz kształtu struktury wytrzymałościowej. Modele generowane są zgodnie z procedurami szczegółowo opisanymi w artykułach stanowiących podstawę dysertacji, jak również nakreślonymi we wcześniejszych rozdziałach niniejszego referatu.
6. W kolejnym etapie analizy CFD zostają powiązane z procesami MES w ramach sprzężonych symulacji typu FSI. Rozkład sił i obciążeń aerodynamicznych uzyskanych w analizie dynamiki płynów przenoszony jest na powierzchnię dyskretnego modelu struktury. Analiza FSI została podzielona na dwa etapy. W pierwszym z nich analizie zostaje poddany model stacjonarny jednej łopaty z symulowanym opływem powietrza. W tej symulacji, w części analizy dotyczącej numerycznej dynamiki płynów uwzględniono zmianę prędkości wzdłuż promienia oraz zmianę kąta napływu poprzez zadanie funkcji zmiany kierunku strumienia napływu w zależności od promienia.
7. Otrzymane wyniki poddawane są ewaluacji pod kątem spełnienia założeń początkowych. W przypadku konieczności korekty konstrukcji algorytm realizowany jest ponownie z uwzględnieniem proponowanych zmian. Etap ten umożliwia wstępną ocenę konstrukcji oraz przeprowadzenie symulacji w znacznie krótszym czasie niż w przypadku symulacji opływu wielołopatowego wirującego wirnika w warunkach nieustalonych.
8. W przypadku pozytywnej oceny jakości wyników z etapu poprzedniego algorytm przechodzi do kolejnej faz. Analizowany jest wariant modelowy wirnika wielołopatowego z uwzględnieniem rzeczywistej prędkości przelotowej, prędkości obrotowej oraz zmienności kąta skoku łopat. W tym przypadku obciążenia aerodynamiczne zostają przeniesione na konstrukcję. Z kolei odkształcenia struktury wywołane obciążeniami zewnętrznymi zostają uwzględnione w kolejnym kroku czasowym symulacji opływu. Dwukierunkowy transfer danych następuje w każdym kolejnym kroku obliczeniowym.

W konsekwencji deformacje i siły masowe są uwzględnianie przy wyliczaniu sił powstających na wirniku. Przykładową siatkę przygotowaną do symulacji pokazano na rys. 20. Przykład zastosowania technik FSI zaprezentowano na konferencji [d].

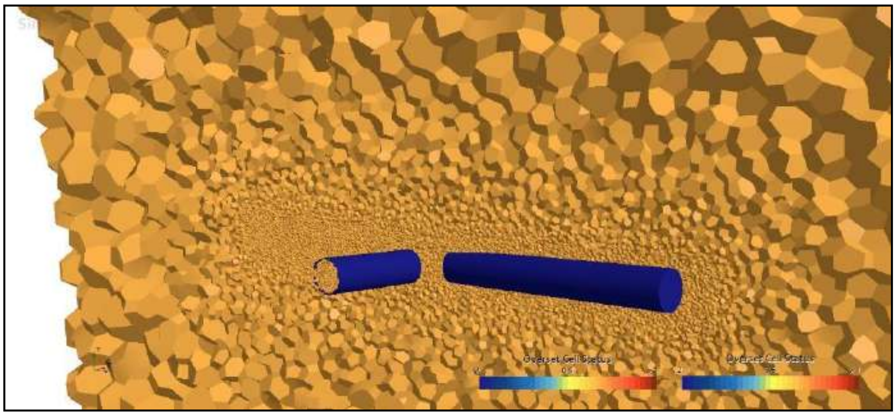

Rys. 20. Model interakcyjny struktury łopaty i siatki aerodynamicznej do symulacji FSI n-łopatowego wirnika nośnego.

9. Wyniki przeprowadzonych obliczeń numerycznych są ponownie oceniane pod kątem wymagań misji z wykorzystaniem parametrów wynikających z analizy rzeczywistych konstrukcji. Oceniane są osiągi oraz ograniczenia. Wyznaczane warianty modelowe są porównywane w celu wyboru tego, który jest najlepiej dostosowany do zadanych preferencji. Wagi cząstkowych funkcji celu odpowiadają wymaganiom przyszłego użytkownika. W przypadku niespełnienia oczekiwań, wyniki są wykorzystywane do ponownej parametryzacji i przeprowadzenia kolejnej iteracji algorytmu.
10. Proces kończy się wyborem jednego bądź kilku rozwiązań spełniających funkcjonał celu. Zoptymalizowane modele mogą być zastosowane w kolejnych iteracjach projektowych.

7.2. Walidacji metody

W badaniach wykorzystano geometrię wirnika nośnego śmigłowca wojskowego oraz rzeczywiste wartości parametrów misyjnych. Przeanalizowano poprawę właściwości konstrukcji oraz dokonano weryfikacji działania algorytmu. Otrzymane wyniki potwierdzają przydatność metody w procesie projektowania wiropłatów. Początkowe parametry obliczeniowe zestawiono w tabeli 5. Kształt i wymiary łopaty są dobierane z przedziału dopuszczalnych wartości rzeczywistych.

Pierwszy etap obliczeń przeprowadzono dla różnych wariantów zaproponowanego kształtu. Postać geometryczną łopaty z parametrycznie zmienianymi wymiarami i z zadaną charakterystyką zwichrzenia zaprezentowano na rys. 21.

Tabela 5. Parametry początkowe symulacji odpowiadające konfiguracji fabrycznej wirnika nośnego

Parametr	Oznaczenie	Wartość
promień	*R*	7.85 [m]
cięciwa łopaty	*c*	0.44 [m]
skręcenie	*v*	12°
nachylenie współcz. siły nośnej	*a*	6.4
prędkość obrotowa wirnika	*n*	255 [rpm]
Liczba Locke'a	*γ*	9.65
Maks. masa startowa (MTOW)	*m*	6400 [kg]
Masa łopaty	*mb*	65.5 [kg]

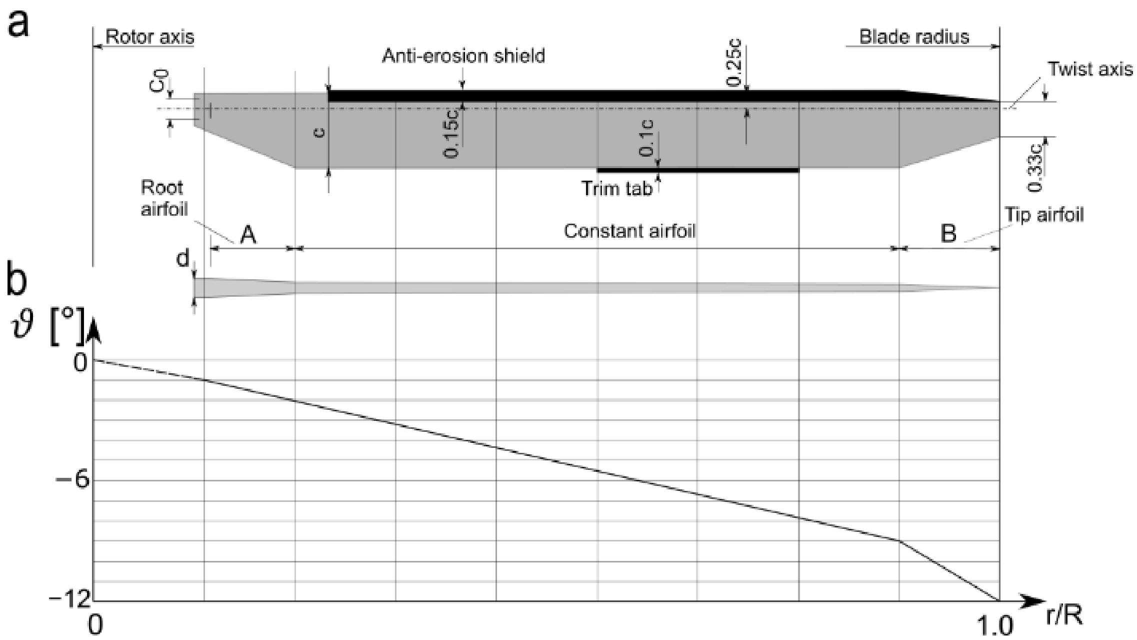

Rys. 21. Geometria łopaty z oznaczeniem parametryzowanych wymiarów i charakterystyką zwichrzenia geometrycznego

W analizowanym przypadku założono zwiększenie możliwości udźwigu śmigłowca o 200 kg, uwzględniając możliwość zwiększenia mocy zespołu napędowego bez konieczności wprowadzania istotnych zmian konstrukcyjnych płatowca. Metodą przeszukiwania przeliczono różne warianty geometryczne wirnika celem wyznaczenia wartości ciągu aerodynamicznego. Jednocześnie zachowano wymaganie technologiczne odnośnie zamocowania łopat w oparciu o istniejącą tarczę sterującą. Ewentualne różnice w ustawieniu łopat byłyby możliwe do zniwelowania poprzez regulacje popychaczy tarczy. Zaproponowane wymiary, wraz z wartościami współczynnika wypełnienia wynikającymi z trymowania i matematycznych obliczeń ciągu zamieszczono w tabeli 6.

Tabela 6. Parametrycznie modyfikowane wymiary wirnika nośnego z wartościami skoku ogólnego odpowiadającymi charakterystycznym prędkościom przelotowym; w pierwszej linii parametry odpowiadające wariantowi fabrycznemu (żółte komórki)

Promień zew.	**Cięciwa**	**Wsp. wypełnienia**	**Skok ogólny dla IAS 50 [km/h]**	**Skok ogólny dla IAS 100 [km/h]**	**Skok ogólny dla IAS 150 [km/h]**	**Skok ogólny dla IAS 200 [km/h]**
R [m]	**c [m]**	**σ**	**θ_0[°]**	**θ_0[°]**	**θ_0[°]**	**θ_0[°]**
7,85	0,44	0,055	4,68	5,05	6,39	9,35
7	0,6	0,084	5,07	5,56	7,19	11,33
7	0,65	0,0899	4,67	5,06	6,67	10,55
7,1	0,6	0,083	4,86	5,35	6,9	10,67
7,1	0,65	0,0912	4,48	4,85	6,4	9,94
7,15	0,6	0,0824	4,76	5,11	6,62	10,46
7,2	0,6	0,0818	4,66	5	6,49	10,06
7,2	0,62	0,0845	4,49	4,89	6,34	9,85
7,2	0,65	0,0886	4,29	4,65	6,02	9,37
7,25	0,6	0,0813	4,56	4,9	6,36	9,86
7,25	0,65	0,088	4,21	4,46	5,9	9,19
7,3	0,65	0,0874	4,12	4,37	5,78	9,02
7,4	0,65	0,0862	3,95	4,2	5,45	8,52
7,4	0,6	0,0796	4,29	4,61	5,87	9,14
7,5	0,6	0,0785	4,04	4,34	5,64	8,36
7,24	0,6	0,0814	4,58	4,92	6,38	9,9
7,24	0,62	0,0841	4,41	4,71	6,24	9,7
7,23	0,62	0,0842	4,43	4,83	6,26	9,74
7,23	0,63	0,0855	4,4	4,68	6,07	9,44
7,22	0,63	0,0857	4,42	4,71	6,1	9,67
7,24	0,61	0,0827	4,54	4,86	6,31	9,8
7,5	0,55	0,072	4,49	4,79	6,12	9,13
7,5	0,54	0,0707	4,54	4,85	6,2	9,42
7,49	0,54	0,0708	4,56	4,87	6,22	9,46
7,5	0,5	0,0655	4,93	5,33	6,68	9,92
7,55	0,5	0,065	4,84	5,22	6,55	9,74
7,6	0,5	0,0646	4,74	5,02	6,43	9,56
7,6	0,48	0,062	4,95	5,27	6,62	9,83
7,5	0,53	0,0694	4,68	5,017	6,28	9,55
7,49	0,53	0,0695	4,7	5,03	6,43	9,58
7,48	0,53	0,0696	4,72	5,05	6,46	9,61
7,48	0,52	0,0683	4,77	5,12	6,55	9,73
7,46	0,52	0,0684	4,81	5,16	6,6	9,81

Propozycje nowych wymiarów zewnętrznych spełniających kryterium technologicznej kompatybilności z istniejącą konstrukcją piasty wirnika i zastosowaną tarczą sterującą (kąty ustawienia łopaty odpowiadające tym samym prędkościom, zbliżone do tych dla łopaty podstawowej) zostały wybrane do ewaluacji w kolejnym kroku. Dla każdego z tych kształtów przeprowadzono kolejne procesy obliczeniowe zgodnie z ustalonym algorytmem (rys. 5) Wyniki zaproponowanych kształtów wraz z parametrami masowymi zaprezentowano w tabeli 7.

Tabela 7 Wymiary i masy łopaty wirnikowej po optymalizacji struktury dla zwiększonego ciągu

PROMIEŃ	CIĘCIWA	MASA ŁOPATY	ŚRODEK CIĘŻKOŚCI
R [m]	**c [m]**	**MB [KG]**	**Z[m]**
7,24	0,61	42,127	4,459
7,49	0,54	37,186	4,612
7,55	0,5	33,527	4,637
7,46	0,62	34,260	4,572

W kolejnym kroku dla każdej z zaproponowanych struktur przeprowadzono analizę FSI w celu sprawdzenie wytrzymałości konstrukcji w zadanych warunkach lotu przy jednoczesnym odkształceniu łopaty z uwzględnieniem wpływu deformacji na siłę nośną. Szczegółowy opis symulacji FSI znajduje się w artykułach będących podstawą dysertacji, natomiast w niniejszym autoreferacie przedstawiono ją w ogólnym zarysie. Analizy FSI potwierdziły bezpieczne poziomy naprężeń występujących w konstrukcji oraz zdolność wirnika do wytworzenia wymaganego ciągu już na etapie symulacji jednołopatowej. Symulacja FSI pełnowymiarowego wirnika wykonana w kolejnej fazie potwierdziła uzyskane wyniki. Przykładowe wyniki odkształceń i naprężeń przedstawiono na rys. 22.

Jednym z głównych celów badania, poza wypracowaniem samej metody optymalizacji aerodynamiczno-strukturalnej, jest zapewnienie, aby zaprogramowany proces był skuteczny i czasowo efektywny. Narzędzia komputerowe pozwalają rozwiązywać bardzo skomplikowane symulacje odwzorowując jak najdokładniej warunki rzeczywiste. Niejednokrotnie jednak czas wymagany do uzyskania wyników jest zbyt długi, aby wykorzystać go w procesie projektowania czy w zastosowaniu do zadań przemysłowych. Celem redukcji czasu symulacji FSI było rozdzielenie jej na dwa etapy, co zostało opisane w poprzednich rozdziałach.

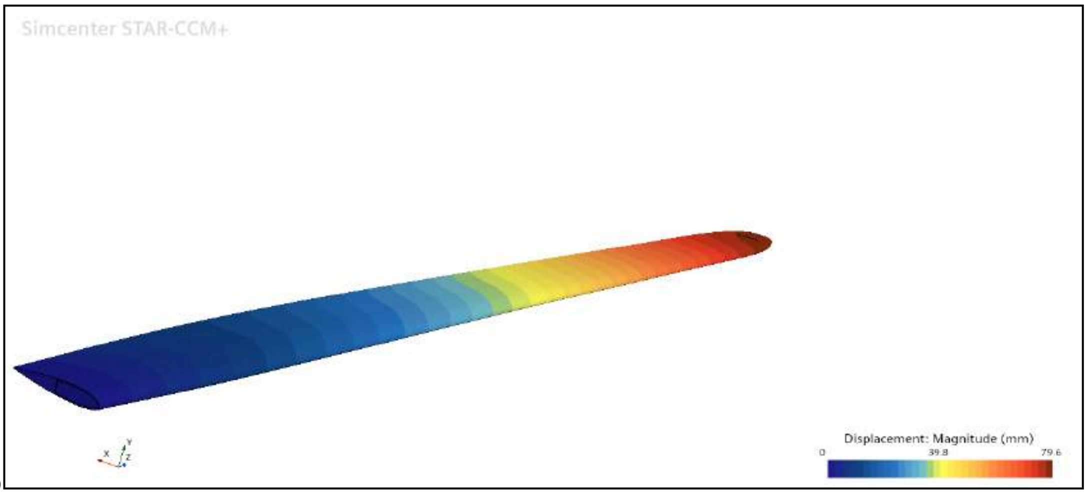

a)

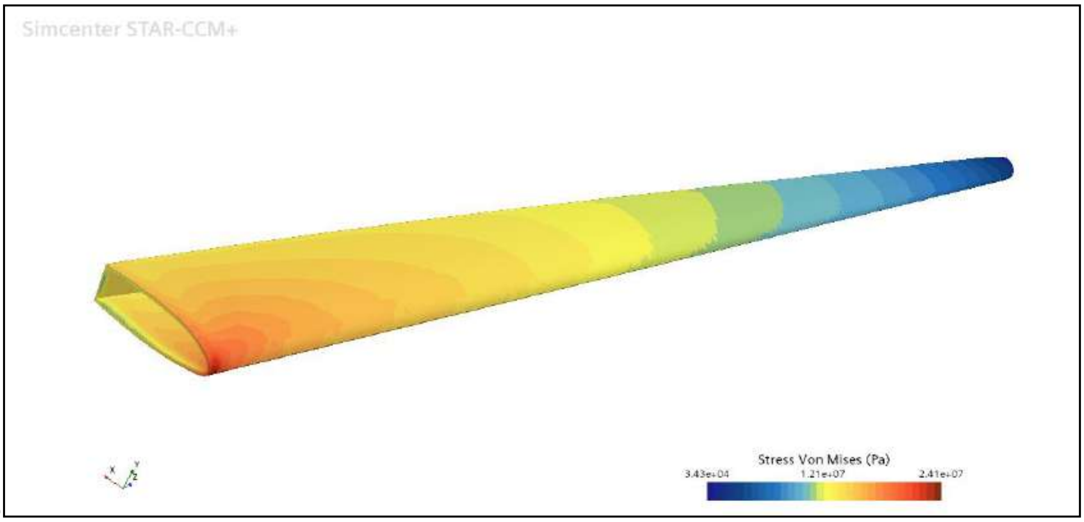

b)

Rys. 22. Wyniki analizy wytrzymałościowej łopaty wirnika po interakcyjnej analizie FSI: a) rozkład odkształceń; b) rozkład naprężeń.

Wszystkie badania symulacyjne zostały przeprowadzone z wykorzystaniem stacji roboczej wyposażonej w dwa procesory Xeon Gold 6152 CPU 2.10GHz z całkowitą liczbą 44 rdzeni fizycznych i 128 GB pamięci RAM. Obliczenia matematyczne wykonywane są na jednym rdzeniu, natomiast symulacje FSI wykorzystują wszystkie dostępne zasoby. Pomiaru czasu dokonywano od rozpoczęcia obliczeń analitycznych do czasu uzyskania zestawu wyników dla badanego wariantu. Całkowity czas do osiągnięcia ostatecznych rezultatów podlegających ocenie według zadanej funkcji kryterialnej zajmuje około 53 godziny. Najbardziej czasochłonnym etapem jest sprzężona analiza FSI aerodynamicznego modelu wirnika nośnego powiązanego ze strukturą modelową MES, która zajmuje 90% czasu realizacji całego procesu. Zestawienie średnich czasów obliczeń etapowych oraz niezbędnych mocy obliczeniowych zamieszczono w tabeli 8.

Tabela 8. Częściowy i całkowity czas przeprowadzenia optymalizacji

Faza symulacji	**Średnia ilośc iteracji na fazę**	**Średni czas na iterację**	**Moc obliczeniowa**
Obliczenia analityczne	30	5 min	1 Rdzeń 2.10GHz
Modelowanie Parametryczne dla CFD	1	2 min	1 Rdzeń 2.10GHz
Modelowanie Parametryczne dla MES	5	7 min	1 Rdzeń 2.10GHz
FSI – Jedna łopata	2	70 min	44 Rdzeń 2.10GHz
FSI – pełny wirnik Nośny	1	48 h	44 Rdzenie 2.10GHz
Czas całkowity		53 h	

8. Podsumowanie wyników i wnioski

W referacie przedstawiono badania własne przeprowadzone w przeciągu pięciu lat prac studyjnych poświęconych problematyce optymalnego projektowania wirników nośnych śmigłowców. Opisana tu autorska metoda modelowej optymalizacji aerodynamiczno-strukturalnej uwzględnia zastosowanie parametryzacji geometrycznej w wielodziedzinowych symulacjach programowych realizowanych na rzecz wyznaczenia możliwie najlepszego wariantu konstrukcyjnego w aspekcie jego wielokryterialnej oceny.

Podstawę analiz modelowych stanowi zaprezentowany w niniejszej pracy matematyczny model optymalizacji. Model jest wykorzystany do przeprowadzenia wieloprocesowej analizy optymalizacyjnej z uwzględnieniem wielokryterialnego funkcjonału jakości. Zmienne decyzyjne zostały wytypowane na podstawie wcześniej przeprowadzonej porównawczej analizy współcześnie eksploatowanych konstrukcji śmigłowcowych. Sformułowany funkcjonał łączy dwa niezależne kryteria jakościowe – funkcję aerodynamicznej efektywności wirnika nośnego oraz funkcję masy konstrukcyjnej obiektu. Tak opracowany funkcjonał jest kluczowym operatorem matematycznym stosowanym w prowadzonych analizach programowych oraz w procesie ewaluacji przyjętej metody. Ma on także znaczenie w kontekście oceny końcowej uzyskanych wyników, przy czym istotne są wtedy wartości współczynników wagowych przypisane do funkcji cząstkowych.

Do przeprowadzenia optymalizacji wirnika nośnego zaproponowano algorytm łączący obliczenia analityczne, parametryzację modeli oraz sprzężoną numeryczną analizę dynamiki płynów z uwzględnieniem deformacji strukturalnych modelowej siatki MES. W celu weryfikacji przydatności algorytmu i skuteczności zadanych obliczeń wstępnie przeprowadzono proces optymalizacji pojedynczej łopaty wirnika wojskowego śmigłowca wielozadaniowego o maksymalnej masie startowej 6400 kg. Warunki lotu zostały ustalone na bazie zapisów z pokładowego rejestratora parametrów lotu.

Zgodnie z proponowanym algorytmem proces optymalizacji poprzedzono analizą istniejących konstrukcji. Analiza wykazała, iż dla śmigłowców o podobnej masie i przeznaczeniu uzyskiwane są lepsze własności osiągowe, w szczególności po ocenie takich parametrów jak obciążenie powierzchni nośnej wirnika czy obciążenie zespołu napędowego. W konsekwencji jako cel analiz przyjęto kierunek poprawy ciągu aerodynamicznego generowanego na dysku wirnika. Wykazano, że podwyższenie ciągu umożliwi zwiększenie maksymalnej masy startowej nawet o 200 kg, przy założeniu niezmienności konstrukcji stosowanego dotychczas zespołu napędowego. Podstawowym założeniem operacji było zachowanie kluczowych cech konstrukcyjnych śmigłowca, czyli brak ingerencji w główne zespoły płatowcowe i napędowe. Jedyną dopuszczalną modyfikacją byłaby zmiana przegubów osiowych w celu ewentualnego zamontowania łopat o nowej, lepiej dostosowanej geometrii. Drugim celem optymalizacji była minimalizacja masy łopat przy zachowaniu wytrzymałości odpowiadającej określonym warunkom lotu.

W efekcie przeprowadzonych obliczeń programowych wyznaczono cztery alternatywne rozwiązania obejmujące nowe kształty łopat i wymiary przekrojowe struktury wewnętrznej. Nowe warianty wirnika muszą spełniać wymagania odnośnie możliwości montażowych, jak również gwarantować poprawę ciągu i tym samym podniesienie masy startowej o 200 kg. Jednocześnie w każdym z nowych wariantów masa łopat podlegała minimalizacji, co przyczyniło się do dodatkowego wzrostu wartości udźwigu o 80 lub nawet 120 kg w zależności od wybranego modelu. W ujęciu wskaźnikowym udźwig mógłby zostać zwiększony o 4,3% lub nawet 5,1%.

Wyznaczone warianty obliczeniowe różnią się pod względem promienia i cięciwy, tym samym również pod względem wymiarów struktury wewnętrznej. Dłuższa cięciwa łopaty zwiększa jej masę, ale jednocześnie powoduje zmniejszenie promienia dysku wirnikowego. Krótsze łopaty mogą zostać zastosowane do wyższych prędkości obrotowych. W rozpatrywanym przykładzie nie ma to zastosowania, jednakże taka opcja jest oczywiście możliwa. Dodatkowo mniejsza powierzchnia wirowania powoduje na pewno zmniejszenie skutecznej powierzchni odbicia radarowego. Dłuższe łopaty powodują znaczącą redukcję masy co przekłada się na lepszy rezultat optymalizacji masowej. W każdym z wariantów pozytywny wynik symulacji FSI potwierdza wyliczenia analityczne wytrzymałości konstrukcji, co pozwala na dopuszczenie proponowanych wariantów geometrii do kolejnych etapów projektowania.

Analizy optymalizacyjne wirnika nośnego przeprowadzone z zastosowaniem dostosowanych modeli parametrycznych opisano szczegółowo w cyklu powiązanych tematycznie publikacji. W opublikowanych artykułach udowodniono, że przeprowadzenie wielokryterialnej optymalizacji, przy właściwym stosowaniu nowoczesnych technik komputerowych, pozwala na uzyskanie konstruktywnych wyników, które będą o wiele bardziej użyteczne, niż wyniki pochodzące z oddzielnych analiz jednodziedzinowych. Zastosowanie metod komputerowych umożliwia precyzyjne wyznaczenie wymiarów geometrycznych preferowanej konfiguracji projektowej wirnika. Ograniczenia wynikające ze szczególnych zaleceń ustalanych dla procesu produkcyjnego mogą wymuszać pewne dodatkowe korekty wymiarowe rozwijanych modeli na późniejszym etapie projektowania.

Przedstawiony w dysertacji algorytm aero-strukturalnej optymalizacji jest dopracowanym metodycznie narzędziem programowym dedykowanym do zastosowania w procesie projektowania nowoczesnych wirników śmigłowcowych. Projektowanie wirnika nośnego to proces złożony, który musi uwzględniać wiele czynników strukturalnych czy aerodynamicznych. Efektem zastosowania algorytmu są gotowe modele, które można zaimplementować w kolejnych fazach projektowania. Możliwe jest ich zastosowanie w analizie także innych zespołów konstrukcyjnych np. piasty wirnika nośnego w połączeniu z tarczą sterującą. Bardzo ważnym aspektem są analizy aerosprężyste wirnika, które stanowią oddzielne rozległe zagadnienie. Przygotowany model może być z powodzeniem stosowany do analiz drgań zarówno pojedynczej łopaty jak i całego zespołu wirnikowego.

Niniejsza praca prezentuje nowatorskie rozwiązanie, które jest efektem oryginalnej koncepcji autorskiej oraz wieloletniej pracy indywidualnej w obszarze modelowania i symulacji struktur wiropłatowych. Powiązanie nowoczesnych metod programowania z matematycznym podejściem do procesu optymalizacji poskutkowało wypracowaniem skutecznej i przydatnej metody projektowej. Metoda jakkolwiek sprawdzona tylko na jednym przykładzie wydaje się być użyteczna w kontekście podjęcia zadania projektowego na rzecz opracowania lub rozwinięcia konstrukcji wirnika nośnego dla klasycznego śmigłowca dowolnej wielkości.

9. Pozostała działalność naukowa zrealizowana w ramach studiów w Szkole Doktorskiej WAT

9.1. Wygłoszenie referatów na międzynarodowych lub krajowych konferencjach tematycznych:

[a] *Aero-strukturalna optymalizacja wirnika nośnego śmigłowca z uwzględnieniem ograniczeń masowych i wytrzymałościowych*, Mechanika w Lotnictwie ML-XXI Kazimierz Dolny, 20-23 maja 2024 r.

[b] *Aerostructural UAV main rotor optimisation algorithm considering mass and strength limitations*, The 19th ASCE ASD Biennial International Conference on Engineering, Science, Construction and Operations in Challenging Environment, Miami, USA, 15-18 kwietnia 2024,

[c] *Aerostructural helicopter main rotor optimisation algorithm considering mass and strength limitations*, 1st International Conference on Vehicle Body Engineering, Porto, Portugalia, 2-3 Listopada 2023.

[d] *Helicopter main rotor FSI analysis using parametric blade model as an application for multidisciplinary optimization*, 13th EASN International Conference, Salerno, Włochy 5-8 Września, 2023.

[e] Helicopter main rotor blade structure parametric optimization using graphic programming language Aerospace Europe Conference 2023 Joint 10th EUCASS – 9th CEAS Conference, Lozanna, Szwajcaria, 9-13 Lipca, 2023.

[f] *Analiza CFD wirnika nośnego śmigłowca dla różnych warunków lotu z wykorzystaniem parametrycznego modelu łopaty z przeznaczeniem do zastosowania w wielokryterialnej optymalizacji*, Mechanika w Lotnictwie ML-XX Kazimierz Dolny, 14-17 listopada 2022 r.

[g] *Kierunki optymalizacji konstrukcji w aspekcie nowoczesnych rozwiązań podwyższających własności osiągowe śmigłowców*, Rozwiązania i Technologie XXI, Konferencja online – Fundacja tygiel, 10.06.2022r.

[h] *Analiza obecnie eksploatowanych konstrukcji śmigłowcowych i ich parametrów konstrukcyjnych pod kątem możliwych kierunków rozwoju i optymalizacji elementów nośnych*, WiWAT 2021, Warszawa, 06-07.12.2021.

9.2. Dodatkowe publikacje w czasie realizacji badań:

[a] Kocjan, J.; Kachel, S.; Rogólski, R. Kierunki optymalizacji konstrukcji w aspekcie nowoczesnych rozwiązań podwyższających własności osiągowe śmigłowców, Rozwiązania i Technologie XXI – skutki i perspektywy rozwoju. Wydawnictwo TYGIEL 2022.

[b] Stanisław Kachel, Robert Rogólski, Jakub Kocjan, Analiza obecnie eksploatowanych konstrukcji śmigłowcowych i ich parametrów konstruktyjnych pod kątem możliwych kierunków rozwoju i optymalizacji elementów nośnych, Wiedza i innowacje wiWAT 2021, Poznań 2021.

9.3. Udział w projektach badawczych:

[a] Metody optymalnego projektowania statków powietrznych w zastosowaniu do poprawy ich własności konstrukcyjnych i aerodynamicznych. Uczelniany Grant Badawczy 2024.

[b] Metody optymalnego projektowania statków powietrznych w zastosowaniu do poprawy ich własności konstrukcyjnych i aerodynamicznych. Uczelniany Grant Badawczy 2023.

[c] Analiza numeryczna osiągów samolotu Su-57 pod kątem wyznaczenia danych wejściowych niezbędnych do symulacji lotu. Październik 2023.

[d] Analiza numeryczna osiągów samolotu MIG-31 pod kątem wyznaczenia danych wejściowych niezbędnych do symulacji lotu. Wrzesień 2023.

[e] Określenie parametrów osiągowych systemu BSP WABIK. Sierpień 2023.

[f] Zastosowanie nowoczesnych metod projektowania optymalnego w zastosowaniu do konstrukcji lotniczych, Uczelniany Grant Badawczy 2022.

9.4. Praktyka zawodowa:

[g] Prowadzenie ćwiczeń laboratoryjnych w języku angielski „Basics of graphics engineering"

[h] Prowadzenie ćwiczeń z przedmiotu „Mechanika Techniczne"

[i] Prowadzenie zajęć laboratoryjnych z przedmiotu „Laboratorium wytrzymałości i nauki o materiałach"

9.5. Kursy, szkolenia zrealizowane w ramach pracy badawczej:

- Szkolenie SIEMENS SIMCENTER STAR CCM+. EC Test Systems. Warszawa 20.02.2023
- Szkolenie Ansys FLUENT – Maszyny wirnikowe oraz metody FSI – maj 2022.
- Szkolenie Abaqus . Politechnika Lubelska. 7-9.01.2022.
- Standard FLIGHTLAB Training. Advanced Rotorcraft Technology. 21-23.09.2021.

10.Bibliografia

[1]–[182]

[1] Y. M. Ignatkin, P. V. Makeev, A. I. Shomov, V. A. Ivchin, *Numerical Study Of The Main Rotor Wake Structures And Induced Velocity Fields At The Tail Rotor Location When Flying Near The Ground*, International Review Of Aerospace Engineering, 14, 4, 2021, S.181–191,

[2] S. Stouti, A. T. Lahlou, I. Lagrat, O. Bouazaoui, H. Mounir, *Prediction Of The Pitch Angle Value For The Bell's 212 Helicopter Main Rotor In A Hover State Configuration Using A Cfd Approach Title*, International Review Of Aerospace Engineering, 17, 5, 2024.

[3] S. Stouti, A. T. Lahlou, I. Lagrat, O. Bouazaoui, H. Mounir, *Impact Of Blade Trailing Edge Devices On Helicopter Rotor Aerodynamics During Hovering Flight*, International Review Of Aerospace Engineering, 17, 2, 2024, S.39–49,

[4] S. Stouti, A. T. Lahlou, I. Lagrat, O. Bouazaoui, H. Mounir, *Exploration And Analysis Of Rotor System Designs With Varying Diameters In The Context Of Helicopter Technology*, International Review On Modelling And Simulations, 17, 2, 2024, S.97–107,

[5] M. Ostwald, *Podstawy Optymalizacji Konstrukcji W Projektowaniu Systemowym*. Poznań, 2016.

[6] A. M. Morris, C. B. Allen, T. C. S. Rendall, *Aerodynamic Optimisation Of Hovering Helicopter Rotors Using Efficient And Flexible Shape Parameterisation*, 2008.

[7] C. B. Allen, A. M. Morris, T. C. S. Rendall, *Cfd-Based Aerodynamic Shape Optimization Of Hovering Rotors*, 2009.

[8] H. Wang, B. Zhang, H. Wang, D. Li, *The Research On Helicopter Rotor Aeroelastic Dynamics Multi-Objective Optimization Solution*, Yingyong Lixue Xuebao/Chinese Journal Of Applied Mechanics, 30, 2, 2013,

[9] R. Ganguli, I. Chopra, *Aeroelastic Optimization Of A Helicopter Rotor To Reduce Vibration And Dynamic Stresses*, Journal Of Aircraft, 33, 4, 1996,

[10] D. Cornette, B. Kerdreux, G. Michon, Y. Gourinat, *Aeroelastic Tailoring Of Helicopter Blades*, Journal Of Computational And Nonlinear Dynamics, 10, 6, 2015,

[11] F. K. Straub, C. B. Callahan, J. D. Culp, *Rotor Design Optimization Using A Multidisciplinary Approach*, Structural Optimization, 5, 1–2, 1992,

[12] S. Kizhakke Kodakkattu, P. Nair, J. M.L, *Design Optimization Of Helicopter Rotor Using Kriging*, Aircraft Engineering And Aerospace Technology, 90, 6, 2018,

[13] X. Liu, B. Zhang, *Study On Aeroelastic Optimal Design Of Composite Blades*, Yingyong Lixue Xuebao/Chinese Journal Of Applied Mechanics, 38, 4, 2021,

[14] F. Tarzanin, D. K. Young, B. Panda, *Advanced Aeroelastic Optimization Applied To An Improved Performance, Low Vibration Rotor*, Annual Forum Proceedings - American Helicopter Society, 1, 1999.

[15] P. P. Friedmann, P. Shanthakumaran, *Optimum Design Of Rotor Blades For Vibration Reduction In Forward Flight.*, Journal Of The American Helicopter Society, 29, 4, 1984,

[16] R. Ganguli, I. Chopra, *Aeroelastic Optimization Of A Helicopter Rotor With Two-Cell Composite Blades*, Aiaa Journal, 34, 4, 1996,

[17] P. P. Friedmann, *Helicopter Vibration Reduction Using Structural Optimization With Aeroelastic/Multidisciplinary Constraints - A Survey*, Journal Of Aircraft, 28, 1, 1991,

[18] R. Ganguli, I. Chopra, *Aeroelastic Optimization Of A Helicopter Rotor With Composite Coupling*, Journal Of Aircraft, 32, 6, 1995,

[19] X. D. Deng, L. Gao, J. H. Deng, *Rotor Blade Tip Shape Optimization For Vibration Reduction Based On Surrogate Model*, Zhendong Gongcheng Xuebao/Journal Of Vibration Engineering, 34, 1, 2021,

[20] J. X. Guo, J. W. Xiang, *Composite Rotor Blade Design Optimization For Vibration Reduction With Aeroelastic Constraints*, Chinese Journal Of Aeronautics, 17, 3, 2004,

[21] C. Johnson, M. Woodgate, G. N. Barakos, *Optimising Aspects Of Berp-Like Rotors Using Frequency-Domain Methods*, In *Notes On Numerical Fluid Mechanics And Multidisciplinary Design*, 2016, 133.

[22] H. Ali, S. Sridhar, N. K. Maiti, M. Vijaya Kumar, *Reduction Of Structural Vibrations On Light Combat Helicopter*, In *Annual Forum Proceedings - Ahs International*, 2015, 2, January.

[23] M. Sinem, K. A. Y. A. Metin Orhan, *Optimization Of Vibration Reduction In A Helicopter Blade With 2 Way Fluid-Structure Interaction*, In *Asme 2018 Conference On Smart Materials, Adaptive Structures And Intelligent Systems, Smasis 2018*, 2018, 1.

[24] C. Rotaru, I. Cîrciu, D. Luculescu, *Lift Capability Prediction For Helicopter Rotor Blade-Numerical Evaluation*, In *Aip Conference Proceedings*, 2016, 1738.

[25] S. Moffatt, N. Griffiths, *Structural Optimisation And Aeroelastic Tailoring Of The Berp Iv Demonstrator Blade*, In *Annual Forum Proceedings - Ahs International*, 2009, 1.

[26] M. Borri, G. L. Ghiringhelli, T. Merlini, *Linear Analysis Of Naturally Curved And Twisted Anisotropic Beams*, Composites Engineering, 2, 5–7, 1992,

[27] H. A. Taymaz, *Helicopter Rotor Blade Vibration Reduction With Optimizing The Structural Distribution Of Composite Layers*, Journal Of Measurements In Engineering, 10, 1, 2022,

[28] R. Ganguli, *Optimum Design Of A Helicopter Rotor For Low Vibration Using Aeroelastic Analysis And Response Surface Methods*, Journal Of Sound And Vibration, 258, 2, 2002,

[29] A. Chattopadhyay, T. R. Mccarthy, N. Pagaldipti, *Multilevel Decomposition Procedure For Efficient Design Optimization Of Helicopter Rotor Blades*, Aiaa Journal, 33, 2, 1995,

[30] R. Celi, *Recent Applications Of Design Optimization To Rotorcraft - A Survey*, Journal Of Aircraft, 36, 1, 1999,

[31] S. Tian *Et Al.*, *Structural Design Optimization Of Composite Rotor Blades With Strength Considerations*, Aiaa Science And Technology Forum And Exposition, 2022,

[32] D. Barwey, D. A. Peters, *Optimization Of Composite Rotor Blades With Advanced Structural And Aerodynamic Modeling*, Mathematical And Computer Modelling, 19, 3–4, 1994,

[33] C. J. He, D. A. Peters, *Optimization Of Rotor Blades For Combined Structural, Dynamic, And Aerodynamic Properties*, Structural Optimization, 5, 1–2, 1992,

[34] N. A. Vu, J. W. Lee, T. P. N. Le, S. T. T. Nguyen, *A Fully Automated Framework For Helicopter Rotor Blades Design And Analysis Including Aerodynamics, Structure, And Manufacturing*, Chinese Journal Of Aeronautics, 29, 6, 2016,

[35] E. J. Saltzman, J. W. Hicks, *In-Flight Lift-Drag Characteristics For A Forward-Swept Wing Aircraft (And Comparisions With Contemporary Aircraft)*, 1994.

[36] D. Lee, Y. Hong, J. Park, K. Yee, *Design Optimization Of Coaxial Rotor Blades For Small Uav Through Physics-Based Free-Wake Adjustment*, Journal Of Computational Fluids Engineering, 27, 4, 2022,

[37] H. M. Lee, J. K. Ryu, S. J. Ahn, O. J. Kwon, *Aerodynamic Design Optimization Of Uav Rotor Blades Using A Genetic Algorithm And Artificial Neural Networks*, Journal Of Computational Fluids Engineering, 19, 3, 2014,

[38] W. Wei, R. Wang, B. Xu, K. Fan, Z. Zhao, B. Zou, *Multi-Objective Optimization Of Rotor Blade Aerodynamic Performance Of Aerial-Ground Platform*, Beijing Ligong Daxue Xuebao/Transaction Of Beijing Institute Of Technology, 42, 8, 2022,

[39] W. A. Klimczyk, *Aerodynamic Design And Optimization Of Propellers For Multirotor*, Aircraft Engineering And Aerospace Technology, 94, 1, 2022,

[40] M. K. Herniczek, D. Jee, B. Sanders, D. Feszty, *Rotor Blade Optimization And Flight Testing Of A Small Uav Rotorcraft*, Journal Of Unmanned Vehicle Systems, 7, 4, 2019,

[41] M. F. Afthon, M. A. Moelyadi, *A Study In Aerodynamic Optimization Of Uav Helicopter Rotor- Blades Planform In Vertical Motion*, Avia, 2, 1, 2021,

[42] M. C. Hsu, Y. Bazilevs, *Fluid-Structure Interaction Modeling Of Wind Turbines: Simulating The Full Machine*, Computational Mechanics, 50, 6, 2012,

[43] C. Grinderslev, S. González Horcas, N. N. Sørensen, *Fluid–Structure Interaction Simulations Of A Wind Turbine Rotor In Complex Flows, Validated Through Field Experiments*, Wind Energy, 24, 12, 2021,

[44] S. W. James *Et Al.*, *Fibre-Optic Measurement Of Strain And Shape On A Helicopter Rotor Blade During A Ground Run: 1. Measurement Of Strain*, Smart Materials And Structures, 31, 7, 2022,

[45] D. Zhangaskanov, S. Batay, B. Kamalov, Y. Zhao, X. Su, E. Kweeng, *High-Fidelity 2-Way Fsi Simulation Of A Wind Turbine Using Fully Structured Multiblock Meshes In Openfoam For Accurate Aero-Elastic Analysis*, Fluids, 7, 5, 2022,

[46] S. Oh, S. H. Kim, *Next Generation Rotorcraft Technologies In Usa And Europe*, Journal Of The Korean Society For Aeronautical & Space Sciences, 42, 8, 2014,

[47] P. De Guillenchmidt, *Calculation Of The Bending Stresses In Helicopter Rotor Blades*, Washington, 1951.

[48] Wilde E., Price H.L, *A Theoretical Method For Calculating Flexure And Stresses In Helicopter Rotor Blades*, Aircraft Engineering, 1965, S.45–54.

[49] P. K. Nguyen, T. K. D. Hoang, *Strength Analysis Of Main Rotor Blades Of Helicopter Uav*, In *International Conference On Engineering Tribology And Applied Technology*, 2021, 111.

[50] B. Plaza, R. Bardera, S. Visiedo, *Comparison Of Bem And Cfd Results For Mexico Rotor Aerodynamics*, Journal Of Wind Engineering And Industrial Aerodynamics, 145, 2015,

[51] Ö. Öğüçlü, *Structural Design And Stress Analysis Of A Helical Vertical Axis Wind Turbine Blade*, Sakarya University Journal Of Science, 2020,

[52] R. Kliza, K. Ścisłowski, K. Siadkowska, J. Padyjasek, M. Wendeker, *Strength Analysis Of A Prototype Composite Helicopter Rotor Blade Spar*, Applied Computer Science, 18, 1, 2022,

[53] D. Goerke, A. L. Le Denmat, T. Schmidt, F. Kocian, E. Nicke, *Aerodynamic And Mechanical Optimization Of Cf/Peek Blades Of A Counter Rotating Fan*, In *Proceedings Of The Asme Turbo Expo*, 2012, 7, Parts A And B.

[54] G. Wilke, *Quieter And Greener Rotorcraft: Concurrent Aerodynamic And Acoustic Optimization*, Ceas Aeronautical Journal, 12, 3, 2021,

[55] R. Jain, *Computational Fluid Dynamics Transition Models Validation For Rotors In Unsteady Flow Conditions*, Journal Of Aircraft, 59, 4, 2022,

[56] S. A. Shah, D. G. Thomson, *Rotorcraft's Multiblade Modelling For An Autogyro*, Science International (Lahore), 29, 5, 2017.

[57] G. N. Barakos, A. J. Garcia, *Cfd Analysis Of Hover Performance Of Rotors At Full- And Model-Scale Conditions*, Aeronautical Journal, 120, 1231, 2016,

[58] G. N. Barakos, T. Fitzgibbon, A. N. Kusyumov, S. A. Kusyumov, S. A. Mikhailov, *Cfd Simulation Of Helicopter Rotor Flow Based On Unsteady Actuator Disk Model*, Chinese Journal Of Aeronautics, 33, 9, 2020,

[59] A. Tremolet, P. M. Basset, *Some Meta-Modeling And Optimization Techniques For Helicopter Pre-Sizing*, In *38th European Rotorcraft Forum 2012, Erf 2012*, 2012, 2.

[60] K. Pahlke, B. Demaret, *Onera And Dlr Contributions To Improve Environmental Friendliness Of Rotorcraft*, Annual Forum Proceedings - Ahs International, 2017.

[61] N. Spyropoulos, G. Papadakis, J. M. Prospathopoulos, V. A. Riziotis, *Investigating The Level Of Fidelity Of An Actuator Line Model In Predicting Loads And Deflections Of Rotating Blades Under Uniform Free-Stream Flow*, Applied Sciences (Switzerland), 11, 24, 2021,

[62] Y. Lei, Y. Huang, H. Wang, *Aerodynamic Performance Of An Octorotor Suav With Different Rotor Spacing In Hover*, Processes, 8, 11, 2020,

[63] A. Samad, G. B. S. Tagawa, F. Morency, C. Volat, *Predicting Rotor Heat Transfer Using The Viscous Blade Element Momentum Theory And Unsteady Vortex Lattice Method*, Aerospace, 7, 7, 2020,

[64] P. Pölzlbauer, A. Kümmel, D. Desvigne, C. Breitsamter, *Numerical Investigation Of An Optimized Rotor Head Fairing For The Racer Compound Helicopter In Cruise Flight*, Aerospace, 8, 3, 2021,

[65] O. Okumuş, M. Şenipek, A. Ezertaş, *Multi-Objective Multi-Fidelity Aerodynamic Optimization Of Helicopter Rotor*, Aiaa Science And Technology Forum And Exposition, 2022,

[66] P. A.S.F. Silva, P. Tsoutsanis, A. F. Antoniadis, *Numerical Investigation Of Full Helicopter With And Without The Ground Effect*, Aerospace Science And Technology, 122, 2022,

[67] S. Oh, D. Park, H. M. Ji, *Development Of Preliminary Conceptual Design/Comprehensive Analysis Programs For Next Generation Rotorcraft*, Journal Of The Korean Society For Aeronautical & Space Sciences, 49, 1, 2021,

[68] J. R. Majhi, R. Ganguli, *Modeling Helicopter Rotor Blade Flapping Motion Considering Nonlinear Aerodynamics*, 2008.

[69] A. Kafkas, S. Kilimtzidis, A. Kotzakolios, V. Kostopoulos, G. Lampeas, *Multi-Fidelity Optimization Of A Composite Airliner Wing Subject To Structural And Aeroelastic Constraints*, Aerospace, 8, 12, 2021,

[70] P. Mohammad Zadeh, A. Mehmani, A. Messac, *High Fidelity Multidisciplinary Design Optimization Of A Wing Using The Interaction Of Low And High Fidelity Models*, Optimization And Engineering, 17, 3, 2016,

[71] G. Droandi, G. Gibertini, *Aerodynamic Blade Design With Multi-Objective Optimization For A Tiltrotor Aircraft*, Aircraft Engineering And Aerospace Technology, 87, 1, 2015,

[72] P. E. Bath, A. L. Gaitonde, D. P. Jones, *Reduced Order Aerodynamics And Flight Mechanics Coupling For Tiltrotor Aircraft Stability Analysis*, 2022.

[73] A. Zanotti, A. Savino, M. Palazzi, M. Tugnoli, V. Muscarello, *Assessment Of A Mid-Fidelity Numerical Approach For The Investigation Of Tiltrotor Aerodynamics*, Applied Sciences (Switzerland), 11, 8, 2021,

[74] A. Jimenez-Garcia, M. Biava, G. N. Barakos, K. D. Baverstock, S. Gates, P. Mullen, *Tiltrotor Cfd Part Ii - Aerodynamic Optimisation Of Tiltrotor Blades*, Aeronautical Journal, 121, 1239, 2017,

[75] G. Zhao, Q. Zhao, P. Li, B. Wang, *Parametric Analyses For Effects Of Rpm And Diameter On Tiltrotor Aerodynamic Performances In Hovering And Cruise Mode*, International Journal Of Aeronautical And Space Sciences, 22, 3, 2021,

[76] Z. Wu, C. Li, Y. Cao, *Numerical Simulation Of Rotor-Wing Transient Interaction For A Tiltrotor In The Transition Mode*, Mathematics, 7, 2, 2019,

[77] W. Stalewski, *Design And Optimisation Of Main Rotor Or Ultralight Helicopter*, Journal Of Kones Powertrain And Transport, 24, 4, 2017.

[78] K. Ferguson, D. Thomson, *Performance Comparison Between A Conventional Helicopter And Compound Helicopter Configurations*, Proceedings Of The Institution Of Mechanical Engineers, Part G: Journal Of Aerospace Engineering, 229, 13, 2015,

[79] E. W. Aiken, R. A. Ormiston, L. A. Young, *Future Directions In Rotorcraft Technology At Ames Research Center*, 2000.

[80] E. Ahci-Ezgi, U. Denecke, S. Emmerling, G. Kuntze-Fechner, P. Rauch, *Evolution Of Fenestron^{tm} Development In Terms Of Safety, Design And Substantiation Characteristics*, In *Annual Forum Proceedings - Ahs International*, 2015, 4, January.

[81] M. Imiela, *Investigation Of Aeroelastic Effects For A Helicopter Main Rotor In Hover*, 2010.

[82] K. Robinson, A. Brocklehurst, *Berp Iv Aerodynamics, Performance And Flight Envelope*, In *34th European Rotorcraft Forum 2008, Erf34*, 2008, 1.

[83] U. Saetti, J. F. Horn, K. S. Brentner, W. Villafana, D. Wachspress, *Rotorcraft Simulations With Coupled Flight Dynamics, Free Wake, And Acoustics*, In *Annual Forum Proceedings - Ahs International*, 2016, 3.

[84] D. P. Schrage, *The Search For An Ideal Bearingless Main Rotor (Bmr) Design*, 2021.

[85] M. Ilie, *A Fully-Coupled Cfd/Csd Computational Approach For Aeroelastic Studies Of Helicopter Blade-Vortex Interaction*, Applied Mathematics And Computation, 347, 2019,

[86] Y. Zhao, Y. Shi, G. Xu, *Helicopter Blade-Vortex Interaction Airload And Noise Prediction Using Coupling Cfd/Vwm Method*, Applied Sciences (Switzerland), 7, 4, 2017,

[87] D. Alfano, P. Cranga, V. Gareton, F. Guntzer, J. F. Hirsch, *The Blue Edge^{tm} Blade Continuation*, 2019.

[88] R. Harrison, S. Stacey, B. Hansford, *Berp Iv The Design, Development And Testing Of An Advanced Rotor Blade*, In *Annual Forum Proceedings - Ahs International*, 2008, 2.

[89] B. Rasuo, *Damage Tolerance And Survivability Of Composite Aircraftstructures*, In *Structural Integrity And Durability Of Advanced Composites: Innovative Modelling Methods And Intelligent Design*, 2015.

[90] B. Rasuo, *An Experimental Methodology For Evaluating Survivability Of An Aeronautical Construction From Composite Materials: An Overview*, *International Journal Of Crashworthiness*, 12, 1. 2007.

[91] L. Li, V. V. Volovoi, D. H. Hodges, *Cross-Sectional Design Of Composite Rotor Blades*, Journal Of The American Helicopter Society, 53, 3, 2008,

[92] *Design Of Composite Gyrocopter Main Rotor Blade Involving Rib And Spar Elements*, Journal Of Engineering, Project, And Production Management, 2019,

[93] B. Rasuo, *Helicopter Tail Rotor Blade From Composite Materials: An Experience*, Sae International Journal Of Aerospace, 4, 2, 2011,

[94] F. L. M. Dos Santos, B. Peeters, H. Van Der Auweraer, L. C. S. Góes, W. Desmet, *Vibration-Based Damage Detection For A Composite Helicopter Main Rotor Blade*, Case Studies In Mechanical Systems And Signal Processing, 3, 2016,

[95] J. H. Jang, S. H. Ahn, *Numerical Analysis Of Bird Strike Resistance Of Helicopter Composite Rotor Blade*, Arpn Journal Of Engineering And Applied Sciences, 14, 19, 2019,

[96] D. Kumar, C. E. S. Cesnik, *New Strategy For Designing Composite Rotor Blades With Active Flaps*, Journal Of Intelligent Material Systems And Structures, 27, 9, 2016,

[97] Y. S. Kang, S. W. Park, J. S. Roh, R. S. Myong, *Computational Investigation Of Effects Of Expanded Metal Foils On The Lightning Protection Performance Of A Composite Rotor Blade*, International Journal Of Aeronautical And Space Sciences, 22, 1, 2021,

[98] T. A. Fitzgibbon, G. N. Barakos, M. A. Woodgate, A. Jimenez-Garcia, *Numerical Simulation Of Different Rotor Designs In Hover And Forward Flight*, In *44th European Rotorcraft Forum 2018, Erf 2018*, 2018, 1.

[99] M. T. Scott, D. Sigl, R. C. Strawn, *Computational And Experimental Evaluation Of Helicopter Rotor Tips For High-Speed Flight*, Journal Of Aircraft, 28, 6, 1991,

[100] T. S. Kalra, V. K. Lakshminarayan, J. D. Baeder, *Effect Of Tip Geometry On A Hovering Rotor In Ground Effect: A Computational Study*, 2013.

[101] C. S. Johnson, M. Woodgate, G. N. Barakos, *Helicopter Berp Tip: Literature Review Of Helicopter Blade Shape Optimisation Methods*, In *Advanced Uav Aerodynamics, Flight Stability And Control: Novel Concepts, Theory And Applications*, 2016, S.309–343.

[102] R. Widjaja, J. W. Lim, R. Jain, M. Potsdam, *Investigation Of Berp-Shape Tip Design On An Apache Rotor Blade*, 2020.

[103] X. Wu, *Current Status, Development Trend And Countermeasure For High-Speed Rotorcraft*, Nanjing Hangkong Hangtian Daxue Xuebao/Journal Of Nanjing University Of Aeronautics And Astronautics, 47, 2, 2015,

[104] T. Berger, M. B. Tischler, J. F. Horn, *High-Speed Rotorcraft Pitch Axis Response Type Investigation*, 2021.

[105] X. Yan, B. Lou, A. Xie, L. Chen, D. Zhang, *A Review Of Advanced High-Speed Rotorcraft*, Iop Conference Series: Materials Science And Engineering, 1102, 1, 2021, S.012006,

[106] Y. Tanabe *Et Al.*, *A Conceptual Study Of High Speed Rotorcraft*, In *40th European Rotorcraft Forum 2014*, 2014, 2.

[107] X. Yan, B. Lou, A. Xie, L. Chen, D. Zhang, *A Review Of Advanced High-Speed Rotorcraft*, Iop Conference Series: Materials Science And Engineering, 1102, 1, 2021,

[108] J. Thiemeier, C. Öhrle, F. Frey, M. Keßler, E. Krämer, *Aerodynamics And Flight Mechanics Analysis Of Airbus Helicopters' Compound Helicopter Racer In Hover Under Crosswind Conditions*, Ceas Aeronautical Journal, 11, 1, 2020,

[109] J. Serafini, M. Cremaschini, G. Bernardini, L. Solero, C. Ficuciello, M. Gennaretti, *Conceptual All-Electric Retrofit Of Helicopters: Review, Technological Outlook, And A Sample Design*, Ieee Transactions On Transportation Electrification, 5, 3, 2019,

[110] K. Van Truong, *Modeling Aerodynamics, Including Dynamic Stall, For Comprehensive Analysis Of Helicopter Rotors*, Aerospace, 4, 2, 2017,

[111] S. Slavik, J. Klesa, J. Brabec, *Propeller Selection By Means Of Pareto-Optimal Sets Applied To Flight Performance*, Aerospace, 7, 3, 2020,

[112] P. Weiand, A. Krenik, *A Multi-Disciplinary Toolbox For Rotorcraft Design*, Aeronautical Journal, 122, 1250, 2018,

[113] W. Stalewski, W. Zalewski, *Aerodynamic Design And Optimisation Of Main Rotors For Light Rotorcrafts*, In *45th European Rotorcraft Forum 2019, Erf 2019*, 2019, 1.

[114] C. Królak, Z. Czyz, K. Siadkowska, R. Kliza, *Cfd Investigation Of The Main Rotor For An Unmanned Helicopter*, In *Journal Of Physics: Conference Series*, 2021, 1736, 1.

[115] L. S. Shabliy, I. B. Dmitrieva, *Conversion Of The Blade Geometrical Data From Points Cloud To The Parametric Format For Optimization Problems*, Arpn Journal Of Engineering And Applied Sciences, 9, 10, 2014.

[116] C. Grabowik, K. Kalinowski, W. Kempa, I. Paprocka, *A Method Of Computer Aided Design With Self-Generative Models In Nx Siemens Environment*, In *Iop Conference Series: Materials Science And Engineering*, 2015, 95, 1.

[117] A. I. Ryazanov, *Automated 3d Modeling Of Working Turbine Blades*, Russian Engineering Research, 36, 9, 2016,

[118] Z. Chen *Et Al.*, *High-Order Redesign Method For Wind Turbine Blade Optimization In Model Test Considering Aerodynamic Similarity*, Ocean Engineering, 202, 2020,

[119] S. Kachel, *Metoda Wielokryterialnego Projektowania Bryły Samolotu Z Uwzględnieniem Misji*. Warsaw, 2011.

[120] W. Stalewski, *Projektowanie I Optymalizacja Aerodynamiczna Wiropłatów*. Warsaw, 2017.

[121] S. Sagimbayev, Y. Kylyshbek, S. Batay, Y. Zhao, S. Fok, T. S. Lee, *3d Multidisciplinary Automated Design Optimization Toolbox For Wind Turbine Blades*, Processes, 9, 4, 2021,

[122] A. Г. Гребеников *Et Al.*, *Analysis Of Design And Technological Features Of The Main Rotor Blades Of Heavy Transport Helicopters*, Open Information And Computer Integrated Technologies, 93, 2021,

[123] L. Ma, Q. Zhao, K. Zhang, X. Zhang, M. Zhao, *Aeroelastic Analysis And Structural Parametric Design Of Composite Rotor Blade*, Chinese Journal Of Aeronautics, 34, 1, 2021,

[124] W. Stalewski, W. Zalewski, *Performance Improvement Of Helicopter Rotors Through Blade Redesigning*, Aircraft Engineering And Aerospace Technology, 91, 5, 2019, S.747–755,

[125] T. A. Fitzgibbon, M. A. Woodgate, G. N. Barakos, *Practical Considerations In Rotor Design Optimisation Studies*, 2021.

[126] G. Wilke, J. Bailly, K. Kimura, Y. Tanabe, *Jaxa-Onera-Dlr Cooperation: Results From Rotor Optimization In Hover*, 47th European Rotorcraft Forum - Conference Proceeding, 2021, S.55–62.

[127] T. Zhang, G. N. Barakos, *Aerodynamic Simulation And Adjoint-Based Optimisation Of Rotorcraft Configurations*.

[128] M. Imiela, *High-Fidelity Optimization Framework For Helicopter Rotors*, In *Aerospace Science And Technology*, Dec. 2012, 23, 1, S.2–16.

[129] J. Bailly, D. Bailly, B. Didier, *Multifidelity Aerodynamic Optimization Of A Helicopter Rotor Blade*, Aiaa Journal, 2019, S.1–13,

[130] E. Tixadou, *Optimisation Of The Structure Of A Helicopter Blade In View Of Reducing Cabin Vibration*, 2021.

[131] A. D'andrea, F. Scorcelletti, *Enhanced Numerical Simulations Of Helicopter Landing Maneuvers In Brownout Conditions*, In *Annual Forum Proceedings - Ahs International*, 2010, 2.

[132] R. W. Du Val, C. He, *Validation Of The Flightlab Virtual Engineering Toolset*, Aeronautical Journal, 122, 1250, 2018, S.519–555,

[133] F. Mastroddi, S. Gemma, *Analysis Of Pareto Frontiers For Multidisciplinary Design Optimization Of Aircraft*, Aerospace Science And Technology, 28, 1, 2013, S.40–55,

[134] H. Chengjian, C. S. Lee, W. Chen, *Rotorcraft Simulation Model Enhancement To Support Design, Testing And Operational Analysis*, Journal Of The American Helicopter Society, 45, 4, 2000, S.284–292,

[135] K. K. T. Thanapalan, *Modelling Of A Helicopter System*, 1st Virtual Control Conference, 2010.

[136] H. Saberi, M. Hasbun, J. Y. Hong, H. Yeo, R. A. Ormiston, *Overview Of Rcas Capabilities, Validations, And Rotorcraft Applications*, In *Annual Forum Proceedings - Ahs International*, 2015, 2, January.

[137] J. W. Lim, *Consideration Of Structural Constraints In Passive Rotor Blade Design For Improved Performance*, Aeronautical Journal, 120, 1232, 2016,

[138] J. W. Lim, *Application Of Parametric Airfoil Design For Rotor Performance Improvement*, In *44th European Rotorcraft Forum 2018, Erf 2018*, 2018, 1.

[139] K. Van Truong, *Modeling Aerodynamics, Including Dynamic Stall, For Comprehensive Analysis Of Helicopter Rotors*, Aerospace, 4, 2, 2017,

[140] L. D. Allen, J. W. Lim, R. B. Haehnel, I. D. Dettwiller, *Rotor Blade Design Framework For Airfoil Shape Optimization With Performance Considerations*, 2021.

[141] T. Aoyama, J. Kawachi, S. Saito, *Effect Of Blade-Tip Planform On Shock Wave Of Advancing Helicopter Blade*, Journal Of Aircraft, 32, 5, 1995,

[142] C. Chen, H. Cheng, P. Sun, C. Zhou, *An Aerodynamic Calculation Model For Anti-Torque System Of Notar*, Mechanika, 24, 2, 2018,

[143] Congressional Budget Office, *Modernizing The Army's Rotary Wing Fleet*, November, 2007, S.39.

[144] S. Robert, *Modeling Attack Helicopter Operations In Theater Level Simulations*, 1996.

[145] E. Ference, *Cace Study Of The Development Of The Apache Attack Helicopter (Ah-64)*, Security, September, 2002, S.1–183, [Online]. Available: Http://Handle.Dtic.Mil/100.2/Ada417536

[146] H. Yeo, W. G. Bousman, W. Johnson, *Performance Analysis Of A Utility Helicopter With Standard And Advanced Rotors*, Journal Of The American Helicopter Society, 49, 3, 2004, S.250–270,

[147] M. G. Rozhdestvensky, A. P. Vaintrub, V. A. Ivchin, *Mi-28n Helicopter - Most Essential Design Features Providing Its Flight Performance*, In *Annual Forum Proceedings - American Helicopter Society*, 1998, 2, S.1275–1284.

[148] W. Stepniewski, *Rotary-Wing Aerodynamics - Volume I Basic Theories Of Rotor Aerodynamics*, I, 1979.

[149] R. Przysowa, B. Gawron, A. Kułaszka, K. P. Hetman, *Polish Experience From The Operation Of Helicopters Under Harsh Conditions Polskie Doświadczenia Z Eksploatacji Śmigłowców W Trudnych Warunkach*, 48, 2018, S.263–299,

[150] A. Ünlü, M. F. Can, G. Yagci, I. Ozerhan, J. A. Asensio, P. Petrone, *Tactical Evacuation Of Casualties By Military Helicopters : Present And Future Aspects*, 2, August, 2013, S.83–88.

[151] D. Novak, T. Bucak, *Helicopter Main Rotor Conceptual Design - Application To A Westland Lynx Helicopter*, 50, 3, 2008, S.169–173.

[152] A. Oldersma, M. J. Bos, F. L. Management, C. Voice, F. Data, *Airframe Loads & Usage Monitoring Of The Ch-47d " Chinook " Helicopter Of The Royal Netherlands Air Force*, 2011, June, S.1–3.

[153] A. Engleder, J. Markmiller, R. Mueller, *The Evolution Of Airbus Helicopters Crashworthy Composite Airframes For Transport Helicopters*, 2015.

[154] C. N. Keys, *Rotary-Wing Aerodynamics - Volume Ii - Performance Prediction Of Helicopters*. 1979.

[155] P. Coleman, *A Survey Of Theoretical And Experimental Coaxial Rotor*, 1997.

[156] M. H. Bae, D. J. Lee, *A Study On Helicopter Maneuver Warfare In Future Battle Field*, 2016.

[157] Eda, *Acceptable Means Of Compliance And Guidance Material For The Certification Of Military Aircraft And Related Products, Parts And Appliances, And Design And Production Organisations Emar 21 Amc & Gm Acceptable*, October, 2016.

[158] J. Xie, Z. Xie, M. Zhou, J. Qiu, *Multidisciplinary Aerodynamic Design Of A Rotor Blade For An Optimum Rotor Speed Helicopter*, Applied Sciences (Switzerland), 7, 6, 2017,

[159] H. Yeo, *Design And Aeromechanics Investigation Of Compound Helicopters*, Aerospace Science And Technology, 88, 2019, S.158–173,

[160] M. Ramasamy, *Measurements Comparing Hover Performance Of Single, Coaxial, Tandem, And Tilt-Rotor Configurations*, Annual Forum Proceedings - Ahs International, 4, 2013, S.2439–2461.

[161] J. Deng, F. Fan, P. Liu, S. Huang, Y. Lin, *Aerodynamic Characteristics Of Rigid Coaxial Rotor By Wind Tunnel Test And Numerical Calculation*, Chinese Journal Of Aeronautics, 32, 3, 2019, S.568–576,

[162] A. Azlan, S. B. Ibrahim, *Power Estimation For Four Seater Helicopter*, 1, 27, 2008, S.78–90.

[163] D. Jordan, J. D. Kiras, D. J. Lonsdale, I. Speller, C. Tuck, C. D. Walton, *Understanding Modern Warfare*, Understanding Modern Warfare, 56, 2001, 2016,

[164] Eda, *Certification Of Military Aircraft And Related Products, Parts And Appliances, And Design And Production Organisations, Emar 21*, June. 2012, S.1–64.

[165] T. Berger, T. Berger, *Handling Qualities Requirements And Control Design For High-Speed Rotorcraft The Pennsylvania State University The Graduate School College Of Engineering Handling Qualities Requirements And Control Design For High-Speed Rotorcraft A Dissertation In © 2019*, December 2019, 2020.

[166] J. Seddon, S. Newman, *Basic Helicopter Aerodynamics*, *Basic Helicopter Aerodynamics*. 2011.

[167] T. Unmack, T. Unmack, *Helicopter Operations*, In *Civil Aviation: Standards And Liabilities*, 2020, S.521–539.

[168] G. Padfield, *Helicopter Flight Dynamics, Second Edition*. 2007.

[169] Easa, *Certification Specifications And Acceptable Means Of Compliance For Large Rotorcraft Cs-29*, July. 2019. [Online]. Available: Https://Www.Easa.Europa.Eu/Certification-Specifications/Cs-29-Large-Rotorcraft

[170] Easa, *Certification Specifications And Acceptable Means Of Compliance For Small Rotorcraft Cs-27*, June, 2020, [Online]. Available: Https://Www.Easa.Europa.Eu/Certification-Specifications/Cs-27-Small-Rotorcraft

[171] A. R. S. Bramwell, G. Done, B. David, *Bramwell ' S Helicopter Dynamic*, 2001.

[172] A. Brocklehurst, G. N. Barakos, *A Review Of Helicopter Rotor Blade Tip Shapes*, Progress In Aerospace Sciences, 56, 2013, S.35–74,

[173] K. Szumański, *Teoria I Badania Śmigłowców W Ujęciu Symulacyjnym*. Warszawa, 1997.

[174] N. A. Vu, J. W. Lee, *Aerodynamic Design Optimization Of Helicopter Rotor Blades Including Airfoil Shape For Forward Flight*, Aerospace Science And Technology, 42, 2015, S.106–117,

[175] A. Tamer, A. Yücekayali, Y. Ortakaya, *Design And Optimization Of Helicopter Rotor For Minimum Power Required*, 6th Aiac Ankara International Aeropsace Conference, September 14-16, 2011.

[176] J. Stanisławski, *A Comparison Of Helicopter Main Rotor Features Due To Stiffness Of Rotor Blade-Hub Connection*, Transactions On Aerospace Research, 2018, 1, 2019, S.119–136,

[177] A. Krenik, P. Weiand, *Aspects On Conceptual And Preliminary Helicopter Design*, 2016, S.1–12.

[178] *Wstęp Do Konstrukcji Śmigłowców : Praca Zbiorowa*, Wyd. 2. Warszawa, 2002.

[179] W. Johnson, *Helicopter Theory*. New York, 1994.

[180] M. H. Sadraey, *Aircraft Design Aerospace Series List Design And Analysis Of Composite Structures: With Applications To Aerospace Structures*. 2013.

[181] D. P. Raymer, *Summary Of : Enhancing Aircraft Conceptual Design Using By Royal Institute Of Technology*, January. 2019.

[182] D. P. Raymer, *Aircraft Design: A Conceptual Approach, Sixth Edition*. 2018.

(strona celowo zostawiona pusta)

Załączniki A – Publikacje naukowe

Załączone publikacje [A1] – [A6] są zbiorem sześciu powiązanych tematycznie artykułów naukowych stanowiących zasadniczy wkład merytoryczny rozprawy doktorskiej. Wszystkie opublikowane prace zostały podane w formie oryginalnych reprintów pobranych bezpośrednio z ogólnodostępnych źródeł internetowych poszczególnych czasopism.

Publikacje zostały załączone wg porządku podanego w Tabeli 1 (str. 8).

PROBLEMY MECHATRONIKI
UZBROJENIE, LOTNICTWO, INŻYNIERIA BEZPIECZEŃSTWA

ISSN 2081-5891 **12, 3 (45), 2021, 27-52**

PROBLEMS OF MECHATRONICS
ARMAMENT, AVIATION, SAFETY ENGINEERING

Review of Modern Helicopter Constructions and an Outline of Rotorcraft Design Parameters

Stanisław KACHEL, Robert ROGÓLSKI, Jakub KOCJAN*

Military University of Technology,
Faculty of Mechatronics, Armament and Aerospace
2 Sylwestra Kaliskiego Str., 00-908 Warsaw, Poland
**Corresponding author's e-mail address and ORCID*:
jakub.kocjan@wat.edu.pl; https://orcid.org/0000-0003-3772-1525

Received: April 8, 2021 / Revised: June 13, 2021 / Accepted: July 3, 2021 / Published: September 30, 2021

DOI 10.5604/01.3001.0015.2427

Abstract. This work contains the results of a modern helicopter construction analysis. It includes the comparison of almost seventy rotorcraft constructions in terms of size in line with EASA requirements – large and small helicopters. The helicopters are also divided because of a mission purpose. The proposed division for large aircrafts is: transport, multipurpose, attack and for small aircrafts: observation, training, and utility. The aircraft construction features are described. Average dimension values of airframes and rotors are shown. Helicopter rotor arrangements are presented in terms of an operational purpose. Next, the rotorcraft design inputs are described. The mathematical formulas for design inputs are given. The ratios are calculated and gathered for the compared aircrafts. Correlation between the analysed parameters is presented on charts. Design inputs are also presented in the paper as a function of MTOW. The function trends are determined to provide an evaluation tool for helicopter designers. In addition, the parameters are presented as possible optimisation variables.

Keywords: aerospace, helicopter, analysis, rotor, military

1. INTRODUCTION

The modern battlefield, according to [1], requires the armed forces to use new technologies and to introduce solutions that will be astonishing for a potential opponent. One of the most important branches of today's warfare are air operations. One of the types of air operations is the support of land and naval actions. The backing can be realised by providing troops with transport, firing, radiolocation, observation and more of what is needed to conduct the operations properly. One of the best aircrafts, to grant all of the mentioned duties, are the rotorcrafts. The helicopters, because of their vertical lift ability and capability to dynamically change their position about all three movement axes and about all three rotational axes, can serve in changeable environment conditions and can adapt to new mission challenges.

From the operational needs there come the prerequisites for a helicopter construction. As it is described in [2], from those conditions there come the first parameters like: payload, speed, range, size etc., everything that is needed to fulfil the mission terms. However, there are some rigid design rules (mechanics, aerodynamics etc.) that depend on a chosen aircraft and its aeronautical arrangement. Taking into consideration reference [3], there are some crucial requirements that an engineer is obliged to consider in planning a new helicopter: external loads, strength and stiffness, durability and reliability, crash safety, manufacturing and maintenance technology. All of the requirements are inputs to start the design process. The conceptual design phase is described by the Design Wheel.

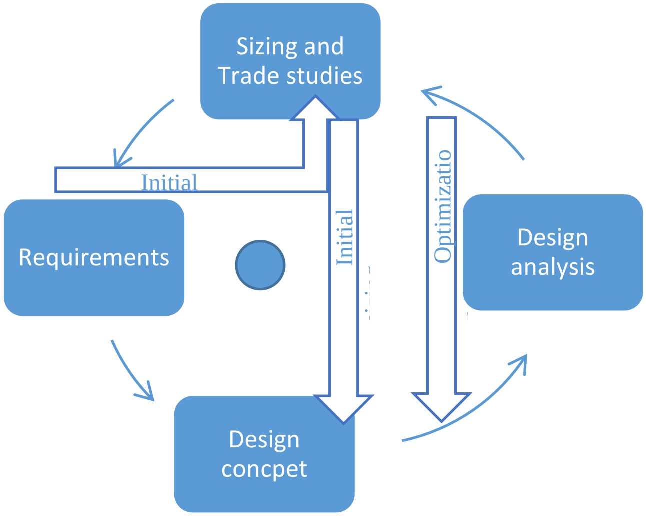

Fig. 1. Design wheel[1]

[1] Adopted from [28].

What needs to be mentioned, because of the subject of analysis, the second source of aircraft requirements comes from legislation – where some design boundaries for civilian or military constructs are enclosed. For example, the civilian helicopters' requirements are described in EASA[2] CS-27 [4] and CS-29 [5]. To adopt this specification to the military environment, EMAR[3] 21 [6] was provided by EDA[4]. The certification specifications point out the requirements for: flight conditions, strength, design and construction, powerplant, equipment and operating limitations. These regulations divide the rotorcraft population into two types: small rotorcraft and large rotorcraft. In this kind of division, the helicopters are catalogued according to their mass and seating capacity.

Because of the described issue, in the next chapter, basing on the EASA's specification, the helicopters' destiny division is proposed. The construction review according to the purpose of the use, will enable to outline the operational problems that were noted during different helicopters' lifecycles.

2. REVIEW OF CURRENT HELICOPTER CONSTRUCTIONS

2.1. Type of the construction because of operating purpose

Because of versatile helicopters usage [7], the manufacturers prepare rotorcrafts' airframes that can be developed into various versions of the same type of aircraft. The modern helicopter frame is prepared for modular replacement of most of the components because of configuration change, or to put in some parts that were improved during an aircraft's lifecycle, for example engines or avionics. However, depending on the mission profile, the basic helicopter construction will be different. As a consequence, some construction division can be proposed:

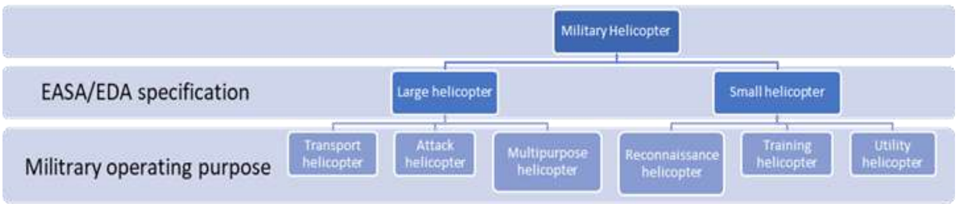

Fig. 2. Helicopter construction classification

[2] European Union Aviation Safety Agency.
[3] European Military Airworthiness Requirements.
[4] European Defence Agency.

The classification, described above, is based on military system requirements and mission effectiveness which are described in [8]. The mentioned conditions determine the performance. While conducting the assigned mission, the helicopter should reach the required level of airspeed, range, and payload. Moreover, a capacity to carry weaponing and resistance to firing may be needed. As it was described in the introduction, these demands determine the rotorcraft construction.

EASA/EDA specification

The EASA legislations regulate the parameters that a helicopter construction must fulfil to be certified [4], [5]. The specifications are broken into subparts which detail the flight, strength, design and construction, powerplant, equipment, operating limitations conditions. For military aircrafts, as stated in EMAR 21 [9], a national law (similar to EASA) is needed to be passed. In accordance with mentioned rules, two main construction categories can be defined. The requirements are also divided into categories which specify certification demands depending on the operation.

Table 1. EASA's helicopter classification

Type	Category	Maximum weight [kg]	Max. seating capacity
Small helicopter	A	≤ 3175	≤ 9
Large helicopter	A	≥ 9072	≥ 10
Large helicopter	B (with category A subparts – C, D, E and F)	> 9072	≤ 10
Large helicopter	B (with category A requirements CS.29.67(a)(2), 29.87, 29.1517 and subparts – C, D, E and F)	≤ 9072	≥ 10
Large helicopter	B	≤ 9072	≤ 10

Rotors' configuration

Before describing the types of military helicopters' construction, it is very important to outline the rotor arrangement of helicopters, the analysis is based on [10]-[12]. The configuration of rotors is determined by the arising torque. The mentioned torque is a consequence of the main rotor's work. The main rotor during flight is acting on the fuselage and generates a reaction moment, which is responding in the opposite direction. To balance the torque and to provide a steady flight, a counter-force is needed. It is realised by an additional rotor/rotors. Three rotors arrangements, which are generally used on military helicopters, are described below. The arrangements are basically independent from the helicopter operating purpose and they can be applied to all of the military types. However, some forms are more likely applicable to certain sorts of construction.

The most popular helicopter rotors' configuration is the Sikorsky configuration with a single main rotor and a small supporting rotor to produce the balancing torque and to control the yaw. Usually, the tail rotor is placed at the end of a tail boom. The auxiliary rotor is set vertically to generate the balancing thrust that acts on an arm about the main rotor axis. In this configuration, the main rotor grants lift, propulsion force, roll and pitch control. This layout is adopted to all kinds of military helicopter constructions. For example, a Polish military multirole helicopter W-3 "Sokol" (Fig. 3) is a typical example of the Sikorsky layout.

Fig. 3. W-3 "Sokol" – single rotor helicopter layout [5]

The second kind of helicopter aerodynamic arrangement is a construction with twin main rotors, this kind of arrangement is well described in [13]. These elements are the same size and loadings, however, they are rotating in opposite directions. As a consequence, the torques produced by the rotors are naturally balancing themselves. The yaw control is gained by contrasting lateral inclination of the rotors' thrusts. The power of the main rotors is not diminished by an additional smaller rotor. The most popular displacement of the rotors on the construction is the fore and aft configuration, however, there are some constructions which were designed with the side-by-side configuration. Nowadays, they are especially used in constructions with tilted rotors. The twin rotor layout was almost only applied to transport helicopters. The most characteristic representative of twin-rotor helicopters is CH-47 "Chinook" (Fig. 4).

[5] Sketch source: Technika Lotnicza i Astronautyczna.1986 (4-5).

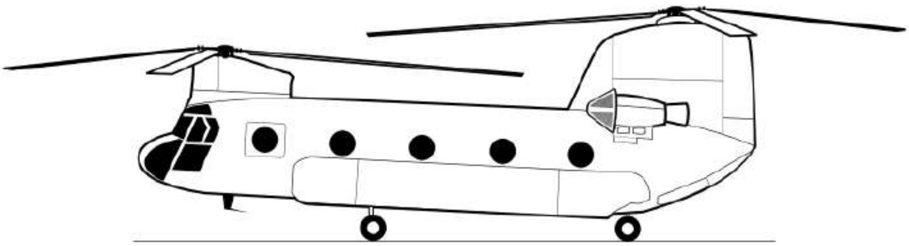

Fig. 4. CH-47 “Chinook” – twin-rotor helicopter layout[6]

The third configuration, which should be described, is a coaxial layout. The international research about this kind of arrangement was summarised in [14]. Coaxial helicopter may be treated as a special kind of a tandem helicopter. No additional tail rotor for balancing the torque is applied, as it was in the twin configuration, the main rotors are compensating each other by rotating in opposite directions. That is why the construction of the helicopter fuselage can be shorter and more compact. Coaxial construction requires rigid rotor blades, and as a consequence, higher, than in the Sikorsky layout, root and shaft bending moments are possible to be tolerated. This gives an opportunity to produce a higher lift force on the advancing and retreating side of the rotors. In the military aircraft it grants a high climb speed and a very high hovering ceiling. The coaxial rotors are mostly used in the Russian helicopter constructions manufactured by “Kamov” company. The representative of a military helicopter with coaxial rotors applied is Ka-52 “Alligator” (Fig. 5).

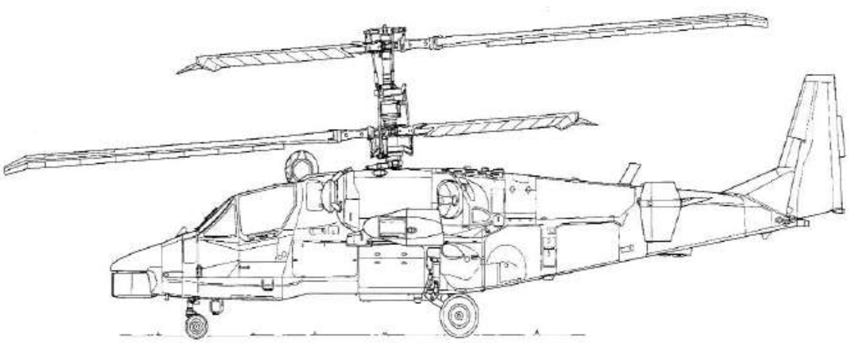

Fig. 5. Ka-52 “Alligator” coaxial-rotor helicopter layout[7]

[6]Sketch source: https://commons.wikimedia.org/wiki/File:CH-47_Chinook_Line_Drawing.svg (last accessed 30.01.2021).

[7] Sketch source: https://www.the-blueprints.com/blueprints/helicopters/kamov/76276/view/kamov_ka-52_alligator_hokum (last accessed 30.01.2021).

Large helicopter

The large military helicopters' family can be divided into three types that determine the rotorcraft elements' construction: transport helicopters, attack helicopters and multipurpose helicopters. These constructions differ in weight, dimensions, equipment and performance. In result the structure of components is also altered.

Transport helicopters conduct supporting missions of military operations. The helicopter tasks in modern warfare are recognised in [15]. Transport helicopters are capable to carry troops, cargo or vehicles. The load can be lifted inside the hold or externally by putting a sling to the prepared attachment point. Transport helicopters are also used for air assault operations, where they are used to deploy troops near the enemy position. In this situation, the high possibility of enemy fire occurs. As a consequence, for transport helicopters' performance, the most important are the payload and the range, next the speed, fire resistance, and survivability. Some transport helicopters are equipped with armament to provide their self-defence.

The described above conditions determine the helicopters' construction. In regard to [16], some features of transport helicopter construction can be indicated. The most important aspect for the vehicle purpose are the dimensions. The main rotor diameter of transport helicopters, according to the rotorcrafts data from [17], is on average of 20 m, however, it depends on the aircraft payload. The heavy lift helicopters have a rotor diameter of 24 m to 34 m. The biggest representative of this group of aircrafts is Mil Mi-26 helicopter (Fig. 6).

Fig. 6. Mi-26 unloading vehicles[8]

[8] Image from the Russian Ministry of Defence.

The fuselage dimensions are on average of 20 m long and of 4.45 m wide. These aircrafts are usually built with two engines, however, some heavy lifts constructions are three-engine. The motors are placed within the upper part of the fuselage, above the cargo hold and crew cabin.

The fuselage is constructed as semimonocoque design. In a transport helicopter it is important to place the bulkheads and the frames in points where internal or external load is going to be attached. These elements are also tasked to concentrate loads. The aircrafts' fuel is usually located underneath the cargo compartment floor, in the bottom part of the hull. The tail rotor diameter, because of a high torque, is proportional to the main rotor diameter and it is wider than in a helicopter with a different operation purpose. The advantage of vertical take-off and landing gives transport helicopters the crucial meaning in tactical operations, rotorcrafts can be used in almost all kinds of terrain conditions to deliver the required cargo. Even when landing is not possible, the load can be deployed in a hovering flight. However, the rotorcrafts' size makes them vulnerable to opponents' detection and fire.

The second type of military helicopters are attack helicopters. According to [18] and [19], these rotorcrafts' primary role is to attack ground targets: infantry, vehicles or fortifications. One of the primary missions of the aircrafts described are close air support operations. In this kind of tasks, attack helicopters are supporting the attack of land forces by heavy fire. Another kind of operations are deep attacks. In deep attacks, helicopters are assigned to precisely destroy the enemy forces that are not in use, however, they can be deployed to operate in the closest time. Because of conducted tasks, these machines are heavily armoured and armed. The aircraft is equipped with cannons, machine guns, rockets or missiles. The most important parameters for the aircrafts' performance are speed and range (flight durability). The velocity is crucial in close fight, it allows the helicopter to avoid being detected and hit. Aircrafts' durability is necessary to allow supporting the operations even when unpredicted circumstances occur.

Construction parameters of helicopters depend on their mission profiles. As it was for transport helicopters, characteristic criterions are the dimensions. The aircrafts' main rotor diameter is on average of 15 m. The fuselage length is quite similar for all of the western constructions and it is on average of 15 m, however, for the Russian attack helicopters they are longer, for example the Mi-28 is 17.5 m long. All attack helicopters are narrow ones. The average fuselage width is 2.25 m. However, the widest Agusta A129 Mangusta is 3.6 m. Rotorcraft minimal size is important to evade the enemy shelling. Decisive is the front narrow shape, it is minimising radar detection and hit opportunity. The special representative of this helicopter family is Kamov Ka-50/52 because of its twin-rotor construction.

The airframe construction is also semimonocoque, however, because of the high possibility of being hit the number of frames and longerons, relative to transport helicopter, is increased. The bulkheads are used for attaching machine guns and cannons. The fittings are needed to be prepared for recoil compensation.

Usually, small wings are attached on the left and right side of the fuselage. Their main purpose is carrying rockets and missiles' launchers, nevertheless, a residual lift force is also produced. On the helicopter's nose, there is a radar mounted, or an observation camera, sometimes a machinegun is placed under the nose section. The engines are installed outside the fuselage on the middle upper left and right side, and the main gear is installed in the hull between them.

Fig. 7. AH-64 attack helicopter[9]

The largest type of military helicopters are the multipurpose (utility) helicopters. In references [20] and [21], these constructions are needed to be available to adjust them to various versions. Utility helicopters are conducting: reconnaissance, attack, transport, medical evacuation, search and rescue or maritime missions. Platform's versatility is the crucial parameter that evaluates the helicopter as a desirable structure. Some aircrafts' versions are prepared by the manufacturer, for example the maritime or search and rescue helicopters, because their equipment, especially radars and cameras, require preparation of electrical installation within the airframe. However, mainly the modern multipurpose airships are made as modular ones. The airframe is prepared to quickly change special equipment and to shape the rotorcraft to a planned mission. This equipment is for example armament, medical equipment, troops' seats or cargo fastening. Depending on a mission profile, some setups can be mounted simultaneously, for example configurations with weaponry and troops' transport. The most characteristic representative of these rotorcrafts' family is UH-60 "Black Hawk".

[9] Image from Boeing official materials.

The multipurpose helicopter's airframe is designed to fulfil all the operational requirements that are defined by the user. As a consequence, the dimensions and the masses of large multi-role aircrafts can be defined somewhere between a transport and a small helicopter. The smallest UH-72A is 10.2 m long and 1.73 m wide with MTOW 3585 kg, on the contrary the H-92 is 17.1 m long and 2.6 m wide with MTOW 12020 kg. However, an average can be specified. For the multipurpose helicopter, the average dimensions are: length of 14.40 m, width of 2.56 m, and a rotor diameter of 15.14 m. The aircraft's proportions are exact to combine all types of an operational purpose. The helicopter's performance is between an attack and a transport helicopter with an average maximum cruise speed of 288 km/h and a range of 700 km. That is 10 km/h less and 100 km more than attack aircrafts, but 10 km/h more and 100 km less than transport aircrafts.

As in all the previously described constructions, the multipurpose rotorcraft airframe is also designed as a semimonocoque structure. A fuselage construction with the number of longerons is more like a transport than an attack helicopter. The longerons and frames are prepared to carry troops or equipment in cargo hold, however, some external fittings are also prepared. The inner structure is arranged with the points where special equipment or passenger seats are safely secured. These points are calculated to carry the loads that came from the mounted devices. Engines and the main gear are placed above the fuselage.

Fig. 8. UH-60M multipurpose helicopter[10]

Small helicopter

With regards to [22] and [23], small military helicopters can be divided into three types of a mission purpose: reconnaissance helicopters, training helicopters and utility helicopters.

[10] Image from Lockhead Martin official materials.

However, most small rotorcrafts are built utility airships that provide all kinds of vertical lift aircrafts missions: transport, evacuation, medical support, reconnaissance, light attack, observation and training. There are only a few constructions that are typically reconnaissance or training rotorcrafts. OH-58D “Kiowa” (Fig. 9) is one of the representatives of observation helicopters. It needs to be added that mostly the observation aircrafts are also lightly armed with guns or missiles. As regards to training machines, the most popular kind of helicopters are Robinsons R22 and R44.

Fig. 9. OH-58D “Kiowa Warrior” reconnaissance helicopter[11]

The small helicopters’ airframes, because of a similar operating purpose, are similar in their constructions. The average fuselage length is of 9.84 m and width is of 1.58 m, where the shortest is the OH-6A with 7.6 m, but its fuselage is the widest with 1.9 m. The narrowest is the prototype CH-14 Aguilucho and the longest is the Bell 429 with 11.73 m. The average maximum cruise speed stays on 252 km/h and it is quite similar for all small helicopters. A range depends on the mission purpose and on assumed load, however, it can be established at 600 km.

The structure of helicopters is designed as semimonocoque, but it differs in some solutions from large helicopters. In this kind of rotorcrafts, the tail boom is more often a pipe which is strengthened with formers and longerons. The popular solving is also using a fenestron instead of a classic tail rotor. The innovative solution is applied on MD Explorer helicopters family, where instead of a tail rotor a NOTAR[12] system is used, the system is well described in [24].

[11]Photo source: https://ghostrecon.fandom.com/wiki/OH-58D_Kiowa?file=OH-58D_Kiowa.jpg, last accessed 12.02.2021.

[12] No tail rotor.

The fuselage is built with frames and longerons, the bulkheads are used to carry the most dangerous loads and loads that come from fittings. Small rotorcrafts are usually single-engine, the rotorcrafts with high MTOW (close to 3175 kg) are twin-engine. In some aircrafts, piston engines are used instead of turbine engines, unlike in large helicopters where only turbine engines are applied. The motors and main gearbox are built upon the fuselage, like it was in the large multipurpose and transport rotorcrafts.

Fig. 10. MD-902 Explorer utility helicopter with NOTAR system[13]

3. COMPARISON OF CONSTRUCTION CHARACTERISTIC PARAMETERS

To compare modern helicopter construction and to outline the dependencies between the design parameters and performance, some characteristics need to be settled. The characteristics will be divided into relative and absolute. The compared absolute qualities are mass, performance and geometry parameters. This correlation is made only to gather and specify some typical features of helicopter types. The most important for further considerations are the relative characteristics. As it is defined in [25], the relative characteristics are calculated ratios, which allow us to measure the influence of main components excellence on aircrafts performance. In the comparison almost seventy modern helicopter constructions were examined.

[13] Image from MD Helicopters official materials.

Absolute parameters

In Table 2 the average main rotor parameters are shown. These statistics are gathered to represent relatives between the rotor geometry and performance. The crucial parameter during the main rotor designing is the blade's tip speed. According to the presented data, the tip speed is similar for all kinds of rotorcrafts. It is a consequence of the fact that the maximum tip's speed is determined by the forward flight conditions. On an advancing blade, the rotor blade speed is summing up with the forward flight speed. Therefore, it appears the possibility of supersonic speed occurrence. According to [26], this phenomenon is a cause of rotor increased noise, vibration and drag. To avoid the undesirable effect, during the conceptual design phase, the main rotor radius and speed are calculated to provide a limited tip velocity. The smaller radius enables us a higher rotor speed implementation. As a result, the overall helicopter performance is mostly constrained by the tip speed. In modern helicopter constructions, the higher rotor velocities are obtained by applying the computer designed blade tip platforms, that postpone the critical Mach number to the higher speeds. The tip shapes are outlined in [27].

Table 2. Absolute main rotor parameters

Helicopter	Average main rotor diameter [m]	Average blade chord [m]	Average rotor speed [rpm]	Average blade tip speed [m/s]
Large	**16.56**	**0.54**	**269.99**	**219.27**
attack	15.22	0.56	275.01	221.01
multipurpose	14.72	0.44	301.20	219.80
transport	22.01	0.64	208.43	217.07
Small	**10.08**	**0.29**	**408.35**	**213.11**
observation	9.62	0.25	412.50	206.71
training	9.90	0.31	409.10	211.29
utility	10.47	0.30	405.33	217.98
Average	**14.24**	**0.43**	**327.91**	**216.69**

Table 3 summarises the comparison of performance parameters for each of helicopters' operational purpose. Some unique features, described in the previous chapter, which came from the operational demands, can be spotted. This summary can also be a base of design inputs, which will fulfil the user needs.

Table 3. Absolute performance parameters

Helicopter	Average MTOW [kg]	Average Rate of climb[m/s]	Average max Vc [km/h]	Average range	Average engines power - max continous [HP]
Large	**9799**	**10.13**	**287**	**693**	**4211**
attack	7428	11.88	294	607	3260
multipurpose	6512	9.72	285	708	2640
transport	19876	8.40	283	777	8807
Small	**2163**	**8.89**	**253**	**601**	**700**
observation	1734	9.35	253	519	476
training	1728	9.40	248	671	515
utility	2593	8.51	255	655	914
Average	**7104**	**9.66**	**275**	**661**	**2971**

Relative parameters

The relative parameters are a good evaluation of the desired constructions. They are also proposed as inputs in the conceptual design phase.

Relative useful load

The relative useful load (M_p) is a ratio that defines the capability of helicopter lift. The relative useful load includes the fuel and the cargo mass. In helicopter missions, the operator is planning the quantity of fuel in the tanks. The rest of a free mass is allocated for the mission purpose. However, to carry more cargo at a shorter range, there are tasks where the tanks are not maximally filled. The ratio is given by the equation:

$$M_p = 1 - \frac{OEW}{MTOW} \tag{1}$$

with: OEW – operating empty weight [kg];
MTOW – maximum take-off weight [kg].

A helicopter designer at the very beginning phase should assume the MTOW. To properly respond to the operator's needs, it is necessary to plan the mass proportions and calculate the payload. The statistics for a relative useful load are shown in Fig. 11. Analysing the ratio in reference to the modern helicopter constructions, some statistics' features can be pointed out. In accordance with the intended use, the transport helicopter has the best lift capability. For the attack helicopters, where the lift is designed only for the armament and the fuel, the relative useful load is at the lower level. The shown statistic can be a base to assess the concept design of the rotorcraft.

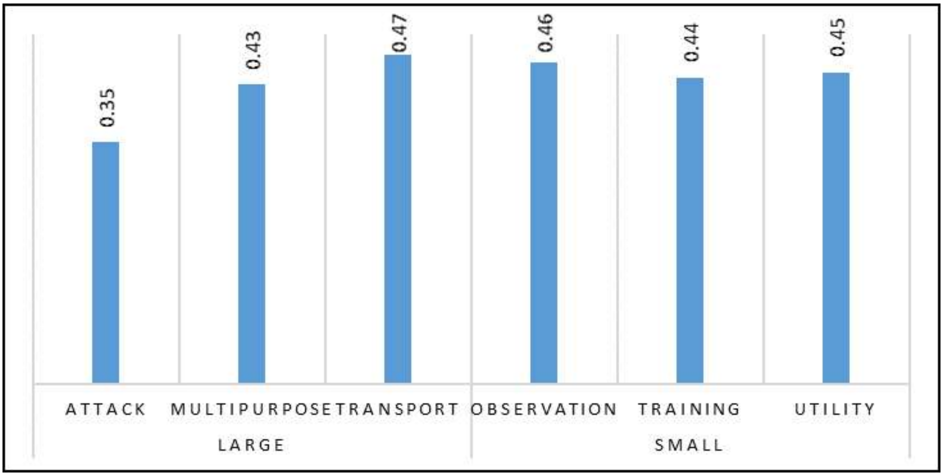

Fig. 11. Relative payload chart

In Figure 12, the trends for small and large helicopters are compared. What can be recognised is the fact that the trend for smaller MTOW is at the higher level. As a consequence, the conclusion can be drawn that the constructions with the smaller MTOWs are better than those for the larger machines. The main cause is the lack of geometry boundaries of the main rotor. This is another argument for the theory which says that achieving the optimal rotor parameters improves the construction performance.

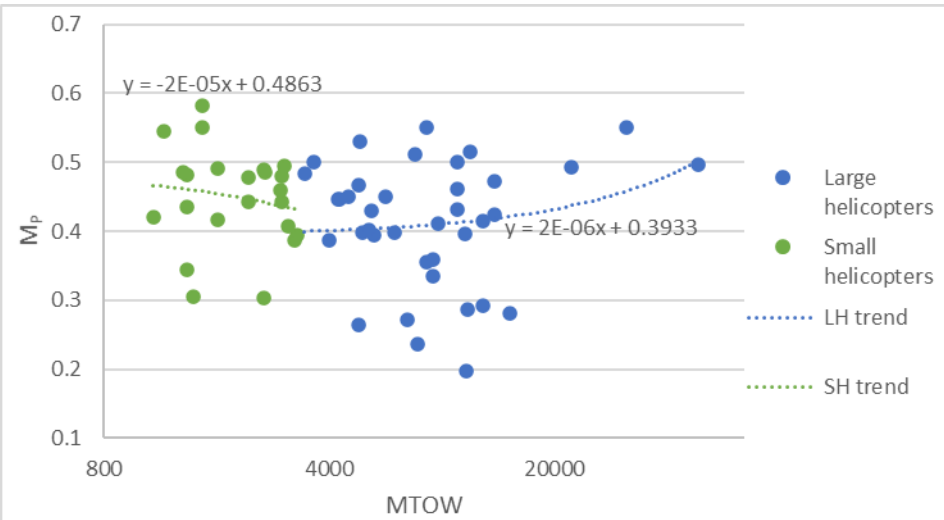

Fig. 12. Relative useful load trends

Disc load and power load

Other relative parameters, that help the designer to check the construction performance, are the disc load and the power load. These ratios, when calculated for the preliminary construction, should be compared to the static values.

The disc load is given by:

$$p = \frac{MTOW}{\pi R^2} \tag{2}$$

where R [m] is the main rotor radius,
and the power load is:

$$q = \frac{MTOW}{N_{PU}} \tag{3}$$

where N_{PU} is the power of the engines.

Clearly, if the ratios are larger, then the construction is more capable to lift the planned mass. The capability comes from the rotor geometry or the engines' power.

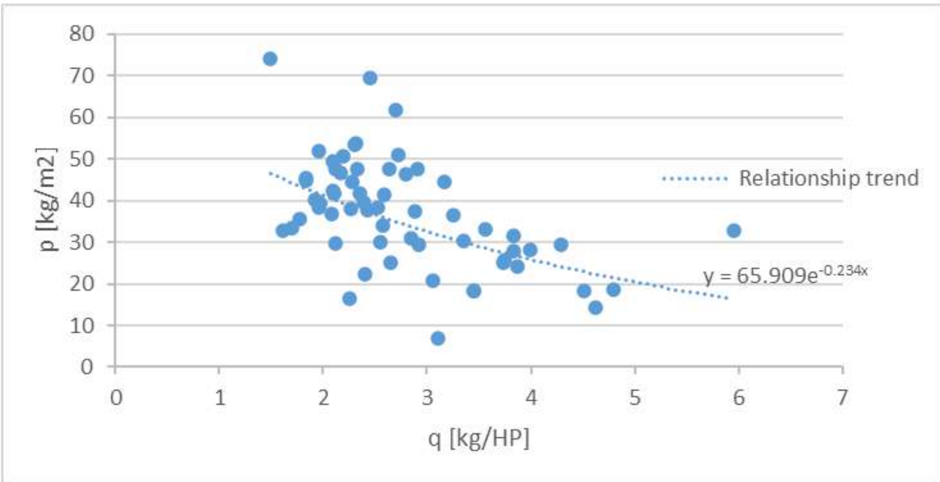

Fig. 13. Relationship between q and p parameters

The statistic relationship between two parameters is shown in Fig. 13. In the chart, the correlation trend is marked. If the disc load is at the higher value, then the power load is lower. The opposite situation takes place if the disc load ratio is bounded by geometry. That is recognised for the large helicopter, where the main rotor radius is longer and there is a risk of critical Mach number occurrence. For smaller constructions, the radius is smaller, and as a result it can be customised to the rotorcraft and it can produce relatively more lift force.

That gives an opportunity to estimate the engines (in a conceptual design phase) with the higher rotor thrust as a calculation input and as a result to obtain lower engine requirements. The statistic average values are presented in Table 4. These figures are good to compare the designed rotorcraft to modern helicopters.

Table 4. Statistic relative parameters

Helicopters	Average M_p	Average p [kg/m2]	Average q [kg/HP]
Large	**0.41**	**42.85**	**2.37**
attack	0.35	42.91	2.27
multipurpose	0.43	39.59	2.37
transport	0.47	49.61	2.46
small	**0.45**	**26.72**	**3.46**
observation	0.46	23.77	3.73
training	0.44	22.58	3.76
utility	0.45	29.97	3.16
All	**0.43**	**37.07**	**2.77**

The two parameters, described above, are another argument for the main rotor optimisation. When the main rotor capability to produce more lift comes from its own parameters, then it is more possible to optimise the powerplant selection with the reduced power requirements.

Rotor solidity

The rotor solidity ratio describes the rotor disc filling with the blades area. In the conceptual design, this parameter, with the statistical database, is fundamental for choosing the number of blades and the blade chord. The rotor solidity is described by:

$$\sigma = \frac{zc}{\pi R} \tag{4}$$

where z is the number of blades,
c [m] is the blade chord and
R [m] is the main rotor radius.

In Figure 14 the relationship between the parameter σ and MTOW is demonstrated. For small constructions, where the rotor velocity is greater, the lift surface can be diminished. However, if the radius and the speed are restrained, the lift is required to be generated by adding more area with the new blade or by extending the chord. Increasing the solidity, the rotor vibrations and mass are simultaneously risen. As a result, the blade loads are expanding. To reduce the rotor solidity, the lift force should be gained by improving the rotor performance with better airfoil or higher speed.

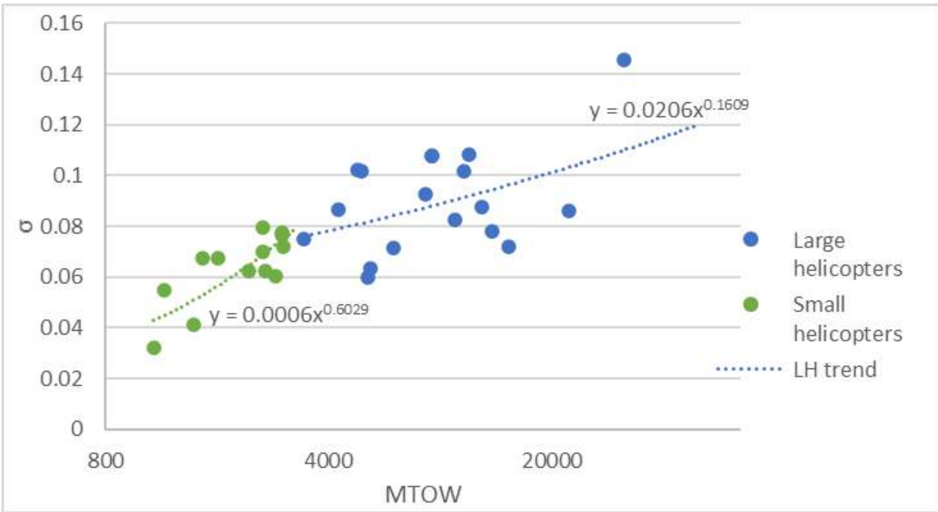

Fig. 14. Rotor solidity

Advance ratio

The advance ratio is a designed input parameter that describes the potential of helicopters' maximum cruising speed in accordance with the rotor's tip speed. It can be compared with statistic data to evaluate the proposed construction. It is described with the equation:

$$\mu = \frac{V_c}{U} \tag{5}$$

with: V_c – maximum cruise speed [m/s];
U – rotor tip speed [m/s].

However, to obtain full information about the rotor's potential, the calculated advance ratio can be also being compared with the maximum advance ratio, which is calculated for the local sound speed:

$$\mu_{max} = \frac{60-a}{\pi n D} - 1 \tag{6}$$

with: a – local sound speed [m/s];
n – number of blades;
D – main rotor diameter [m].

In Figure 15, both parameters are shown. It demonstrates that the rotors with the smaller MTOW, and as the result smaller geometry, have a capacity to increase the performance without the hazard of closing to critical Mach number. On the other side, the ratio can be a proof of the fact that modern rotor blades can be optimised, to increase the cruising speed, with the retraction of the critical Mach number at the higher speed.

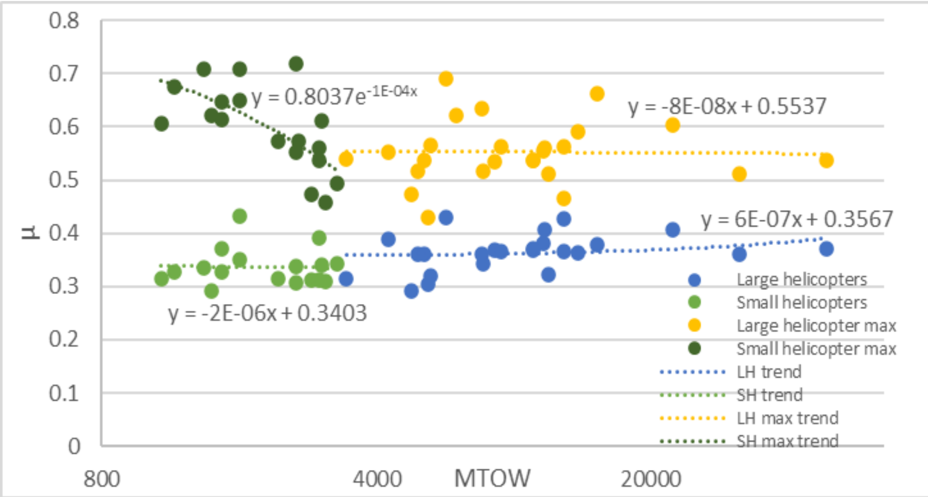

Fig. 15. Advance ratio comparison

Aspect Ratio

The aspect ratio is defining the proportion of blade chord to blade radius.

$$\lambda = \frac{c}{R} \tag{7}$$

Basing on the statistics data, shown in Fig. 16, a trend cannot be defined, however, the parameter can be bounded by the 0.04 to 0.08 value. The average value for all kinds of helicopters equals 0.06.

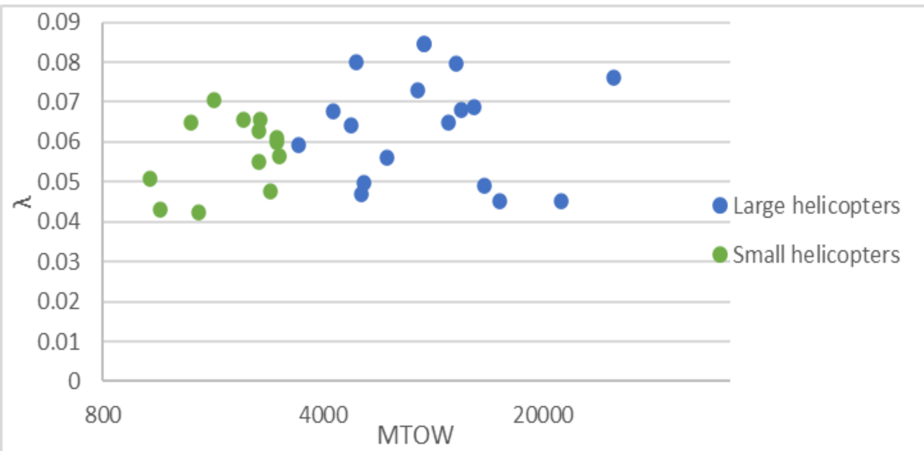

Fig. 16. Aspect ratio

Lock number

The lock number is a crucial ratio that defines the relationship between aerodynamic parameters and inertia forces acting on the blade.

The parameter is calculated with the equation:

$$\gamma = \frac{\rho a_0 c R^4}{I_\beta} \tag{8}$$

with: ρ – air density [kg/m^3];
a_0 – main rotor blade's lift curve slope [1/rad];
I_β – flap moment of inertia [kgm^2].

For military helicopters the Lock Number reaches values from 5 to almost 12. As it is shown in Fig. 17, when the MTOW increases, the ratio is also getting the higher rate. Rotor blades, with the higher Lock Number value, are less resistant to flapping, because of a limited moment of inertia placed in a denominator, with the greater geometric dimensions.

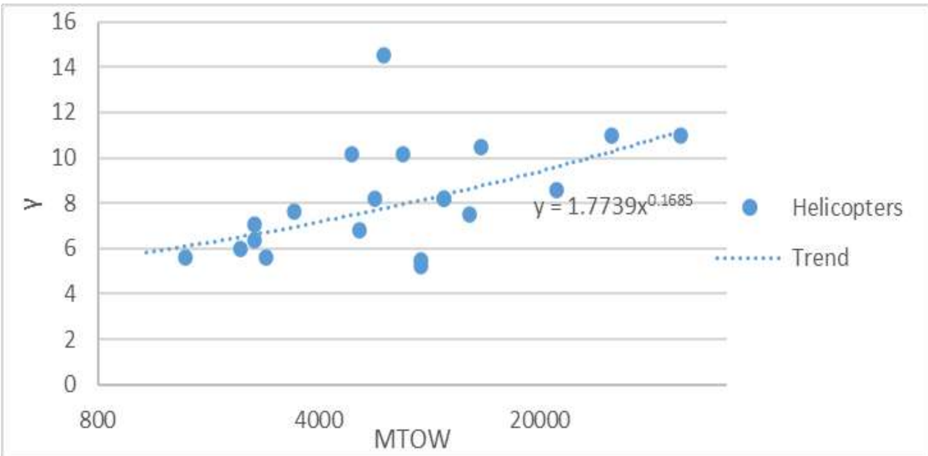

Fig. 17. Lock number

4. DESIGN INPUTS IN PRELIMINARY DESIGN

In order to show the implementation of design inputs in the preliminary phase of the design process, the main rotor initial calculations are presented. The main rotor estimation is the first step in a helicopter design.

4.1. Estimation of Maximum Take-off Weight

From operation prerequisites, there comes the MTOW. Taking into consideration the average values and descriptions, proposed in the previous chapters, some gross weight can be assumed. The Relative Useful Load ratio is applicable in this step to evaluate the required load capability in comparison with statistical data.

4.2. Calculation of a rotor radius

One of the first steps of the main rotor estimations is defining the rotor radius. The Disc Load factor, based on the gathered data, is a good design input to provide the radius length. Comparing the given operational demands with statistics, the first value of the rotor radius can be determined.

4.3. Calculation of tip velocity

The next point of a rotor design is a tip velocity estimation. This possibility provides an Advance Ratio. Taking into consideration the demanding maximum cruise speed, the tip velocity is able to be settled.

4.4. Calculation of a blade number and a chord value

Taking into consideration the Aspect Ratio from statistical data and Rotor Solidity, a blade number and a chord length can be obtained. Combining the mentioned Design Inputs into a function allows us to calculate the rotor parameters as expected.

4.5. Choosing an airfoil and inertial characteristic

The crucial phase of a preliminary main rotor design is choosing an airfoil. One of the proposed criteria of selecting the profile is the inertial characteristic of the blade. Taking into consideration the statistical Lock Number, and assuming the desirable flapping moment of inertia, the lift curve slope can be estimated. Its value helps the designer to choose the correct airfoil for the planned aircraft.

4.6. Iterative procedure

The proposed implementation of the Design Inputs should be applied to the iterative procedure as it is shown in Fig. 1 of the Design Wheel. The procedure can be implemented into numeric computing software or CAD environment to calculate the best helicopter parameters.

4.7. Design inputs calculated for a multipurpose helicopter

To show the Design Inputs in numbers, the calculations for the W-3 helicopter are proposed. The W-3 helicopter is a good example of rotorcrafts that were classically designed without using modern CAD/CAE/CFD software. Table 5 data are a basis for a further rotorcraft optimisation. Improving the ratios allows us to gain the better aircraft performance.

Table 5. Calculated design inputs

Parameter	**Equation**	**Numbers**	**Result**	**Average parameter for helicopters with similar MTOW (±1500 kg)**
Relative useful load	$M_p = 1 - \frac{OEW}{MTOW}$	$1 - \frac{3850}{6400}$	0.398	0.43
Disc load	$p = \frac{MTOW}{\pi R^2}$	$\frac{6400}{\pi \cdot 15.7^2}$	33.06	39.40
Power load	$q = \frac{MTOW}{N_{PU}}$	$\frac{6400}{2 \cdot 1100}$	2.9	2.23
Rotor solidity	$\sigma = \frac{zc}{\pi R}$	$\frac{4 \cdot 0.44}{\pi \cdot 15.7}$	0.071	0.07
Advance ratio	$\mu = \frac{V_c}{U}$	$\frac{72.2}{209.62}$	0.34	0.34
Maximum Advance Ratio	$\mu_{max} = \frac{60 - a}{\pi n D} - 1$	$\frac{60 - 340}{\pi \cdot 255 \cdot 15.7} - 1$	0.62	0.56
Aspect Ratio	$\lambda = \frac{c}{R}$	$\frac{0.44}{7.85}$	0.56	0.05
Lock number	$\gamma = \frac{\rho a_0 c R^4}{I_\beta}$	$\frac{1.21 \cdot 6.303 \cdot 0.44 \cdot 7.85^4}{1207}$	9.82	9.97

5. CONCLUSIONS

The analysis of constructions of modern military helicopters provides a diversified basis for a rotorcraft design. The airframes' distributions were based on EASA legislation, which allows a future designer to use the data in the projects that correspond, from the very beginning, with the applicable law.

In accordance with a mission purpose, characteristic features of helicopters constructions were shown in this work. The provided information is ready to be used in the conceptual design phase. Taking into consideration the operator's needs, a designer has a ready-to-use data that allows us to prepare a fist-look rotorcraft design, which is able to fulfil the modern warfare requirements.

The design inputs, presented in the third chapter, are accessible to evaluate the conceptual calculations and to assess their usefulness with comparison to other modern constructions. The ratios, given in the paper can also be used to calculate basic rotor dimensions and performance parameters.

The crucial conclusion of the work is that all of the rotor parameters determine helicopter's performance. Next phases of a conceptual design are based on the main rotor calculations. Power prediction and tail rotor parameters are limited by the obtained results. More efficient main rotor generates a better quality of input numbers for the next design stages, for example in the engines selection the main rotor thrust is the element of the equations. It could provoke lower power requirements, however, the powerplant selection is a separate optimisation problem which is not objective of this work and more conditions is needed to be considered.

It was also shown, that the existing helicopter can be an object of improvement for researches. The design inputs, presented in the work, can be indicators to evaluate the construction and to point the optimisation directions.

The need for rotor enhancement emerges in different helicopters lifecycle stages. This paper's considerations will serve as a basis for preparing the main rotors model with modern optimisation methods – using CAD, CAE, and CFD environments combined with mathematical multi-criteria optimisation calculations.

FUNDING

The authors received no financial support for the research, authorship, and/or publication of this article.

REFERENCES

[1] Jordan Dawid, James D. Kiras, James D. Lonsdale, Ian Speller, Christopher Tuck, C. Dale Walton. 2016. *Understanding Modern Warfare*, Cambridge University Press.

[2] Padfield Gareth. 2007. *Helicopter Flight Dynamics (Second Edition)*, AIAA Education Series.

[3] *Wstęp do konstrukcji śmigłowców: praca zbiorowa* (Wydanie 2). 2002. Warszawa: Wydawnictwa Komunikacji i Łączności.

[4] EASA. 2020. *Certification Specifications and Acceptable Means of Compliance for Small Rotorcraft CS-27*. Available online: https://www.easa.europa.eu/certification-specifications/cs-27-small-rotorcraft.
[5] EASA. 2019. *Certification Specifications and Acceptable Means of Compliance for Large Rotorcraft CS-29*.
[6] EDA. 2012. *Certification of Military Aircraft and Related Products, Parts and Appliances, and Design and Production Organisations, EMAR 21*, 1-64.
[7] Unmack Tim. 2020. Helicopter Operations. In *Civil Aviation: Standards and Liabilities*, London: Taylor and Francis Group, Imprint: Informa Law from Routledge.
[8] US Army Command. 1972. *Engineering Design Handbook. Helicopter Engineering. Part one. Preliminary design*.
[9] EDA. 2016. *Acceptable Means of Compliance and Guidance Material For The Certification of Military Aircraft and Related Products, Parts and Appliances, and Design and Production Organisations EMAR 21 AMC & GM*.
[10] Wayne Johnson. 1994. *Helicopter Theory*. New York: Dover Publications.
[11] Bramwell A.R.S., David Balmford, George Done. 2001. *Bramwell's Helicopter Dynamic*. American Institute of Aeronautics & Astronautics.
[12] Seddon M. John, Simon Newman. 2011. *Basic Helicopter Aerodynamics*. John Wiley and Sons Ltd.
[13] Stepniewski W. 1979. *Rotary-Wing Aerodynamics – Volume I Basic Theories of Rotor Aerodynamics*.
[14] Coleman P. Colin. 1979. *A Survey of Theoretical and Experimental Coaxial Rotor*. National Aeronautics and Space Administration (NASA).
[15] Bae Myeang-Hyen, Dock-Joo Lee. 2016. *A Study on Helicopter Maneuver Warfare in Future Battle Field*. KAIST.
[16] Engleder Alexander, Johannes Markmiller, Roland Mueller. 2015. The Evolution of Airbus Helicopters Crashworthy Composite Airframes for Transport Helicopters. In *Proceedings of the 41st European Rotorcraft Forum*.
[17] *Jane's All the World's Aircraft – 2004-2005* (ed. Paul Jackson). 2004. Jane's Information Group.
[18] Ference. W. Edward. 2002. *Cace Study of the Development of the Apache Attack Helicopter (AH-64)* (thesis). Monterey, CA, USA: Naval Postgraduate School.
[19] Hume S. Robert. 1996. *Modeling Attack Helicopter Operations in Theater Level Simulations* (Master's thesis). Monterey, CA, USA: Naval Postgraduate School.
[20] Kee Stephen Glen. 1983. *Guide for Conceptual Helicopter Design* (thesis). Monterey, CA, USA: Naval Postgraduate School.

[21] Congress of the United States, Congressional Budget Office. 2007. *Modernizing the Army's Rotary Wing Fleet*. Pub. No. 2898

[22] MD Helicopters. 2014. *MD500E – Technical Description*. Report No. MD14022801-500ETD.

[23] Eurocopter. 2015. *Technical Data – Eurocopter AS 350 B3*. Report No. 350 B3 09.101.01 E

[24] Chen Chen, Han Cheng, Peng Sun, Zhou Chang Chun. 2018. "An Aerodynamic Calculation Model for Anti-Torque System of NOTAR". *Mechanika* 24 (2) : 213-220.

[25] Krenik A., P. Weiand. 2016. Aspects on Conceptual and Preliminary Helicopter Design. In *Proceedings of the Deutscher Luft- und Raumfahrtkongress 2016*, 1-12.

[26] Aoyama Takashi, Jeiji Kawachi, Shigeru Saito. 1995. "Effect of Blade-Tip Planform on Shock Wave of Advancing Helicopter Blade". *Journal of Aircraft* 32 (5) : 955-961.

[27] Brocklehurst A., George N. Barakos. 2013. "A Review of Helicopter Rotor Blade Tip Shapes". *Progress in Aerospace Sciences* 56 : 35-74.

[28] Raymer P. Daniel. 2018. *Aircraft Design: A Conceptual Approach* (Sixth Edition). American Institute of Aeronautics & Astronautics.

Przegląd nowoczesnych konstrukcji śmigłowcowych wraz ze wskazaniem parametrów projektowych wiropłatów

Stanisław KACHEL, Robert ROGÓLSKI, Jakub KOCJAN

Wojskowa Akademia Techniczna,
Wydział Mechatroniki, Uzbrojenia i Lotnictwa
ul. gen. Sylwestra Kaliskiego 2, 00-908 Warszawa

Streszczenie. Praca zawiera wyniki analizy współczesnych konstrukcji śmigłowcowych. Obejmuje porównanie prawie siedemdziesięciu konstrukcji wiropłatów podzielonych ze względu na rozmiar: zgodnie z wymaganiami EASA – duży i mały śmigłowiec. W ramach rozmiaru statki powietrzne zostały podzielone ze względu na cel misji. Proponowany podział dla dużych śmigłowców to: transportowe, wielozadaniowe i szturmowe, natomiast dla małych: obserwacyjne, szkoleniowe, użytkowe. Wyszczególniono najważniejsze cechy konstrukcyjne wiropłata. W pracy zaprezentowano średnie wartości wymiarów płatowców i wirników. Przedstawiono również układ wirników śmigłowca pod kątem przeznaczenia operacyjnego. Finalnie opisano parametry projektowe przydatne w projektowaniu wstępnym. Parametry opisano za pomocą wzorów matematycznych oraz dla każdego z nich zaprezentowano na wykresie zebrane dane statystyczne. W artykule pokazano zależność parametrów w funkcji maksymalnej masy startowej statków powietrznych. Wyznaczono trendy w celu dostarczenia narzędzi do oceny projektowanych śmigłowców. Dodatkowo przedstawiono możliwość wykorzystania parametrów jako zmiennych optymalizacyjnych.

Słowa kluczowe: lotnictwo, śmigłowiec, analiza, wirnik, wojsko materials

MDPI

Article

Helicopter Main Rotor Blade Parametric Design for a Preliminary Aerodynamic Analysis Supported by CFD or Panel Method

Jakub Kocjan [1,*], Stanisław Kachel [2] and Robert Rogólski [2]

[1] Doctoral School, Military University of Technology, ul. gen. Sylwestra Kaliskiego 2, 00-908 Warsaw, Poland
[2] Faculty of Mechatronics, Armament and Aerospace, Military University of Technology, ul. gen. Sylwestra Kaliskiego 2, 00-908 Warsaw, Poland; stanislaw.kachel@wat.edu.pl (S.K.); robert.rogolski@wat.edu.pl (R.R.)
* Correspondence: jakub.kocjan@wat.edu.pl

Abstract: This work is the preliminary part of a research program which is aimed at finding some new methods and design solutions for helicopter main rotor multidisciplinary optimization. The task was to develop a parametric geometric model of a single-blade main rotor applicable for varied methods of numerical aerodynamic modeling. The general analytical assumptions for the parametric main rotor design were described. The description of the main rotor blade parametric design method based on Open GRIP graphical programming was presented. Then, the parametric model of a blade was used for aerodynamic models independently developed for panel method and advanced CFD solver. The results obtained from the CFD simulations and panel analysis for main rotor aerodynamics were compared and assessed using analytical calculations. The calculations and simulations for a single-blade and completed rotor were performed for different helicopter weights and rotor pitch angles. The results of different computer aerodynamic analysis environments were compared for the possibility of their application in an optimization loop. This is preliminary work that describes only a partial problem that could be used in the future as part of a comprehensive methodology for aerodynamic and structural optimization of a helicopter rotor. As an output of the research, new options for main rotor optimization are developed. The combined parametric modeling with aerodynamic analysis, as described in this paper, provide the preliminary design for a main rotor spiral, as an element of the optimization loop.

Keywords: helicopter main rotor; rotor blade; geometric modeling; aerodynamic panel method; CFD

Citation: Kocjan, J.; Kachel, S.; Rogólski, R. Helicopter Main Rotor Blade Parametric Design for a Preliminary Aerodynamic Analysis Supported by CFD or Panel Method. *Materials* **2022**, *15*, 4275. https://doi.org/10.3390/ma15124275

Academic Editors: Panagiotis G. Asteris and Satyam Panchal

Received: 31 March 2022
Accepted: 13 June 2022
Published: 16 June 2022

1. Introduction

Military rotorcrafts that are currently operating are mostly constructions that were designed in the second half of the twentieth century. The constructions (in the preliminary and detail design phases) were prepared with classic mathematical calculations, eventually supported with CAD. With improved computerized options, design processes have been fully transferred to virtual environments. New aircraft structures are fully designed using computer methods; however, the structures of the existing constructions have also been modeled using engineering software, which is described in [1].

The most popular engineering design solution using CAD is a point and click method. A more comprehensive design method is to prepare a model that is generated as a result of entered parameters, which can be obtained by using scripting in the environment's language; an example of parametric blade optimization is shown for a wind turbine blade in [2], and for a main rotor blade in [3]. The parametric design includes options to quickly change the model's features without time-consuming 3D modeling. It is important to note that the influence of parametric change can be rapidly checked in numerous variants.

The helicopter rotor blade is an element which can be successfully adapted to parametric design, because of mathematical functions which precisely describe blade features. The parametric model is the first step to prepare the main rotor optimization process [4]. Some examples have been shown in different works: parametric airfoil design [5–7], structural design [8,9], and aerodynamic design [10]. A good parametric analysis of the rotor blade framework is presented in [11]. In this research, the parametric model was prepared using GRIP modeling language, which is an integral part of the Siemens NX environment. The usage of GRIP in parametric modeling was conducted in [12–14].

The proposed graphical programming language offers the possibility to prepare a geometric and structural model of the aircraft element. The designed part is fully described by the program script. In addition, the elements' features can be calculated from mathematical functions, for example, polynomials for shape parametrization. After programming the structure, Open GRIP offers the possibility to analyze the inertia physiognomy of the body. The obtained data are the basis for the strength calculation. The program also grants a function for preparing forms which can be filled by the user. Therefore, some parameters can be changed during the design loop, without changing the program code. In the future, it is crucial to prepare a full parametric optimization. An effective approach to main rotor blade optimization was proposed in [8,10,15–18], and effective optimization of rotor construction was proposed in [19].

This work is part of a research program that is aimed at finding the best rotorcraft construction optimization solutions. The first step of the research program was an analysis of modern helicopter constructions and an outline of design parameters that are crucial in helicopter main rotor design. The results of the analysis showed that there is a field were rotor construction can be improved in accordance with modern combat field requirements which are dynamically changing due to fast technological improvements. The results, with charts and a comparison of parameters were published in [20].

On the basis of construction comparisons, we conducted a study of new design methods or combinations of some separate solutions. The aim of the study was to provide a versatile, accurate main rotor model that could be analyzed, validated, as well as quickly and easily changed in the optimization process. As a new approach to rotorcraft design, we combined the parametric programming CAD model generator with the CFD and panel method, with the goal of providing new possibilities for improving the construction optimization procedure. The effects and possibilities of CFD main rotor studies that were implemented in the main rotor development procedure were well presented in [21–23]. In addition, a CFD analysis, as a base for a strength analysis because of load prediction, was clearly shown in [24].

The development of the method started with the main rotor blade, as the main element that generates thrust. An existing rotor blade model was taken as a basis to conduct and authenticate the method. As previously described in the Introduction, the blade model was prepared using the parametric method in GRIP language. GRIP language was chosen because it is user-friendly graphical programming code for easily preparing the model with extensive built-in possibilities for quickly calculating the inertia parameters of the generated model, which could be used in further optimization steps, which is crucial when the strength of the construction is taken into consideration in the optimization loop. Further, the model was validated using the CFD and panel methods, and the thrust results were compared with the analytical calculations. The methods were also compared with each other to choose the appropriate procedure to perform the most efficient optimization. To the best of our knowledge, similar studies that combined the proposed methods for rotorcraft main rotor design and main rotor optimization procedure have not been conducted.

This paper is organized as follows: The research methods are described in Section 4, where the mathematical model, which is the basis for the parametric programming, is defined, and in the second part of this section, the CFD and panel method settings are given; the validation results are described in Section 3; and the results are discussed and concluded in Section 4.

2. Research Methods

2.1. Parametric Description of a Single-Blade Rotor with Aspect of Its Geometrics and Aerodynamics

The construction process of helicopter rotor blades requires consideration of fatigue, strength, stiffness, cost, and vibrations. The rotor blade works in a changeable environment, and therefore, the designer has to take into consideration all of the parameters that transform during flight. Periodic changes in the flow velocity on the blade section can modify the angle of attack and the Mach number, and as a consequence, can change the aerodynamic coefficients. Blade turns (relative to hinge axis) and blade deformation cause a periodic change in inertial forces and provoke a cyclic modification in the angles of attack and flow velocity. The flexibility of the main rotor blades and their work in a strong centrifugal force field induce an inseparable connection between loads and deformations. An analysis of the problems mentioned and also the noise level or flow disturbance requires a versatile evaluation of the main rotor blade's work conditions. Effective blade aerodynamic modeling was proposed in [25].

The precise blade geometric design is crucial for obtaining the required main rotor power. As described in [26], the geometric parameters of the blade are the following:

- **Radius** The length of the blade measured from the axis of rotation to the tip;
- **Chord** The length of the blade measured from the airfoil leading edge to the trailing edge and, for a tapered blade, it is the function of local radius;
- **Airfoil** The cross-sectional shape that determines the aerodynamic parameters of the blade, i.e., lift, drag and momentum coefficients;
- **Contour shape** This is the final shape of the blade, which depends on the chord function and tip shape;
- **Geometric twist** Variation of the airfoil angle between the chord and a plane of rotation along the radius;
- **Aerodynamic twist** Variation of the airfoil shape along the radius;
- **Position and shape of trim tabs** Defines the possibility to adjust the rotating blade to the plane of rotation.

The area of a blade root airfoil transfers the whole load from the rotating aerodynamic surface to the blade grip sticking out of a rotor head block. The shape of the root is dictated by the build conception and the adopted aerodynamic solutions. The geometric twist is usually settled on several degrees. The shape of the rotor tip depends on the aerodynamic problems, for example, achieving the speed of sound or the noise level. An analysis of rotor blade tips was described in [27]. According to the mentioned work, there are three main types of helicopter tip designs: BERP tip, the parabolic tip, and the swept (tapered) tip. An example of a main rotor blade is shown in Figure 1.

To evaluate the prepared parametric model, a theoretical lift calculation must be conducted. The lift can be calculated in vertical flight using the blade element theory combined with the momentum theory. The first assumptions are the mass conservation equation for rotor disc:

$$\dot{m} = \rho A v_i \tag{1}$$

and the momentum conservation equation for hoovering rotor:

$$T = \dot{m} w \tag{2}$$

The energy conservation equation is the work of the rotor to change the rate of energy in fluid:

$$T v_i = \frac{1}{2} \dot{m} w^2 \tag{3}$$

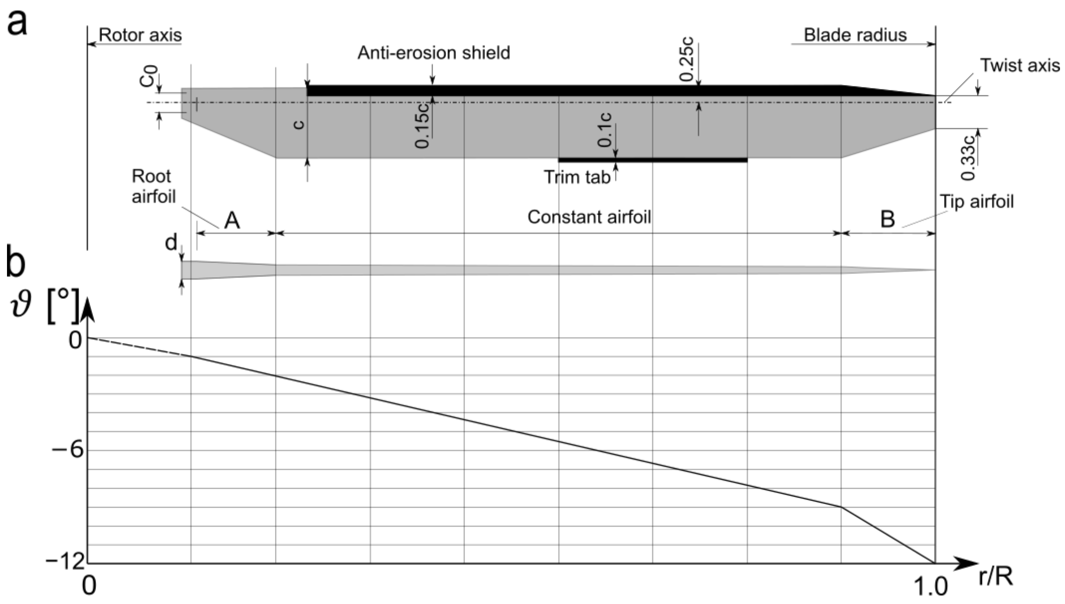

Figure 1. The geometry of the main rotor blade: (**a**) Rotor shape (c, chord and c_0, mounting holes spacing); (**b**) blade parameters ($\alpha_S(r/R)$, geometric twist angle in dependence on nondimensional radius; A and B, airfoil change zone; d, blade thickness) (figure prepared by authors).

The calculation is based on the thrust coefficient, as a function of pitch angle and inflow angle, and is given [28,29]:

$$C_T = \int_0^1 \frac{a\sigma}{2}(\vartheta - \delta)r^2 dr \quad (4)$$

where a is the lift curve slope, σ is the rotor solidity, ϑ is the pitch angle, δ is the inflow angle, and r is the current radius.

According to Figure 2, the inflow angle δ can be defined by:

$$\delta = arctg(\frac{W + v_i}{\Omega r}) \quad (5)$$

where W is the vertical velocity, v_i is the induced velocity, and Ω is the rotor angular velocity.

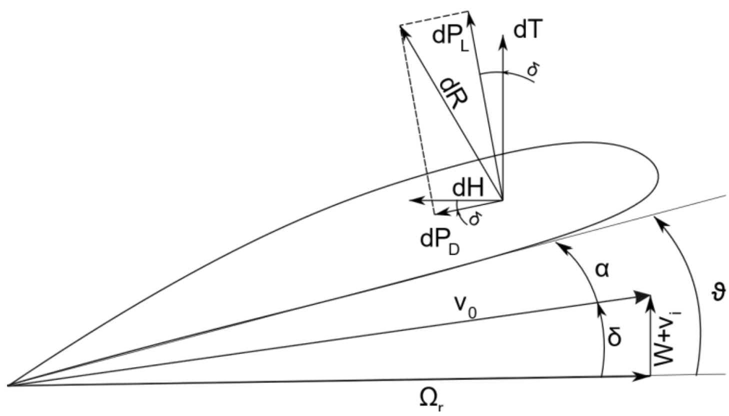

Figure 2. Blade element aerodynamic forces (figure prepared by the authors).

To calculate the induced velocity, for required thrust in hover, the equation solved from the momentum theory is given:

$$v_i = \sqrt{\frac{T}{2\rho A}} \tag{6}$$

where T is the rotor thrust, ρ is the air density, and A is the rotor planform area. For hover, the W velocity equals 0.

The inflow angle can be defined with the inflow ratio as $\lambda_i = \delta/r$, therefore, the thrust coefficient will transform to:

$$C_T = \int_0^1 \frac{a\sigma}{2}\left(\vartheta r^2 - \lambda r\right) dr \tag{7}$$

Rotor performance can be calculated with the combination of the blade element theory with the momentum theory. Therefore, the induced velocity can be determined for nonhomogeneous inflow distribution, by using the differential form of the momentum theory:

$$dC_T = 4\lambda_i \lambda r dr \tag{8}$$

with the blade element theory C_T equation form.

As a result, for hover where $\lambda_c = 0$, the inflow ratio for the induced velocity is:

$$\lambda_i = \frac{a\sigma}{16}\left[\sqrt{1 + \frac{32}{a\sigma}\vartheta r} - 1\right] \tag{9}$$

The σ rotor solidity equation is necessary, which, in this work, is nonuniform along the blade span as a consequence of non constant chord. The rotor solidity is calculated as:

$$\sigma = \int_0^1 \frac{bc(r)}{\pi R} dr \tag{10}$$

where b is the number of blades, $c(r)$ is the chord in function of radius, and R is the rotor radius.

The thrust coefficient is the function of radial location of the blade measured from the centre of rotation to the blade tip. It is calculated as an integral with the r limits from 0 to 1. However, to obtain better quality results, a tip loss factor can be proposed [30]:

$$B = 1 - \frac{ac(r=1)}{2R} \tag{11}$$

The tip loss factor is taken as an upper limit of the coefficient integral. The thrust losses are also a result of the root cutout. It is usually 10% to 30% of the blade radius. Including tip loss factor and root cutout, the thrust integration is:

$$T = \frac{1}{2}\rho a b \Omega^2 R^2 \int_{r_R}^{B} c(\vartheta - \delta) r^2 dr \tag{12}$$

According to [22], the mean lift coefficient for the main rotor blade can be determined:

$$\overline{C}_L = \frac{6C_T}{\sigma} \tag{13}$$

The calculations described above were all prepared in MATLAB. The estimated mathematical thrust model is the basis for the CFD computation evaluation.

The program build is defined using the algorithm presented in Figure 3. The code is constructed as a loop to look for the collective angle required for a given aircraft weight.

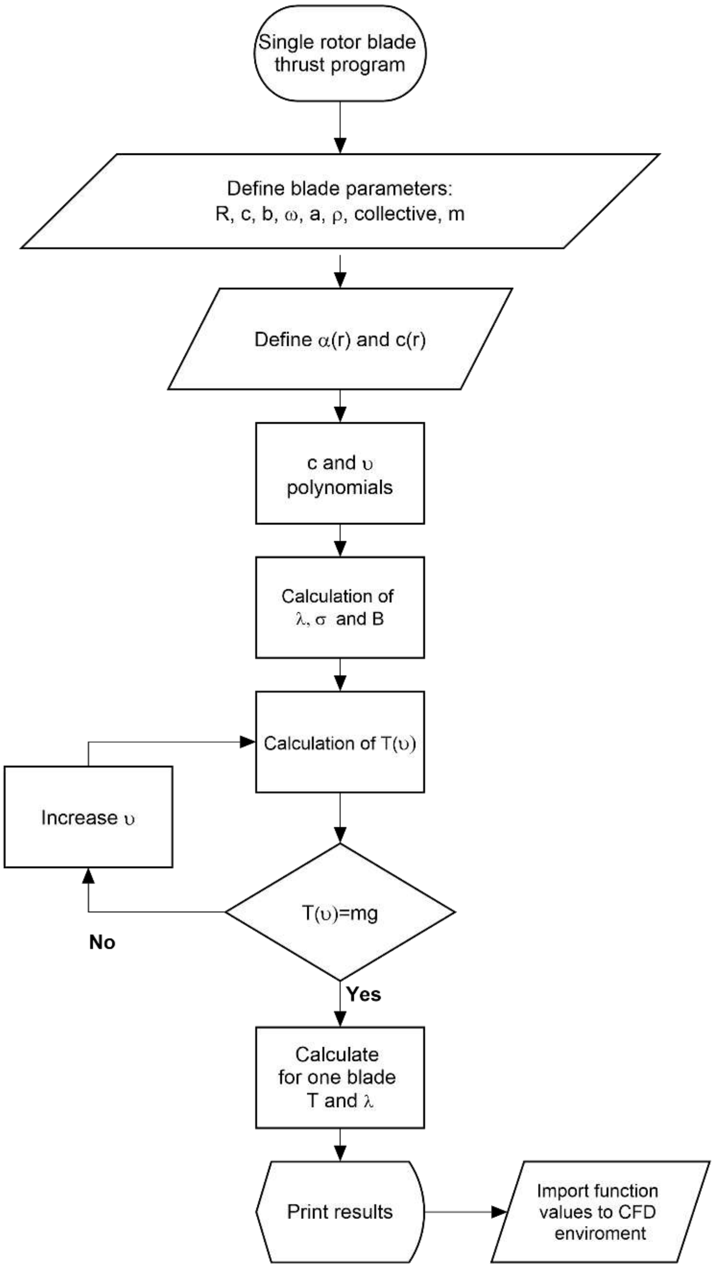

Figure 3. The algorithm developed in Matlab for determining the distribution of the blade's parameters and its aerodynamic thrust.

It starts by defining the input parameters that can be obtained from first cut calculations and the mission flight conditions. In the beginning, the collective is positioned at 0° angle. Next, the position radius coordinates are defined for the twist and chord values in the given sections. The thrust is a radius position integral, and therefore, all program functions are defined as dependent on x. Using the chord and twist values, the chord and twist polynomials are interpolated. These polynomials are also used in the GRIP program to create the blade geometrics. Next, the inflow angle, the rotor solidity, and tip loss factor are given. All the specified equations are inputs to the thrust integral which is bounded by the root cutout and the tip loss factor. The blade attack angle is calculated using the pitch angle with addition of collective. The thrust equation is computed using loop. The collective angle is increased in each step until the result is similar to the hover required force for the assumed mass. The determined collective is used for the CFD analysis to check the parametric model aerodynamic parameters. The procedure described above can be applied for the hover case calculations and for vertical or horizontal flight conditions as well.

To present the possibilities of Matlab calculations for future main rotor optimization, a multi-dimensional analysis was conducted. The main rotor thrusts were calculated for different numbers of blades, twist angles, and mean chord values. The computations were made for the collective angle 7.47°. The distribution of thrust values as a function of twist angle and chord value are shown in Figures 4–6. As predicted, the highest thrust value is obtained for a five-blade rotor, although the reference system is a four-blade rotor, corresponding to the rotor design of the Polish W-3 Sokol helicopter.

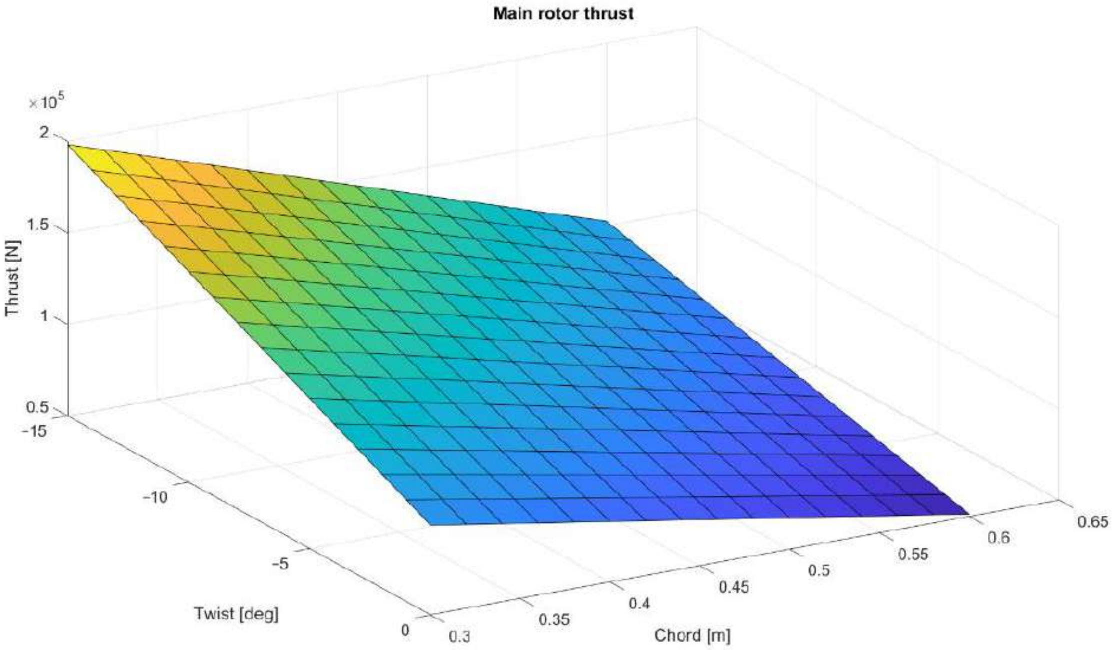

Figure 4. Three-blade rotor thrust distribution as a function of twist and mean chord.

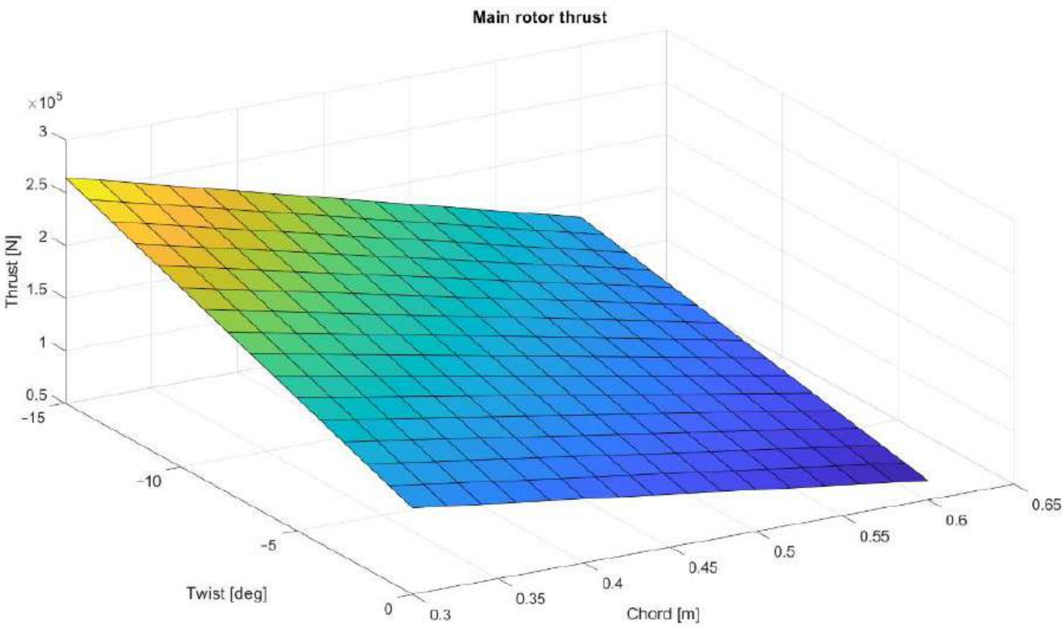

Figure 5. Four-blade rotor thrust distribution as a function of twist and mean chord.

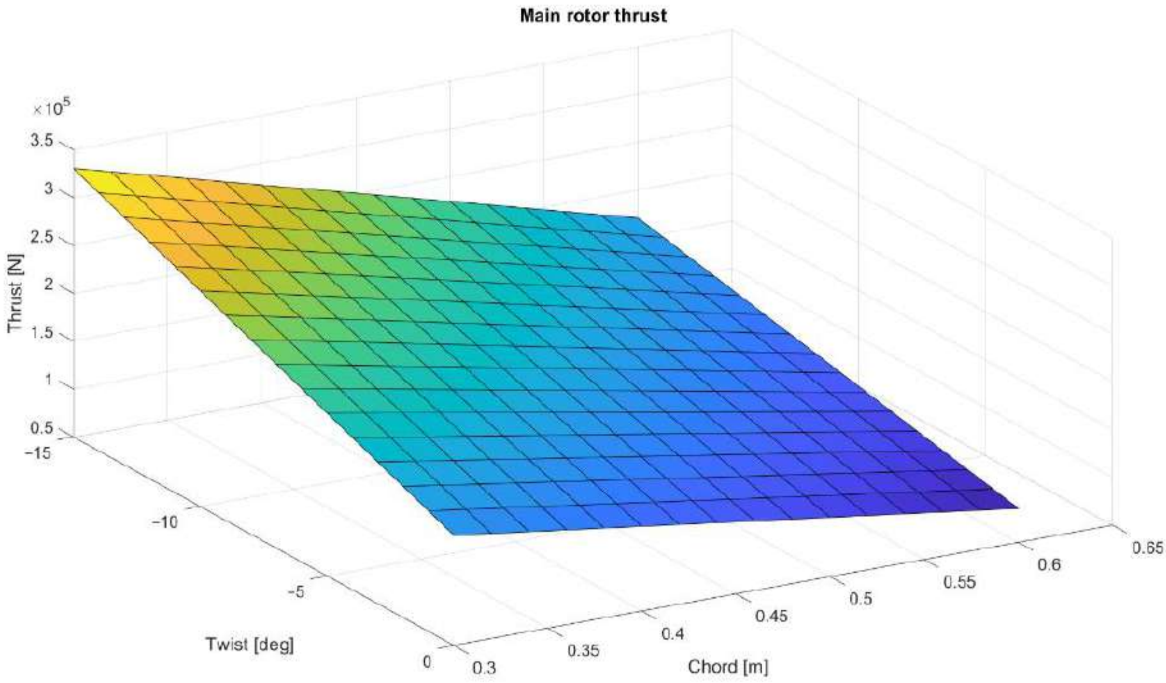

Figure 6. Five-blade rotor thrust distribution as a function of twist and mean chord.

2.2. Modeling the Blade Geometrics and Aerodynamics Using Proprietary Software Applications

The calculations of the blade were performed for an existing main rotor blade of a Polish military W-3 SOKOL helicopter. The model could be easily modified with different parameters. The technical specifications are shown in Table 1, however, some details such as the blade and tip shape (which are provided from design documentation) cannot be published. The simulation was performed for the aerodynamic calculations, therefore, it was modeled as an empty shell only to provide the blade shape.

Table 1. Main rotor technical specifications.

Rotor radius	7.85 m
Blade mean chord	0.44 m
Blade airfoil	NACA 23015
Geometric twist	−12°
Root cutout	0.21R
Root incidence angle	5.34°

Figure 7 shows the original algorithm dedicated to the rotor blade parametric modeling. The rotor blade parametric models were prepared in Siemens NX Open Grip language. It is a programming language that can draw a CAD model with commands and is able to execute advanced customized operations in a more effective way than interactive NX operations. Numerous interactive operations can be executed using GRIP language. It is possible to draw geometric objects using control of parameters or load data from a file to modify the geometrics. Exemplary program code for parametric modeling of the blade geometrics is presented in Listing 1.

Listing 1. Part of GRIP code with blade surface generation.

```
....
SPL3(K+1)=SPLINE/PT0(1..N-1) $$ upper surface
SPL4(K+1)=SPLINE/PT1(1..N-1) $$ lower surface
dfi=fi(4)*cr+fi(3)*cr+fi(2)*cr+fi(1)


MAT=MATRIX/XYROT,-dfi
SPL1(K+1)=TRANSF/MAT,SPL3(K+1)
SPL2(K+1)=TRANSF/MAT,SPL4(K+1)
$$ LN(K+1)=TRANSF/MAT,LN1(K+1)


PT2(K+1)=POINT/ENDOF,XSMALL,SPL1(K+1)
PT3(K+1)=POINT/ENDOF,XLARGE,SPL1(K+1)
PT4(K+1)=POINT/ENDOF,XLARGE,SPL2(K+1)
LN(K+1)=SPLINE/PT3(K+1),PT4(K+1)


DELETE/PT0,PT1,SPL3,SPL4,LN1


IFTHEN/K<M
K=K+1
JUMP/L10:
ELSE
JUMP/L40:
ENDIF


L40:
A=&POINT(PT3(1))
B=&POINT(PT4(1))


SPLC(1)=SPLINE/PT2(1..K+1)
SPLC(2)=SPLINE/PT3(1..K+1)
SPLC(3)=SPLINE/PT4(1..K+1)
SSRF(1)=BSURF/MESH,SPLC(1..2),WITH,SPL1(1..K+1),TYPE,3,TOLER,.01,.01
SSRF(2)=BSURF/MESH,SPLC(1),SPLC(3),WITH,SPL2(1..K+1),TYPE,3,TOLER,.01,.01


SSRF(3) = RLDSRF/SPLC(2),,SPLC(3)


SSRF(4) =RLDSRF/SPL1(1),,SPL2(1)
SSRF(5) =RLDSRF/SPL1(K+1),,SPL2(K+1)
BLD(1)=SEW/SSRF(1..5)
....
```

The program prepared for generating the main rotor blade was easy to modify, and the blade parameters could be changed without needing to repeat an interactive method. The blade radius, chord, chord distribution, twist, and airfoil shape could be easily changed to generate a model with new features. The process of parametric model generation is presented in Figures 8 and 9.

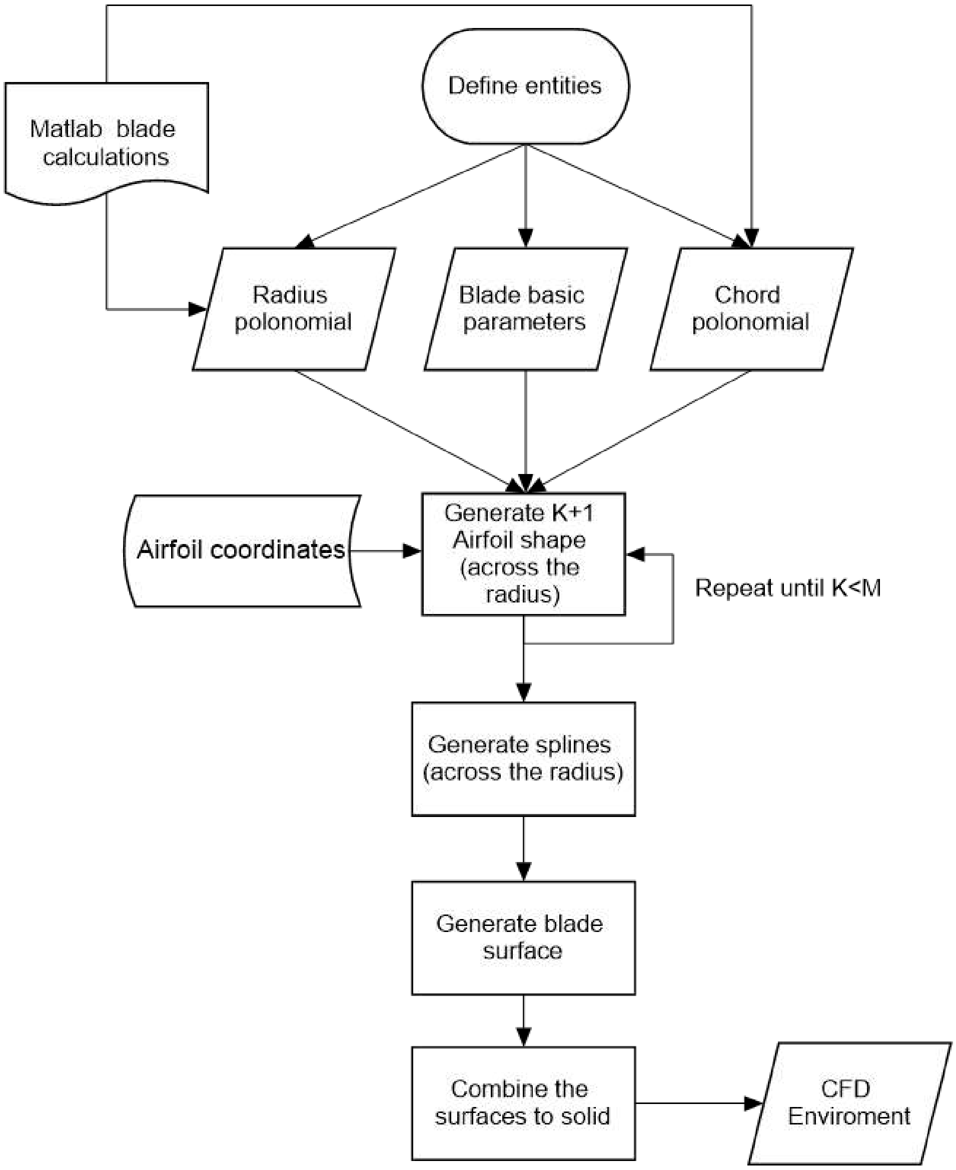

Figure 7. Diagram of the algorithm for parametric programming of the main rotor blade geometrics.

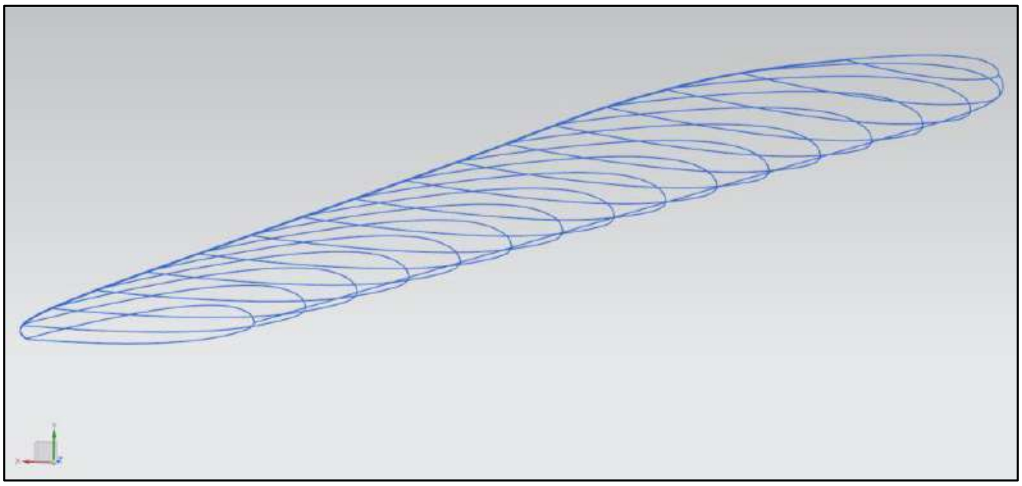

Figure 8. Main rotor blade shape curves.

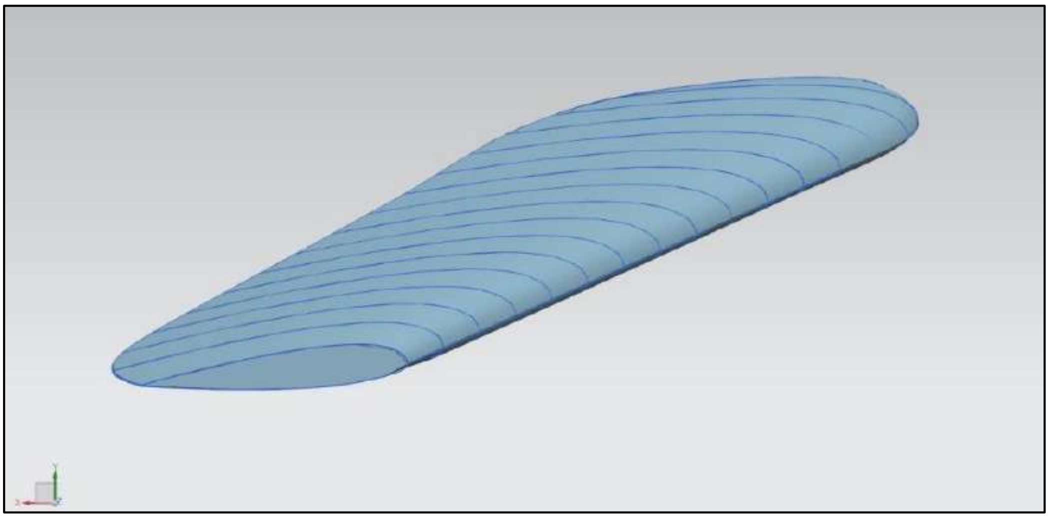

Figure 9. Model generated with defined curves.

2.3. *Aerodynamic Modeling of a Single-Blade and Complete Main Rotor*

The generated model was implemented in two computer environments to evaluate the properties of the obtained blade shape. The main rotor blade was implemented in a CFD software, i.e., ANSYS Fluent and an aerodynamic modeling software, i.e., DARcorporation Flightstream. The domain for CFD was prepared in ANSYS Spaceclaim. The air density in the simulations was 1.25 kg/m^3 and it was constant.

The implementation was conducted to assess the model and to prepare its applicability in further research; however, it was also conducted to compare two different tools for aerodynamic rotorcraft analysis with mathematical calculation. With the results of the CFD analysis, a further strength analysis is possible. In addition, the CFD analysis is a crucial step in the optimization process of a modern main rotor blade design.

2.3.1. One Blade CFD Modeling in ANSYS Fluent

In ANSYS Fluent, a one blade CFD model was prepared. The fluid domain was prepared using Ansys Spaceclaim. It was generated with a quarter of a sphere and half of a cylinder. The air enclosure were 20 m long and high, and the width of the enclosure was 10 m. A hybrid mesh was built for the computational area using the ANSYS Mesh module. Body and face sizing were used with inflation to generate the correct mesh. The boundary layer was modeled using the full thickness option. It was set at 20 mm for 25 layers with a growth ratio of 1.2. The obtained y+ value was 8. The maximum element size was set at 1000 mm, with a size reduction closer to the blade of 20 mm. The 3D bodies were transformed into a tetrahydra mesh with prismatic components within the boundary layer. The mesh consisted of almost 2,837,051 elements. The mesh is shown in Figure 10.

The boundary conditions are presented in Figure 11. The blade is fixed in the enclosure which is modeled by combining half of a hemisphere with a cylinder. In addition, to obtain correct body sizing, a smaller cuboid enclosure was made around the blade, and by naming the object faces, an air flow direction was projected.

To imitate the main rotor blade working environment, velocity change, pitch, and inflow angle were implemented with mathematical expressions. A velocity change was realized by an expression that raised the inflow speed with the span. To model a change in the inflow angle, the inflow directions on the X and Y axes were expressed using the cosine of the X axis and sine of the Y axis. The inflow angle was calculated from the inflow ratio with the Matlab program. Table 2 presents the inflow input function to model the air flow over the blade. The polynomial was a 4th grade polynomial, the higher grades gave similar results. The functions values changed with the span.

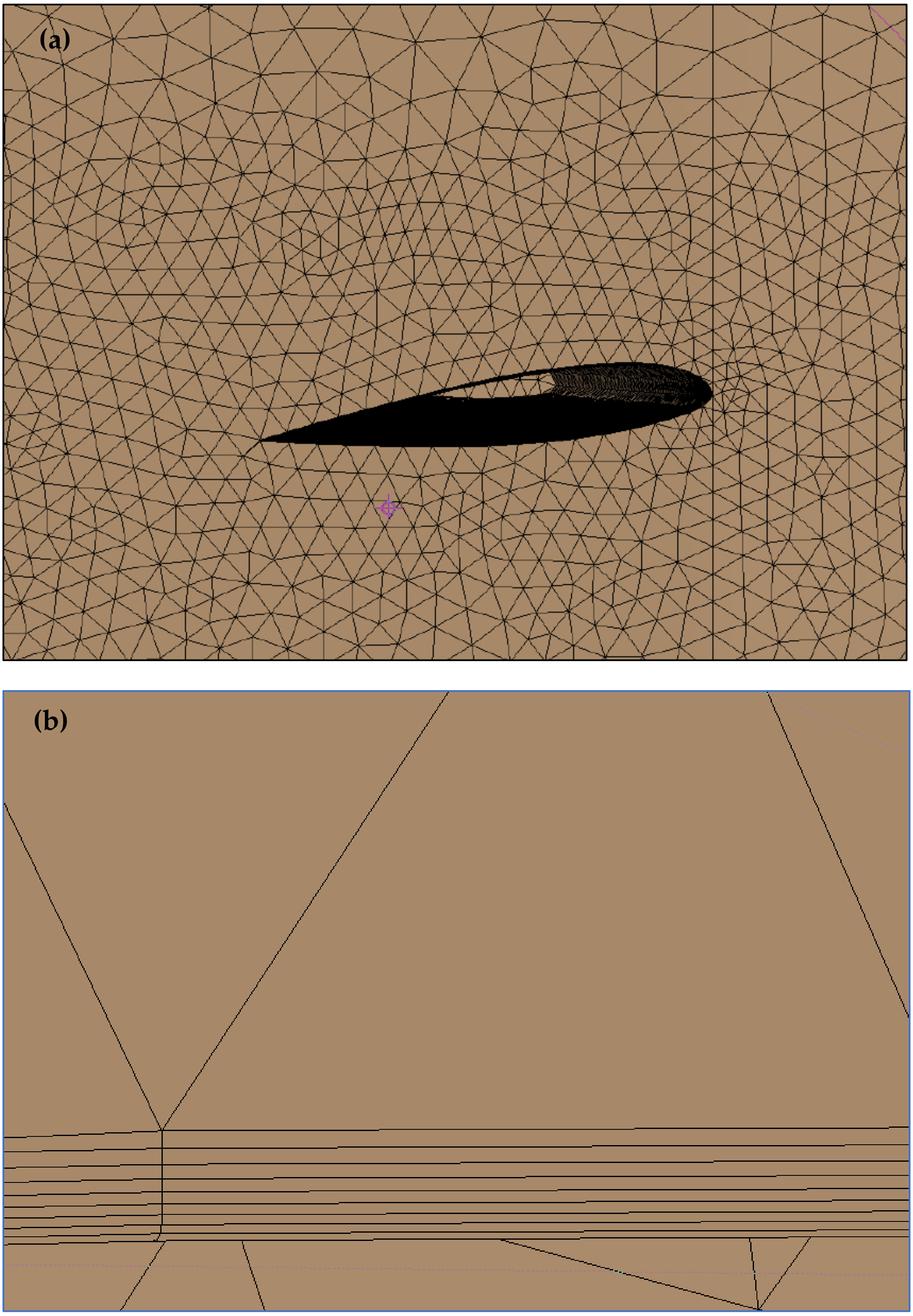

Figure 10. Rotor blade mesh with boundary layer: (**a**) Mesh; (**b**) boundary layer.

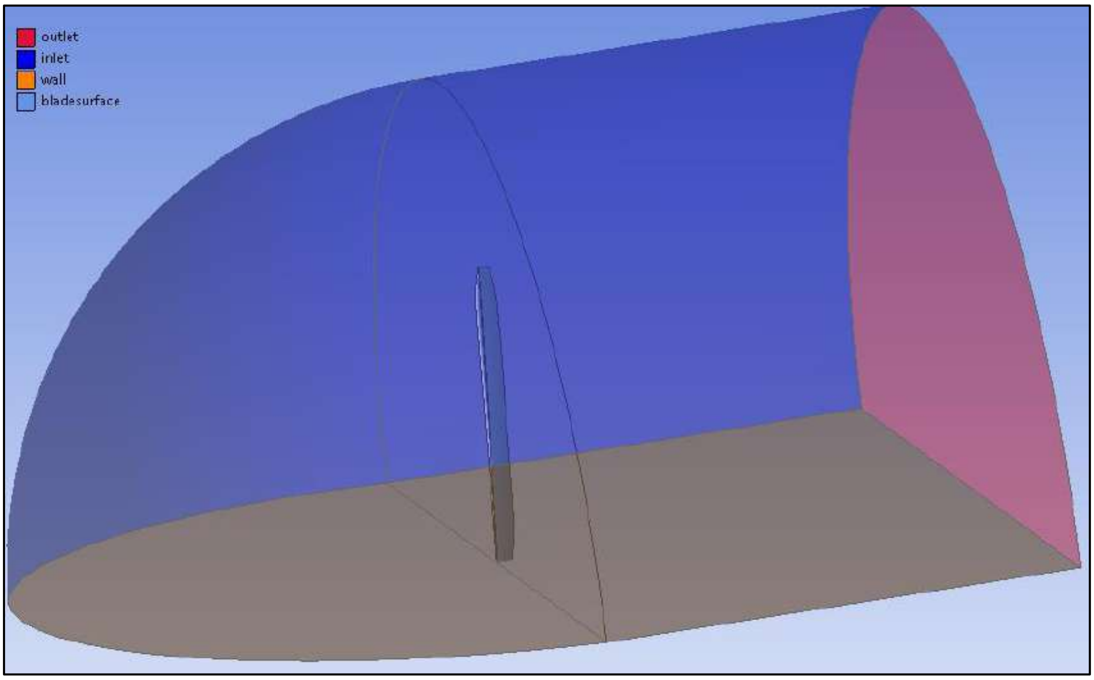

Figure 11. Single-blade model boundary conditions.

Table 2. Example of the inflow functions for the inflow modeling in the FLUENT rotor blade analysis.

Inflow X direction function for 5.96 pitch angle	cos(PI/180 × (5.96 − (−1.40420898843306 × 10^{-5} × (z/7.85[m])^3 + 0.00154624103083247 × (z/7.85[m])^2 − 0.0591574921598430 × (z/7.85[m]) + 1.07777970150355)))
Inflow Y direction function for 5.96 pitch angle	sin(PI/180 × (5.96 − (−1.40420898843306 × 10^{-5} × (z/7.85[m])^3 + 0.00154624103083247 × (z/7.85[m])^2 − 0.0591574921598430 × (z/7.85[m]) + 1.07777970150355)))

The viscosity model which was used for simulations was k-omega SST. It was applied because it is recommended for rotating machinery.

2.3.2. One Blade Panel Modeling in FligtStream

In the second aerodynamic environment, a main rotor blade model was also prepared. The parametric blade model was easily implemented. Software was used to import the CAD files from commercial software, and therefore, the tool could be used in the optimization loop.

In the Flightstream, the mesh is generated only on the studied element. It does not required from user preparing an enclosure and environment. The mesh is generated automatically by the software. Because of the simplicity of the software, the inflow angle and the change of the pitch angle were modeled with the blade position in the reference frame. Velocity change was simulated by the build "shear" freestream option and prepared input .txt file with the velocity magnitude across the span. The advantage of the solver is the fact that the model for conducting a simulation is ready to use three–four times faster than in the Fluent environment. However, rotorcrafts are complex constructions that work in versatile conditions, and therefore, some working states may not be imitated. The solver was setup with steady viscous parameters. The solver setup is shown in Figure 12.

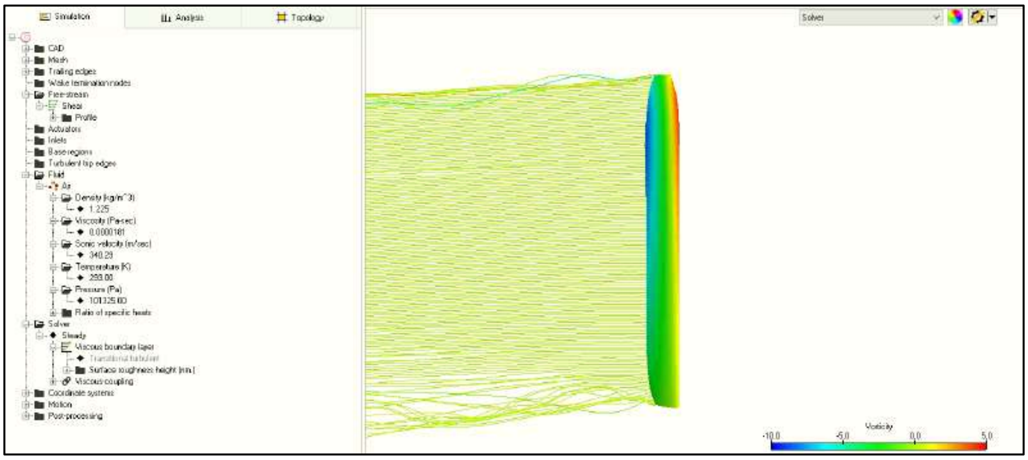

Figure 12. One blade panel code model with solver setup.

2.3.3. Main Rotor CFD Modeling in ANSYS Fluent

In the second stage of the research, the blades were multiplied and positioned in a rotational plane. The fluid domain were also modeled in Spaceclaim. A mesh was built for the computational area using the Mesh Ansys module. The boundary conditions are presented in Figure 12. Body sizing and inflation were used to generate the correct mesh. The boundary layer was modeled using the full thickness option. The air enclosure was 75 m long and wide, and the height of the enclosure was 25 m. The maximum element size was set at 2000 mm, with a size reduction closer to the blade of 20 mm. The boundary layer was modeled using the full thickness option. It was set at 20 mm for 25 layers with a growth ratio of 1.2. The obtained y+ value was 8. The 3D bodies were transformed into a triangular mesh. The mesh consisted of nearly 5,300,000 elements.

The blades were placed in the enclosure which was modeled with cuboid. In addition, to obtain correct body sizing, a smaller cylinder enclosure was made around the blades. By naming the object faces, an air flow direction was projected. The analysis was performed with mesh motion, and therefore, there was no inlet, because the air flow was provoke by the rotating blades. The boundary conditions are presented on Figure 13.

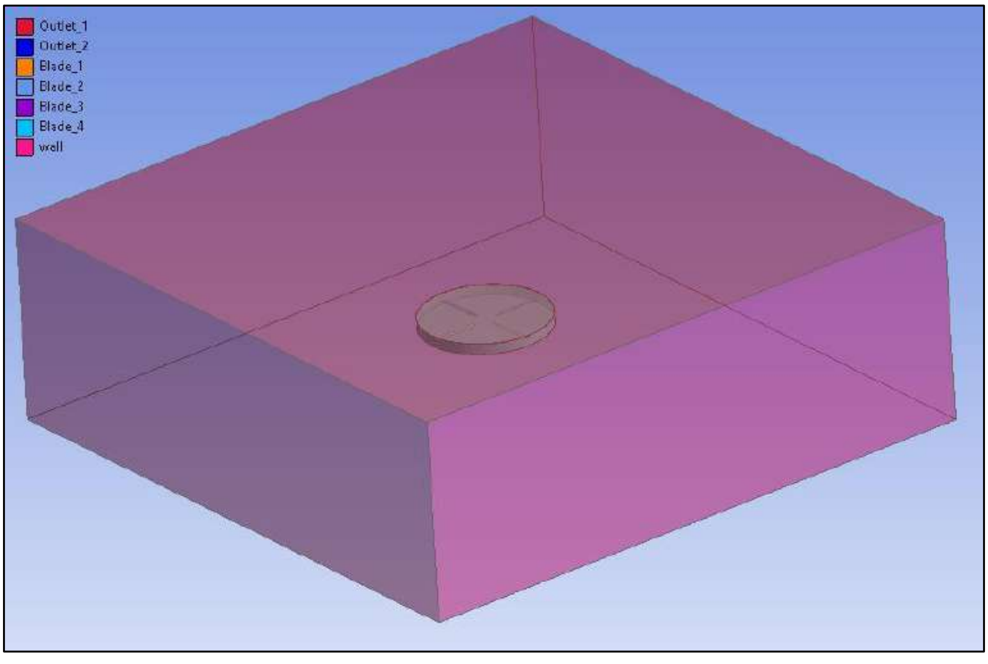

Figure 13. Four blade model boundary conditions.

The blades were set at the pitch angle calculated for the required thrust. The models were set to rotate with the main rotor angular speed. The inflow angle was assumed to be generated in the solver with the rotational movement. The viscosity model for the simulation that produced the most accurate results with the lowest time consumed was realizable k-epsilon with scalable wall function.

2.3.4. Main Rotor Panel Modeling in FligtStream

Since the modeling was performed using CFD software, the panel environment was also tested to provide results for parametric modeling in the optimization procedure. The model building was more time-consuming and it was easy to make a mistake, because the pitch angle and inflow angle were modeled by the blade's position. The blades were multiplied and positioned in a rotational plane. The mesh was generated the same way as it was generated for the one blade case. The cases were calculated with an unsteady solver. The rotational movement was modeled with motion settings, where the angular velocity and rotation axis could be defined.

3. Results

The evaluation results are shown in Tables 1 and 2. In both cases, the parametric model has no issues when implemented. Calculations of the aerodynamic thrust were conducted for selected design weight values corresponding to those from the range of operating weights of the W-3 Sokol helicopter (i.e., between 4900 and 6400 kg).

Table 3 shows the comparison of the results of Fluent and Flightstream stationary blade modeling with mathematical calculations for a given thrust and the required collective angle for that thrust. The collective angles were calculated using thrust Equation (9) using Matlab procedure, combining the blade element theory with the momentum theory. According to the obtained results, shown in Figure 14, CFD modeling resulted in a high accuracy of expected resultant forces; both solvers produced similar results. However, for lower thrust, Flightstream, which is mainly designated to steady simulations, delivered a more accurate result.

During the preparation of the stationary simulation, it is crucial to model the exact inflow conditions. The main advantage of this type of imitation is the short time for the solver calculations. As compared with a four blade rotary model, it provides the results about 9–10 times faster. It also offers the possibility of checking the different collective values and inflow angle using one model and solver settings. This type of simulation is a good choice for evaluating the first cut blade loads.

Table 4 presents the comparison of results from Fluent and Flightstream for the main rotor model with modeled rotational movement. The mathematical assumptions are the same as in the steady model. The results presented in Figure 15 show that, for the rotary model, definitely better results are obtained with the Fluent solver. The Flightstream environment gives the most accurate findings with the unsteady solver, nevertheless, they is a 20% difference btween the mathematical and CFD solver model. The advantage of the Flighstream simulation is the duration of calculation. For the Ansys software, the calculations with mesh preparation last about 3 h (for a 30 threads computer station); with the DARcorporation solver, the simulation with meshing is ready in up to 30 min (with 8 threads). Despite the results, the Flightstream simulation can be used, when a designer needs to take a first look at the rotor aerodynamics behavior. However, to obtain accurate findings, a CFD simulation needs to be conducted.

The rotary model provides the calculations and forces that can be used in further analysis. It can be applied to the strength model and can calculate the required mass parameters to sustain the blade loads. Combining the models' mass loads from rotary motion can also be simulated.

Table 3. Results obtained from analyses of the one blade model.

Simulation Input Parameter			Fluent		Flightstream	
Weight (kg)	Analytical Thrust (N)	Collective (°)	CFD Thrust (N)	Δ (%)	Panel Method Thrust (N)	Δ (%)
6400	15,696	7.47	15,591	0.67%	15520	1.12%
6000	14,715	7.06	14,870	1.05%	14850	0.92%
5600	13,734	6.66	14,041	2.24%	14150	3.03%
5200	12,753	6.26	13,242	3.83%	12602	1.18%
4900	12,017	5.96	12,592	4.78%	12133	0.96%

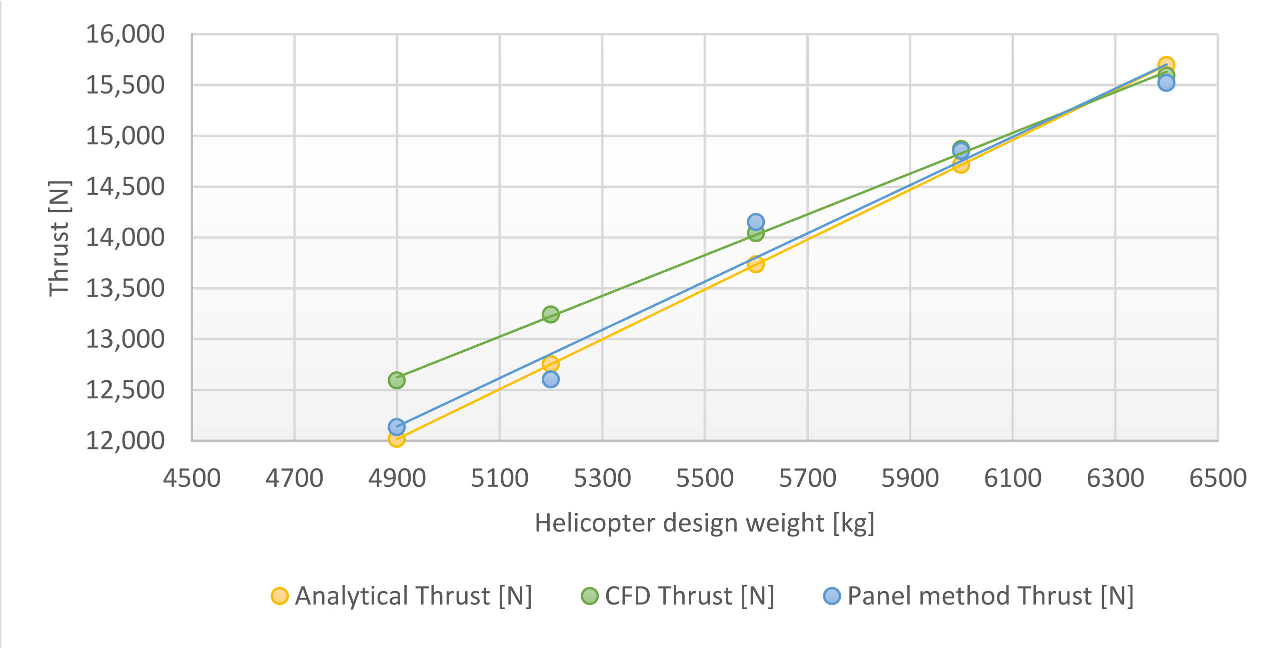

Figure 14. Line graphs of aerodynamic thrust dependencies for the one blade model.

Table 4. Results obtained from analyses of the complete rotor model.

Simulation Input Parameter			Fluent		Flightstream	
Weight (kg)	Analytical Thrust (N)	Collective (°)	CFD Thrust (N)	Δ (%)	Panel Method Thrust (N)	Δ (%)
6400	62,784	7.47	64,472	2.69%	74186	18.16%
6000	58,860	7.06	58,504	0.60%	71112	20.82%
5600	54,936	6.66	55,862	1.69%	68917	25.45%
5200	51,012	6.25	52,044	2.02%	63205	23.90%
4900	48,069	5.95	49,175	2.30%	59462	23.70%

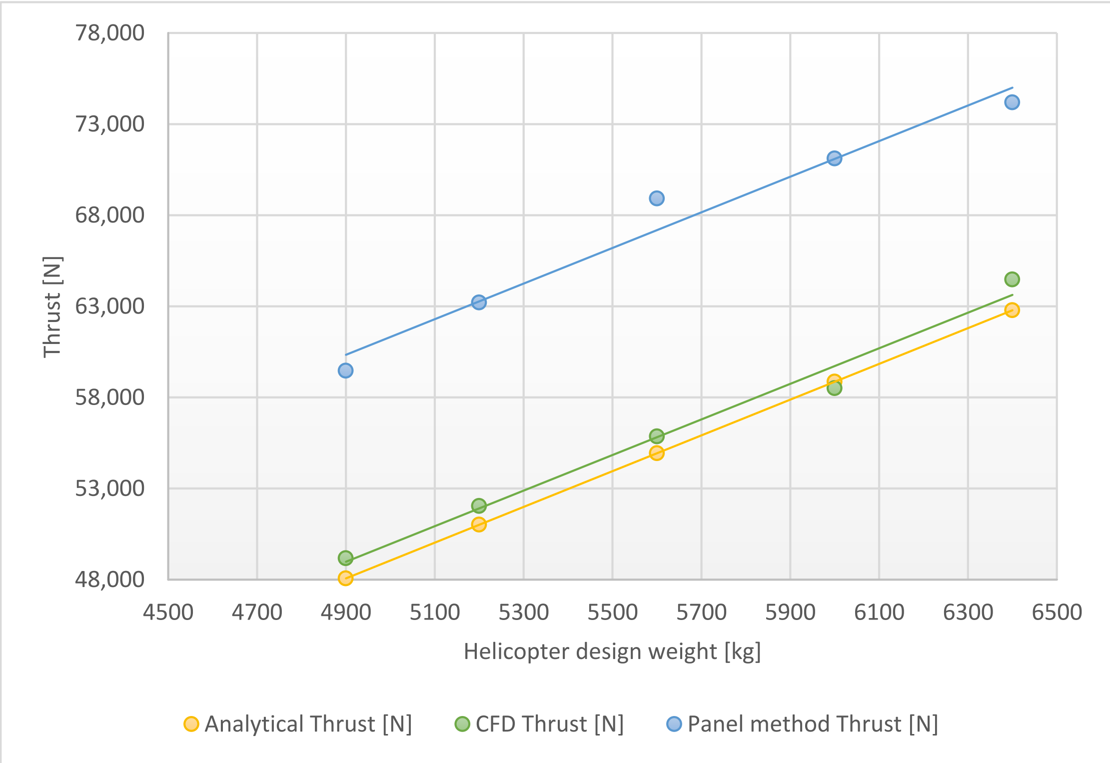

Figure 15. Line graphs of aerodynamic thrust dependencies for the complete rotor model.

4. Conclusions

As stated in the Introduction, this work is part of an aerospace construction optimization research program. It is the second step in preparing the optimization loop for rotorcraft constructions.

In this research, it was confirmed that graphical programming language with a user-friendly syntax is a good solution for this type of geometric modeling. The commands are intuitive and easy to use. The code is short and the blade model is generated within a few seconds. In addition, the language offers an inertia analysis for solids, which is planned to be used in future research on the optimal blade design. The generated model was versatile and easy to adjust in different environments. There were no compatibility problems with the CFD solvers.

The parametric model behaved as it was assumed. The CFD analysis confirmed that the generated shape had the aerodynamic features that were preferred during the design phase. The mathematical assumptions of the inflow angle were confirmed with the rotary CFD model.

This research shows a new approach to rotor blade inflow modeling. The stationary blade with complex air flow analytical model gives correct results and consumes less computer power and time. Therefore, it is possibile to implement this type of simulation in the preliminary design of a main rotor, which is useful in optimization studies. Combining the stationary blade with parametric modeling is the first stage of optimization to evaluate a construction and to enhance the first cut shape. This method provides an initial shape in a short period of time. Therefore, even when the calculations are combined with mechanical analysis (FSI), the analysis time is reduced. Finally, the iterative procedure for optimization studies is proposed in Figure 16. In the first phase, the CFD model can be replaced with a panel code environment. To summarize, the results of this study can serve as a basis for developing a main rotor aerostructural model (combining aerodynamic properties and finite element structure) for further strength analysis, where both the aerodynamic and weight loads can be considered. In future work, in accordance with the research program, the CFD and FE model will be combined using scripting methods to prepare an optimization loop to find a design shape that fulfils modern combat field requirements and offers the best mass properties.

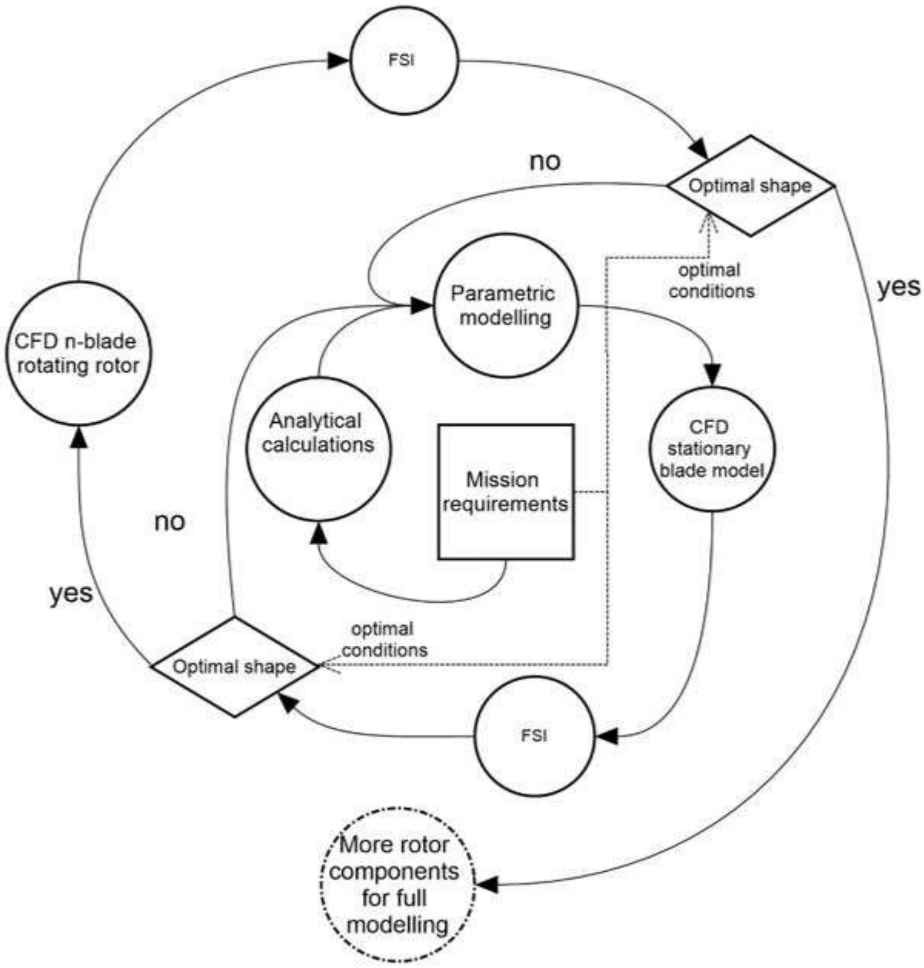

Figure 16. Graphical proposal of design spiral with results of the studies.

Author Contributions: Conceptualization, J.K., R.R. and S.K.; methodology, J.K.; software, J.K.; validation, R.R. and J.K.; formal analysis, J.K.; writing—original draft preparation, J.K.; writing—review and editing, R.R.; visualization, J.K.; supervision, S.K.; project administration, S.K. All authors have read and agreed to the published version of the manuscript.

Funding: The methods and results presented in this paper have been obtained during research works conducted within the university research project entitled "Methods of optimal design of aircraft and helicopters in application to improve their design and aerodynamic properties". This work was financed by the Military University of Technology (Warsaw, PL), in 2022, under research project UGB-782.

Institutional Review Board Statement: Not applicable.

Informed Consent Statement: Not applicable.

Data Availability Statement: Program code is available at: https://github.com/jakubkocjan/parametricrotordesign (accessed on 30 March 2022).

Acknowledgments: The present work was conducted as part of the Aerospace Constructions research program. The authors gratefully acknowledge their support.

Conflicts of Interest: The authors declare no conflict of interest.

Nomenclature

A	Main rotor disc area
a	Main rotor blade lift curve slope
B	Tip loss factor
b	Number of blades
C_L	Lift coefficient
C_T	Thrust coefficient
c	Blade chord
$\dot{m}$	Mass flux through the rotor disc
R	Main rotor blade total radius
r	Main rotor blade current radius position
T	Main rotor thrust
v_i	Main rotor induced velocity in hover
w	Rotor induced velocity in far wake
W	Climb velocity
δ	Inflow angle
ρ	Air density
λ	Total inflow ratio
λ_c	Climb inflow ratio
λ_i	Induced inflow ratio
σ	Rotor solidity
ϑ	Pitch angle
Ω	Rotor angular velocity

Abbreviations

CAD	Computer-aided design
CAM	Computer-aided manufacturing
CAE	Computer-aided engineering
CFD	Computational fluid dynamics
GRIP	Graphic integrated programming
FSI	Fluid structure interaction
BERP	British engineering rotor program
MATLAB	Matrix laboratory-multi-paradigm programming language and numerical computing environment
SIEMENS NX	CAD/CAM/CAE software developed from Unigraphics system

References

1. Stalewski, W.; Zalewski, W. Performance Improvement of Helicopter Rotors through Blade Redesigning. *Aircr. Eng. Aerosp. Technol.* **2019**, *91*, 747–755. [CrossRef]
2. Sagimbayev, S.; Kylyshbek, Y.; Batay, S.; Zhao, Y.; Fok, S.; Lee, T.S. 3D Multidisciplinary Automated Design Optimization Toolbox for Wind Turbine Blades. *Processes* **2021**, *9*, 581. [CrossRef]
3. Ma, L.; Zhao, Q.; Zhang, K.; Zhang, X.; Zhao, M. Aeroelastic Analysis and Structural Parametric Design of Composite Rotor Blade. *Chin. J. Aeronaut.* **2020**, *34*, 336–349. [CrossRef]
4. Fitzgibbon, T.A.; Woodgate, M.A.; Barakos, G.N. Practical Considerations in Rotor Design Optimisation. In Proceedings of the 47th European Rotorcraft Forum, Virtual, 7–9 September 2021.
5. Lim, J.W. Application of Parametric Airfoil Design for Rotor Performance Improvement. In Proceedings of the 44th European Rotorcraft Forum 2018, ERF 2018, Delft, The Netherlands, 18–21 September 2018; Volume 1.
6. Vu, N.A.; Lee, J.W. Aerodynamic Design Optimization of Helicopter Rotor Blades Including Airfoil Shape for Forward Flight. *Aerosp. Sci. Technol.* **2015**, *42*, 106–117. [CrossRef]
7. Allen, L.D.; Lim, J.W.; Haehnel, R.B.; Dettwiller, I.D. Rotor Blade Design Framework for Airfoil Shape Optimization with Performance Considerations. In Proceedings of the AIAA SciTech 2021 Forum, Online, 11–15 January 2021.
8. Tixadou, E. Optimisation of the structure of a helicopter blade in view of reducing cabin vibration. In Proceedings of the 47th European Rotorcraft Forum, Virtual, 7–9 September 2021.
9. Гребеников, А.Г.; Дьяченко, Ю.В.; Коллеров, В.В.; Коцюба, В.Ю.; Малков, И.В.; Урбанович, В.А.; Воронько, И.А. Analysis of Design and Technological Features of the Main Rotor Blades of Heavy Transport Helicopters. *Open Inf. Comput. Integr. Technol.* **2021**, *93*, 59–103. [CrossRef]

10. Bailly, J.; Bailly, D.; Didier, B. Multifidelity Aerodynamic Optimization of a Helicopter Rotor Blade. *AIAA J.* **2019**, *57*, 3132–3144. [CrossRef]
11. Roy, A.M. Finite Element Framework for Efficient Design of Three Dimensional Multicomponent Composite Helicopter Rotor Blade System. *Eng* **2021**, *2*, 69–79. [CrossRef]
12. Ryazanov, A.I. Automated 3D Modeling of Working Turbine Blades. *Russ. Eng. Res.* **2016**, *36*, 751–754. [CrossRef]
13. Shabliy, L.S.; Dmitrieva, I.B. Conversion of the Blade Geometrical Data from Points Cloud to the Parametric Format for Optimization Problems. *ARPN J. Eng. Appl. Sci.* **2014**, *9*, 1849–1853.
14. Grabowik, C.; Kalinowski, K.; Kempa, W.; Paprocka, I. A Method of Computer Aided Design with Self-Generative Models in NX Siemens Environment. In Proceedings of the IOP Conference Series: Materials Science and Engineering, Mamaia, Romania, 17–20 June 2015; Volume 95.
15. Stalewski, W. *Design and Aerodynamic Optimization of Rotorcraft (Polish Translated)*; Institute of Aviation: Warsaw, Poland, 2017.
16. Stalewski, W.; Zalewski, W. Aerodynamic Design and Optimisation of Main Rotors for Light Rotorcrafts. In Proceedings of the 45th European Rotorcraft Forum 2019, ERF 2019, Warsaw, Poland, 17–20 September 2019; Volume 1.
17. Tamer, A.; Yücekayali, A.; Ortakaya, Y. Design and Optimization of Helicopter Rotor for Minimum Power Required. In Proceedings of the 6th AIAC Ankara International Aeropsace Conference, Ankara, Turkey, 14–16 September 2011.
18. Xie, J.; Xie, Z.; Zhou, M.; Qiu, J. Multidisciplinary Aerodynamic Design of a Rotor Blade for an Optimum Rotor Speed Helicopter. *Appl. Sci.* **2017**, *7*, 639. [CrossRef]
19. Slavik, S.; Klesa, J.; Brabec, J. Propeller Selection by Means of Pareto-Optimal Sets Applied to Flight Performance. *Aerospace* **2020**, *7*, 21. [CrossRef]
20. Kachel, S.; Rogólski, R.; Kocjan, J. Review of Modern Helicopter Constructions and an Outline of Rotorcraft Design Parameters. Problems of Mechatronics. *Armament Aviat. Safety Eng.* **2021**, *12*, 27–52.
21. Pölzlbauer, P.; Kümmel, A.; Desvigne, D.; Breitsamter, C. Numerical Investigation of an Optimized Rotor Head Fairing for the RACER Compound Helicopter in Cruise Flight. *Aerospace* **2021**, *8*, 66. [CrossRef]
22. Samad, A.; Tagawa, G.B.S.; Morency, F.; Volat, C. Predicting Rotor Heat Transfer Using the Viscous Blade Element Momentum Theory and Unsteady Vortex Lattice Method. *Aerospace* **2020**, *7*, 90. [CrossRef]
23. Lei, Y.; Huang, Y.; Wang, H. Aerodynamic Performance of an Octorotor SUAV with Different Rotor Spacing in Hover. *Processes* **2020**, *8*, 1364. [CrossRef]
24. Spyropoulos, N.; Papadakis, G.; Prospathopoulos, J.M.; Riziotis, V.A. Investigating the Level of Fidelity of an Actuator Line Model in Predicting Loads and Deflections of Rotating Blades under Uniform Free-Stream Flow. *Appl. Sci.* **2021**, *11*, 12097. [CrossRef]
25. Truong, K.V. Modeling Aerodynamics, Including Dynamic Stall, for Comprehensive Analysis of Helicopter Rotors. *Aerospace* **2017**, *4*, 21. [CrossRef]
26. *Wstęp do Konstrukcji Śmigłowców: Praca Zbiorowa*, 2nd ed.; Wydawnictwa Komunik. i Łączn.: Warszawa, Poland, 2002; ISBN 8320611571.
27. Brocklehurst, A.; Barakos, G.N. A Review of Helicopter Rotor Blade Tip Shapes. *Prog. Aerosp. Sci.* **2013**, *56*, 35–74. [CrossRef]
28. Seddon, J.; Newman, S. *Basic Helicopter Aerodynamics*; John Wiley & Sons, Ltd.: Hoboken, NJ, USA, 2011.
29. Johnson, W. *Helicopter Theory*; Dover Publications: New York, NY, USA, 1994; Volume 12.
30. Bramwell, A.R.S.; Done, G.; David, B. *Bramwell 's Helicopter Dynamic*; Elsevier: Amsterdam, The Netherlands, 2001.

JOURNAL OF THEORETICAL AND APPLIED MECHANICS
61, 4, pp. 793-805, Warsaw 2023
https://doi.org/10.15632/jtam-pl/171748

PARAMETRIZATION OF THE MAIN ROTOR AND WORKING ENVIRONMENT FOR DIFFERENT FLIGHT CONDITIONS – COMPUTATIONAL FLUID DYNAMICS ANALYSIS AS AN APPLICATION FOR MULTIDISCIPLINARY OPTIMIZATION

Jakub Kocjan
Military University of Technology, Doctoral School, Warsaw, Poland
e-mail: jakub.kocjan@wat.edu.pl (corresponding author)

Stanisław Kachel, Robert Rogólski
Military University of Technology, Faculty of Mechatronics, Armament and Aerospace, Warsaw, Poland
e-mail: stanislaw.kachel@wat.edu.pl; robert.rogolski@wat.edu.pl

The paper shows a method of aerodynamic modelling of the whole rotor and exemplary results obtained from complex analyses. The analytical basis of rotor aerodynamics for different phases of the helicopter flight is shown. The analytical calculations are provided to model a single blade motion according to its azimuth angle and to validate the obtained results. The parametric design method is shown to be applied for different blade planform shapes and various section airfoils. The Computational Fluid Dynamics (CFD) fluid domain for the flow around the blade is also prepared using a parametric method. The parametric graphic script is developed to create the flow domain for a one-blade simulation or for a complete n-bladed rotor effect. The obtained blade model with enclosure is implemented into CFD environment. The method for fluid mesh preparation and the way of defining its properties are given. The simulation is carried out as transient for the n-bladed rotor. In this simulation, various flight conditions are taken into account. Real rotary motion of the blades is simulated with artificially enforced mesh motion. The obtained numerical results are compared then with analytical assumptions. The simulation findings which are the inputs for further analysis are shown with graphical representations. As an output of the research, new options for main rotor optimization are developed. The usage of combined parametric modelling confirmed with aerodynamic analysis for different flight conditions is shown in the work as a new perspective for design optimization of the main rotor.

Keywords: helicopter, main rotor, rotor blade, geometric modelling, computational fluid dynamics (CFD)

1. Introduction

The Russian invasion on Ukraine revised the usage of helicopters on modern battlefield. The need of preparing constructions that are capable to provide better features for comprehensive military operations is observed more than in any other conflict in XXI's century. As a consequence, a lot of countries are improving existing structures and searching for brand new solutions of VTOL vehicles (Oh *et al.*, 2021). Therefore, also in Polish Military University of Technology, a development of rotorcraft design methods is being conducted as an activity included in a complex research program which is aimed at finding new approaches and design solutions for needs of structural or aeroelastic optimization. This work is a second part of the recalled research program. The first one was focused on preparing a parametric blade model and its analytical and CFD validation for further analysis. The research were preceded with comparative analysis of commonly used helicopter configurations. The results of evaluation and proposals for construction improvements were published in (Kachel *et al.*, 2021).

The parametrization of the blade provides a less time-consuming solution for the preliminary design phase. The advantages of parametric blade modeling were demonstrated in numerous publications including (Sagimbayev *et al.*, 2021; Ma *et al.*, 2021). What is more in this stage of the study, the fluid enclosures for CFD analysis are also parametrized and generated by the prepared program. The usage of parametric models to fulfill the required features of shape and structure is shown in (Lim, 2018; Allen *et al.*, 2021) for airfoil design, (Tixadou, 2021; Grebenikov *et al.*, 2021) for strength design and (Bailly *et al.*, 2019) for aerodynamics. Some model tasks from the above works defined with parametrization declared both for aerodynamic shape, blade structure and fluid domain are highly advanced numerical problems. Solving such problems generally demands applying Fluid Structure Interactions (FSI) techniques, which gives optional results varied due to different design configurations. Simulations of the rotor aerodynamic and aeroelastic effects, taking into account sensitivity analysis due to key design parameters, significantly support the decision-making process in relation to the selection of optimal utility variants.

In the research described here, for preparation parametric models and fluid enclosures, some specific programming language was used. Examples of parametrization in the modelling using GRIP language were shown in (Ryazanov, 2016; Shabliy and Dmitrieva, 2014; Grabowik *et al.*, 2015). Open GRIP (Graphic Interactive Programming) available in Siemens NX CAD environment is a language that provides a possibility to create an external solid body or internal structure geometry of any airframe part. Virtual elements are generated with the use of commands and parameters defined with a specific programming code. The GRIP language is dedicated for research processes, because it grants an option for inertia properties of the generated model. The obtained model features can be used for aerodynamic or strength analyses carried out in further stages of the simulations. The logical conditions that are enclosed in the program code can be used to prepare loops which will provide a possibility of strength calculation with fitting the best dimensions. As an output, a geometry generator is prepared with initial optimization functions. Other main rotor optimization studies with focusing on aerodynamic optimization were presented in (Stalewski, 2017a,b; Xie *et al.*, 2017; Stalewski and Zalewski, 2019; Okumuş *et al.*, 2022) while optimization procedure for best flight performance was shown in (Slavik *et al.*, 2029).

The aim of the research presented herein is to analyze the aerodynamic rotor model in different flight conditions. The new approach is to provide geometry with enclosures prepared to be applied into CFD environment, where different flight conditions with real main rotor motion could be evaluated and compared. One of the examples of CFD usage for strength analysis was presented in (Spyropoulos *et al.*, 2021). There are some main research institutes that are focused on main rotor optimization problems, ONERA French Aerospace Lab and DLR German Aerospace Center for instance. They published several methods of solving the optimization problem using CFD methods (Goerke *et al.*, 2012; Wilke, 2021; Jain, 2022). However, there were no parametrization of the rotor blade shape, position and entire fluid domains simultaneously for given flight conditions, which is the main goal of this research in order to provide a comprehensive tool for future combined optimization solutions.

As it was mentioned above, the solutions for the optimization process which are being developed in the mentioned research program, started with evaluating the blade and assessing the methods for further analysis. The preliminary results from the initial stage of investigations were published in (Kocjan *et al.*, 2022). In this research, geometry of the existing rotor was taken as an example for evaluating the proposed solution. The GRIP program code for the modeling was developed by adding the option for enclosures preparation and expand possibilities to enter more parameters of the main rotor by end-user. The dimensions of enclosures are adequate to rotor dimensions.

The prepared model will be a basis for fluid dynamics computation using Ansys Fluent. The parameters of main rotor movement will be calculated from analytic formulae. The value of collective pitch control and a change of cyclic control are calculated with the use of a MATLAB code. Then the calculated values are inputs for CAD model generation and then for CFD motion simulation. Furtherly, the mesh for numerical simulation is generated with the Fluent meshing tool. The mesh size decreases as it approaches the blade surface. The inflation model is also applied. In the research, a poly-hexcore mesh was used. The prepared mesh is configured for calculation using sliding mesh options. The mesh motion is described with outcomes of analytical calculations, which were earlier prepared. During the studies, the mesh size was adapted to obtain best results within a reasonable time. The results were compared with the assumptions. The lift and drag values were used to evaluate the model and to check if the parametrized rotor model with air domains is applicable to CFD environment and if the obtained numerical results, especially pressure distributions, are reasonable and eventually acceptable. To the best of co-authors' knowledge, similar research merging the proposed methods for the helicopter main rotor design and main rotor optimization operation has not been performed so far.

This paper is organized in a specifically intended way. The research methods are described in Sections 2 and 3, where the mathematical model, which is the basis for parametric programming, is defined. In Section 3, the parametric programming is described. The mesh properties and simulation setup are presented in Section 4. The results and evaluation of the method is discussed in Section 5. The research methods and outputs, with application to next phases of the program are concluded in Section 6.

2. Analytical model for parametrization

2.1. Mathematical model

The conditions of operation of the main rotor are complex and impose on a designer a necessity to check all of the working aspects. Before performing, an optimization loop for parametrization of main rotor features must be introduced.

The first data to be introduced are blade parameters. To obtain required operational capabilities, the blades construction requires to take into consideration both geometric and aerodynamic characteristics. The flow periodic changes, flexibility of blades and conditions of operation in the presence of a strong centrifugal force imply a relationship between pressure loads and deformations of the material. The blades were well parametrized in the previous step of the research (Kocjan *et al.*, 2022), the deformations are going to be considered in the further phases.

In the presented studies, the conditions of the n-bladed main rotor operation are analyzed and transformed as input parameters for geometry generation and numerical CFD simulation. To prepare a rotor model which is ready to be implemented into Ansys Fluent, in accordance with (Johnson, 1994; Bramwell *et al.*, 2001), pitch angles should be calculated for the main rotor trim conditions. The trim of the rotor is calculated from the thrust, pitching moment for lateral and longitudinal movement

$$\theta(\psi) = \theta_0 - A_1 \cos\psi - B_1 \sin\psi \tag{2.1}$$

where the angles are calculated for different flight conditions. The helicopter speed is given in calculation as a dimensionless speed ratio. To find the longitudinal cycling pitch angle, the first step is to calculate the H-force coefficient in the disc plane

$$h_{cD} = \frac{1}{4}\mu\delta \tag{2.2}$$

As a result, the disc incidence can be calculated as follows

$$\alpha_D = -\frac{1}{w_c}\Big(\frac{1}{2}\mu^2 d_0 + h_{cD}\Big) \tag{2.3}$$

where d_0 is the fuselage drag ratio and w_c is the weight coefficient. Now the mean inflow ratio relative to the disc plane can be obtained in the following way

$$\lambda_D = (\mu\alpha)_D - \lambda_i \tag{2.4}$$

The next step for the rotor trim is to calculate the collective pitch angle which will be used for GRIP program to prepare the main rotor geometry installed for designated flight conditions. The collective pitch is calculated from the main rotor thrust expression

$$t_{cd} = \frac{a}{4}\left(\frac{2}{3}\theta_0\frac{1-\mu^2+\frac{9\mu^4}{4}}{1+\frac{3\mu^2}{2}} + \lambda_D\frac{1-\frac{\mu^2}{2}}{1+\frac{3\mu^2}{2}}\right) \tag{2.5}$$

Further, in order to obtain the longitudinal cycling pitch angle, it is crucial to calculate the flapping coefficient

$$a_1 = \frac{2\mu\Big(\frac{4\theta_0}{3} + \lambda_D\Big)}{1+\frac{3\mu^2}{2}} \tag{2.6}$$

Therefore, the B_1 angle (with the assumptions for a change of the center of gravity – h and f) is ready to be calculated

$$B_1 = \frac{a_1 + C_{mf} + h_{cD}h - w_c f}{w_c + C_{ms}} \tag{2.7}$$

where C_{mf} is the pitching moment coefficient for fuselage and C_{ms} is the pitching moment coefficient due to hinge offset. Then, to get the lateral cyclic pitch angle, the lateral flapping coefficient should be given with the following expression

$$b_1 = \frac{\frac{4}{3}(\mu a_0 + 1.1v^2\lambda_i)}{1+\frac{\mu^2}{2}} \tag{2.8}$$

In consequence, the lateral cyclic pitch angle can be written as

$$A_1 = -b_1 - \frac{w_c f + \frac{T_t}{W}t_c h_t}{t_c h + C_{ms}} \tag{2.9}$$

At the end of analytical consideration, for the main rotor evaluation, its drag force is needed and it can be calculated from the expression

$$D = \frac{P}{V} + X \tag{2.10}$$

where P is the power required for the evaluated flight conditions, X is a force acting in the longitudinal direction. The X-force can be estimated with the formula

$$X = -T\sin\alpha_D - H_D\cos\alpha_D$$

2.2. Analytical calculations for preparing the simulation

All calculation formulae described above were all prepared in MATLAB software. The outputs of calculations are a basis for geometry generation in GRIP program and then for model configurations applicable in Ansys Fluent.

It starts with the input parameters of the designed blade and flight conditions. The blade planform is defined with a specific polynomial function. Next, the rotor solidity factor is calculated as an integral. Using MATLAB functions required for the collective pitch are possible to be established. The weight coefficient, fuselage drag ratio, inflow velocity and disc incidence are computed. After that, the inflow ratio relative to the disc plane can be processed. The program in the further step is solving equation (2.5) to obtain the collective pitch value. Next stage of the calculations is to estimate the flapping coefficients. The pitching moment coefficient is assessed at the subsequent step. With the flapping and pitching moment coefficient, the B_1 angle is ready to be computed. After obtaining the first angle, the second is calculated similar to the first using the equations mentioned above. The MATLAB source code used for all described calculations is shown in Fig. 1.

The calculated collective pitch is modelled in CAD geometry. The collective pitch angles are a basis for the rotor cyclic pitch movement modelled then in Ansys Fluent.

```
a1DEG=rad2deg(a1)

hcd2=1/4*u*del+a*lamd/4*(1/2*a1-u*tet0)

alfd2=-(0.5*u^2*d0*cos(tc)+hcd2)/wc-tc
ud2=u*cos(alfd2)
lamd2=ud2*alfd2-lami

a0=y/8*(tet0*(1-19*u^2/18+3*u^4/2)/(1+3*u^2/2)+4/3*lamd2*(1-u^2/2)/(1+3*u^2/2))
dtf=(1-sin(alfd2)/(1+sin(alfd2)))
b1=4*((u*a0+1.1*dtf^(1/2)*lami)/3)/(1+u^2/2)
qc=del*(1+3*u^2)/8-lamd2*wc-u*hcd

Cms=b*Mb*xg*e/(2*Solid*A*R)
B1=a1+(Cmf+hcd2*h-wc*f)/(wc*h+Cms)
B1=simplify(B1)
axis=simplify(a1-B1)
B1=rad2deg(B1(1,1))
B1=simplify(B1)


 H=hcd2*ro*A*om^2*R^2*Solid
 P=qc*ro*A*om^3*R^3*Solid

 X=-W*sin(alfd2)-H*cos(alfd2)
D=P\V+X
D=simplify(D)

alfd2=simplify(alfd2)
a1=simplify(a1)
axis=simplify(rad2deg(a1)-B1)

alfHT=simplify(D/W+H/W)
alfHT=simplify(rad2deg(alfHT))


Q=qc*ro*Solid*A*om^2*R^3



%%mass=@(x) Mb.*(x/(0.79*R)-0.21/0.79)        % mass function
%%Inert=@(x) mass(x).*x.^2

```

Fig. 1. Example of MATLAB numerical code for preliminary calculations

3. Parametric model for simulation process

The main goal of this research is to obtain a new approach for main rotor blade modelling, which will be implemented into the main rotor optimization loop. The goal is achieved using Open

GRIP code, which is implemented into Siemens NX. The program was taken from the first stage of the studies and improved. The program algorithm is shown in Fig. 2.

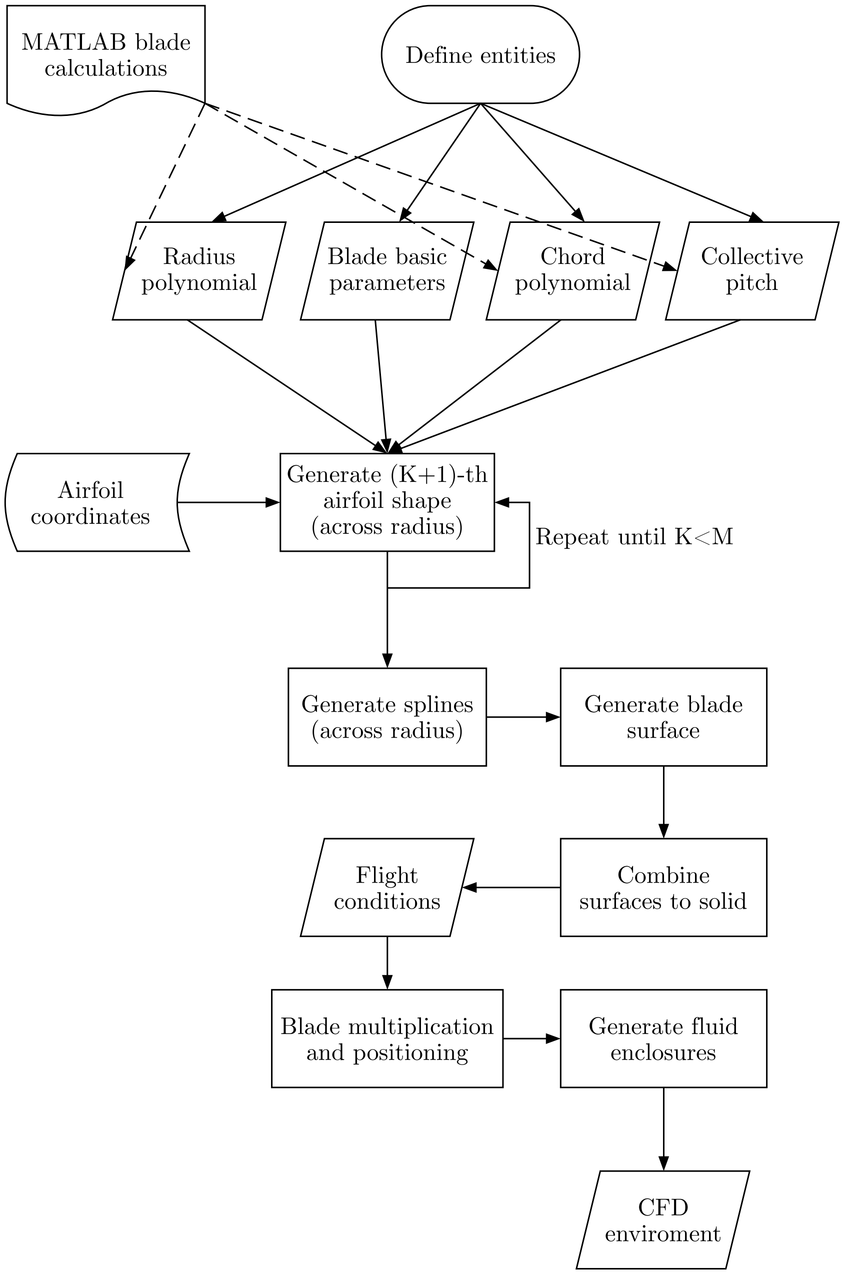

Fig. 2. Enhanced algorithm for generating parametric geometry model

The geometry of the model is parametrized in the program using all main rotor geometrical dimensions. The user is able to enter the blade basic parameters into a popup input window. The first parameters are the number of blades, rotor radius and blade chord. The airfoil is generated from the text file with coordinates, so the user can prepare the blade for any chosen airfoil geometry. The next stage of parametrization is to enter the polynomial coefficient for blade twist and blade chord, so the blade chord and twist can change along the span. With the prepared solution, the blade shape can be freely changed with accordance to analytically calculated values. The windows with applets for introducing control parameters are shown in Figure 5. The shape generation is based on inbuilt GRIP commands for the line and splines, which provides the desired shape. The number of sections to create the geometry can also be chosen. An example of generating the blade geometry is shown in Fig. 3.

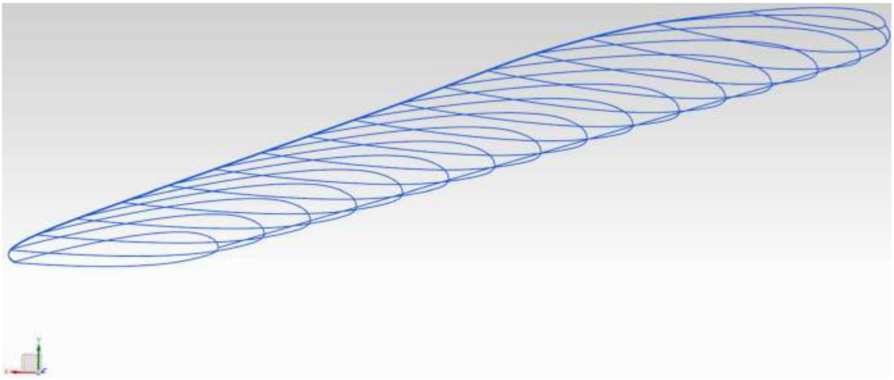

Fig. 3. Blade parametrisation

The second stage of parametrization is the n-bladed rotor. The blades are positioned with the angles that were trimmed analytically. Each blade is positioned at a different angle in accordance to their initial azimuthal position in simulation.

The next phase is generation of fluid enclosures for multi-moving mesh simulation. In the code, the volumes of fluid domains are programmed proportionally to the rotor dimensions. The domains are generated as follows: the main air enclosure as a cuboid for forward flight and as a cylinder for hover, rotor enclosure as a cylinder with each blade havig its own cylinder domain. The space geometry of applicable enclosure variants is presented in Fig. 4. The selectable flight conditions – forward flight or hovering are possible to be chosen by the user.

(a) (b)

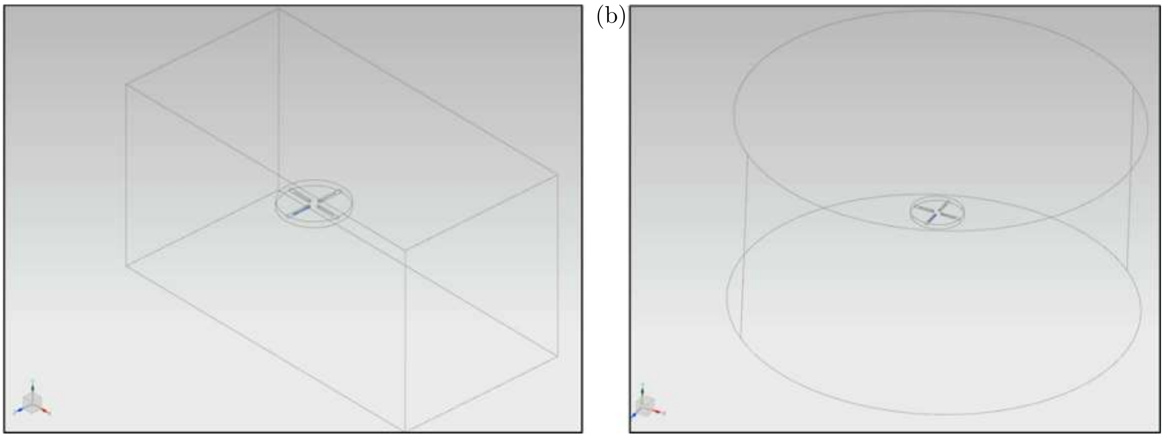

Fig. 4. Fluid domains: (a) for forward flight, (b) for hovering flight

(a) (b)

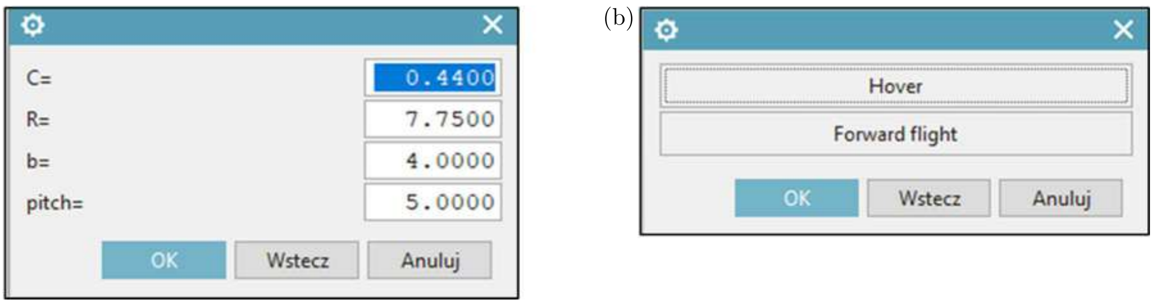

Fig. 5. User input options: (a) blade parameters, (b) flight conditions

The ready to simulation geometry is generated in few seconds, so the designer can prepare different models for CFD analysis in a short time.

4. Mesh and simulation properties

The model for CFD simulations was prepared in Ansys Fluent. The generated geometry with fluid domains was imported into the mentioned environment. To generate the fluid mesh of finite volume elements, the Fluent Mesher was used. It was chosen because of the future automatization of the process. This software provides a full path of activities that are necessary to generate the ready-to-use mesh. Body sizing, face sizing and inflation options were used to prepare a correct simulation. The boundary layer was generated using the aspect ratio options. The air enclosure size was calculated from the rotor dimensions. The ratios chosen to obtain correct domains were defined in the following way: X for the air enclosure, Y for the rotor enclosure and Z for the blade enclosures. The maximum size of a single volume element was set as 5000 mm, the elements on the blade were set to a value of 10 cm spanwise and chordwise. The inflation was set for 15 layers with 80 aspect ratio. The $y+$ value was established at an average value of 300, which gave the boundary layer a wall function. The mesh was generated as a poly-hexcore mesh and consisted of approximately 10^6 elements (depending on the model). An example of the prepared mesh is shown in Fig. 6.

Fig. 6. Polyhexcore mesh of fluid volume elements

The domains were named adequate to their destinations. The velocity inlet for the forward flight was set as a pressure far-field – velocity inlet, and the end of the cuboid was provided as a pressure outlet. The pressure far-field – velocity inlet option in Ansys Fluent provides a possibility to set the inlet velocity direction and magnitude with the vector coordinates. The contact regions were named to identify the internal connection between the domains in the preparing of the solution. K-ω SST viscosity model was chosen for the simulation, because it is recommended for solving CFD rotor tasks. The viscosity model results with the $y+$ for wall function boundary layer treatment were checked whether it gave satisfying results without extending calculation, what would be for more complex boundary layer simulations. The time step for transient simulation was set at 0.001 s. The convergence for each time step was settled for continuity at 10^{-5} with 100 iterations. The fluid domain with declared boundary conditions and the rotor model inside is presented in Fig. 7.

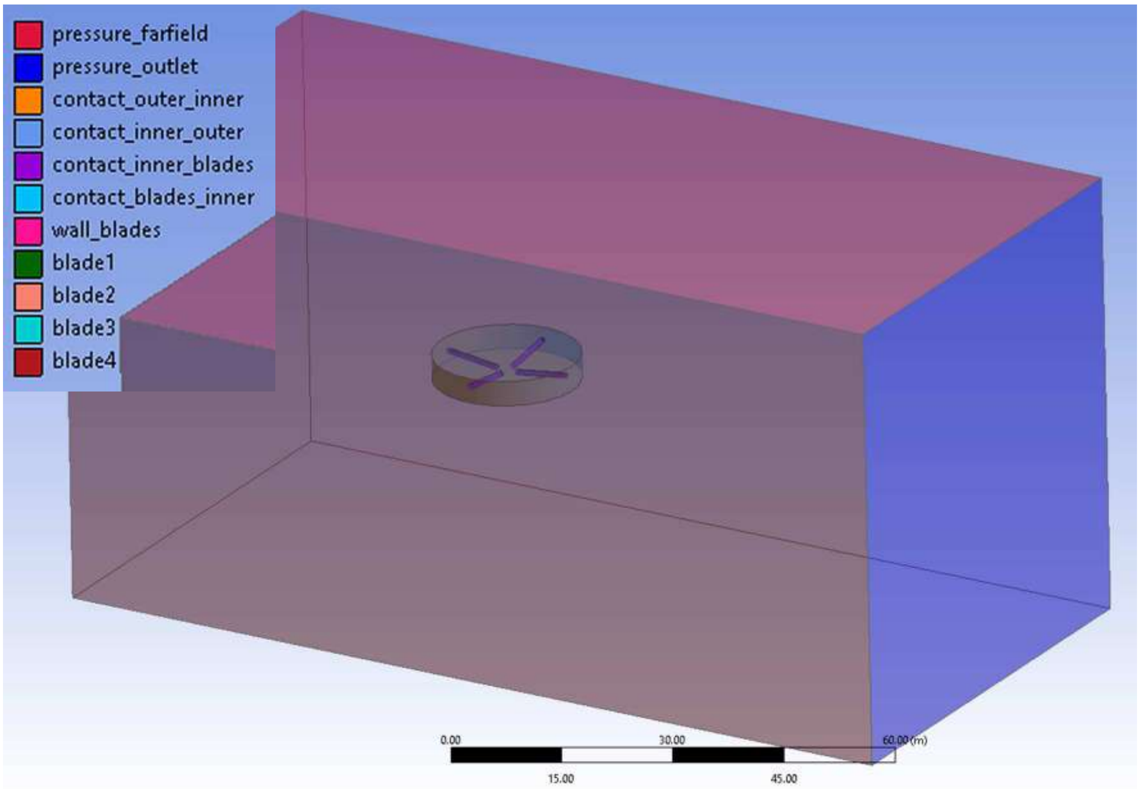

Fig. 7. The fluid domain with boundary conditions and the rotor model enclosure defined for the CFD process

5. Results

As a basis for CFD calculations, the rotor geometry of the rotorcraft W-3 Sokol was taken. The parameters of the helicopter are: radius – 7.85 m, chord – 0.44 m, rotational speed – 255 rpm, weight 6400 kg. The lift force should be adequate to the aircraft weight and the drag force is calculated from analytical assumptions. The first cut calculation was made for the existing rotor dimensions and features. The rotor position and movement were calculated in MATLAB program described in Section 2.2. For evaluation of the method, various rotor dimensions and flight parameters were used. The angles for the preparation of simulation are shown in Table 1.

Table 1. Calculated angles for simulation

Case No.	Collective [deg]	B_1 [deg]	A_1 [deg]	Tip path angle [deg]
1	11.12	3.46	−3.72	10.75
2	11.52	5.26	−4.87	10.71
3	8.31	2.52	−3.45	7.44
4	9.85	5.48	−5.48	7.43
5	9.48	3.10	−4.38	7.83

The calculated results are presented in Table 2. It shows that the assumptions which were made for the movement simulation and calculations are correct. The values of basic rotor forces are similar to those calculated, the average difference between the results and analytical calculations is at 4%. The comparison is made with analytical calculations of the drag force and helicopter weight. The lift force that is required for flight of the helicopter is generated adequately to the needs.

Table 2. Simulation results

Case No.	Analytical assumptions					CFD simulation	
	Weight	MR radius [m]	Blade chord [m]	Flight speed [km/h]	Drag [N]	Lift [N]	Drag [N]
1	62784	7.85	0.3	100	1276	61706	1256
2	62784	7.85	0.3	150	2870	63708.25	2982
3	62784	7.85	0.44	100	1276	61537	1139
4	62784	7.85	0.44	200	5098	62625	5132
5	62784	7	0.6	100	1276	66850	1295

In consequence, working conditions of rotor blades can be evaluated using the obtained results. The major finding, that will be used in optimization loop (which will be aimed at mass reduction of the blades and stiffness improvement), is the pressure distribution. Examples of pressure distributions are shown in Fig. 8.

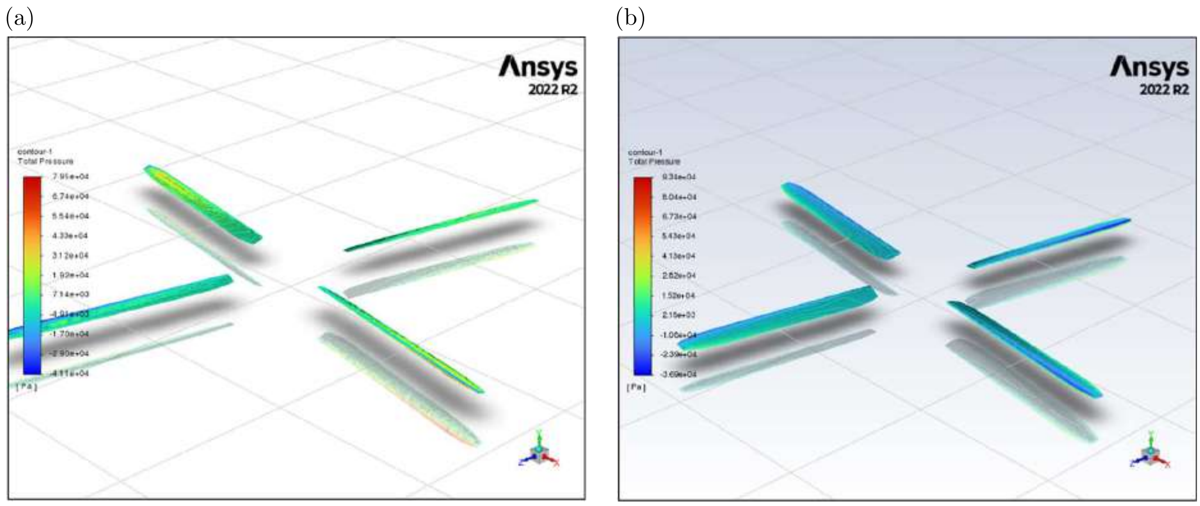

Fig. 8. Pressure distribution: (a) case 1, (b) case 2

The pressure distribution for the calculated flight case enables determination of the load acting on rotor blade surfaces during their rotary movement. Different flight conditions and different blade geometry can be evaluated by the designer. To obtain these results with application of the proposed method, 6 to 8 hours is needed, where 15 minutes is 3D model preparation, 45 min to 2 h is mesh and simulation preparation, the rest is Fluent processing time (which is also depending on mesh parameters).

The proposed way of model preparation and calculation of simulation parameters provides information about the influence of parametrisation on the obtained dimensions. The required drag and lift are the same for different flight parameters, however the angles of rotor disc and blade pitch positions are changing depending on blades dimensions. With CFD simulation, the proposed modelling was proved to be correct and applicable to next steps of rotor optimisation.

6. Conclusions

As it is described at the beginning of this paper, this research is a part of the program aimed at finding new solutions for rotorcraft structures design using optimization methods. This is a next step for preparing a full rotor model which will be optimized to obtain the best mass and stiffness characteristics.

It is confirmed that developing the rotor model with fluid enclosures, using parametric modelling, provides a versatile tool to quickly prepare different rotor geometries for CFD analysis. The code properties provide a possibility to prepare correct fluid domains. The enclosures are generated proportionally to rotor dimensions. The Open GRIP syntax Boolean options, to cut out the volumes from wider areas, enables an exact model preparation, which is ready to be analyzed using dedicated software. The model compatibility problem with software did not occur during the calculations. Using the parametric modeling significantly reduced the time of simulation preparation for different geometries and flight conditions.

The CFD analysis confirmed the expected results. The mathematical model of the rotor movement led to similar forces that were inputs for analytical calculations. The generated domains and models were easily configured for mesh simulation. The interior contacts for mesh interaction during simulation of motion were correctly corresponding with the indented contact regions.

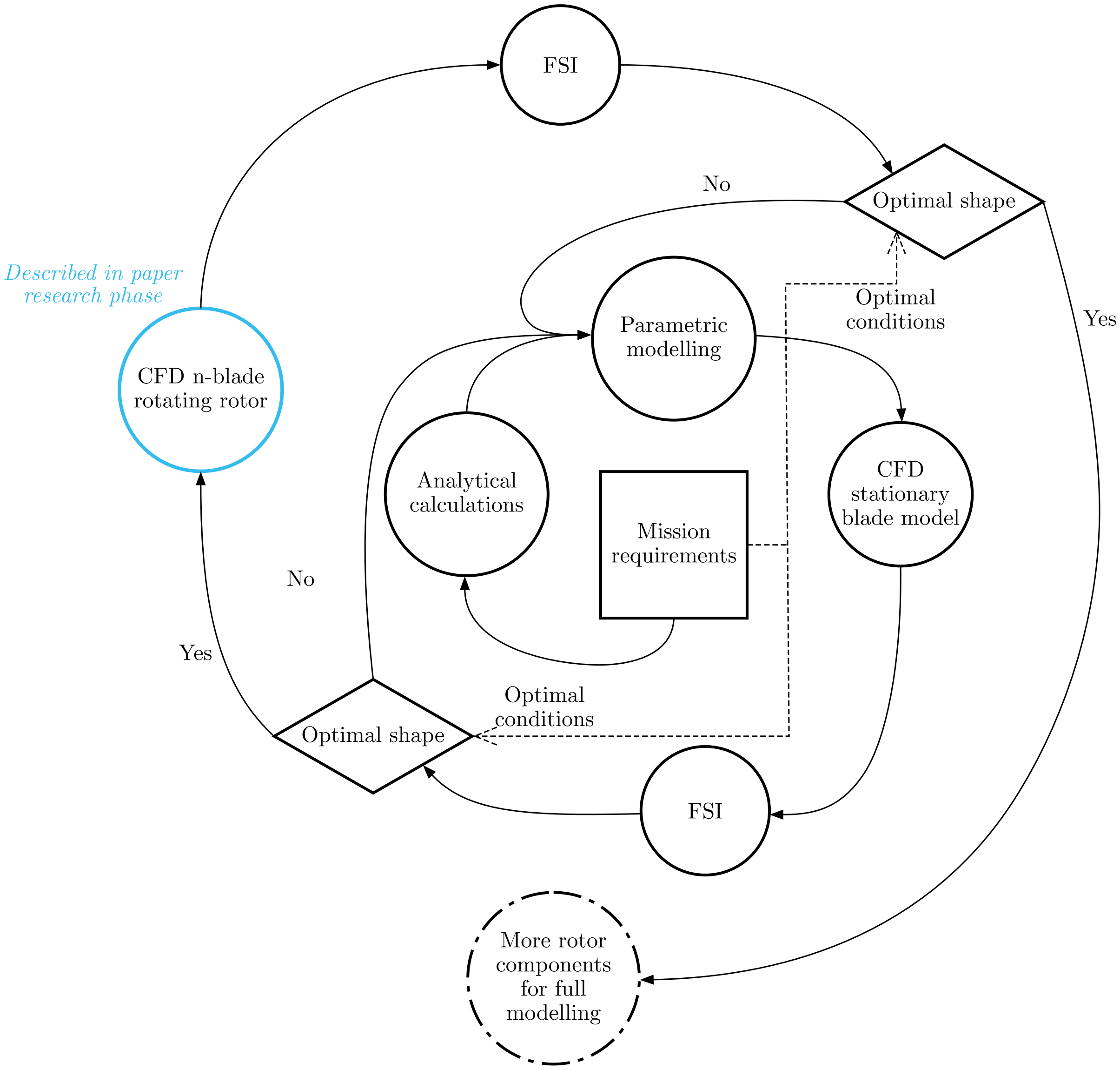

Fig. 9. Design spiral for rotor optimization

The simulation results showed that the model was correctly prepared. However, providing all required conditions to replicate the working environment of the real rotor, the simulation of the rotor movement and a change of pitch angles was time and memory consuming. But in fact it is a necessary condition to obtain correct results.

The studies shows a new way of preparing and conducting main rotor CFD simulations using a parametric approach. The parametric modelling reduces the total time of simulations. The results obtained showed the working conditions of the main rotor blades in terms of pressures, velocity or turbulence. The outputs can now be combined in Ansys with FEM analysis and calculated simultaneously using the FSI procedure.

The advantage of the procedure is fidelity of the simulation. This kind of simulations provides high fidelity results, that can be used to evaluate parameters of prepared blades such us the shape and strength structure. This will be a next phase of the proposed optimization loop. The application of the studies described in this paper is only a one of many activities included in the optimization procedure illustrated with the so called design spiral. It is shown in Fig. 9.

Acknowledgement

The methods and results presented in this paper have been obtained during research works conducted within a university research project entitled "Methods of optimal design of aircraft to improve its structural and aerodynamic properties". It was financed by the Military University of Technology (Warsaw, Poland), in in 2022 and 2023, under the university research project UGB-782/2022 and UGB-819/2023.

Data Availability Statement

Program code is available at: https://github.com/jakubkocjan/parametricrotordesign (accessed on 30 November 2022).

The work and its results were presented during the conference "Mechanika w Lotnictwie, ML-XX 2022".

References

1. Allen L.D., Lim J.W., Haehnel R.B., Dettwiller I.D., 2021, *Rotor Blade Design Framework for Airfoil Shape Optimization with Performance Considerations*, Engineer Research and Development Center
2. Bailly J., Bailly D., Didier B., 2019, Multifidelity aerodynamic optimization of a helicopter rotor blade, *AIAA Journal*, **57**, 8, 3132-3144
3. Bramwell A.R.S., Done G., David B., 2011, *Bramwell's Helicopter Dynamic*, Butterworth--Heinemann, Linacre House, Jordan Hill, Oxford
4. Grabowik C., Kalinowski K., Kempa W., Paprocka I., 2015, A method of computer aided design with self-generative models in NX Siemens environment, *IOP Conference Series: Materials Science and Engineering*, **95**, 1
5. Grebrnikov A.G., *et al.*, 2021, Analysis of design and technological features of the main rotor blades of heavy transport helicopters, *Open Information and Computer Integrated Technologies*, **93**
6. Goerke D., Le Denmat A.L., Schmidt T., Kocian F., Nicke S., 2012, Aerodynamic and mechanical optimization of CF/PEEK blades of a counter rotating fan, *Proceedings of the ASME Turbo Expo*, **7**, Parts A and B
7. Jain R., 2022, Computational fluid dynamics transition models validation for rotors in unsteady flow conditions, *Journal of Aircraft*, **59**, 4
8. Johnson W., 1994, *Helicopter Theory*, Dover Publications, New York
9. Kachel S., Rogólski R., Kocjan J., 2021, Review of modern helicopter constructions and an outline of rotorcraft design parameters, *Problems of Mechatronics Armament Aviation Safety Engineering*, **12**, 3

10. Kocjan J., Kachel S., Rogólski R., 2022, Helicopter main rotor blade parametric design for a preliminary aerodynamic analysis supported by CFD or panel method, *Materials*, **15**, 12
11. Lim J.W., 2018, Application of parametric airfoil design for rotor performance improvement, *44th European Rotorcraft Forum 2018, ERF 2018*, **1**
12. Ma L., Zhao Q., Zhang K., Zhang X., Zhao M., 2021, Aeroelastic analysis and structural parametric design of composite rotor blade, *Chinese Journal of Aeronautics*, **34**, 1
13. Oh S., Park D., Ji H.M., 2021, Development of preliminary conceptual design/comprehensive analysis programs for next generation rotorcraft, *Journal of the Korean Society for Aeronautical and Space Sciences*, **49**, 1
14. Okumuş O., Senipek M., Ezertas A., 2022, Multi-objective multi-fidelity aerodynamic optimization of helicopter rotor, *AIAA SCITECH 2022 Forum*
15. Ryazanov A.I., 2016, Automated 3D modeling of working turbine blades, *Russian Engineering Research*, **36**, 9
16. Sagimbayev S., Kylyshbek Y., Batay S., Zhao Y., Fok S., Lee T.S., 2021, 3D multidisciplinary automated design optimization toolbox for wind turbine blades, *Processes*, **9**, 4
17. Shabliy L.S., Dmitrieva I.B., 2014, Conversion of the blade geometrical data from points cloud to the parametric format for optimization problems, *ARPN Journal of Engineering and Applied Sciences*, **9**, 10
18. Slavik S., Klesa J., Brabec J., 2020, Propeller selection by means of pareto-optimal sets applied to flight performance, *Aerospace*, **7**, 3
19. Spyropoulos N., Papadakis G., Prospathopoulos J.M., Riziotis V.A., 2021, Investigating the level of fidelity of an actuator line model in predicting loads and deflections of rotating blades under uniform free-stream flow, *Applied Sciences*, **11**, 24
20. Stalewski W., 2017a, Design and optimisation of main rotor for ultralight helicopter, *Journal of KONES Powertrain and Transport*, **24**, 4
21. Stalewski W., 2017b, *Design and aerodynamic optimization of rotorcraft* (in Polish), Warsaw
22. Stalewski W., Zalewski W., 2019, Aerodynamic design and optimisation of main rotors for light rotorcrafts, *45th European Rotorcraft Forum 2019, ERF 2019*, **1**
23. Tixadou E., 2021, Optimisation of the structure of A helicopter blade in view of reducing cabin vibration, *Proceedings of the 47th European Rotorcraft Forum*, Google Scholar
24. Wilke G., 2021, Quieter and Greener rotorcraft: concurrent aerodynamic and acoustic optimization, *CEAS Aeronautical Journal*, **12**, 3
25. Xie J., Xie Z., Zhou M., Qiu J., 2017, Multidisciplinary aerodynamic design of a rotor blade for an optimum rotor speed helicopter, *Applied Sciences*, **7**, 6

Manuscript received April 24, 2023; accepted for print August 3, 2023

EASN-2023 IOP Publishing
Journal of Physics: Conference Series **2716** (2024) 012031 doi:10.1088/1742-6596/2716/1/012031

Helicopter main rotor FSI analysis using parametric blade model as an application for multidisciplinary optimization

J Kocjan[1], S Kachel[2], R Rogólski[2]

[1] Doctoral School, Military University of Technology, ul. gen. Sylwestra Kaliskiego 2, 00-908, Warsaw, Poland
[2] Faculty of Mechatronics, Armaments and Aviation, Military University of Technology, ul. gen. Sylwestra Kaliskiego 2, 00-908, Warsaw, Poland

Corresponding author's e-mail: jakub.kocjan@wat.edu.pl

Abstract. This work is part of a research program aimed at finding new approaches and design solutions for helicopter main rotor modelling using multidisciplinary optimization. It is the fourth stage of an individual research program that includes preliminary tasks such as parametric modelling of a single blade, CFD modelling of a full main rotor for different flight conditions, and preliminary structural modelling of a blade. The main goal of this work is to present the parametric modelling of the rotor blade body and structure as an application for complex simulation. The paper demonstrates the method of advanced analysis of the entire rotor and provides exemplary results obtained from complicated analyses. The analytical foundation for combined fluid-structure analysis is presented. The parametric design method is shown to be applicable for different blade planform shapes and various section airfoils. The blade CFD fluid domain is also prepared using the parametric method, as well as the blade's inner structure. The simulation parameters from the previous stages of research, which serve as inputs to the FSI analysis, are outlined. These previously obtained parameters are combined and introduced into an FSI simulation to assess their compatibility and applicability. The configuration procedure of the analysis and the boundary conditions are presented. The obtained numerical results are then compared with analytical assumptions. The simulation products, which serve as inputs for further analysis, are presented with graphical representations. The time and memory consumption of the simulation are outlined. The application of the described work in an optimization loop is proposed. As a result of this research, new options for main rotor optimization are developed. The paper demonstrates some crucial possibilities of FSI analysis in the described simulation cases. The use of combined parametric modeling with fluid-structure interaction analysis for different flight conditions is presented as a new perspective for multidisciplinary design optimization of a helicopter rotor system.

1. Introduction

Modern military helicopters are designed to operate in various flight conditions and environments, with manufacturers and governments working together to enhance their effectiveness in military operations. There are currently two main streams of rotorcraft design. The first focuses on finding new aerodynamic configurations, such as combining the construction of the main rotor with a pusher propeller. [1], [2]. The second stream aims to enhance existing helicopter designs by improving aerodynamic and structural solutions.[3]–[5].

EASN-2023 IOP Publishing
Journal of Physics: Conference Series **2716** (2024) 012031 doi:10.1088/1742-6596/2716/1/012031

The Polish Military University of Technology is also involved in developing new rotorcraft design possibilities. This work is part of a comprehensive research program aimed at optimizing the aerodynamics and structure of the main rotor. This article represents the fourth phase of the research program, following previous analyses of rotorcraft construction and main rotor computational fluid dynamics (CFD) using parametric modeling. The program were preceded with an rotorcraft construction analysis which results were published in [6]. The latter parts included the main rotor CFD analysis using parametric modeling and preparing the blade structure using parametrization, this work were published in [7]. In each phase the parametrization of the model is used because of planned optimization loop.

Parametrization of the rotor blade allows designers to explore different blade shapes and structures using geometric parameters or dimensionless coefficients. This method offers advantages in terms of time efficiency and the ability to evaluate various design variants The benefits of parametrization for rotor blades have been described in [8], [9]. In this study, parametric models are used to generate the CFD fluid domain and the blade's inner structure. Examples of using parametric models for airfoil shape and structure and aerodynamic performance are also provided in [10], [11] for an airfoil shape and [12]–[14] for structure and aerodynamic performance.

The parametric models for blade shape, fluid domains, and inner structure were created using a graphic programming language called GRIP, which is provided with Siemens NX software. GRIP allows users to generate the desired shape of any airframe part by combining commands and inputting parameters. The language also includes inertia analysis functions, enabling initial strength calculations within the code. By combining logical functions, the designed shape can be initially optimized. Examples of using the GRIP language are shown in [15]–[17].

To achieve the research objectives and find new solutions for main rotor blade optimization, a combination of CFD analysis and structural finite element analysis (FEA) is required. To accurately describe the phenomenon, these tools can be combined in a fluid-structure interaction (FSI) simulation. FSI simulations allow for the examination of the influence of aerodynamic loads on the structure and the subsequent impact of deformation on the generated loads. While FSI is commonly used in wind turbine simulations [18]–[20], its application in rotorcraft simulations is less frequently described in published studies.

In this phase of the study, previously evaluated and prepared solutions for CFD main rotor analysis and blade structure preparation using parametric modeling were utilized. The blade's parametric model was generated using geometric and shape parameters, with the geometry based on an existing helicopter rotor. The codes developed generate the geometry of the rotor blades for the CFD part of the FSI analysis and the blade with the inner structure for the MES part of the simulation. The GRIP program code allows end users to input blade parameters and vary the geometries for simulation testing.

The simulation was prepared using a CFD environment, with the movement of the blades analytically calculated. MATLAB was used to determine the values of collective pitch control and cyclic control, which were then inputted into the CFD simulation to simulate rotor movement under different flight conditions. Meshes were generated for the CFD domain and MES analysis, with mesh sizes chosen to obtain acceptable results within a reasonable time frame. The FSI simulation was conducted, starting with a one-way analysis where aerodynamic loads were transferred to the model, followed by a two-way FSI simulation using solver coupling. The construction was evaluated to ensure it met the strength requirements for desired performance possibilities. To the best of the co-authors' knowledge, similar research combining the proposed methods for helicopter main rotor design and optimization has not been conducted before.

EASN-2023 IOP Publishing
Journal of Physics: Conference Series **2716** (2024) 012031 doi:10.1088/1742-6596/2716/1/012031

2. Blade parametric model for FSI analysis

2.1 CFD model for FSI analysis

The working environment of a rotor is very complex due to the axial rotation and simultaneous change of the rotor blade angles as a function of azimuth. To prepare a model for FSI analysis, both a CFD and FEM model must be prepared. The CFD model is prepared with the shape of the air domain, which depends on the simulation conditions. The blade shape is generated using user-inserted dimensions and the proposed airfoil shape. An example of blade shape parametrization is presented in Figure 1. Additionally, the domain for analysis is prepared in accordance with the blade shape. A different domain is prepared for n-bladed rotor simulation, and a different domain is prepared for 1-blade simulation. The preparation and analysis of the CFD model for the optimization procedure were presented in [21].

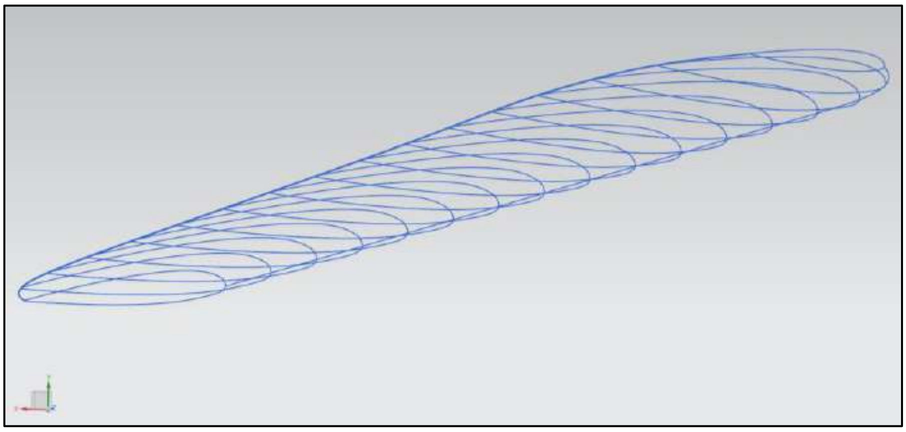

Figure 1 Blade parametrization

2.2 FEM model for FSI analysis

The FEM model for FSI analysis is also parametrized. To adjust the structure, initial stress calculations need to be conducted. Analytical calculations are performed using MATLAB, and the final internal shape fitting is implemented in the GRIP programming language. The generated shape is based on a real blade structure, consisting of a composite spar and skin in the front, and honeycomb in the back. The spar is filled with foam to maintain its shape. The shape of the parametrized blade is presented in Figures 2A and 2B. The Figure 2A shows the inner structure of the geometry. The parts are highlighted using different colours: green – skin, brown – spar, grey – honeycomb and beige – foam. The image 2B describes the full shape of the generated blade with the chord change across the span.

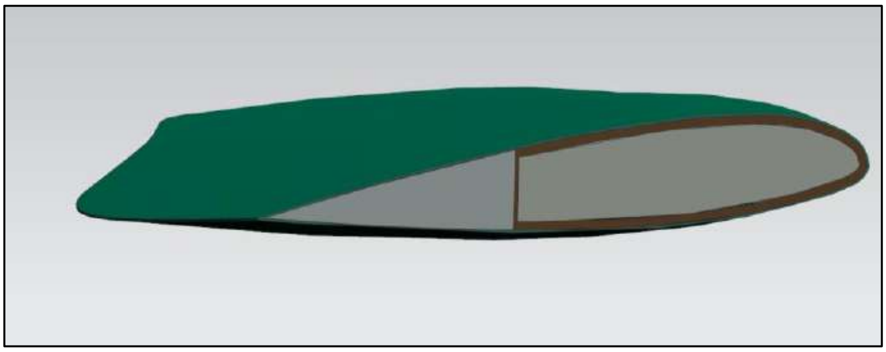

Figure 2A Blade structure parametrization

EASN-2023 IOP Publishing
Journal of Physics: Conference Series **2716** (2024) 012031 doi:10.1088/1742-6596/2716/1/012031

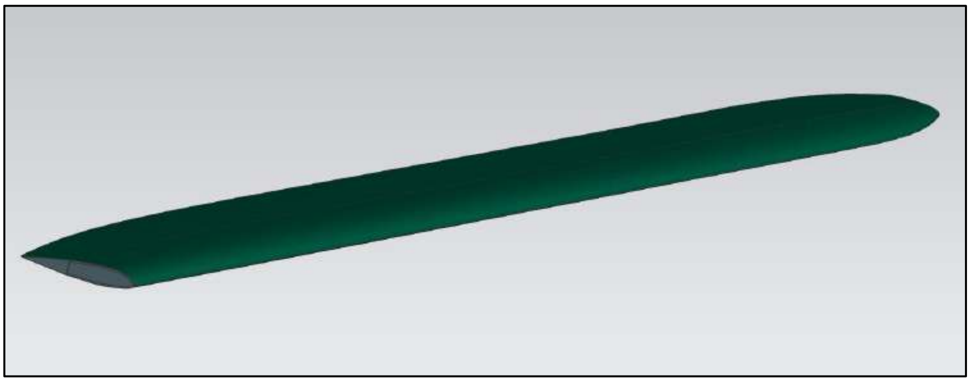

Figure 2B Blade structure parametrization

3. FSI analysis in optimisation procedure

The proposed research aims to combine aero-structural optimization in a loop to achieve improved performance and strength of the main rotor. The final stage of the research involves using FSI analysis to evaluate the model and make changes to the geometrical model of the CFD and FEM models. The procedure is illustrated in Figure 3.

The procedure begins with determining the mission requirements, which serve as the basis for the performance requirements that need to be met. These requirements are essential for designing a rotorcraft capable of fulfilling its intended missions, such as payload, forward speed, and climb. To determine reasonable parameters, existing constructions designed for similar missions are analyzed. The trends identified from this analysis serve as a reference for proposing initial geometric and aerodynamic parameters for the main rotor blade.

The next step in the procedure involves analytical calculations. During this phase, the blade trimming is determined based on the required rotorcraft mass and airspeed. This allows for the establishment of the aerodynamic loads on the blade. Combined with the mass moments of inertia from centrifugal force, flap, and lag moments, these calculations provide the moments acting on the rotor blade's strength elements. The results of the mathematical analysis serve as inputs for parametric modeling.

Parametric modeling is used to generate the blade shape using the dimensions obtained from the trim and performance calculations. The pitch angle of the rotor blade and the blade position angles for the CFD analysis are also provided. This enables the generation of the air domain for single rotor blade or n-bladed main rotor CFD simulations. The second part of parametric modeling involves creating the blade with its inner strength structure. The dimensions of the spar are calculated within the GRIP code and applied to a chosen number of blade cutouts. This allows for mass reduction, as the spar thickness is determined by the strength requirements. The shape of the foam inside the spar and the geometry of the honeycomb section from the trailing edge to the spar are also generated. The CAD models for CFD and FEM applications serve as inputs for FSI simulations, as shown in Figure 3.

EASN-2023 IOP Publishing
Journal of Physics: Conference Series **2716** (2024) 012031 doi:10.1088/1742-6596/2716/1/012031

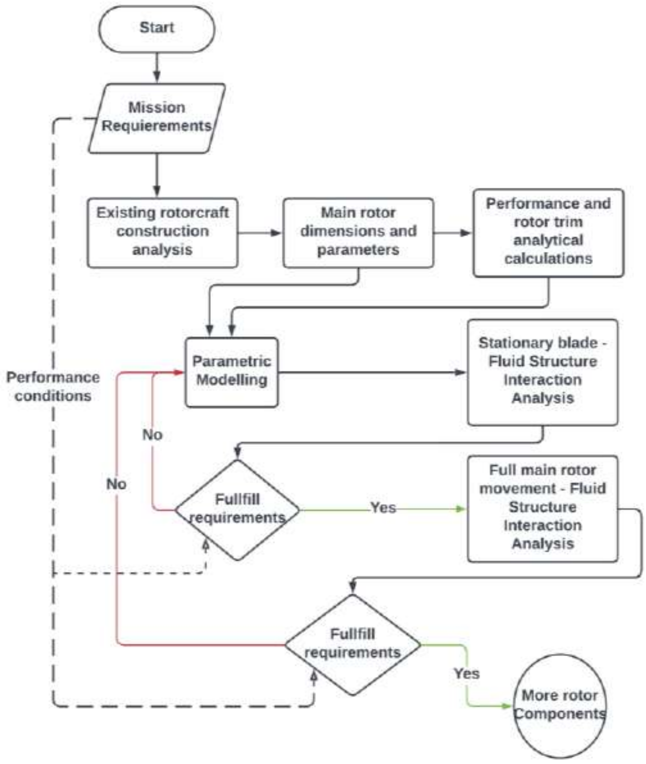

Figure 3 Optimization procedure

Firstly, the single blade simulation is conducted, where the model of a blade in the air domain is combined with the structural model. The airflow is modeled in a steady simulation using the inflow angles that were determined during the analytical calculation of thrust and trim. This method is less computationally demanding and takes much less time to obtain numerical results.

The initial step is to check the deformations of a blade in a one-way FSI simulation, where the loads are transferred from the CFD into the FEM model. This allows for a quick assessment of the reasonableness of the results.

The second step is a two-way FSI simulation, where the loads are transferred to the FEM model and then the deformation of the rotor blade is transferred to the CFD model to assess the influence of the deformation on the produced aerodynamic forces. The results of this part of the research are described in this work.

The construction is evaluated to determine if it fulfills the requirements of the strength elements and performance conditions. If any requirements are not met, the parameters of the model are adjusted and the construction is re-evaluated.

The next stage is to analyze the main rotor blade in its working environment under different flight conditions. The CFD simulation is prepared for an n-bladed rotor, with the simulated blade motion dependent on its azimuthal position. The resulting aerodynamic forces will be combined with the structural FEM model to apply the deformation to the rotor model. The results of this simulation will also be evaluated to determine if the construction meets the requirements.

4. Preliminary FSI simulation.

4.1 Simulation properties

The FSI simulation was prepared using Siemens Star CCM+. The geometry for the CFD and FEM analysis was imported into the software, ensuring no collisions between the CAD geometry and the

EASN-2023 IOP Publishing
Journal of Physics: Conference Series **2716** (2024) 012031 doi:10.1088/1742-6596/2716/1/012031

simulation environment. The mesh was generated using the automated mesh function, which can be applied to new geometries in an automated process. The minimum size of the surface elements was set at 1% of the base element, which was established at 0.5 m. The boundary layer was also applied. The skin of the blade and the spar were meshed using the thin mesher option, with polyhedral elements used for the fluid and tetrahedral elements used for the solids.

The boundary conditions for the CFD parts were set as a velocity inlet, pressure outlet, and wall for the blade surface. In Star CCM+, the solver parameters were set simultaneously in the continua options. The fluid part of the simulation was set as an unsteady simulation using the K-Omega SST turbulence model.

For the FEM simulation, an unsteady simulation was also applied. To simulate the different materials of the blade components, the multi-part and multi-component solid solver was used, with the solid stress option. The blade was fixed at the root, and the load was applied to simulate the centrifugal force. The time step for the simulation was set at 0.001s, with 30 inner iterations and the continuity stopping criterion for each time step.

4.2 Exemplary simulation results

To verify the capabilities of the simulation, hover conditions for the MTOW of 4900 were simulated. The inflow conditions were prepared using data obtained from earlier stages of the research. The forces created on the blade were similar to those required for hover. Figure 3 shows the blade displacement, with some areas that should be further examined under more complex flight conditions. Figure 4 shows the resultant stress in the blade spar, with areas that also need to be checked for endurance during flight. It can be observed that the construction has the potential to be thinner, but this should be evaluated under different flight conditions.

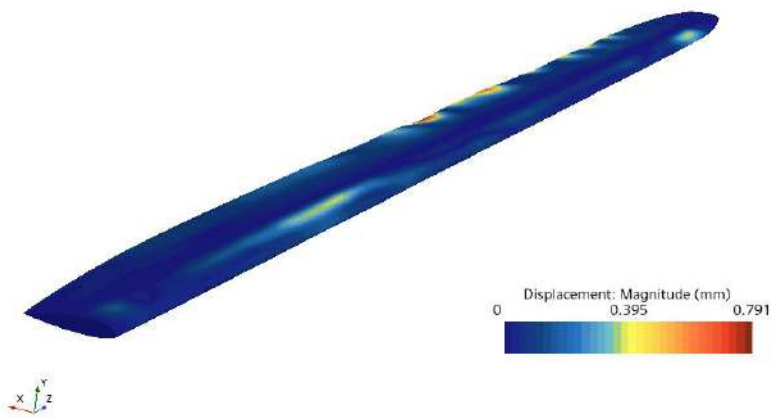

Figure 4 Blade displacement for the hover with MTOW 4900 kg

EASN-2023 IOP Publishing
Journal of Physics: Conference Series **2716** (2024) 012031 doi:10.1088/1742-6596/2716/1/012031

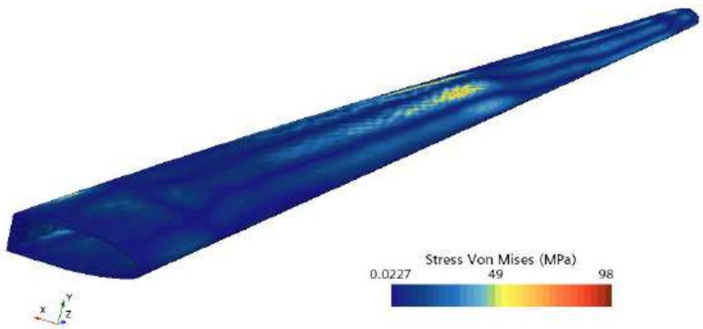

Figure 5 Spar stress results for the hover with MTOW 4900 kg

5. Conclusion

As described in the introduction, this paper presents the next stage of our research program, which aims to explore new methods for main rotor design using modern techniques within an optimization loop. In this step, one-blade two-way FSI simulations were conducted as an initial step before preparing the FSI analysis of a blade with its motion due to rotational movement and pitch change in an azimuth function.

The results confirm that the blade parametric model is a quick and efficient solution for preparing FSI simulations. The CFD and FEM models were generated in just a few minutes using the prepared code. The compatibility between the CFD domain and the FEM model was ensured by subtracting the exact blade shape from the domain. There were no issues with mesh generation, and the models were compatible with the software.

The results of the CFD analysis align with the analytical expectations and previous standalone CFD simulations. The mathematical model of the inflow for the one-blade simulation provides accurate results.

The FEM analysis, as part of the FSI simulation, demonstrated the influence of the pressure load on the blade. The stress on the strength elements and the displacement of the blade were analyzed to identify weak points in the structure and make necessary design corrections. These design corrections will be implemented using dedicated software or code to facilitate the optimization loop.

This study presents a new approach to aerostructural analysis of main rotor blades using a parametric approach. The application of parametric geometry significantly reduces design time. The results serve as a foundation for preparing a structural model for full n-bladed main rotor FSI analysis, which includes the motion of the main rotor blades.

Another benefit of this procedure is the flexibility it offers in changing the external blade shape or inner strength structure shape. This is crucial for developing an optimization loop that can identify the best aerodynamic properties and strength elements to meet performance requirements.

Funding: The methods and results presented in this paper have been obtained during research works conducted within the university research project entitled “Methods of optimal design of aircraft to improve their structural and aerodynamic properties”. This work was financed by the Military University of Technology (Warsaw, PL), in 2023, under the university research project UGB-819/ 2023.

References

[1] S. Oh, D. Park, H. M. Ji, *Development of Preliminary Conceptual Design/Comprehensive Analysis Programs for Next Generation Rotorcraft*, Journal of the Korean Society for Aeronautical & Space Sciences, 49, 1, 2021,

EASN-2023 IOP Publishing
Journal of Physics: Conference Series **2716** (2024) 012031 doi:10.1088/1742-6596/2716/1/012031

[2] S. Oh, S. H. Kim, *Next Generation Rotorcraft Technologies in USA and Europe*, Journal of the Korean Society for Aeronautical & Space Sciences, 42, 8, 2014,
[3] K. Pahlke, B. Demaret, *ONERA and DLR contributions to improve environmental friendliness of rotorcraft*, 2017.
[4] W. Stalewski, *DESIGN AND OPTIMISATION OF MAIN ROTOR FOR ULTRALIGHT HELICOPTER*, Journal of KONES Powertrain and Transport, 24, 4, 2017.
[5] K. Robinson, A. Brocklehurst, *BERP IV aerodynamics, performance and flight envelope*, in *34th European Rotorcraft Forum 2008, ERF34*, 2008, 1.
[6] S. Kachel, R. Rogólski, J. Kocjan, *Review of Modern Helicopter Constructions and an Outline of Rotorcraft Design Parameters*, Problems of Mechatronics Armament Aviation Safety Engineering, 12, 3, 2021,
[7] J. Kocjan, S. Kachel, R. Rogólski, *Helicopter Main Rotor Blade Parametric Design for a Preliminary Aerodynamic Analysis Supported by CFD or Panel Method*, Materials, 15, 12, 2022,
[8] S. Sagimbayev, Y. Kylyshbek, S. Batay, Y. Zhao, S. Fok, T. S. Lee, *3D multidisciplinary automated design optimization toolbox for wind turbine blades*, Processes, 9, 4, 2021,
[9] L. MA, Q. ZHAO, K. ZHANG, X. ZHANG, M. ZHAO, *Aeroelastic analysis and structural parametric design of composite rotor blade*, Chinese Journal of Aeronautics, 34, 1, 2021,
[10] J. W. Lim, *Application of parametric airfoil design for rotor performance improvement*, in *44th European Rotorcraft Forum 2018, ERF 2018*, 2018, 1.
[11] L. D. Allen, J. W. Lim, R. B. Haehnel, I. D. Dettwiller, *Rotor blade design framework for airfoil shape optimization with performance considerations*, 2021.
[12] E. Tixadou, *OPTIMISATION OF THE STRUCTURE OF A HELICOPTER BLADE IN VIEW OF REDUCING CABIN VIBRATION*, 2021.
[13] А. Г. Гребеников *et al.*, *ANALYSIS OF DESIGN AND TECHNOLOGICAL FEATURES OF THE MAIN ROTOR BLADES OF HEAVY TRANSPORT HELICOPTERS*, Open Information and Computer Integrated Technologies, 93, 2021,
[14] J. Bailly, D. Bailly, B. Didier, *Multifidelity Aerodynamic Optimization of a Helicopter Rotor Blade*, AIAA Journal, 2019, s.1–13,
[15] A. I. Ryazanov, *Automated 3D modeling of working turbine blades*, Russian Engineering Research, 36, 9, 2016,
[16] L. S. Shabliy, I. B. Dmitrieva, *Conversion of the blade geometrical data from points cloud to the parametric format for optimization problems*, ARPN Journal of Engineering and Applied Sciences, 9, 10, 2014.
[17] C. Grabowik, K. Kalinowski, W. Kempa, I. Paprocka, *A method of computer aided design with self-generative models in NX Siemens environment*, in *IOP Conference Series: Materials Science and Engineering*, 2015, 95, 1.
[18] M. C. Hsu, Y. Bazilevs, *Fluid-structure interaction modeling of wind turbines: Simulating the full machine*, Computational Mechanics, 50, 6, 2012,
[19] C. Grinderslev, S. González Horcas, N. N. Sørensen, *Fluid–structure interaction simulations of a wind turbine rotor in complex flows, validated through field experiments*, Wind Energy, 24, 12, 2021,
[20] D. Zhangaskanov, S. Batay, B. Kamalov, Y. Zhao, X. Su, E. Kweeng, *High-Fidelity 2-Way FSI Simulation of a Wind Turbine Using Fully Structured Multiblock Meshes in OpenFoam for Accurate Aero-Elastic Analysis*, Fluids, 7, 5, 2022,
[21] J. Kocjan, S. Kachel, R. Rogólski, *Parametrization of the main rotor and working environment for different flight conditions – Computational Fluid Dynamics analysis as an application for multidisciplinary optimization*, Journal of Theoretical and Applied Mechanics, 2023, s.793–805,

Parametric structure optimization of a main rotor blade as an application for FSI analysis in main rotor optimization process

Jakub Kocjan
Doctoral School, Military University of Technology, Warsaw, Poland, and
Robert Rogólski
Faculty of Mechatronics, Armament and Aerospace, Military University of Technology, Warsaw, Poland

Abstract

Purpose – Modern warfare and modern battlefield are very demanding. The recent conflicts showed that the usage of the helicopters is very limited and only the best constructions are able to provide support for the operations. The purpose of this research is to show the possibilities of new design tool for main rotor aerostructural optimization. It is a next chapter of the research that is aimed at finding new solutions for rotorcraft constructions.

Design/methodology/approach – This work presents a method of preliminary structure optimization of the main rotor blade using parametric modeling. It is the next step in the main rotor optimization studies. It is the next step after preparing the parametric model for the external shape CFD analysis. As a basis for parametric blade structure calculations, the analytical model is provided in this paper. The equations of rigid blade loads and, as a consequence of the strength elements, stresses are shown. The parametric blade modeling is conducted using the Graphic Integrated Programming language. The parametric design method is shown to be used for various blade planform models and different section airfoils. The structure of a blade is generated automatically after the user enters the parameters. The code-inbuilt analysis systems provide a quick inertia examination of the generated geometry, which is the basis for further optimization. The program calculates the blade loads and verifies them with the given material conditions and proposed safety factors. In the analysis, composite materials for the strength elements were proposed.

Findings – The results of this research showed the application of parametrization into the main rotor blade design loop. It was presented that the main rotor blade structure can be enhanced using fluid-structure interaction (FSI) methods. The time saving with the implementation the process into design loop is shown.

Practical implications – This work can be practically used in the main rotor blade design process. It provides the possibilities to check various blade aerodynamic configuration in a structure strength aspect.

Originality/value – To the best of the authors' knowledge, there were no published research that combines the main rotor FSI analysis. The method, which is presented in the work, provides a new approach to a rotorcraft design. The application of the parametrization and combining it with the FSI method gives a novel solution for helicopters construction enhancement.

Keywords Helicopter, Rotorcraft, Optimization, Main rotor, Fluid-structure interaction

Paper type Research paper

Introduction

The recent military conflicts have prompted a reassessment of the possible operations that helicopters can conduct on the modern battlefield. The need for constructions capable of providing enhanced characteristics for widespread military operations has been acknowledged by manufacturers and national authorities. Consequently, many countries are upgrading current configurations and exploring new solutions for vertical take-off and landing vehicles. Therefore, at the Military University of Technology, studies focused on finding new approaches and design possibilities for rotorcraft are

The current issue and full text archive of this journal is available on Emerald Insight at: **https://www.emerald.com/insight/1748-8842.htm**

Aircraft Engineering and Aerospace Technology
97/1 (2025) 37–51
Emerald Publishing Limited [ISSN 1748-8842]
[DOI 10.1108/AEAT-03-2024-0084]

This work was financed by the Military University of Technology (Warsaw, PL) under the two following research projects: No. UGB 22-732/2024/WAT entitled: Aerodynamic design of aircraft in terms of optimizing selected performance parameters; No. UGB 22-734/2024/WAT entitled: Design of light aircraft lifting structures in terms of optimizing strength and aeroelastic properties of the airframe. Both grants were carried out in the Institute of Aviation Technology (Faculty of Mechatronics, Armament and Aerospace of the Military University of Technology) in the year 2024 as university statutory activities funded by the Ministry of National Defence of the Republic of Poland.

Received 29 March 2024
Revised 12 July 2024
Accepted 5 September 2024

underway. The research began with an evaluation of helicopter construction features and parameters responsible for rotorcraft performance. The analysis considered nearly 70 of the newest helicopter designs from around the world. The results of this comparison were published in Kachel *et al.* (2021).

The main goal of the entire research is to develop a multicriteria optimization procedure to provide a solution using the newest computer-aided design methods. There are several main approaches to resolving optimization problems nowadays. The results of research focused on main rotor aerodynamic optimization are published in Okumuş *et al.* (2022), Stalewski (2017), Stalewski and Zalewski (2019), Tamer *et al.* (2011) and Xie *et al.* (2017), whereas an example addressing strength problems is shown in Spyropoulos *et al.* (2021). Some research institutes concentrate on main rotor optimization problems, such as the ONERA French Aerospace Lab and the DLR German Aerospace Centre. Their results are presented in Goerke *et al.* (2012), Pahlke and Demaret (2017), Tremolet and Basset (2012) and Wilke (2021, 2024). The proposed solution involves using parametrization in CAD geometry design. The benefits of using this approach were presented in Sagimbayev *et al.* (2021) and MA *et al.* (2021). Parametrization is also currently used for airfoil design (Allen *et al.*, 2021; Lim, 2018; Vu and Lee, 2015), structural design (Tixadou, 2021; Гребеников *et al.*, 2021) and aerodynamic design (Bailly *et al.*, 2019). Therefore, the second step, following comparative analysis, was the preparation of the main rotor blade shape as a parametric model using the Graphic Integrated Programming (GRIP) language. The evaluation of the model's application in CFD analysis was published in Kocjan *et al.* (2022). In addition, in further research, the CFD fluid domains were parametrized and simultaneously generated with a full n-bladed rotor for CFD analysis under different flight conditions. The aim of preparing the CFD environment and parametrizing the rotor model and its enclosures is to obtain a solution for quick preparation of (fluid-structure interaction) analysis.

The second part of preparing the FSI analysis involves setting up a finite element structural loads simulation. Therefore, to integrate it with the optimization procedure, a parametric structural model also needs to be prepared. This paper presents the preparation of a model for further analysis with preliminary strength analytical calculations. The preparation of the CAD parametric model is conducted using the GRIP language, which is implemented in Siemens NX software. Examples of GRIP usage are shown in Grabowik *et al.* (2015), Ryazanov (2016) and Shabliy and Dmitrieva (2014). This language provides the capability to generate external body or inner structural parts of the airframe that are currently being designed. Within the code, mathematical calculations, logical conditions and geometry creation are possible. The main advantages of the presented solution, which will be demonstrated in this research, include mass and inertia analysis built within the code. The functions offer the possibility to obtain numerical features of any geometry shapes, which can be used to prepare an optimization procedure. The program code presented in this paper, which generates geometry preliminarily prepared and calculated for given flight conditions, is prepared by the authors.

Another approach to main rotor blade optimization is the aeroelastic features optimization. Researches that are conducted nowadays are focused on enhancing features that concerns also the vibration of the blade. One of the most interesting studies are the influence of the BERP-like blade tip on working conditions and aeroelastic response (Johnson *et al.*, 2016; Moffatt and Griffiths, 2009). In this kind of studies also the computer methods are used. Some examples of the CFD analysis including vibrations analysis are shown in Allen *et al.* (2009) and Cornette *et al.* (2015). However, the exploration that are aimed at single or multicriteria optimization, that takes into account the main rotor blades aeroelastic attributes, are valuable and shows the procedures to obtain the best main rotor attributes. This is also the aim of research described in this paper. Very good examples of the optimization mentioned above are (Ganguli and Chopra, 1996; Guo and Xiang, 2004; Kizhakke Kodakkattu *et al.*, 2018; Liu and Zhang, 2021; Morris *et al.*, 2008; Straub *et al.*, 1992; Tarzanin *et al.*, 1999; Wang *et al.*, 2013). As it can be spotted there is many research that provides the solution for optimization and vibration reduction; however, there is not many published papers that use the FSI method for that purpose. One example is presented in Sinem and Metin Orhan (2018).

The optimization of the blade structure is described in Barwey and Peters (1994), Chattopadhyay *et al.* (1995), He and Peters (1992), Tian *et al.* (2022), and Vu *et al.* (2016) in which various aspects of the structure are taken into consideration. The most significant for the presented research are the strength considerations in aspects of its aerodynamic loads; however, the proposed procedures have not been developed using modern computational techniques. The example of modern optimization research where the advanced analysis is presented was published in Salh Eddine *et al.* (2023).

Taking into consideration the conducted analysis of research that were performed in helicopter main rotor design enhanced with optimization techniques, there is lack of the studies that combine the parametrization of the rotor blade for both numerical and analytical analysis, where the analytical model takes into consideration the inertia and mass features of the structure.

The novelty of this study lies in combining analytical research with computer analysis of the blade structure to obtain exact mass and inertia parameters and optimize the shape of the spar across various spar cross-sections.

The analytical analysis for generating the structure is conducted using MATLAB software. Originally developed codes, with implemented mathematical formulas, calculate main rotor loads and bending moments. The generated loads are presented graphically as functions of radius and azimuth. The natural frequencies are also shown in charts. The process of generating the load and frequency shapes is automated and implemented into the code. The program recalculates the inertia parameters at selected cross sections of the blade, providing a comprehensive tool for analyzing structural features and working conditions. Consequently, the designer can quickly evaluate the case and identify possible weak points and faults.

Calculated loads are transferred into a CAD parametric optimization program (prepared using GRIP), where the shape is formed and assessed to meet the given material properties using an optimization procedure. The research also introduces features of modern composite structures.

To the best of the authors' knowledge, the approach presented in this paper has not been combined in any known research, making it unique in main rotor blade structure design studies.

Analytical model

Main rotor aerodynamic load

To estimate the main rotor aerodynamic loads for structural analysis, it is necessary to calculate the main rotor trim angles. The method of trimming was described in the previous phase of the study (Kocjan *et al.*, 2022) Trimming can be performed for all types of flight conditions. Finding pitch angles and flap angles is the first step in determining the main rotor blade load:

$$\theta(\psi) = \theta_0 - \theta_1 \cos(\psi) - \theta_2 \sin(\psi) \tag{1}$$

$$\beta(\psi) = \beta_0 - \beta_1 \cos(\psi) - \beta_2 \sin(\psi) \tag{2}$$

where θ are pith angles, β are flap angles and the ψ is rotor blade azimuth. The rotor motion is shown in Figure 1.

The rotor thrust which can be assumed as a rotor lift is given with the equation:

$$dT = \frac{1}{2} a\rho\left(\theta U_T^2 + U_p / U_{UT}\right) dr \tag{3}$$

where a is the lift curve slope and ρ is the air density. However, to calculate the thrust an velocity components at the blade are needed to be estimated:

$$U_p = \Omega \mathrm{R}\left(\lambda' - \frac{x\dot{\beta}}{\Omega} - \mu\beta\cos\psi\right) \tag{4}$$

$$U_T = \Omega \mathrm{R}(\mathrm{x} + \mu \sin\psi) \tag{5}$$

where Ω is main rotor rotational velocity, R is the rotor radius, and μ is the advance ratio. The inflow ratio is given with:

$$\left(\lambda' = (V\sin\alpha_D - \nu_i)/\Omega \mathrm{R}\right. \tag{6}$$

where V is the rotorcraft velocity α_D is rotor disc angle of attack and ν_{i} is the rotor induced velocity.

Rotor blade normal modes and frequencies

Estimating the bending shapes of the rotor blade requires calculating the natural frequencies and normal modes. There is no single technique or procedure to determine the values of vibration parameters. For this research, the Rayleigh–Ritz method was chosen, and the algorithm used is based on (Wilde and Price, 1965) In this method, the energy equation of the rotating beam is minimized:

$$\epsilon = \int_0^R \left\{ EI\left(\frac{d^2y}{dr^2}\right)^2 + \frac{1}{2}\overline{m}\Omega^2(R^2 - r^2)\left(\frac{dy}{dr}\right)^2 - m\omega^2 y^2 \right\} dr \tag{7}$$

where E is the Young Modulus, I is the second moment of area, y is the natural mode shape and ω is the natural frequency.

The applied method of solution provides possibilities for using the method in numerical software. The equation is transformed into matrix form, with each part being transformed into Fourier series. This allows for the application of nonconstant mass distribution into the procedure and enables the utilization of the orthonormality properties of Fourier series. To further simplify the procedure, the spanwise coordinate is given as $x = \pi r/R$. Then the equation's components are:

$$\frac{EI(x)\pi^2}{R} = \sum_1^\infty p_n \cos nx \tag{8}$$

$$\frac{\overline{m}\Omega^2 R^2(\pi^2 - x^2)}{2\pi^2} = \sum_1^\infty q_n \cos nx \tag{9}$$

$$y = a_0 x - \sum_1^\infty a_n \sin nx \tag{10}$$

Substituting the parts of energy expression we get:

$$E = \int_0^\pi \left\{ \left(\sum_1^\infty p_n \cos nx\right)\left(\sum_1^\infty n^2 a_n \sin nx\right)^2 + \left(\sum_1^\infty q_n \cos nx\right) \left(a_0 - \sum_1^\infty n a_n \sin nx\right)^2 - r_0\omega^2\left(a_0 x - \sum_1^\infty a_n \sin nx\right)^2 \right\} dx \tag{11}$$

These equation can be written in a matrix form and A and B are symmetric matrices with p and q coefficients:

$$\left(A^{-1}B - \frac{I}{\Gamma^2}\right)\underline{a} = 0 \tag{12}$$

where $\Gamma^2 = 2\omega^2 r_0$ and a is the matrix of coefficients of normal modes shape. Calculating the latent roots of the matrix $A^{-1}B$ the natural frequencies and shapes are obtained.

Rotor flapping blade bending moment

After preparing the earlier results, the bending moment can be estimated for different spanwise coordinates and azimuthal locations. The first step is to establish the external forces on the blade. These external forces consist of:

- the elementary lift $\mathrm{dT}=\mathrm{dF_a}$;
- the blade weight $m'gdx$;
- centrifugal force of rotation $m'\omega^2 r\beta dx$;
- the force inertia for flapping $-mx\ddot{\beta}$;
- the force of inertia of deflection $-mx\ddot{y}$;
- the centrifugal force of flapping $m'x\dot{\beta}2$;

Figure 1 Rotor velocity and blade motion

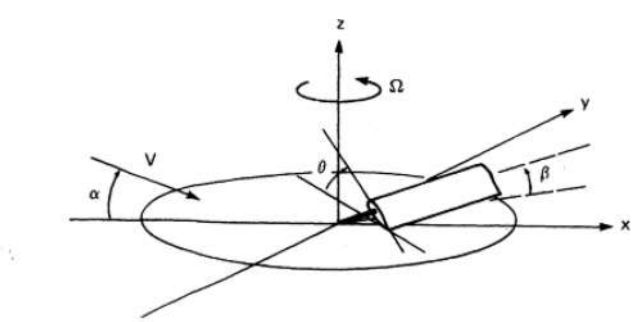

Source: Reproduced from Johnson (1994)

- the Coriolis force due to the simultaneous action of blade deflection and flapping motion $-2\dot{\beta}\dot{y}m'$; and
- corrective term of the damping of the lift force due to the flexural elastic deformation of the blade $-K\dot{y}$.

In this calculation, the Euler–Bernoulli beam theory was chosen. In this theory, the main assumptions are that the cross section of the beam is rigid (i.e. no deformations occur in the plane of the cross section), and shear deformations are neglected. The cross section remains plane, unstretched and normal to the deformed axis of the beam after deformation.

Authors resigned from using the Timoshenko beam theory, which is mostly used in the case of short or thick beams where shear effects can be significant. This theory includes the effects of shear deformation. As a result, the difference in Timoshenko theory is that after deformation, the cross section of the beam is no longer normal to the beam axis. As mentioned above, this effect can be neglected.

The differential equation of the blade is then:

$$\frac{d^2}{dx^2}\left(EI\frac{d^2y}{dx^2}\right)-\omega^2\frac{d}{dx}\left(\frac{dy}{dx}\int_x^R m'(a+\xi)d\xi\right)+m'\ddot{y}+K\dot{y} = \frac{dF}{dx}-m'g-mx\ddot{\beta}-m'\omega^2 r\beta \quad (13)$$

The differential equation must be fulfilled by four conditions, which specify the integration constants:

$$y=0 \ \text{for}\ x=0 \quad (14)$$

$$EI\frac{d^2y}{dx^2}=0\ \text{for}\ x=0\ \text{and for}\ x=R-a \quad (15)$$

$$\frac{d^2}{dx^2}\left(EI\frac{d^2y}{dx^2}\right)=0\ \text{for}\ x=R-a \quad (16)$$

To solve the deflection equation the second member, which is independent of the deflection can be put into function $dF_d=\mathrm{dFa}-\ m'g-\ m'\omega 2\ x-mx\ddot{\beta}$. We also put: $\int_x^R m'(a+\xi)d\xi=S$ so the final form is:

$$\frac{d^2}{dx^2}\left(EI\frac{d^2y}{dx^2}\right)-\omega^2\frac{d}{dx}\left(s\frac{dy}{dx}\right)+m'\ddot{y}+K\dot{y}=\dot{F}'_d(x,t) \quad (17)$$

The applied calculation formula estimates the distribution of bending moment to the third harmonic of natural shape. This method was chosen due to its compatibility with the MATLAB environment.

Initially, we use the natural deflection functions of the rotor blade to solve it. For simplicity, we consider the vibration state to be undamped. The bending moment is assumed to result from the forces acting on the rigid blade. In addition, the time function can be expanded into a series of periodic functions, represented as $\psi=\omega t$, therefore:

$$M_{rig}=M_0+M_a\cos\psi+M_b\sin\psi+M_{2a}\cos2\psi+M_{2b}\sin2\psi+M_{3a}\cos3\psi+M_{3b}\sin3\psi\ldots \quad (18)$$

This moment concerns the distribution of external force F'_d which constitute the second term of the equation. These forces should also be resolved at each point as a series of deflection distributions correlated with the natural mode shape. The natural functions can always be resolved into series. The proposed series take form:

$$F'_d=g_0m'\eta_0+g_1m'\eta_1+g_2m'\eta_2+\ldots \quad (19)$$

where g_i is the function a function of time only and η_i is the bending natural function of the order i.

The i order deflection of the main rotor blade affects at each point the natural mode function, it is given by function:

$$y_i=h_i\eta_i \quad (20)$$

where h_i is the function of time. The deflection is obtained by superposing the many natural deflections of the blade vibrating at the corresponding natural frequencies, using the h_i function which defines the amplitude and phase. Therefore, for the i-order frequency:

$$h_i\frac{d^2}{dx^2}\left(EI\frac{d^2\eta_i}{dx^2}\right)-h_i\omega^2\frac{d}{dx}\left(s\frac{d\eta_i}{dx}\right)+h_im'\ddot{y}=g_im'\eta_i \quad (21)$$

Next, the natural vibrations of a freely vibrating blade with an angular velocity ω allow an infinite quantity of solutions, using η *sinvt* a function a limiting conditions and the below function is satisfied:

$$\frac{d^2}{dx^2}\left(EI\frac{d^2\eta}{dx^2}\right)-\omega^2\frac{d}{dx}\left(s\frac{d\eta}{dx}\right)=\nu^2m'\eta_i \quad (22)$$

As a consequence, for the natural function we obtain a rotating beam function for every natural frequency:

$$\frac{d^2}{dx^2}\left(EI\frac{d^2\eta_i}{dx^2}\right)-\omega^2\frac{d}{dx}\left(s\frac{d\eta_i}{dx}\right)=\nu_{i,\omega}^2m'\eta_i \quad (23)$$

where $\nu_{i,\omega}$ is the corresponding function of natural frequency at the ω speed of rotation.

When the equations are simplified, the result is:

$$h_i\nu_{i,\omega}^2+\ddot{h}_i=g_i \quad (24)$$

The functions given above $h_i\ g_i$ are periodic with respect to ψ, so there can be transformed into series:

$$h_i=h_{i,0}+h_{i,a}\cos\psi+h_{i,b}\sin\psi+h_{i,2a}\cos2\psi+h_{i,2b}\sin2\psi+h_{i,3a}\cos3\psi+h_{i,3b}\sin3\psi\ldots \quad (25)$$

$$g_i=g_{i,0}+g_{i,a}\cos\psi+g_{i,b}\sin\psi+g_{i,2a}\cos2\psi+g_{i,2b}\sin2\psi+g_{i,3a}\cos3\psi+g_{i,3b}\sin3\psi\ldots \quad (26)$$

Therefore, the differential equation can be written:

$$\sum_{i=0}^{i=\infty}\left[h_i\frac{d^2}{dx^2}\left(EI\frac{d^2\eta_i}{dx^2}\right)-h_i\omega^2\frac{d}{dx}\left(s\frac{d\eta_i}{dx}\right)+h_im'\ddot{y}\right]=\sum\nolimits_{i=0}^{i=\infty}g_im'\eta_i \quad (27)$$

Limiting the equation to third harmonic and resolving the identification of the coefficients, it can be reduced into:

$$h_{i,0}\nu_{i,\omega}^2 = g_{i,0} \tag{28}$$

$$h_{i,a}\left(\nu_{i,\omega}^2 - \omega^2\right) = g_{i,a} \tag{29}$$

$$h_{i,b}\left(\nu_{i,\omega}^2 - \omega^2\right) = g_{i,b} \tag{30}$$

$$h_{i,2a}\left(\nu_{i,\omega}^2 - 4\omega^2\right) = g_{i,2a} \tag{31}$$

$$h_{i,2b}\left(\nu_{i,\omega}^2 - 4\omega^2\right) = g_{i2b} \tag{32}$$

$$h_{i,3a}\left(\nu_{i,\omega}^2 - 9\omega^2\right) = g_{i,3a} \tag{33}$$

$$h_{i,3b}\left(\nu_{i,\omega}^2 - 9\omega^2\right) = g_{i3b} \tag{34}$$

To determine the g_i it is needed to multiply the members of the equation (19) by η_i and conduct integration over the blade.

Taking into consideration the orthogonality condition:

$$\int_0^R m'\eta_i\eta_j dx = 0 \qquad i \neq j \tag{35}$$

it provides:

$$\int_0^R F'_d\eta_i dx = g_i\int_0^R m'\eta_i{}^2 dx \tag{36}$$

$$g_i = \frac{\int_0^R F'_d\eta_i dx}{\int_0^R m'\eta_i{}^2 dx} \tag{37}$$

Next, the bending moment on the deformable main rotor blade is computed. The single harmonic acting the outside forces, produces the elastic deformation:

$$\sum_{i=1}^{i=\infty}\left[g_{i,na}m'\eta_i\cos n\psi + g_{i,nb}m'\eta_i\sin n\psi\right] \tag{38}$$

which is:

$$\sum_{i=1}^{i=\infty} y_{i,n}\left\{\begin{matrix} a \\ b \end{matrix}\right. = \sum_{i=1}^{i=\infty} h_{i,n}\left\{\begin{matrix} a \\ b \end{matrix}\right. \eta_i \tag{39}$$

When the terms h_i are replaced by values which are obtained from (28–34), the corresponding bending moment:

$$M_{elast\ n}\left\{\begin{matrix} a \\ b \end{matrix}\right. = \frac{g_{i,n}\left\{\begin{matrix} a \\ b \end{matrix}\right.}{\nu_{i,\omega}^2 - n^2\omega^2} - EI\frac{d^2\eta_i}{dx^2}\left\{\begin{matrix} \cos n\psi \\ \sin n\psi \end{matrix}\right. \tag{40}$$

Because the natural functions exhibit minimal variation with changes in angular velocity, the ith order natural function at $\omega = 0$, is comparable to the same natural function for the standard angular velocity. This simplification incurs an error of only 3%, making it suitable for application in this solution.

As a consequence, the natural function η_i fulfills the equation (23) and:

$$\frac{d^2}{dx^2}\left(EI\frac{d^2\eta_i}{dx^2}\right) = \nu_{i,0}^2 m'\eta_i \tag{41}$$

In result:

$$EI\frac{d^2\eta_i}{dx^2} = \nu_{i,0}^2\iint_x^R m'\eta_i dx d\xi \tag{42}$$

After replacing in (40) the value of $EI\frac{d^2\eta_i}{dx^2}$ with (42), the elastic blade bending moment equation is obtained, which is can be integrated along the blade:

$$M_{elast\ n}\left\{\begin{matrix} a \\ b \end{matrix}\right. = \sum_{i=1}^{i=\infty}\left(\frac{\nu_{i,0}^2}{\nu_{i,\omega}^2 - n^2\omega^2} g_{i,n}\left\{\begin{matrix} a \\ b \end{matrix}\right.\iint_x^R m'\eta_i dx d\xi\right) \tag{43}$$

The value of the g_i is calculated from (37) for the azimuth values for a given acting forces. The expansion of the g_i into Fourier series expresses the coefficient:

$$g_{i,n}\left\{\begin{matrix} a \\ b \end{matrix}\right. \tag{44}$$

Practical bending moment calculation procedure

Considering the equation calculation, a practical calculation method is proposed in de Guillenchmidt (1951). This method offers a step-by-step solution that can be applied to numerical calculations. The first step, as described earlier, involves calculating the natural functions and corresponding natural frequencies of both rotating and nonrotating blades. In the second step, we evaluate the values:

$$\int_0^R m'\eta_1{}^2 dx\int_0^R m'\eta_2{}^2 dx\int_0^R m'\eta_3{}^2 dx \tag{45}$$

Next step is to determine the outside forces on the rigid main rotor blade for different ψ (minimum eight positions with 45° spacing), so the position are evaluated for:

$$\int_0^R F'_d\eta_1 dx\int_0^R F'_d\eta_2 dx\ \int_0^R F'_d\eta_3 dx \tag{46}$$

Taking into consideration the (37) equation the function are calculated:

$$g_1 = \frac{\int_0^R F'_d\eta_1 dx}{\int_0^R m'\eta_1{}^2 dx}\ g_2 = \frac{\int_0^R F'_d\eta_2 dx}{\int_0^R m'\eta_2{}^2 dx}\ g_3 = \frac{\int_0^R F'_d\eta_3 dx}{\int_0^R m'\eta_3{}^2 dx} \tag{47}$$

The function (47) can be developed into Fourier series. The series are produced to third harmonic of ψ:

$$\begin{matrix} g_{1,0} & g_{1,a} & g_{1,b} & \cdots & g_{1,3b} \\ g_{2,0} & g_{2,a} & g_{2,b} & \cdots & g_{2,3b} \\ g_{3,0} & g_{3,a} & g_{3,b} & \cdots & g_{3,3b} \end{matrix} \tag{48}$$

The bending moments are calculated for each harmonic and for different station on the blade span using equation:

$$M_x = \sum_{i=1}^{i=3} M_{i,x} \tag{49}$$

The inner functions are estimated with:

$$M_{i,x} = \iint_x^R m' \eta_i dx d\xi \big[A_{i,0} + A_{i,1}\cos\big(\psi - \psi_{i,1} - \varphi_{i,1}\big) + A_{i,2}\cos\big(2\psi - \psi_{i,2} - \varphi_{i,2}\big) + A_{i,3}\cos\big(3\psi - \psi_{i,3} - \varphi_{i,3}\big)\big] \tag{50}$$

where

$$A_{i,0} = \frac{\nu_{i,0}^2}{\nu_{i,\omega}^2} g_{i,0} \tag{51}$$

$$A_{i,n} = \frac{\nu_{i,0}^2 \sqrt{g^2{}_{i,na} + g^2{}_{i,nb}}}{\sqrt{\left(\nu_{i,\omega}^2 - n^2\omega^2\right)^2 + n^2\Phi^2\omega^4}} \tag{52}$$

$$\tan\psi_{i,n} = \frac{\omega^2 n\Phi}{\left(\nu_{i,\omega}^2 - n^2\omega^2\right)} \tag{53}$$

$$\tan\varphi_{i,n} = \frac{g_{i,nb}}{g_{i,na}} \tag{54}$$

Optimization method

As it was mentioned in introduction this paper presents the part of research that is aimed at finding solutions for main rotor optimization problem. The proposed algorithm for the entire program is presented on Figure 2. The structure optimization is an inner procedure inside the presented loop. It is included inside the "parametric modelling" element, where the outer shape and CFD enclosures are generated, as well as the blade inner structure.

The inner structure optimization is performed using computer techniques; however, some mathematical assumptions must be made. This procedure is a single-criterion mass reduction process while maintaining the required strength. The mathematical description is presented below:

- *Decision variables*: h – spar height, d – honeycomb wall position, t – spar thickness
- *Parameters*: material properties, flight conditions
- *Constraints*: σdop > σmax(h, d, t) – strength condition; $h > 0$, $t > 0$, max airfoil thickness position > d >0
- *Criteria*: $m(h, d, t) \rightarrow$ minimum

The process of resolving main rotor blade stresses and subsequently optimizing the shape is divided into steps, with each step described in consecutive chapters.

The first phase of the proposed method involves resolving the mathematical model presented in Chapter 2. This model was implemented in the MATLAB environment to solve equations and compute values for rotor parameters. The results serve as the basis for a customized GRIP program to assess the best structural shape.

Figure 2 Main rotor optimization research algorithm

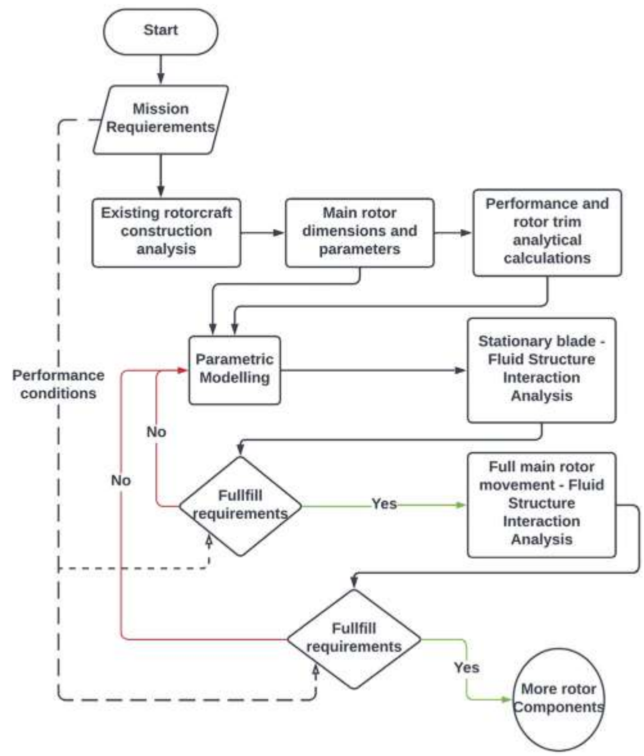

Analytical solving

The problem was divided into two separate codes. The first one was prepared for the main rotor trim, involving calculations of blade loads. The second one focused on blade mode shapes, natural frequencies, and finally, the determination of bending moment values and distribution.

To initiate the calculations, the first code begins with declaring the geometric and aerodynamic parameters of the main rotor. Basic helicopter parameters, especially weight, are also included. In the input section, initial blade mass parameters are declared. These parameters can be based on an existing blade or estimated using statistical data from similar constructions. Such statistics were compiled in the initial phase of the research program (Kachel *et al.*, 2021).

In addition, the user declares the flight conditions under which the main rotor blade stresses are evaluated. These conditions describe the flight with the forward speed and climb, and include the statistical change of the center of gravity as a function of velocity. The forward speed is also calculated in the form of an advance ratio.

The next step involves parameterizing the rotor chord and twist so that their values can vary along the span. The calculated coefficients will also be used in the program that generates the geometry for structural evaluation.

The subsequent stage of the procedure involves trimming the main rotor pitch and flap angles. The code has been partially prepared in previous phases of the research. Trim angles are determined by resolving acting forces horizontally and vertically with reference to the rotor-disc plane. After acquiring the trim angles, the blade aerodynamic loading can be determined. By solving the equations of velocity components, the lift distribution is obtained. Examples of aerodynamic loading distribution generated using the MATLAB environment are shown in Figure 3, whereas the total aerodynamic loading is depicted in Figure 4. These figures illustrate that the calculated loading offers a means to evaluate the rotor's working conditions. It can be seen that the behavior of aerodynamic forces slightly changes with inflow ratio increase. Especially on advancing blade position (azimuth 135° represents the transition position), where the influence of maximum forward speed, due to the inflow angle change, is reducing the aerodynamic force. The blade geometric twist is provided to reduce the diminish the negative force value.

The second calculation program, which receives the aerodynamic loading from the first procedure, is used to find first the natural modes and frequencies and next solve the bending moment equation. It also includes the declaration of inputs part of the code, where the geometry and mass dimensions of the rotor are given. In this phase, the stiffness declaration is provided as a function of material Young modulus and moment of inertia. The stiffness alters along the span due to the change of cross section of the blade spar. The moments of inertia are established using the GRIP program, which will be described later.

Furthermore, the program calculates the natural mode shapes and frequencies. The calculation procedure implemented in the code is described in section Rotor blade normal modes and frequencies. Matrices are prepared to compute the vibration quantities up to the 8th harmonic. Using the built-in functions of MATLAB, the results are easily obtained. Functions are transformed into Fourier series using the Fourier Series integral definition, and then matrices of coefficients are constructed. The eigenvalues of the matrices equation are determined using MATLAB's built-in functions. The characteristics can be evaluated for every shape of a blade and materials that are used. Exemplary results for the rotor blade (W-3 helicopter rotor blade shape) are depicted in Figure 5. The natural function value is normalized and the radius is parameterized as a function of π.

Figure 3 Aerodynamic loading distribution for different inflow ratio (flight speed)

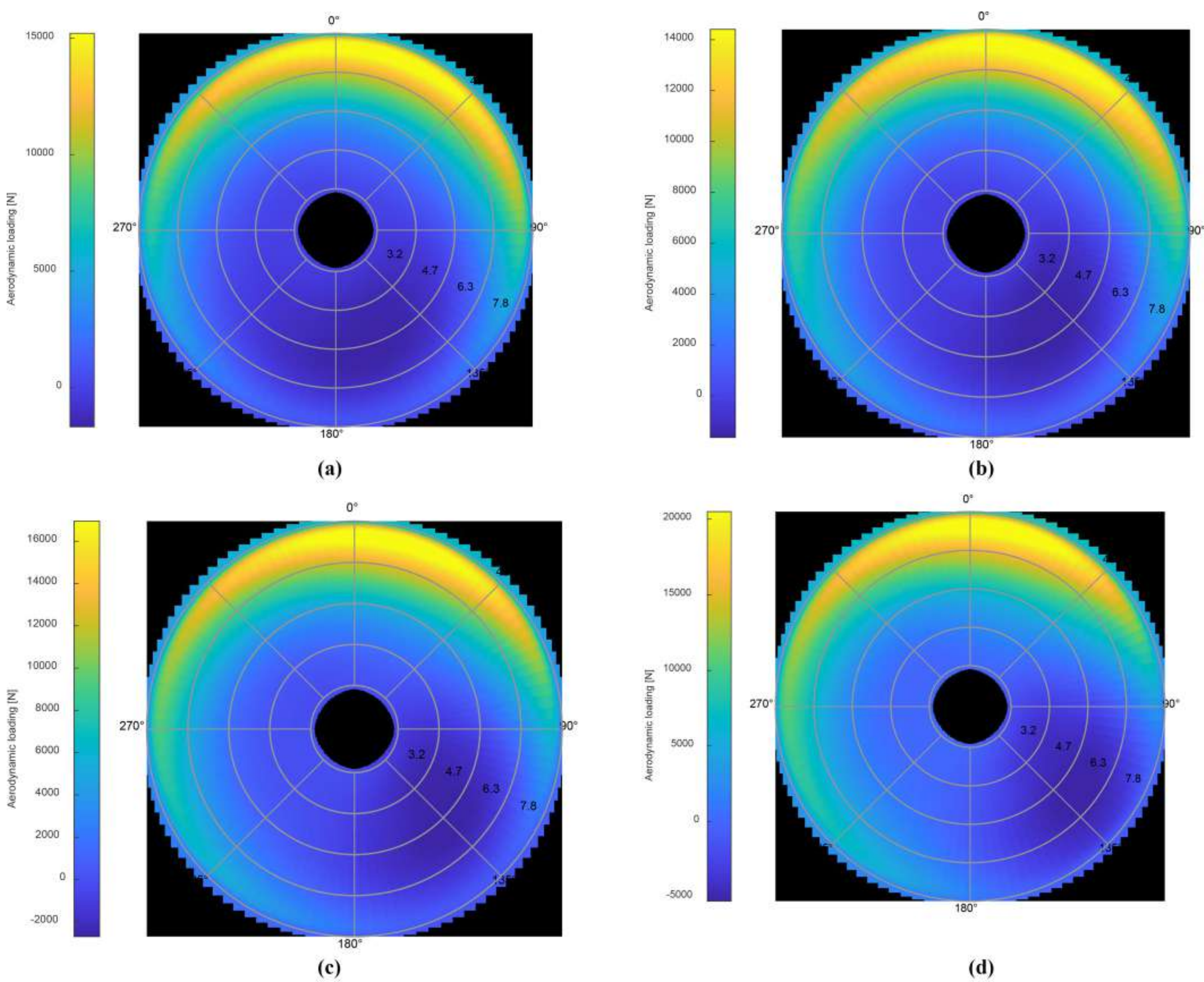

Note: (a) $\mu = 0.1$; (b) $\mu = 0.15$; (c) $\mu = 0.2$; (d) $\mu = 0.25$

Figure 4 Aerodynamic loading in function of radius for: $\mu = 0.1$

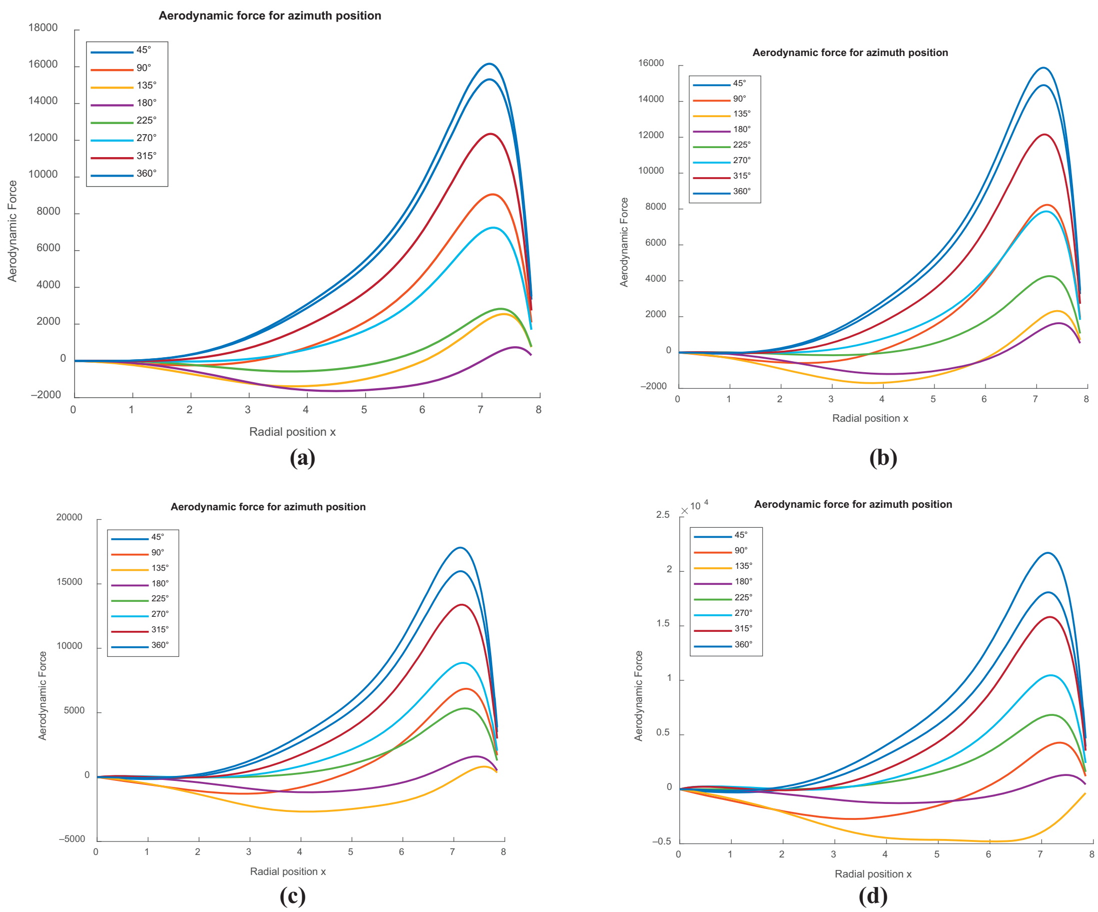

Note: (a) $\mu = 0.1$; (b) $\mu = 0.15$; (c) $\mu = 0.2$; (d) $\mu = 0.25$

In the next step of the code execution, the bending moment for the first three harmonics is obtained. The outside forces, established in the first program and described in section Main rotor aerodynamic load, are input for the aerodynamic loading. The damping coefficient is estimated, and then the outside force and mass distribution are correlated with the natural vibration shape. The procedure is applied as follows: the time functions g_i are calculated for each harmonic, and the resultant equations are substituted into the bending moment function, respectively, to the harmonic number. The calculations end with summing the total bending moment, which is a function of radius and azimuth. An example of the values of bending moment depending on the radius and azimuth is shown in Figure 6. The maximum bending moment values are written into a file to serve as input for geometry strength analysis.

Graphics integrated programming

The primary objective of this study is to develop a new method for preparing the main rotor blade geometry for FSI analysis and optimization. The aim is to reduce the time consumption of complex simulations and find the best strength structure by combining analytical calculations with the capabilities of open GRIP inertia analysis code, which is an integral part of Siemens NX. The program has been partially used because the initial stages of the study, as the external geometry needs to be exact for further FSI simulations, ensuring connections of corresponding faces.

The blade model is parametrized in the program using main rotor geometric features. The designer can input values into a popup input window, corresponding with the input values from MATLAB programs. The first parameter is the blade chord and rotor radius. The airfoil is shaped from a text file with the coordinates, allowing the operator to prepare the geometry for any chosen airfoil. The next phase of parametrization involves polynomial coefficients for twist and chord of the blade, allowing them to vary along the span. The outer model is filled with the structure. The inner assembly of the blade is based on existing solutions, with the main spar and filling in the leading edge part, and a honeycomb structure in the trailing edge part. An illustration of the CAD model is shown in Figure 7.

With the prepared solution, the blade shape can be freely changed in accordance with the analytically calculated values. The shape building process relies on built-in GRIP commands for lines and splines, which are used to create the requested shape.

Furthermore, the program conducts the analysis and strength calculation. Using integral commands, the mass and inertia analysis of the cross sections and the entire 3D geometry are performed. As a result, the moment of inertia of cross sections is obtained. The density of the parts is programmed by the user,

Figure 5 Natural modes and frequencies

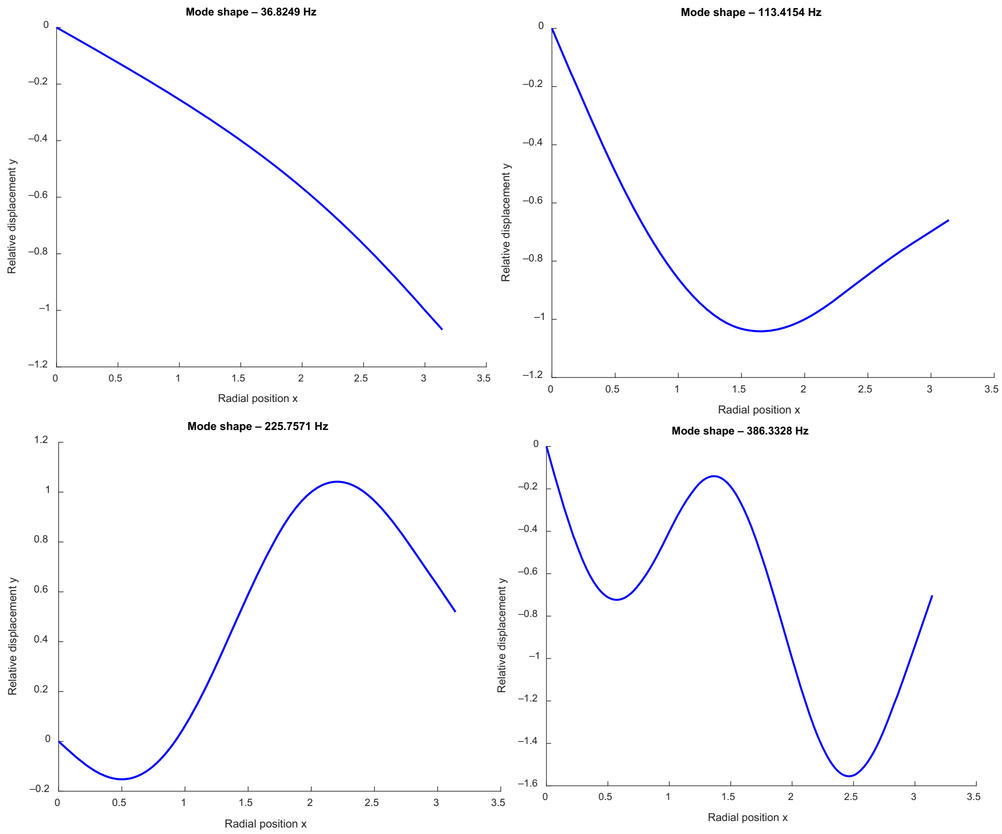

Figure 6 Main rotor blade bending moment function

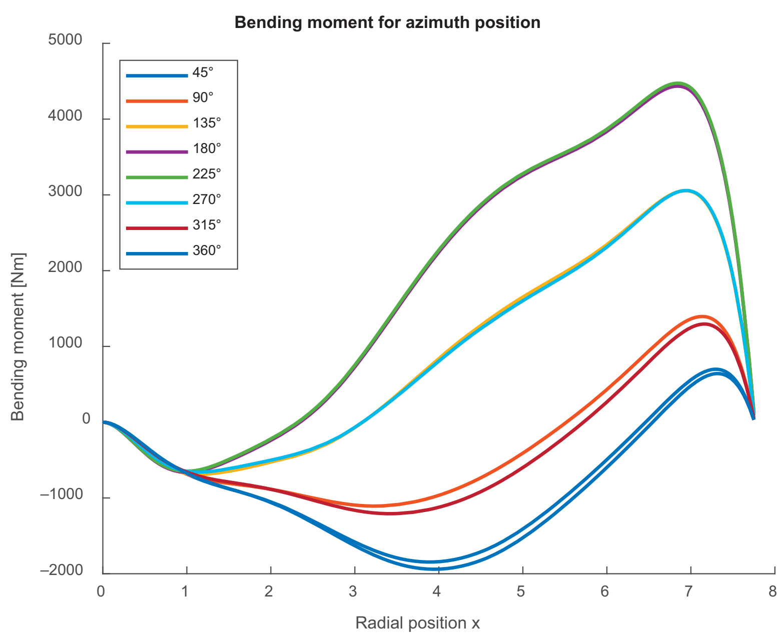

allowing the 3D analysis to provide the total mass of the blade and the mass of the components. The moment acting on a blade in respective sections is loaded from the file generated previously. The strength equations are programmed within the code. Stresses are calculated for each cross section using bending moment values and the moment of inertia from the GRIP analysis. Finally, it is checked whether the required stiffness is sufficient for the given loads. The program adjusts the spar

Figure 7 Main rotor blade CAD model for calculation

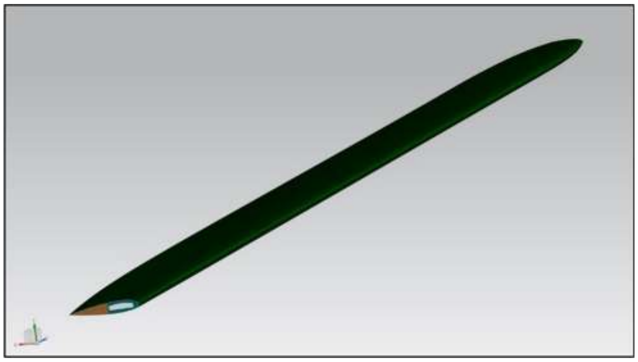

dimensions to meet the stiffness requirement and iterates the calculation until the requirements are met. The iterative procedure modifies the dimensions in each step and evaluates the new shape. A safety factor of 1.2 is proposed, but it can be changed by the user. As a result, a CAD geometry is provided, which can be applied in further complex analysis. An example of the code with analysis options is shown in Figure 8.

Example of results

The steps that were described in the previous chapters were combined into an optimization procedure. The entire procedure is shown in Figure 9.

To demonstrate the capabilities of the procedure, the W-3 helicopter main rotor blade was recalculated using the original blade dimensions and modern materials applied to the proposed structure. The properties of the composite materials used are presented in Table 1.

The procedure was conducted within six iteration loops. The mass reduction and change of the center of mass are shown in Table 2.

In each step, the change of the cross section and consequently the change of the moment of inertia is considered. The geometry is generated automatically, and the output is provided as the blade CAD model. The spar cross section varies along the span in accordance with the calculated bending moments.

Evaluation of the model

To validate the generated model, a one-way FSI simulation is conducted. One-way FSI was chosen to check the optimized structure in simulated blade working conditions. The CFD simulation is proposed as stationary, so the forces produced are transferred one-way to the structure. This approach allows for the assessment of stresses and deformations. In the next research step, a two-way FSI for transient n-blade simulation will be established, taking into consideration the evaluated structure as described in this paper. The CFD part of the simulation is configured for a single-blade fluid enclosure, as demonstrated in the previous part of the research published in Kocjan *et al.* (2022). The pressure distribution from the mentioned CFD simulation is applied to the FEM model. According to MATLAB calculations, the flight conditions for a blade at an azimuthal position of 360° are simulated. The inflow is parameterized using calculated functions. An example of pressure distribution is shown in Figure 10.

Figure 8 Code example

```
SPAR(4)=BSURF/MESH,LNS5(3..4),WITH,LNS3(1..K),TYPE,3,TOLER,.01,.01
SPAR(5)=BSURF/MESH,LNS5(4),LNS5(1),WITH,LNS4(1..K),TYPE,3,TOLER,.01,.01
SPAR(6)=AUTOSF/LNS1(1),LNS2(1),LNS3(1),LNS4(1)
SPAR(7)=AUTOSF/LNS1(K),LNS2(K),LNS3(K),LNS4(K)
SPAR(8)=SEW/SPAR(2..7)

BLD(7)=SEW/SSRF(6..9)
MAT=MATRIX/TRANSL,0,0,0
BLD(5)=TRANSF/MAT,BLD(7)
SPAR(1)=TRANSF/MAT,SPAR(8)

BLD(6)= SUBTRA/BLD(8),WITH,BLD(7),CNT,c $$ enclosure


DELETE/LN,PT2,PT3,PT4,PT5,PT6,SPLC



PLN(1)=PLANE/YZPLAN,C0/3+wall
BLD(1..2)= SPLIT/BLD(5),WITH,PLN(1)

PLN(2)=PLANE/XYPLAN,A(3)+1
SEC(1..3)= SECT/BLD(1),WITH,PLN(2)
BND(1)=BOUND/SEC(1..3)
BND(2)=BOUND/LNS1(1),LNS2(1),LNS3(1),LNS4(1)
ANLSIS/TWOD,BND(1),MMETER,wyn2
ANLSIS/TWOD,BND(2),MMETER,wyn3






PRINT/'--------Spar Cross section analysis-----------'
PRINT/USING,'Cross section area Fdz=#@@@@@@.@@ [mm^2]',wyn2(2)-wyn3(2)
PRINT/USING,'Moment of Intertia Idz=#@@@@@@@.@@ [mm^4]',wyn2(9)-wyn3(9)
PRINT/USING,' center of mass:  X=#@@@@@@@@@@@@.@@@ mm',wyn2(3)
PRINT/USING,'                  Y=#@@@@@@@@@@@@.@@@ mm',wyn2(4)
PRINT/USING,' center of mass:  X=#@@@@@@@@@@@@.@@@ mm',wyn3(3)
PRINT/USING,'                  Y=#@@@@@@@@@@@@.@@@ mm',wyn3(4)
```

Aircraft Engineering and Aerospace Technology
Volume 97 · Number 1 · 2025 · 37–51

Figure 9 Initial structure optimization procedure

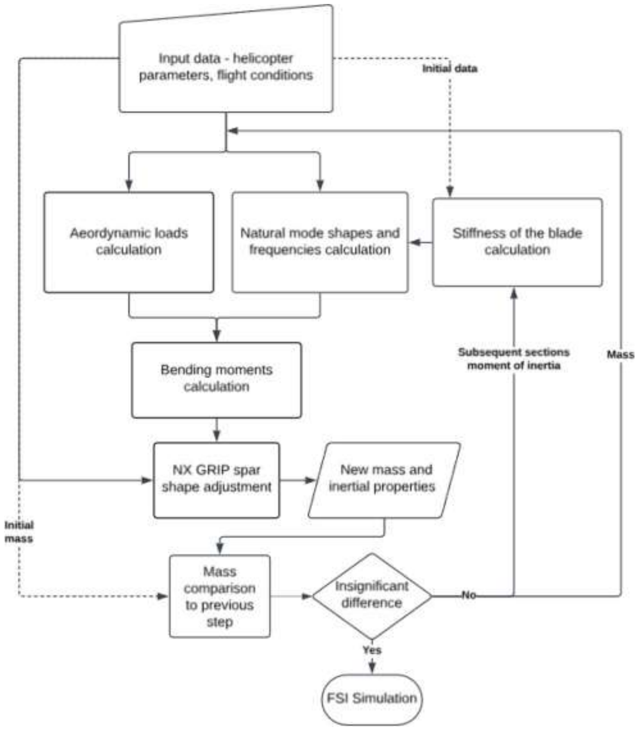

The pressure is transferred to the model generated from the CAD geometry prepared using the algorithm described in this study. The mesh was prepared using the tetrahedral mesher and thin mesher options. The base element size was set at 500 mm, with a target surface size of 0.025 m and a minimum surface size of 0.005 m. The meshing process was fully automated for the imported geometry. The results of the simulation confirm the parameters of the construction and provide information that the model is fully applicable in the FEM analysis environment. Examples of deformation and stresses are shown in Figures 11 and 12.

Discussion

This research introduces a new methodology for preparing geometry for subsequent FEM and FSI analyses. The first section outlines the analytical assumptions for the

Table 2 Iteration results

Step	Mass [kg]	Center of mass [m from rotor axis]
1	60	4.73
2	40.01	4.91
3	35	4.76
4	34.43	4.74
5	34.70	4.79
6	34.70	4.79

proposed solution, including calculations for loads and vibrations. The second part provides details on solving analytical problems using modern computer environments, accompanied by a description of the structural optimization method. Furthermore, an example of the resultant geometry with mass effects is presented, along with an evaluation using FSI calculations.

It has been demonstrated that the generated CAD model is fully compatible with FEM software and that meshes can be generated for even extremely complex blade shapes.

The proposed solution offers a novel approach to helicopter design. First, it addresses procedures for resolving natural mode shapes and vibrations of rotating blades, followed by blade trimming under various flight conditions. Furthermore, it provides aerodynamic loading of the blade as a function of radius and azimuth. Finally, the research includes the generation and preparation of a preliminary optimized main rotor blade structural model. These solutions can be used independently or combined for any blade shape and flight conditions.

The results of this research are valuable for reducing the time required to create and evaluate final models for various blade configurations. It is crucial to note that the model has been validated and is ready for implementation in further two-way FSI simulations for full rotor geometry.

To evaluate the solution, the proposed geometry is based on the existing rotor blade shape and dimensions. The forces were calculated using real mission objective parameters (e.g. velocity, height and payload). The flight parameters were also based on data from the Flight Data Recorder. An example of a 1-h flight is shown in Figure 13. The indicated velocity presented in the figure is effective from 50 km/h, due to the stream velocity from the rotor; however, it was not cut out to include the moments when the rotorcraft is on the ground.

Table 1 Material properties

Material property	Gr/E woven cloth	S-glass/E woven cloth	Nomex honeycomb
Young's modulus (E11) [Mpa]	1.69E + 03	6.45E + 02	4.06
Young's modulus (E22) [Mpa]	1.69E + 03	6.26E + 02	4.06
Young's modulus (E33) [Mpa]	2.36E + 02	1.60E + 02	4.06
Shear modulus (G12) [Mpa]	1.32E + 02	1.00E + 02	6.82
Shear modulus (G13) [Mpa]	1.32E + 02	1.00E + 02	6.82
Shear modulus (G23) [Mpa]	1.32E + 02	1.00E + 02	6.82
Poisson ratio (v12)	6.76E − 06	1.65E − 05	4.35E − 05
Poisson ratio (v13)	4.64E − 05	3.92E − 05	4.35E − 05
Poisson ratio (v23)	4.64E − 05	3.92E − 05	4.35E − 05
Density [kg/m^3]	1.60E + 03	1.80E + 03	6.41E + 01

Figure 10 Pressure distribution on the blade

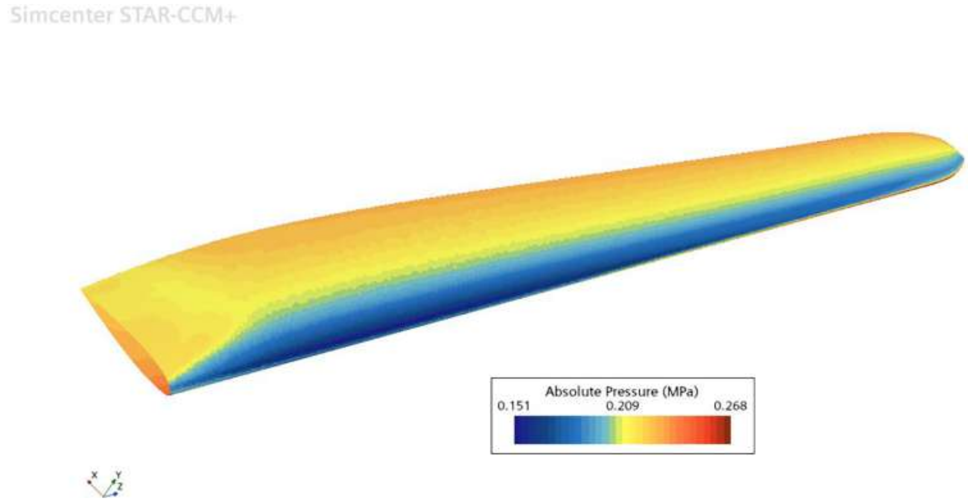

Figure 11 Blade deformation

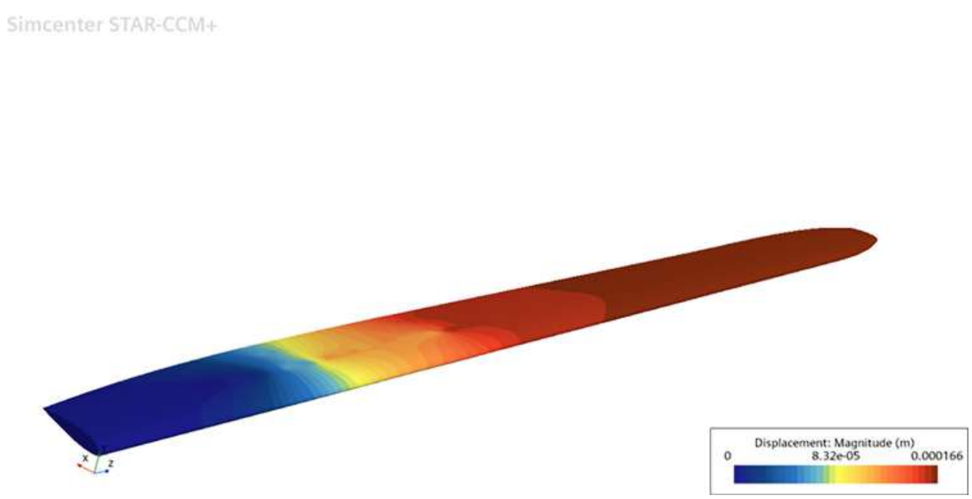

The proposed method is part of wider research; however, the studies described in this paper can be used as a stand-alone procedure during rotorcraft design. The tool can be used to assess the inner structure without integrating it with the proposed rotorcraft optimization procedure. Nevertheless, in this phase, it is limited to the Sikorsky helicopter layout. Nevertheless, the challenge of covering of the various blades structure was achieved for that layout.

Compared to existing design procedures, the main advantage of the presented solution is the versatility of the tool for various blade shapes, materials and environmental conditions, which can be examined in a short time. Practically, it can be implemented in the preliminary design phase of the rotorcraft, allowing many options to be evaluated and some to be chosen for the next design steps. It can also be implemented into the rotor blade lifecycle to assess the existing construction using data acquired during the rotorcraft's life – flight data, maintenance data, airworthiness data, etc.

Conclusion

The initial optimization of the structure is presented in this paper, showcasing a combination of analytical calculations and computer numerical analysis. The optimization of the spar shape was conducted in six steps, with the process lasting approximately 40 min. By parametrizing the spar dimensions in subsequent selected sections, shape optimization was achieved, resulting in the minimum mass of the spar, which has a significantly greater density compared to the remaining elements of the blade.

Considering the potentially time-consuming nature of computer calculations, particularly when simulating an articulated main rotor using FSI, the method outlined in the paper offers an original method to reducing the time required for model preparation for analysis. By inputting desired performance parameters and previously obtained aerodynamic features, the structure can be adapted to fit any proposed blade.

Figure 12 Stress distribution in the blade structure

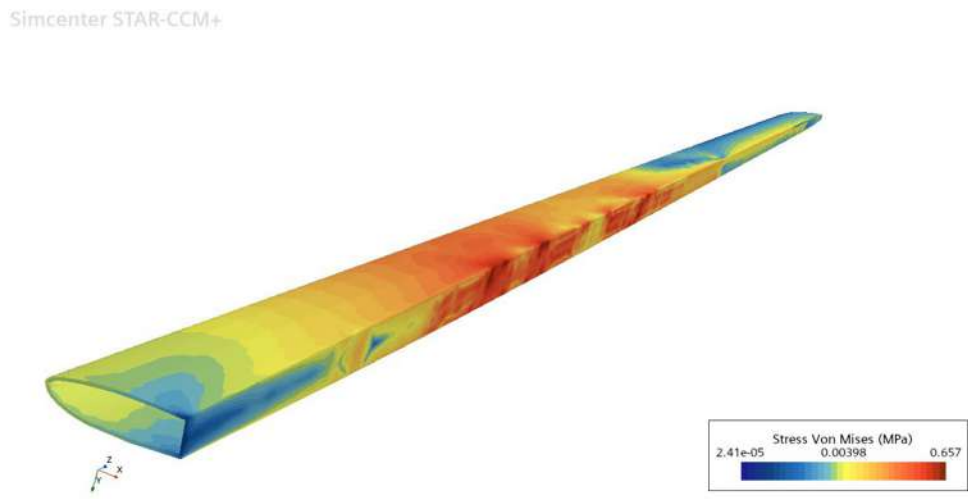

Figure 13 Indicated air speed, barometrical height and g-force

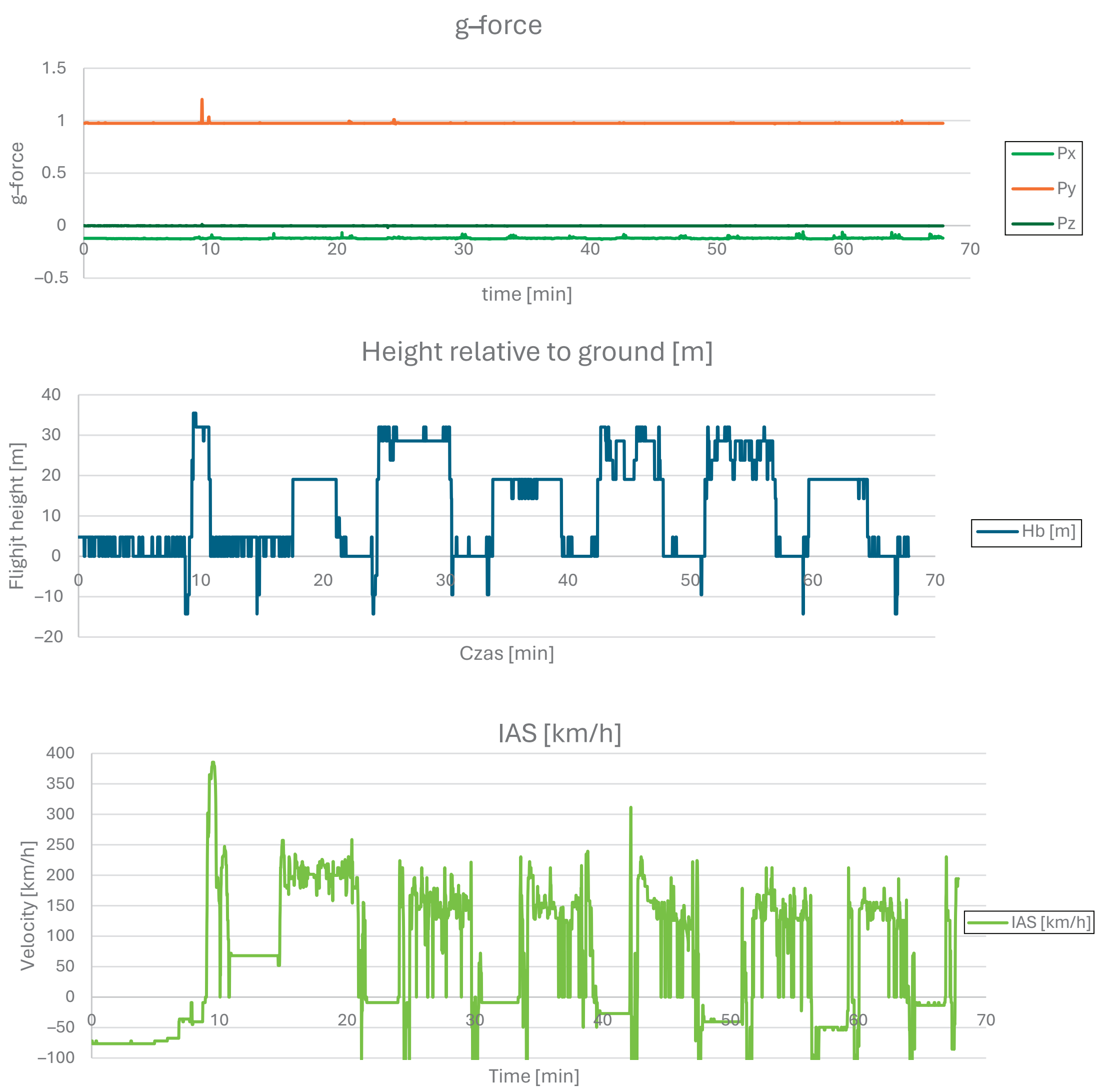

The evaluation of the structure, provided with one-way FSI analysis, demonstrates that the geometry is suitable for CAD/CAE software. Introducing a tool, such as the one presented in this paper, which automates mesh preparation, ensures repeatability of the process for future designs.

In conclusion, the research objectives have been achieved. The preparation method of the model using optimization techniques is ready to be used independently or can be integrated into a comprehensive optimization loop, as intended by the authors for further research endeavors. What is more, even though it is part of a research, the tool is ready to use and can be implemented into the design process as described and used to calculate and assess the blade structure. It can be used in industry to optimize not only the structure but also provide more efficient design and lifecycle analysis.

References

Allen, C.B., Morris, A.M. and Rendall, T.C.S. (2009), "CFD-based aerodynamic shape optimization of hovering rotors", Collection of Technical Papers – *AIAA Applied Aerodynamics Conference*, doi: 10.2514/6.2009-3522.

Allen, L.D., Lim, J.W., Haehnel, R.B. and Dettwiller, I.D. (2021), "Rotor blade design framework for airfoil shape optimization with performance considerations", AIAA Scitech 2021 Forum, doi: 10.2514/6.2021-0068.

Bailly, J., Bailly, D. and Didier, B. (2019), "Multifidelity aerodynamic optimization of a helicopter rotor blade", *AIAA Journal*, Vol. 57 No. 8, pp. 1-13, doi: 10.2514/1.J056513ï.

Barwey, D. and Peters, D.A. (1994), "Optimization of composite rotor blades with advanced structural and aerodynamic modeling", *Mathematical and Computer Modelling*, Vol. 19 Nos 3/4, doi: 10.1016/0895-7177(94)90064-7.

Chattopadhyay, A., McCarthy, T.R. and Pagaldipti, N. (1995), "Multilevel decomposition procedure for efficient design optimization of helicopter rotor blades", *AIAA Journal*, Vol. 33 No. 2, pp. 223-230, doi: 10.2514/3.12424.

Cornette, D., Kerdreux, B., Michon, G. and Gourinat, Y. (2015), "Aeroelastic tailoring of helicopter blades", *ASME. J. Comput. Nonlinear Dynam*, 1 November, Vol. 10 No. 6, p. 061001, doi: 10.1115/1.4027717.

de Guillenchmidt, P. (1951), "Calculation of the bending stresses in helicopter rotor blades", Washington, DC.

Ganguli, R. and Chopra, I. (1996), "Aeroelastic optimization of a helicopter rotor to reduce vibration and dynamic stresses", *Journal of Aircraft*, Vol. 33 No. 4, pp. 808-815, doi: 10.2514/3.47018.

Goerke, D., Le Denmat, A.L., Schmidt, T., Kocian, F. and Nicke, E. (2012), "Aerodynamic and mechanical optimization of CF/PEEK blades of a counter rotating fan", *Proceedings of the ASME Turbo Expo*, Vol. 7, pp. 21-33, doi: 10.1115/GT2012-68797.

Grabowik, C., Kalinowski, K., Kempa, W. and Paprocka, I. (2015), "A method of computer aided design with self-generative models in NX siemens environment", *IOP Conference Series: Materials Science and Engineering*, Vol. 95, p. 012123, doi: 10.1088/1757-899X/95/1/012123.

Guo, J.X. and Xiang, J.W. (2004), "Composite rotor blade design optimization for vibration reduction with aeroelastic constraints", *Chinese Journal of Aeronautics*, Vol. 17 No. 3, pp. 152-158, doi: 10.1016/S1000-9361(11)60230-6.

He, C.J. and Peters, D.A. (1992), "Optimization of rotor blades for combined structural, dynamic, and aerodynamic properties", *Structural Optimization*, Vol. 5 Nos 1/2, pp. 37-44, doi: 10.1007/BF01744694.

Johnson, C., Woodgate, M. and Barakos, G.N. (2016), "Optimising aspects of BERP-like rotors using frequency-domain methods", *Notes on Numerical Fluid Mechanics and Multidisciplinary Design*, Vol. 133, p. 639, doi: 10.1007/978-3-319-27386-0_15.

Kachel, S., Rogólski, R. and Kocjan, J. (2021), "Review of modern helicopter constructions and an outline of rotorcraft design parameters", *Problems of Mechatronics Armament Aviation Safety Engineering*, Vol. 12 No. 3, pp. 27-52, doi: 10.5604/01.3001.0015.2427.

Kizhakke Kodakkattu, S., Nair, P. and Ml, J. (2018), "Design optimization of helicopter rotor using kriging", *Aircraft Engineering and Aerospace Technology*, Vol. 90 No. 6, pp. 937-945, doi: 10.1108/AEAT-12-2016-0250.

Kocjan, J., Kachel, S. and Rogólski, R. (2022), "Helicopter main rotor blade parametric design for a preliminary aerodynamic analysis supported by CFD or panel method", *Materials*, Vol. 15 No. 12, p. 4275, doi: 10.3390/ma15124275.

Lim, J.W. (2018), "Application of parametric airfoil design for rotor performance improvement", 44th European Rotorcraft Forum 2018, ERF 2018, Vol. 1.

Liu, X. and Zhang, B. (2021), "Study on aeroelastic optimal design of composite blades", *Yingyong Lixue Xuebao/Chinese Journal of Applied Mechanics*, Vol. 38 No. 4, doi: 10.11776/cjam.38.04.A011.

Ma, L., Zhao, Q., Zhang, K., Zhang, X. and Zhao, M. (2021), "Aeroelastic analysis and structural parametric design of composite rotor blade", *Chinese Journal of Aeronautics*, Vol. 34 No. 1, pp. 336-349, doi: 10.1016/j.cja.2020.09.055.

Moffatt, S. and Griffiths, N. (2009), "Structural optimisation and aeroelastic tailoring of the BERP IV demonstrator blade", *Annual Forum Proceedings - AHS International*, Vol. 1.

Morris, A.M., Allen, C.B. and Rendall, T.C.S. (2008), "Aerodynamic optimisation of hovering helicopter rotors using efficient and flexible shape parameterisation", Collection of Technical Papers – *AIAA Applied Aerodynamics Conference*, doi: 10.2514/6.2008-7338.

Okumuş, O., Şenipek, M. and Ezertaş, A. (2022), "Multi-objective multi-fidelity aerodynamic optimization of helicopter rotor", AIAA Science and Technology Forum and Exposition, AIAA SciTech Forum 2022, doi: 10.2514/6.2022-2099.

Pahlke, K. and Demaret, B. (2017), "ONERA and DLR contributions to improve environmental friendliness of rotorcraft", *Annual Forum Proceedings - AHS International*.

Ryazanov, A.I. (2016), "Automated 3D modeling of working turbine blades", *Russian Engineering Research*, Vol. 36 No. 9, pp. 751-754, doi: 10.3103/S1068798X16090203.

Sagimbayev, S., Kylyshbek, Y., Batay, S., Zhao, Y., Fok, S. and Lee, T.S. (2021), "3D multidisciplinary automated design optimization toolbox for wind turbine blades", *Processes*, Vol. 9 No. 4, p. 581, doi: 10.3390/pr9040581.

Salh Eddine, D., Smail, K., Mahfoudh, C. and Lyes, T. (2023), "Robust optimization of the aerodynamic design of a helicopter rotor blade based on multi-fidelity meta-models", *Proceedings of the Institution of Mechanical Engineers, Part E: Journal of Process Mechanical Engineering*, Vol. 237 No. 3, pp. 615-634, doi: 10.1177/09544089221111593.

Shabliy, L.S. and Dmitrieva, I.B. (2014), "Conversion of the blade geometrical data from points cloud to the parametric format for optimization problems", *ARPN Journal of Engineering and Applied Sciences*, Vol. 9 No. 10, pp. 1849-1853.

Sinem, M. and Metin Orhan, K.A.Y.A. (2018), "Optimization of vibration reduction in a helicopter blade with 2 way fluid-structure interaction", ASME 2018 Conference on Smart Materials, Adaptive Structures and Intelligent Systems, SMASIS 2018, Vol. 1, doi: 10.1115/SMASIS2018-8017.

Spyropoulos, N., Papadakis, G., Prospathopoulos, J.M. and Riziotis, V.A. (2021), "Investigating the level of fidelity of an actuator line model in predicting loads and deflections of rotating blades under uniform free-stream flow", *Applied Sciences (Switzerland)*, Vol. 11 No. 24, p. 12097, doi: 10.3390/app112412097.

Stalewski, W. (2017), "design and optimisation of main rotor for ultralight helicopter", *Journal of KONES Powertrain and Transport*, Vol. 24 No. 4, p. 24.

Stalewski, W. and Zalewski, W. (2019), "Aerodynamic design and optimisation of main rotors for light rotorcrafts", 45th European Rotorcraft Forum 2019, ERF 2019, Vol. 1.

Straub, F.K., Callahan, C.B. and Culp, J.D. (1992), "Rotor design optimization using a multidisciplinary approach", *Structural Optimization*, Vol. 5 Nos 1/2, pp. 70-75, doi: 10.1007/BF01744698.

Tamer, A., Yücekayali, A. and Ortakaya, Y. (2011), "Design and optimization of helicopter rotor for minimum power required", *6th AIAC Ankara International Aeropsace Conference*, No. September 14-16.

Tarzanin, F., Young, D.K. and Panda, B. (1999), "Advanced aeroelastic optimization applied to an improved performance, low vibration rotor", *Annual Forum Proceedings – American Helicopter Society*, Vol. 1, pp. 183-194.

Tian, S., Tao, F., Du, H., Yu, W., Lim, J.W., Haehnel, R., Wenren, Y., *et al* (2022),. "Structural design optimization of composite rotor blades with strength considerations", AIAA Science and Technology Forum and Exposition, AIAA SciTech Forum 2022, doi: 10.2514/6.2022-2454.

Tixadou, E. (2021), "optimisation of the structure of a helicopter blade in view of reducing cabin vibration".

Tremolet, A. and Basset, P.M. (2012), "Some meta-modeling and optimization techniques for helicopter pre-sizing", 38th European Rotorcraft Forum 2012, ERF 2012, Vol. 2.

Vu, N.A. and Lee, J.W. (2015), "Aerodynamic design optimization of helicopter rotor blades including airfoil shape for forward flight", *Aerospace Science and Technology*, Vol. 42, pp. 106-117, doi: 10.1016/j.ast.2014.10.020.

Vu, N.A., Lee, J.W., Le, T.P.N. and Nguyen, S.T.T. (2016), "A fully automated framework for helicopter rotor blades design and analysis including aerodynamics, structure, and manufacturing", *Chinese Journal of Aeronautics*, Vol. 29 No. 6, pp. 1602-1617, doi: 10.1016/j.cja.2016.10.001.

Wang, H., Zhang, B. and Li, D. (2013), "The research on helicopter rotor aeroelastic dynamics multi-objective optimization solution", Vol. 30, pp. 217-222, doi: 10.11776/cjam.30.02.B103.

Wilde, E. and Price, H.L. (1965), "A theoretical method for calculating flexure and stresses in helicopter rotor blades", *Aircraft Engineering and Aerospace Technology*, Vol. 37 No. 2, pp. 45-54.

Wilke, G. (2021), "Quieter and greener rotorcraft: concurrent aerodynamic and acoustic optimization", *CEAS Aeronautical Journal*, Vol. 12 No. 3, pp. 495-508, doi: 10.1007/s13272-021-00513-x.

Wilke, G. (2024), "Jaxa-onera-dlr cooperation: results from rotor optimization in hover".

Xie, J., Xie, Z., Zhou, M. and Qiu, J. (2017), "Multidisciplinary aerodynamic design of a rotor blade for an optimum rotor speed helicopter", *Applied Sciences (Switzerland)*, Vol. 7 No. 6, p. 639, doi: 10.3390/app7060639.

Гребеников, АГ., Дьяченко, ЮВ., Коллеров, ВВ., Коцюба, ВЮ., Малков, ИВ., Урбанович, ВА. and Воронько, ИА. (2021), "Analysis of design and technological features of the main rotor blades of heavy transport helicopters", *Open Information and Computer Integrated Technologies*, Vol. 93, pp. 59-103, doi: 10.32620/oikit.2021.93.04.

Further reading

Johnson, W. (1994), *Helicopter Theory, Dover Publications, INC*, Dover Publications, New York, NY.

Rotaru, C., Cîrciu, I. and Luculescu, D. (2016), "Lift capability prediction for helicopter rotor blade-numerical evaluation", *AIP Conference Proceedings*, Vol. 1738, doi: 10.1063/1.4952208.

Corresponding author

Jakub Kocjan can be contacted at: jakub.kocjan@wat.edu.pl

This paper is available online at www.praiseworthyprize.org
International Review of Aerospace Engineering (I.RE.AS.E), Vol. 18, N. 2
ISSN 1973-7459 April 2025

Aerostructural Helicopter Main Rotor Optimization Considering Mass and Strength Limitations

Jakub Kocjan[1], Robert Rogólski[2]

Abstract – *The ongoing military conflicts necessitate the construction of systems with superior characteristics for extensive military operations. To keep pace with global advancements, the Military University of Technology is enhancing design solutions. This work presents the final stage of research aimed at optimizing the main rotor to achieve the best performance according to mission profiles, while considering structural strength limits and mass reduction. The goal of the multicriteria optimization is described using mathematical functions. An optimization functional and a method for finding an optimal solution are proposed. The optimization procedure involves a combination of computer methods, calculations, and Fluid-Structure Interaction (FSI) simulations. The unsteady aerodynamic forces, influenced by structural deformation, are simulated for different flight conditions, based on data obtained from flight recorders. The CAD model and calculations are fully parameterized to allow rapid adjustments to input dimensions. The optimization loop is presented as an algorithm, demonstrating the implementation of earlier stages of the research. The paper concludes with potential applications of the algorithm in existing or new design projects. The research introduces a novel solution for main rotor blade design, providing the capability to quickly evaluate different constructions in accordance with mission requirements.*

***Keywords**: Helicopter, Main Rotor, Optimization, Aerodynamics, FSI, Multicriteria Optimization, Algorithm, Rotor Blade, Forward Flight, Hover Flight*

Nomenclature

a	Lift curve slope
c	Chord
D	Dimensional constraint
d	Main rotor blade honeycomb width
E	Economic constraint
g_i	Inequality constraint function
h	Main rotor blade spar height
h_j	Equality constraint function
m	Helicopter mass
M	Maintenance constraint
m_b	Blade mass
n	Number of decision variables
n_r	Rotor angular velocity
p	Number of constant parameters p=N-n
Q	Criterion function
Q	Quality constraint
q	Partial criteria
R	Radius
T	Rotor thrust
w	Rotor solidity
w_1, w_2	Weigh coefficient
X	Set of feasible solutions
x	Vector of parameters
Y	New set of feasible solutions
γ	Lock number
ν	Twist
σ_{max}	Allowable stress
σ_{str}	Blade stress
φ_i	Inequality constraint function
CAD	Computer Aided Design
CAE	Computer Aided Engineering
CFD	Computational Fluid Dynamics
FEM	Finite Element Method
FSI	Fluid Structure Interaction
GRIP	Graphic Integrated Programming - programming language
MTOW	Maximum Takeoff Weight
NORM	Average values for normalizing the functions

I. Introduction

Recent military conflicts have led to a reevaluation of the roles helicopters can achieve on the modern battlefield.

Manufacturers and national authorities recognize the necessity for designs that offer improved capabilities for extensive military operations. As a result, numerous countries are modernizing existing configurations and investigating innovative solutions for VTOL (Vertical Take-Off and Landing) vehicles. The two main streams of

Available online by April 30th, 2025 https://doi.org/10.15866/irease.v18i2.25996

rotorcraft enhancement can be identified. The first focuses on the development of the Sikorsky configuration. The designs are being developed to provide better performance within the limits of the classic helicopter aerodynamic layout. The second stream involves the development of high-speed rotorcraft. The high-velocity goal is achieved by adding an extra propeller to produce thrust, while lift is generated by the main rotor. Consequently, the Military University of Technology is also taking part in developing new methods and algorithms for aircraft structure optimization. One branch of this research focuses on finding new solutions for rotorcraft in the classic layout stream. The main objective of this research is to develop a multicriteria optimization procedure utilizing the latest computer-aided design methods. There are several contemporary approaches to solving optimization problems. Each solution, even if it is a multicriteria procedure, needs to focus on only certain aspects of the functioning rotor blade. These approaches focus on enhancing the helicopter's speed, sound, power, etc., primarily aiming to provide better aerodynamic features. The optimization can be achieved using various methods; however, most of them are focused only on one aspect of the construction. The findings of research focused on main rotor aerodynamic optimization are published in [1]-[6].

In Europe, there are two main institutes focused on enhancing main rotor design. These institutes are the leaders in European rotorcraft research: the ONERA French Aerospace Lab and the DLR German Aerospace Centre. Their results are presented in [7]-[11]. The process described in the paper combines two CAE methods for analyzing the construction's working conditions. Firstly, it involves CFD analysis for the main rotor and blade shape evaluation. The research that also shows the usage of computational fluid dynamics for the described topic is presented in [12]-[15]. This research also involves structural optimization. In this field, recently published research is focused on strength analysis using previously acquired data or calculated forces. Recent studies focused on structural optimization are described in [16]-[19], where different aspects of the structure are considered.

These studies mainly consider structural optimization; the aerodynamic aspect is not the subject of a comprehensive mutual analysis. This paper outlines the optimization procedure resulting from three years of study. The research was divided into phases to concentrate on each element of the optimization algorithm. Each phase underwent evaluation through presentations at international conferences and the publication of findings in scientific journals. The first step, which is a novelty in recent research, began with the analysis of helicopter construction, where nearly 70 helicopter designs were evaluated and compared using absolute and relative values. The results of this analysis were published in [20].

The second stage was aimed at preparing the parametric model for fluid dynamics computational environments and comparing the results of simulations to select the best solution for further work. The research was described in detail and published in [21]. The parametrization of the model is developed using the GRIP (Graphic Integrated Programming) language, which is implemented in Siemens NX software. Examples of GRIP usage are demonstrated in [22]-[24]. This language provides the ability to generate external surfaces or internal structural components of the airframe that are currently being designed. In the third part, the simulations were enhanced by developing a parametric model of the rotor blade, including the parametrization of the fluid enclosure for different flight conditions. The model was generated for planned simulations, with the n-bladed rotor initially set up for these simulations. Computational Fluid Dynamics (CFD) calculations were made and compared with existing rotor parameters to validate the findings. The results were shown in [25]. The next stage was aimed at preparing the structural model for Finite Element Model (FEM) analysis, which would be combined with CFD as Fluid-Structure Interaction (FSI). The structural model was also parametrized, and the inner structure of the blade was reproduced and generated. This phase of the study was described and published in [26].

This paper is organized in a specific manner. The research methods are described in Section II, where the mathematical model, which forms the basis for parametric programming, is defined, along with a description of the entire algorithm. Section III presents the results of parametric programming. The research methods and findings are discussed in Section IV, and the work is summarized and concluded in Section V.

II. Research Method

II.1. Mathematical Model of Optimization

Every design is defined by the previously described set of parameters. If each of these parameters is assigned a specific value, the entire design can be described by a set of n numbers, where n is the number of characteristics describing the design. The design is thus a vector x in an N-dimensional Euclidean space. The vector of parameters describing the defined properties of the design is the mathematical model of the structure:

$$\bar{x} = (x_1, x_2, \dots, x_N), \;\; \bar{x} \in R^N \tag{1}$$

The coordinates of vector x can be divided into constant parameters and parameters determined during optimization – decision variables (design variables):

$$\bar{x} = (x_1, \dots, x_n, x_{n+1}, \dots, , x_N) \tag{2}$$

where: $x_1, \dots, x_n$ ate decision variables, $x_{n+1}, \dots, , x_N$ are else constant parameters, n is the number of decision variables, p is the number of constant parameters $p=N-n$.

Equality constraints take the form of:

$$h_j(x_1, \dots, x_n) = 0, \qquad j = 1,2, \dots, m \tag{3}$$

and inequality constraints take the form of:

$$g_i = (x_1, \ldots, x_n) \geq 0 \tag{4}$$

or:

$$\varphi_i = (x_1, \ldots, x_n) \geq 0, \quad i = 1,2, \ldots, q \tag{5}$$

The set of feasible solutions is the set of points in an n-dimensional Euclidean space that satisfy the conditions described by Equations (4) and (5). Denoting this set by X and assuming that it is non-empty, we obtain the mathematical formulation of the first principle of construction:

$$\bar{x} \in X, \qquad X \subset R^n \tag{6}$$

Construction $\bar{x}$ that satisfies Equation (6) is called a good construction. According to the second principle of construction, among the good constructions, the best – optimal – construction is chosen based on the adopted criterion. The criterion is expressed by the function $Q(\bar{x}) = Q(x_1, \ldots, x_n)$. As a result of appropriately selecting decision variables, the objective function should reach its minimum or maximum value:

$$Q(\bar{x}) \to Q_{opt}(\bar{x}^*) = \begin{cases} Q_{\min} \\ Q_{\max} \end{cases} \tag{7}$$

where:

$$\bar{x}^* = (x_1^*, \ldots, x_n^*) \in X \tag{8}$$

is an optimal construction.

For the task of minimizing the objective function, the second principle of construction can be written as:

$$(\bar{x}^* \in X): \left\{ \bigwedge_{\bar{x} \in X} Q(\bar{x}) \geq Q(\bar{x}^*) \right\} \tag{9}$$

and for maximalization task:

$$(\bar{x}^* \in X): \left\{ \bigwedge_{\bar{x} \in X} Q(\bar{x}) \leq Q(\bar{x}^*) \right\} \tag{10}$$

A mathematical model is crucial for the correct solution of an optimization task. It allows the translation of reality into a physical model using mathematical functions. The models used should accurately reflect the real problem, as computer methods can sometimes evaluate cases that have no engineering relevance. However, it is suggested that the model should be as simple as possible, including only the required construction parameters. In some cases, the optimization task requires using more than one criterion – these kinds of problems are called multicriteria optimization tasks. Mathematical model of structure optimization consists of:

- a set of decision variables and other parameters describing the design;
- a set of constraints (limiting conditions);
- the objective function (or set of objective functions), which is a mathematical representation of the optimization criterion.

In accordance with the structure model (2), the construction can be treated as a vector in the construction space. When the coordinates of that vector are numbers, the construction space is an n-dimensional Euclidean space. If the coordinates of that vector are functions, the construction space is a functional n-dimensional Hilbert space. The construction parameters are divided into parameters and decision variables. The set of decision variables is defined by the decision variables vector in a new space, which is reduced in relation to the construction space. This new space is called a design space:

$$\bar{x} \in R^n \subset R^N \tag{11}$$

where $n = N - p$, N is number of construction parameters, n is number of decision variables and p is number of parameters defined by the constructor. The feasible region (feasible set, set of feasible solutions) is a subspace (subset) of the design space:

$$X \subset R^n \tag{12}$$

The feasible region is formed by imposing equality and inequality constraints on the construction. After considering the discussed groups of constraints, the feasible region is the product of the following sets:

$$X = E \cap D \cap Q \cap M \tag{13}$$

where E is the economic constraint, D is the dimensional constraint, Q is the quality constraint and M is the maintenance constraint. The objective function (optimization criterion) can be represented as an operator that transforms the feasible region X into another region Y.

This operator transforms the decision variable R^n into the space R^q, known as the criterion, objective, cos function or quality space.

II.2. Multicriteria Optimization Problem

Nevertheless, the optimization solution presented in this study is a multicriteria optimization problem, in which the mathematical model described above should be developed.

Multi-criteria optimization involves formulating a superior optimization criterion, which is a set of partial criteria for evaluating the construction. This approach is commonly found in optimal design, based on a systematic analysis of the problem. Designers often must solve problems where the construction must simultaneously meet several, often conflicting criteria.

This creates a decision problem, which involves determining the importance of each criterion. In the design process, the designer should strive to achieve their objectives as effectively as possible (the second principle of construction). The entire design procedure can be treated as a decision-making process. In their work, the designer should consider the following assumptions:

- It is possible to choose a solution only from the set of feasible solutions;
- The designer has at their disposal a self-created or externally imposed value system that allows for the evaluation of solutions;
- The designer is able to determine which solutions are considered better, those that are preferred based on the adopted value system;
- The designer is able to justify and defend their satisfying choice, which is considered optimal in their assessment.

The described situation is called the problem of optimal choice. If the value system allows specifying evaluation criteria, then the problem becomes a multicriteria optimization problem. Solving this problem requires determining the set of feasible solutions and their evaluations.

The task requires defining a vector function through which the set of evaluations will be mapped. A characteristic feature of multicriteria optimization is obtaining a set of optimal solutions with varying degrees of compromise between the individual criteria. Due to its mathematical properties, the description of the optimal choice problem is very complicated and, from an engineering point of view, not very useful. The designer uses other decision support techniques to make the optimal choice. Multi-criteria engineering optimization, as a tool for system design, must be characterized by:

- The application of a systematic approach;
- The use of primarily discrete sets of decision variables, providing solutions of a practical nature;
- The use of multi-criteria evaluation of solutions using decision-making methods.

In accordance with [27], The general mathematical model of multi-criteria optimization is presented as follows:

1. Given that $X \subset R^n$ is a set defined by a system of inequalities and equalities:

$$X := \{\bar{x} \in R: \bar{g}(\bar{x}) \geq \bar{0}, \bar{h}(\bar{x}) = \bar{0}\} \tag{14}$$

   where the mapping $\bar{g}: R^n \to R^m$ is the description of the system of m functions:

$$g_i: R^n \to R, (i \in \overline{1,m}) \tag{15}$$

   and a mapping $\bar{h}: R^n \to R^p$ is the description of the system of p functions:

$$h_i: R^n \to R, (i \in p), p < n \tag{16}$$

   The mappings $\bar{g}, \bar{h} \in C^1(\bar{x})$ form the set of feasible solutions, with the vector $\bar{g}(\bar{x})$ representing the set of inequality constraints and the vector $\bar{h}(\bar{x})$ representing the set of equality constraints. The vector $\bar{x}$ is a specific design solution, a vector of decision variables;
2. Given is the mapping $\bar{f}: R^n \to R^q, q > 1,$ defined by a system of q functions (partial criteria) $f_k: R^n \to R, (k \in \overline{1,q})$;
3. According to the designer preferences, there is a requirement to minimize or maximize the partial objective functions $f_k (k \in \overline{1,q})$ over the set *X*.

In this work, the optimization process will be conducted using modern computational methods. Therefore, when solving a problem defined mathematically using modern design methods, the process must be aligned with practical considerations, i.e., the goal of obtaining concrete solutions. Assuming that optimization criteria have been established, the steps to determine the optimal solution are as follows:

- Normalization of partial objective functions;
- Scalarization of the normalized objective function with weight coefficients;
- Defining a set of compromises;
- Defining the preference function set;
- Choosing a subset of preference solutions;
- Deciding in accordance with the designer's preferences.

II.3. Aerostructural Main Rotor Optimization Mathematical Model

To achieve the goal of the research, in accordance with Subsection II.2 of this article, the mathematical model of main rotor optimization needs to be established. The construction features were chosen as the elements of the mathematical model sets:

1. The decision variables:
   a) c – main rotor blade chord;
   b) R – main rotor radius;
   c) h – main rotor blade spar height;
   d) d – main rotor honeycomb width.
2. Parameters:
   a) materials properties;
   b) airfoil properties;
   c) rotor rotational speed;
   d) flight conditions.
3. Constraints:
   a) strength condition - $\sigma_{str} > \sigma_{max}(h,d)$;
   b) geometric condition - $R > 0,\ c > 0, h > 0,\ d > 0$;
   c) effect of blade deformation on thrust variation - *T*(*t*);
   d) maximum blade pitch - $\theta < \theta_{max}$.
4. Objective functions:
   a) performance criterion - $T(c,R) \geq MTOW(h,d)$;
   b) solidity criterion - $w(R,c) \to max$;
   c) blade mass criterion - $mb(h,d) \to min$;
   d) mass forces criterion - $F(m') \leftrightarrow$ balancing the moment generated by aerodynamic forces.

The partial objective functions are scalarized and normalized to prepare a multicriteria objective function of main rotor aerostructural optimization:

$$\tilde{F}(c,R,h,d) = w_1\tilde{T}\big(\sigma(c,R)\big) + w_2\tilde{m}(h,d) \tag{17}$$

where w_1 is the weight associated with aerodynamic performance, which depends on the mission profile and helicopter configuration, w_2 is the weight associated with mass, which also depends on the mission profile and helicopter configuration, $\tilde{T}$ is the normalized thrust function $\tilde{T} = \frac{T(\sigma(c,R))}{TNORM}$, $\tilde{m}$ is the normalized mass function $\tilde{m} = \frac{\tilde{m}(h,d)}{mNORM}$, NORM is the the average reference value for a given type of helicopter and the expected mission profile, calculated based on statistical data. To solve the problem and obtain a design that fulfills the designer's preferences, an appropriate optimization method needs to be chosen.

In engineering solutions where the aim is to find designs that not only meet the engineer's preferences but can also be produced and tested for durability, discrete optimization methods are commonly used. By combining computer methods with analytical calculations, this research proposes a state-space search method with local search of solutions. The initial solution is based on an existing rotorcraft blade construction or is preliminarily generated based on analytical assumptions and existing construction analysis.

II.4. Aerostructural Main Rotor Optimization Algorithm

To solve the problem, the mathematical model presented in Section 2.3 is realized using the support of computer techniques to obtain a solution that fulfills the designer's preferences. The computer CAD/CAE/CFD environments were combined to provide a discrete optimization solution. The schematic of the algorithm is presented in Figure 1.

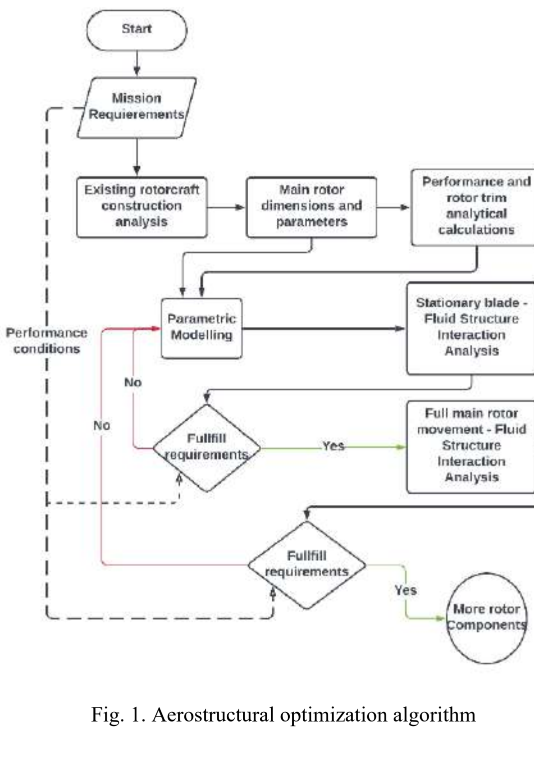

Fig. 1. Aerostructural optimization algorithm

The algorithm was developed during the last few years, each of the elements presented on chart were evaluated and the effects were published in [20], [21], [25], [26], [28]. Below a short brief of the entire process is presented.

The procedure steps are described below:

1) To begin the process, the mission requirements should be established. Depending on the helicopter's utilization, the operational requirements determine the performance aspects of the rotorcraft. The performance features are used to evaluate the resultant design shape and structure. In two milestones (the FSI analysis), the obtained results are compared with the prerequisites and evaluated to see if they produce the demanded capabilities. Negative assessment results provide information on which construction feature should be changed to achieve the desired potential and offer feedback to the parametric blade model. In the phase of preparing the initial shape, the mission requirements are used in the next step to choose the coefficients and physical dimensions responsible for the desired performance capability;
2) The second step of the optimization procedure is comparing the mission requirements with the analysis [20], [21], [25], [28] of existing rotorcraft constructions. The analysis was prepared using data from almost all helicopter constructions that the authors were able to acquire from manufacturers' websites, brochures, scientific articles, helicopter books, catalogues, etc. The constructions were divided in accordance with their size and utilization purpose. The first comparison was made using physical dimensions such as geometric features of the rotor or the maximum takeoff weight. The second was performed using dimensionless coefficients proposed in the helicopter construction problem literature. The trends of coefficient changes in accordance with the helicopter's weight and size were established. By analyzing the charts with the mission requirements, the regions for possible enhancement of existing construction solutions can be identified. In these regions, the exact design parameters can be chosen as optimization variables and parameters. Using the variables and the mission requirements, the multicriteria objective function can be prepared, as described in Section II.3. For the state-space search method, rotor variants are proposed;
3) The proposed initial blade dimensions and parameters are a result of the comparison described above. They serve as inputs for the parametric modeling and the performance and trimming calculations;
4) The trim and performance calculations are based on the analytical model of the rotor work, the mathematical model was presented in details in previous works. The computations are based on input parameters and solved using computer techniques. The results of the programs are the performance estimation with the main rotor blade trimming. The trimming is realized for any flight conditions, the blades collective and cyclic pitch and flapping angles are established.

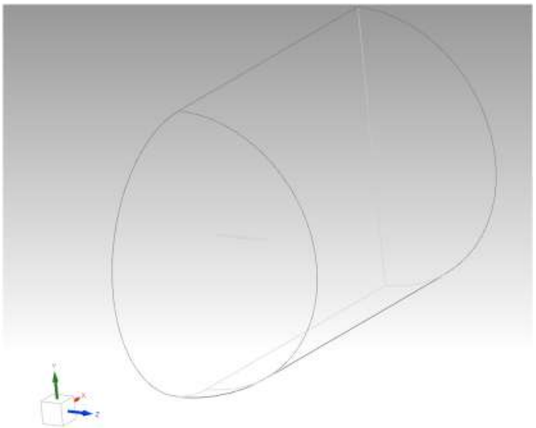

Fig. 2. One blade simulation generated model

This phase also provides the lift force calculations for blade bending moment assumption in parametric modeling of inner structure. Blade position angles, along with rotor dimensions, serve as the basis for the blade CAD parametric model;

5) The essential part of the procedure is the parametric modelling of the rotor. The CAD models are prepared as input into combined CFD and FEM simulation. Simultaneously outer shape with fluid enclosures is prepared, firstly for one blade CFD analysis, and next for full rotor simulation. The parametric CAD model is generated using GRIP language which is built inside the design software. The code was prepared to be used for any blade shape that is proposed by the designer. The examples of the generated blade shape with enclosure is presented on Figure 2 and Figure 3. As mentioned, also the model for FEM analysis is parametrized. However, to enhance the process, the preliminary structure optimization as an inner procedure was established. The structure is evaluated, using analytical calculations, to be prepared for the bending moments produced by the predicted lift. The natural mode shapes are taken into consideration during bending moment calculations. The iterative loop uses the GRIP program and its inner inertial and mass analysis functions combined with mathematical calculation software. The process in details was described in [24]. The structure optimization procedure is presented on Figure 5. The example of resultant model for FEM simulation is given on Figure 4.
6) The models for CFD and MES are merged into FSI simulation. To optimize the entire process, the FSI simulation is divided into two steps. Firstly, a single-blade model is simulated. In this phase, the model is stationary, and the inflow is simulated using prepared equations. In this phase the structure is checked to confirm that analytical assumptions were correct, the required lift is produced and structure is designed to carry the aerodynamical loads. This step provides the time save in entire process. This kind of FSI simulation is not relatively time consuming and allows to make corrections or try different configuration of the blade dimensions in reasonable time. Example of simulation mesh configuration is shown in Figures 6;
7) The construction is checked, in accordance with the objective function and the best solution for the performance requirements is found using a state space search method;

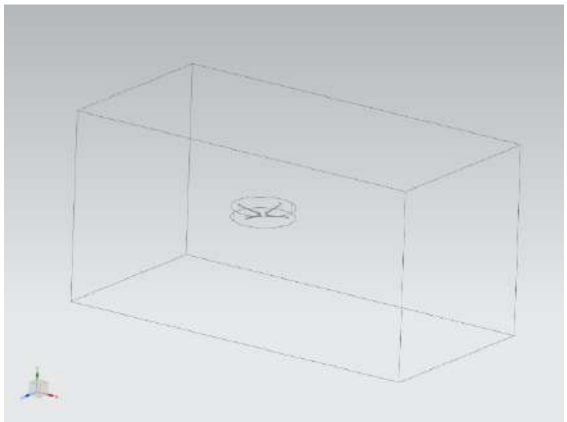

Fig. 3. Full rotor CAD generated model for forward flight simulation

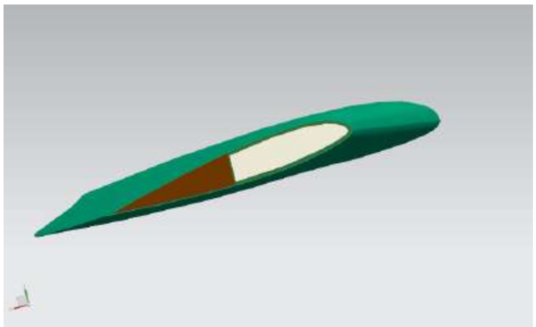

Fig. 4. Structural model for FEM simulation

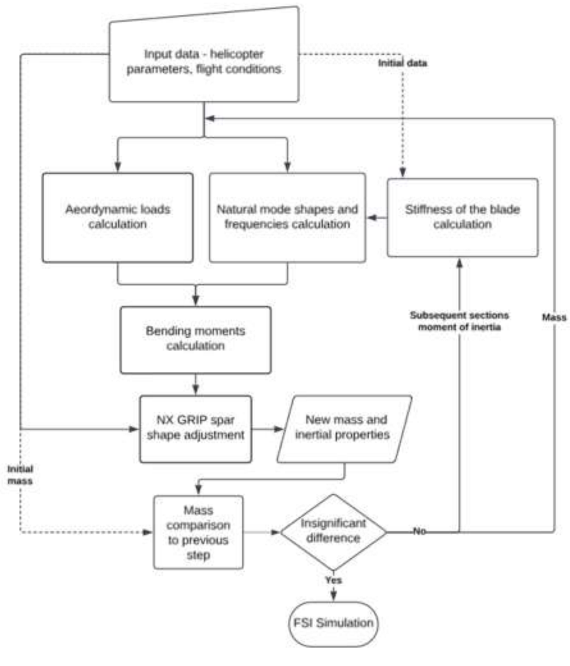

Fig. 5. Initial structure optimization procedure

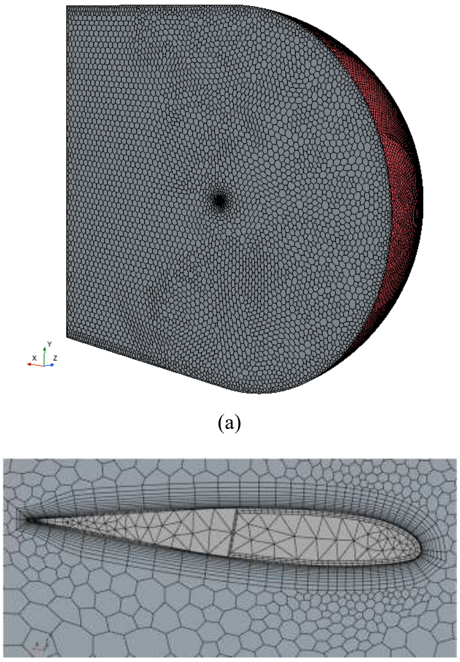

(a)

(b)

Figs. 6. One blade FSI simulation: (a) Fluid domain, (b) close up for structure and boundary layer mesh

8) If the founded construction meets the requirements and is identified as the optimal solution for that phase, it is then translated into second step an inflight n-bladed rotor simulation, where real flight conditions and rotor movement are represented.
   This is also an FSI simulation where the forces that are produced during flight are transferred to structural analysis and then the displacement is translated into CFD simulation. This is reproduced in each time step, so the deformation and mass forces are considered in the simulation and affects the resultant forces. The example of simulation mesh configuration, where the interfaces are visible, is shown on Figure 7;
9) The outcomes of the simulation are again assessed in accordance with the mission requirements. The construction is checked with the performance features and the construction limitations. The variants are compared to find the best fulfillment of the objective function. The weight of the partial functions represents the intention of the designer, what is preferred to be more important in optimization process. If the construction fails to meet the aerostructural requirements, the results are used to adjust the parametric model dimensions of the outer shape or inner structure. The iteration starts again as it is shown on Figure 1;
10) The process ends with an one or few rotor propositions that fulfill the objective function and provide the best required features. The model is ready to use in further helicopter development.

III. Results

The result of the research is a new method for main rotor blades design, which combines computer design methods to obtain the best main rotor blade shape and structure. The basis for the validation of the research is the W-3 helicopter's main rotor geometry. The blades are parametrized using the real geometric dimensions and tip shape with the parameters of airfoil. The initial parameters are presented in Table I. The blade planform shape is shown in Figure 6. As it was described earlier the blade planform and dimensions can be adopted from any blade shape.

III.1. Mathematical Calculation with Parametric Modelling

The configuration of the rotor blade shape for given conditions can vary depending on the intended utilization of the helicopter. To demonstrate the possibilities of this method, an optimization proposal for the baseline blade described above is presented. The calculations begin by identifying various blade shape configurations that meet the technological constraints for blade pitch and cyclic angles while providing the required thrust. This paper proposes an optimization of an existing rotor based on the parameters outlined in Table I.

Considering the limitations of the power plant, rotor shaft, and main rotor hub steering rods, the performance improvement was calculated for a 200 kg increase in MTOW. The criterion for the first cut of the calculation procedure was to provide better performance with maintaining similar pitch angles. The differences of the pushrods settings can be eliminated using normal maintenance procedure of adjusting the swashplate for rotor trimming. Using the state space search ne values were found. The proposed blade shapes (with rotor solidity values), along with values resulting from analytical thrust calculations, are shown in Table II.

The shapes, listed in Table II, that fulfill the construction criterion for swashplate angles (to maintain within the values that were initial for the existing construction) are chosen for inner shape parametric modelling. For each of chosen planforms, the blade strength structure was optimizes as it was described in [24]. The resultant shapes with the proposed minimum weights are shown in Table III. The models prepared are next evaluated using FSI to prove its strength and performance capabilities. The simulations were prepared using the method which was described above, and showed in details in the papers from previous stages of the work.

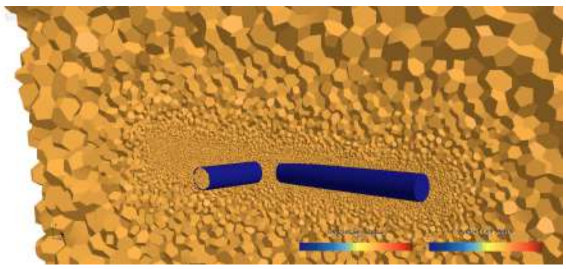

Fig. 7. Full rotor FSI simulation

TABLE I
INITIAL PARAMETERS FOR THE METHOD VALIDATION

Parameter	Letter	Value
Radius	*R*	7.85 m
Chord	*c*	0.44 m
Twist	ν	12°
Lift curve slope	*a*	6.4
Rotor angular velocity	*nr*	255 rpm
Lock number	γ	9.65
MTOW	*m*	6400 kg
Blade mass	*mb*	65.5 kg

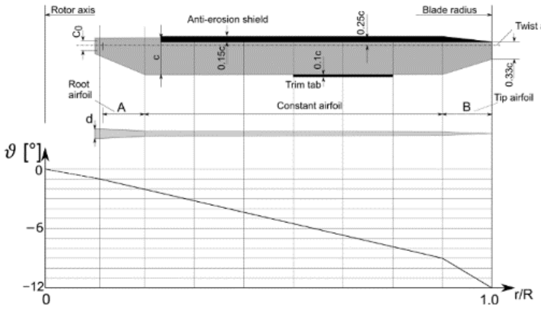

Fig. 7. The geometry of the main rotor blade: Rotor shape (c, chord and c0, mounting holes spacing), and blade parameters (αS(r/R), geometric twist angle in dependence on nondimensional radius; A and B, airfoil change zone; d, blade thickness)

TABLE II
CALCULATED ROTOR DIMENSIONS WITH THE COLLECTIVE PITCH VALUES FOR CHARACTERISTICS IAS

Radius R [m]	Chord c [m]	Rotor solidity	Collective pitch for IAS 50 [km/h] θ0[°]	Collective pitch for IAS 100 [km/h] θ0[°]	Collective pitch for IAS 150 [km/h] θ0[°]	Collective pitch for IAS 200 [km/h] θ0[°]
7,85	0,44	0,055	4,68	5,05	6,39	9,35
7	0,6	0,084	5,07	5,56	7,19	11,33
7	0,65	0,0899	4,67	5,06	6,67	10,55
7,1	0,6	0,083	4,86	5,35	6,9	10,67
7,1	0,65	0,0912	4,48	4,85	6,4	9,94
7,15	0,6	0,0824	4,76	5,11	6,62	10,46
7,2	0,6	0,0818	4,66	5	6,49	10,06
7,2	0,62	0,0845	4,49	4,89	6,34	9,85
7,2	0,65	0,0886	4,29	4,65	6,02	9,37
7,25	0,6	0,0813	4,56	4,9	6,36	9,86
7,25	0,65	0,088	4,21	4,46	5,9	9,19
7,3	0,65	0,0874	4,12	4,37	5,78	9,02
7,4	0,65	0,0862	3,95	4,2	5,45	8,52
7,4	0,6	0,0796	4,29	4,61	5,87	9,14
7,5	0,6	0,0785	4,04	4,34	5,64	8,36
7,24	0,6	0,0814	4,58	4,92	6,38	9,9
7,24	0,62	0,0841	4,41	4,71	6,24	9,7
7,23	0,62	0,0842	4,43	4,83	6,26	9,74
7,23	0,63	0,0855	4,4	4,68	6,07	9,44
7,22	0,63	0,0857	4,42	4,71	6,1	9,67
7,24	0,61	0,0827	4,54	4,86	6,31	9,8
7,5	0,55	0,072	4,49	4,79	6,12	9,13
7,5	0,54	0,0707	4,54	4,85	6,2	9,42
7,49	0,54	0,0708	4,56	4,87	6,22	9,46
7,5	0,5	0,0655	4,93	5,33	6,68	9,92
7,55	0,5	0,065	4,84	5,22	6,55	9,74
7,6	0,5	0,0646	4,74	5,02	6,43	9,56
7,6	0,48	0,062	4,95	5,27	6,62	9,83
7,5	0,53	0,0694	4,68	5,017	6,28	9,55
7,49	0,53	0,0695	4,7	5,03	6,43	9,58
7,48	0,53	0,0696	4,72	5,05	6,46	9,61
7,48	0,52	0,0683	4,77	5,12	6,55	9,73
7,46	0,52	0,0684	4,81	5,16	6,6	9,81

TABLE III
MAIN ROTOR BLADE PARAMETRIC STRUCTURAL MODEL – ESTIMATED WEIGHT AND CENTER OF GRAVITY

Radius *R* [m]	Chord *c* [m]	Blade mass m_b [kg]	Center of gravity *z* [m]
7,24	0,61	42,127	4,459
7,49	0,54	37,186	4,612
7,55	0,5	33,527	4,637
7,46	0,62	34,260	4,572

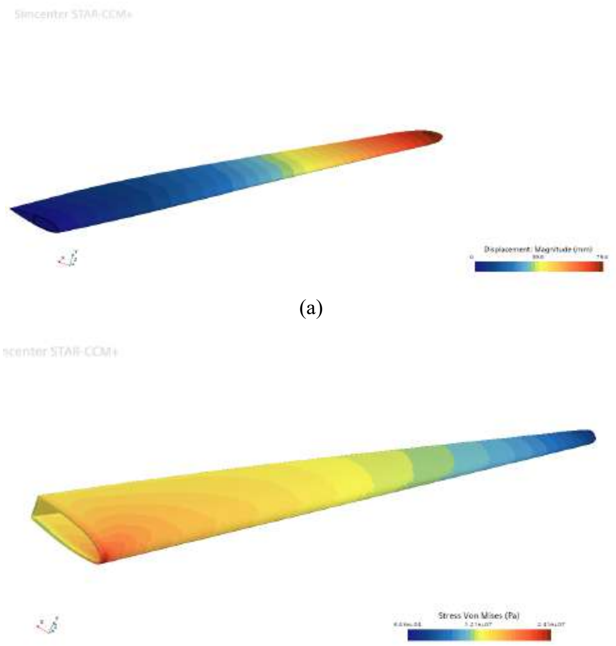

(a)

(b)

Figs. 8. Structural analysis: (a) displacement, (b) stress

III.2. Time and Power Consumption

One of the main goals of the prepared procedure is to develop a time- and energy-efficient method for the main rotor design process. The procedure was optimized to minimize solution time. Calculations were performed on a workstation with two Xeon Gold 6152 CPU 2.10 GHz processors, with total 44 physical cores and 128 GB of RAM memory. While the software uses a single core for solving equations, the FSI analysis utilizes all cores to achieve accurate results quickly. The model's parametrization and structural shape generation were conducted on the same hardware, with software which is also using single-core processing. The time was measured from the beginning of the process until obtaining final result.

The total time to obtain a set of results that is ready to be assessed by the designer in accordance with optimization goal, was about 53h. The most time consuming is the Full Rotor FSI analysis, which takes average 90% of the process. The mean partial and total time for calculations and evaluating the constructions in presented in Table IV.

TABLE IV
PARTIAL AND TOTAL TIME OF THE OPTIMIZATION PROCEDURE

Phase	Average Iterations required	Average Time per iteration	Power
Analytical Calculation	30	5 min	1 core 2.10 GHz
Parametric Modelling CFD	1	2 min	1 core 2.10 GHz
Structural Parametric Modelling	5	7 min	1 core 2.10 GHz
One Blade FSI	2	70 min	44 cores 2.10 GHz
Full Rotor FSI	1	48 h	44 cores 2.10 GHz
Full time		53 h	

IV. Discussion

The article presents the summary and results of new main rotor design method which combines the parametrization of the model, new engineering computing solutions and optimization methods. As an output of the optimization process, four shapes are proposed as an example of the procedure's possibilities, each with different blade mass but the same performance capabilities.

The shapes differ in radius and chord dimensions, and consequently, in the inner dimensions. A wider chord provides a higher blade mass, but with a reduction in rotor radius. Shorter blades can be applied to constructions with higher rotational speeds. Shorter blades also provide a smaller rotor disk, which decreases the helicopter's radar cross-section. Longer blades with shorter chords offer a lower mass, resulting in a better final outcome for mass reduction optimization. The mathematical model of optimization was presented in this work. The mathematical assumptions for optimization are required to correctly address the optimization goal by the designer, also providing awareness of the parameters considered during the process. The correct parameters are chosen in accordance with the construction evaluation, which was the first step of the research. The mathematical function is also used for the final result evaluation to determine if the required features of the construction were obtained, taking into consideration the weight assigned by the designer to the partial functions. The paper provides a description of the designed algorithm, with details of each phase of the process. The workflow was divided into parts, which were evaluated and published separately. To present the possibilities of the method, an existing rotor blade was adopted and processed within the optimization loop. The working environment for the blade was based on data from the Flight Data Recorder. The results of the analytical calculations, strength evaluation, and FSI simulation are shown. The connection between subsequent phases, which leads to the final results, is presented. The procedure eliminates some of the possible solutions at each step to ultimately obtain a few that fulfill the requirements.

Possible solutions that best fit the optimization goal and meet the requirements are proposed. Due to the complexity of the main rotor assembly with the hub and swashplate, the blade shapes are aero-structurally optimized and ready to be used as input for further helicopter construction investigations. As an output of the optimization process, presented as an example of the procedure's possibilities, four shapes are proposed with different blade masses and the same performance capabilities. The shapes differ in radius and chord dimensions, and consequently in the inner dimensions. A wider chord provides a higher blade mass, but with a reduction in rotor radius. Shorter blades can be applied to constructions with higher rotational speeds. Shorter blades also provide a smaller rotor disk, which decreases the helicopter's radar cross-section. Longer blades with shorter chords offer a lower mass, resulting in a better final outcome for mass reduction optimization.

V. Conclusion

The scope of the research was to combine the aerodynamic analysis with structural evaluation, using full model parametrization, in the multicriteria optimization process. Based on the mathematical multicriteria optimization model, the algorithm was developed using modern engineering solutions and evaluated. The aim of the entire research was to provide a ready-to-use universal algorithm for main rotor blade design. The second goal was to prove that combining computational solutions can provide more efficient results than using them separately.

However, it is crucial to appropriately design the system of different tools intended to work together. The presented paper provides the final description of four years of research and development. It was proven that the aims were achieved. The algorithm was designed and tested, based on real dimensions and FDR data from a military helicopter. The research offers a new solution for aero-structural optimization. This approach can be applied to helicopter design or to the improvement of existing structures. The method was also developed to reduce design time and optimize computational power usage. It was demonstrated that the method provides a tool for the fast evaluation of various design alternatives. The aero-structural optimization method presented in the previous articles and summarized in this work is a ready-to-use solution for the modern helicopter design process.

Moreover, it can be developed for use in UAV design processes. The parametrization also offers the possibility of being applied to construction projects, such as space design projects, by incorporating environmental conditions. Main rotor design is a complex process that requires consideration of numerous structural and aerodynamic factors. This study focuses on the performance and strength characteristics of the blade.

However, the next step in the algorithm implementation should involve modeling a fully articulated rotor hub with mounted blades. The type of hinges used and the blade installation method should be analyzed for strength properties. A crucial aspect of rotor head design is evaluating aeroelasticity and vibration characteristics, which represent distinct and essential areas of rotor system research. In terms of helicopter construction improvement, high-speed rotorcraft are now being rapidly developed to provide high-speed transportation while maintaining vertical takeoff and landing capability. These rotorcraft use the main rotor for lift generation, combined with propellers responsible for thrust. The presented research could also be applied to this type of design; however, certain corrections to the mathematical model are required, and real flight data must be incorporated to validate the solution.

Acknowledgements

This work was financed by the Military University of Technology (Warsaw, PL) under the two following research projects: No. UGB 22-732/2024/WAT entitled: Aerodynamic design of aircraft in terms of optimizing selected performance parameters; No. UGB 22-734/2024/WAT entitled: Design of light aircraft lifting structures in terms of opti-mizing strength and aeroelastic properties of the airframe. Both grants were carried out in the Institute of Aviation Technology (Faculty of Mechatronics, Armament and Aerospace of the Military University of Technology) in the year 2024 as university statutory activities funded by the Ministry of National Defence of the Republic of Poland.

References

[1] O. Okumuş, M. Şenipek, A. Ezertaş, Multi-Objective Multi-Fidelity Aerodynamic Optimization of Helicopter Rotor, *AIAA Science and Technology Forum and Exposition*, 2022.

[2] W. Stalewski, *Design and Aerodynamic Optimization of Rotorcraft*. Warsaw, 2017.

[3] W. Stalewski, W. Zalewski, Aerodynamic design and optimisation of main rotors for light rotorcrafts, in *45th European Rotorcraft Forum 2019, ERF 2019*, 2019, 1.

[4] W. Stalewski, W. Zalewski, Performance improvement of helicopter rotors through blade redesigning, *Aircraft Engineering and Aerospace Technology*, 91, 5, 2019, s.747–755.

[5] J. Xie, Z. Xie, M. Zhou, J. Qiu, Multidisciplinary aerodynamic design of a rotor blade for an optimum rotor speed helicopter, *Applied Sciences (Switzerland)*, 7, 6, 2017.

[6] W. Stalewski, Design and Optimisation of Main Rotor or Ultralight Helicopter, *Journal of KONES Powertrain and Transport*, 24, 4, 2017.

[7] D. Goerke, A. L. Le Denmat, T. Schmidt, F. Kocian, E. Nicke, Aerodynamic and mechanical optimization of CF/PEEK blades of a counter rotating fan, in *Proceedings of the ASME Turbo Expo*, 2012, 7, PARTS A AND B.

[8] K. Pahlke, B. Demaret, ONERA and DLR contributions to improve environmental friendliness of rotorcraft, *Annual Forum Proceedings - AHS International*, 2017.

[9] A. Tremolet, P. M. Basset, Some meta-modeling and optimization techniques for helicopter pre-sizing, in *38th European Rotorcraft Forum 2012, ERF 2012*, 2012, 2.

[10] G. Wilke, Quieter and Greener rotorcraft: concurrent aerodynamic and acoustic optimization, *CEAS Aeronautical Journal*, 12, 3, 2021.

[11] G. Wilke, J. Bailly, K. Kimura, Y. Tanabe, JAXA-ONERA-DLR Cooperation: Results From Rotor Optimization in Hover, *47th European Rotorcraft Forum - Conference Proceeding*, 2021, s.55–62.

[12] C. Królak, Z. Czyz, K. Siadkowska, R. Kliza, CFD investigation of the main rotor for an unmanned helicopter, in *Journal of Physics: Conference Series*, 2021, 1736, 1.

[13] Lahlou, A., Stouti, S., Lagrat, I., Bouazaoui, O., Mounir, H., Prediction of the Pitch Angle Value for the BELL's 212 Helicopter Main Rotor in a Hover State Configuration Using a CFD Approach, (2024) *International Review of Aerospace Engineering (IREASE)*, 17 (5), pp. 159-167.
doi: https://doi.org/10.15866/irease.v17i5.25389

[14] Ignatkin, Y., Makeev, P., Shomov, A., Ivchin, V., Numerical Study of the Main Rotor Wake Structures and Induced Velocity Fields at the Tail Rotor Location When Flying Near the Ground, (2021) *International Review of Aerospace Engineering (IREASE)*, 14 (4), pp. 181-191.
doi: https://doi.org/10.15866/irease.v14i4.19744

[15] Stouti, S., Lahlou, A., Lagrat, I., Bouazaoui, O., Mounir, H., Impact of Blade Trailing Edge Devices on Helicopter Rotor Aerodynamics During Hovering Flight, (2024) *International Review of Aerospace Engineering (IREASE)*, 17 (2), pp. 39-49.
doi: https://doi.org/10.15866/irease.v17i2.24685

[16] D. Barwey, D. A. Peters, Optimization of composite rotor blades with advanced structural and aerodynamic modeling, *Mathematical and Computer Modelling*, 19, 3–4, 1994.

[17] A. Chattopadhyay, T. R. McCarthy, N. Pagaldipti, Multilevel decomposition procedure for efficient design optimization of helicopter rotor blades, *AIAA Journal*, 33, 2, 1995.

[18] S. Tian et al., Structural Design Optimization of Composite Rotor Blades with Strength Considerations, *AIAA Science and Technology Forum and Exposition*, 2022.

[19] N. A. Vu, J. W. Lee, T. P. N. Le, S. T. T. Nguyen, A fully automated framework for helicopter rotor blades design and analysis including aerodynamics, structure, and manufacturing, *Chinese Journal of Aeronautics*, 29, 6, 2016.

[20] S. Kachel, R. Rogólski, J. Kocjan, Review of Modern Helicopter Constructions and an Outline of Rotorcraft Design Parameters, *Problems of Mechatronics Armament Aviation Safety Engineering*, 12, 3, 2021.

[21] J. Kocjan, S. Kachel, R. Rogólski, Helicopter Main Rotor Blade Parametric Design for a Preliminary Aerodynamic Analysis Supported by CFD or Panel Method, *Materials*, 15, 12, 2022.

[22] A. I. Ryazanov, Automated 3D modeling of working turbine blades, *Russian Engineering Research*, 36, 9, 2016.

[23] L. S. Shabliy, I. B. Dmitrieva, Conversion of the blade geometrical data from points cloud to the parametric format for optimization problems, *ARPN Journal of Engineering and Applied Sciences*, 9, 10, 2014.

[24] C. Grabowik, K. Kalinowski, W. Kempa, I. Paprocka, A method of computer aided design with self-generative models in NX Siemens environment, in *IOP Conference Series: Materials Science and Engineering*, 2015, 95, 1.

[25] J. Kocjan, S. Kachel, R. Rogólski, Parametrization of the main rotor and working environment for different flight conditions – Computational Fluid Dynamics analysis as an application for multidisciplinary optimization, *Journal of Theoretical and Applied Mechanics*, 2023, s.793–805.

[26] J. Kocjan, R. Rogólski, Parametric structure optimization of a main rotor blade as an application for FSI analysis in main rotor optimization process, *Aircraft Engineering and Aerospace Technology*, 96, 2024.

[27] M. Ostwald, *Fundamentals of Structural Optimization in System Design*. Poznań, 2016.

[28] J. Kocjan, S. Kachel, R. Rogolski, Helicopter main rotor FSI analysis using parametric blade model as an application for multidisciplinary optimization, in *Journal of Physics: Conference Series*, 2024, 2716, 1.

Authors' information

[1]Doctoral School, Military University of Technology, ul. gen. Sylwestra Kaliskiego 2, 00-908 Warsaw, Poland.

[2]Faculty of Mechatronics, Armament and Aerospace, Military University of Technology, ul. gen. Sylwestra Kaliskiego 2, 00-908 Warsaw, Poland.

Jakub Kocjan was born in Ruda Slaska (Poland) in 1989. He graduated from the Faculty of Mechatronics and Aerospace of Military University of Technology in 2013 (currently – Faculty of Mechatronics, Armament and Aerospace of MUT) obtaining the degree of M.Sc. in aerospace engineering. In years 2013-2023 he performed his duties as a helicopter engineer in the military. He starts his studies at MUT Doctoral School in 2020. His studies and scientific interests are related to problems of rotorcraft construction, strength, aerodynamics and design optimization problems.

Robert Rogólski, PhD was born in Warsaw (Poland) in 1975. He graduated from the Faculty of Armament and Aerospace of Military University of Technology in 1999 (currently – Faculty of Mechatronics, Armament and Aerospace of MUT) obtaining the degree of M.Sc. in aerospace engineering. In years 1999-2000 he performed his duties as an aircraft section commander in the military Training Centre of Aircraft Engineering of the Polish Air Forces. In 2000 he returned to the MUT and did his doctoral studies in the field of dynamics of aircraft structures. He received the Doctor's degree in 2005. His professional and scientific interests are related to problems of aircraft construction and airframe strength, aeroelasticity, UAV design and prototyping, strength and dynamics of rotor machines. During his scientific and educational work (since 2000) he took part in about twenty research projects. At present he is an assistant professor in Institute of Aviation Technology in the Faculty of Mechatronics, Armament and Aerospace of MUT

Załączniki B – kody źródłowe

B1. Kody źródłowe MATLAB

Program A – trymowanie wirnika nośnego

```
clc
clearvars


Vfl=200 % helicopter flight speed km/h

R=7.85             % rotor radius [m]
c=0.44        % rotor chord [m]

b=4                     % number of blades [m]
rpm=255               % rotor angular velocity [RPM]
a=6.4                 % lift curve slope [rad]
ro=1.225                 % air density [kg/m^3]
G=6600                % weight
vc=0
om=rpm*pi/30                          % rotor angular velocit [rad/s]
W=G*9.81
del=0.01%08*4*a               % profile drag coeficient
tc=0;                   % climb angle
Sfp=2.7                % equivalent fuselage flat plate area [m]
y= 9.65                 % lock nnumber
Mb= 42.5% 65.5                % blade mass [m]
xg=4.640/R  %%%3.612/7.85
e=0.04
A=pi*R^2                % rotor disc area
collective=0
mn=0
twist=-12


V=Vfl/3.6
u=V/(om*R)              % advance ratio
Cmf=0
h=0.25
f=0.01
lt=13.781-4.285
K=0

x=[0  0.21 0.275 0.36 0.45 0.54 0.63 0.72 0.81 0.9 0.95 0.975 0.98 0.99 1]  %
blade coordinates
relc=[0  0.732 0.943 1 1 1 1 1.0955 1.05 1.05 0.827 0.664 0.5 0.5 0]    % chord
dimensions
twist=[5.34  5.34 5.15 4.12 3.031.94 0.85 -0.24    -1.33 -2.42 -3.03 -3.33 -3.63
-3.63 -3.63] % twist value

cg=4.21

Ib=Mb*cg^2
lock=ro*a*c*R^4/Ib
%y= lock
 r=@(x) R*x                             % radius funciotn
```

```
p=polyfit(x,relc,8)
p2=polyfit(x,twist,1)
syms r xx
chord=@(x) polyval(p,x)*c% chord function

chordx=poly2sym(p,xx)*c
chordr=subs(chordx,xx,r/R)
chord2=double(subs(chordr,r,4))
chord3=double(subs(chordr,r,7.85))
plot(x,polyval(p,x))
%fplot(@(r) chordr(r), [0 R], 'b-', 'LineWidth', 1.5);

twistf=deg2rad(-11.8142114712274*(r/R)+8.23642780874989)              % twist
function
B=1-chord(1)/(2*R)

sig=@(x) (b.*chord(x))/(pi.*R)        % rotor soilidity

Solid=integral(sig,0.21,B)
%Solid=b*c/(pi*R)
d0=Sfp/(Solid*A)
wc=W/(ro*Solid*A*om^2*R^2)
v0= (W./(2*ro*pi*R.^2)).^(1/2)      % mean induced velocity

hcd=0.25*u*del

alfd=-(0.5*u^2*d0+hcd)/wc
alfddeg=rad2deg(alfd)

Vm=u*om*R/v0

vi0=1/Vm

lami=vi0*v0/(om*R)

ud=u*cos(alfd)

lamd=ud*alfd-lami

syms tet

eqn= a/4*(2/3*tet*(1-u^2+9*u^4/4)/(1+3*u^2/2)+lamd*(1-u^2/2)/(1+3*u^2/2)) == wc

S=solve(eqn,tet)

tet0=vpa(S(1,1),4)

 exitFLAG = 0


while ~exitFLAG

alfddeg=rad2deg(tet0)
alfddeg=simplify(alfddeg)

a1=2*u*(4*tet0/3+lamd)/(1+3*u^2/2)
a1DEG=rad2deg(a1)

hcd2=1/4*u*del+a*lamd/4*(1/2*a1-u*tet0)
```

```
alfd2=-(0.5*u^2*d0*cos(tc)+hcd2)/wc-tc
ud2=u*cos(alfd2)
lamd2=ud2*alfd2-lami

a0=y/8*(tet0*(1-19*u^2/18+3*u^4/2)/(1+3*u^2/2)+4/3*lamd2*(1-u^2/2)/(1+3*u^2/2))
dtf=(1-sin(alfd2)/(1+sin(alfd2)))
b1=4*((u*a0+1.1*dtf^(1/2)*lami)/3)/(1+u^2/2)
qc=del*(1+3*u^2)/8-lamd2*wc-u*hcd

Cms=b*Mb*xg*e/(2*Solid*A*R)
B1=a1+(Cmf+hcd2*h-wc*f)/(wc*h+Cms)
B1=simplify(B1)
axis=simplify(a1-B1)
B1=rad2deg(B1(1,1))
B1=simplify(B1)


 H=hcd2*ro*A*om^2*R^2*Solid
 P=qc*ro*A*om^3*R^3*Solid

 X=-W*sin(alfd2)-H*cos(alfd2)
D=P\V+X
D=simplify(D)

alfd2=simplify(alfd2)
a1=simplify(a1)
axis=simplify(rad2deg(a1)-B1)

alfHT=simplify(D/W+H/W)
alfHT=simplify(rad2deg(alfHT))


Q=qc*ro*Solid*A*om^2*R^3



%%mass=@(x) Mb.*(x/(0.79*R)-0.21/0.79)        % mass function
%%Inert=@(x) mass(x).*x.^2

%%Ib=integral(Inert,0.21,R)
cg=4.21

Ib=Mb*cg^2
lock=ro*a*c*R^4/Ib

eps=lami/u

Tt=simplify(Q/lt)
ht=2.216/R

b1=(4*(u*a0+1.1*dtf^(1/2)*lami)/3)/1+(u^2/2)-8/lock*eps/(1+u^2/2)*a1

rad2deg(b1)


A1=-b1-(wc*f+(Tt/W)*tc*ht)/(wc*h+Cms)
```

```
xrot=cos(a0)
yrot=sin(a0)

teta=alfddeg
B1=simplify(B1)
A1=simplify(rad2deg(A1))
a0=simplify(rad2deg(a0))

tet0=tet0
tet1=deg2rad(A1)
tet2=deg2rad(B1)
bet0=deg2rad(a0)
bet1=a1
bet2=b1

twist=-12
tettw=deg2rad(twist)*r/R
syms psi r t x

K=1.2
vi=vi0*(1+r/R*K*cos(psi))
%psi=om*t
tet=tet0-twistf-tet1*cos(psi)-tet2*sin(psi) %+tettw*r

%tet=tet0-tet1*cos(psi)-tet2*sin(psi) %+tettw*r
tetsim=tet0-tet1*cos(psi)-tet2*sin(psi)

bet=bet0-bet1*cos(psi)-bet2*sin(psi)
ut=r+u*sin(psi)

ur=u*cos(psi)
lam=(V*sin(alfd-a1)-vi)/(om*R)
%lam=u*tan(alfd)+lami

betp=(bet1*sin(psi)-bet2*cos(psi))
%up=lam+r*diff(bet,t)+u*bet*cos(psi)


UP=om*R*(lam-(r/R)*diff(bet,psi)-u*bet*cos(psi))
UT=om*R*(r/R+u*sin(psi))

inc=tet+atan(UP/UT)

%dT=1/2*ro*a*(tet*UT^2+UP*UT)*c
dT=1/2*ro*a*(tet*UT^2+UP*UT)*chordr

Tn(psi)=int(dT,r,0.21,B*R)
Tnr(r)=int(dT,psi,0,2*pi)
T=(1/(2*pi)*int(Tn,psi,0,2*pi))

if abs(W/b-T) < 500        % find collective loop
    exitFLAG=1
else
    if W/b-T <0
        tet0=tet0*(0.98)
        exitFLAG=0
    else
    tet0=tet0*(1.02)
    exitFLAG=0
```

```
    end
end
end

figure

fplot(@(psi) Tn(psi), [0 2*pi], 'b-', 'LineWidth', 1.5);
%fplot(@(r) Tnr(r), [0 R], 'b-', 'LineWidth', 1.5);
xticks([0 pi/2 pi 3/2*pi 2*pi ])
xticklabels({'0','1/2\pi','\pi','3/2\pi','2\pi'})
xlabel('Azimuth angle [rad]')
ylabel('Aerodynamic loading [N]')
legend
hold off
%%added
figure
%tiledlayout(2,4)
hold on
for n=1:8
dT2=subs(dT,psi,2*pi*n/8)
dTx(x)=subs(dT2,r,x)
%nexttile
fplot(@(x) dTx(x), [0 R], 'LineWidth',
1.5,'DisplayName',[num2str(360*n/8),char(176)]);

%title(['Bending moment for - ',num2str(360*n/8),char(176),' azimuth position'])

end
xlabel('Radial position x')
ylabel('Aerodynamic Force')
title(['Aerodynamic force for azimuth position'])
%added
legend('Location','northwest')
hold off


N =100
x = linspace(0.21*R,1*R,N); % radius
y = linspace(2*pi,0,N); % in degrees
[X,Y]=meshgrid(x,y);
%Z=T2(X,deg2rad(Y))
Z=double(subs(dT, {r,psi}, {X,Y}));

isequal(X,Z)
%plot(deg2rad(Y),Z)
figure;


[~,c]=polarPcolor(x, rad2deg(y), transpose(Z),'Nspokes',9)%,'ncolor',15);
%title(['Rotor Lift distribution for advance ratio u=',u])
ylabel(c,'Aerodynamic loading [N]')

double(subs(tetsim,psi,pi))
double(subs(bet,psi,pi))

rad2deg(double(subs(tetsim,psi,pi)))
rad2deg(double(subs(bet,psi,pi)))
alfddeg
Solid
```

Program B – Wyliczanie momentu gnącego łopaty

```
clearvars -except dT bet r psi
dFa=dT
R=7.46            % rotor radius [m]
c=0.52             % rotor chord [m]
b=4                    % number of blades [m]
rpm=255                % rotor angular velocity [RPM]
a=6.4                 % lift curve slope [rad]
ro=1.293             % air density [kg/m^3] 0.07516 1.293
G=6600 % weight
m=34.203    %34.697
md= m/R %         *47.88


om=rpm*pi/30                            % rotor angular velocit [rad/s]

x=0:pi/16:pi
EI=[44.11 43.29 40.86 38.54 31.92 22.63 13.00 7.54 5.22 4.41 3.48 2.90 2.90 2.90
3.02 2.90 0.58]*10^3*0.45359237
data = importdata('stiffness.txt') ;
syms xx
div=7.4
mass=
[0,m/div,m/div,m/div,m/div,m/div,m/div,m/div,m/div,m/div,m/div,m/div,m/div,m/div,m
/div,m/div,0]
p=polyfit(x,mass,6)
m=@(x) polyval(p,x)
masfun=poly2sym(p,xx)
masfun1=double(subs(masfun,xx,3.14))
masfun2=double(subs(masfun,xx,1.21))

mx=poly2sym(p,xx)
m2=subs(mx,xx,pi*r/R)
mint=double(int(m2,r,0,R))
dF=dFa-m2*om^2*r*bet-m2*r*diff(bet,psi,2)-m2*9.81

fplot(@(x) m(x), [0 pi], 'b-', 'LineWidth', 1.5);
exitFLAG=0

%rigity distribution
pol= polyfit(x,data(1:17,1),6)
EIP=@(x) polyval(pol,x)


n=1
while ~exitFLAG
if n< 16          % find collective loop
    exitFLAG=0
else

    exitFLAG=1
end

fun=@(x) (2/pi)*(EIP(x).*cos(n.*x))
p(n)=integral(fun,0,pi)
n=n+1
end
fun0=@(x) (2/pi)*(EIP(x))
```

```
p0=integral(fun0,0,pi)

exitFLAG=0
n=1
while ~exitFLAG
    if n< 16
    exitFLAG=0
else

    exitFLAG=1
end

mfun=@(x) (m(x)*om^2.*R^2.*(pi^2-x.^2))/(2*pi^2)
fun=@(x) (2/pi)*(mfun(x).*cos(n.*x))
q(n)=integral(fun,0,pi)
n=n+1
end

fun0=@(x) (2/pi)*(mfun(x))
q0=integral(fun0,0,pi)

r0=md*R^2/pi^2

A=  [2*p0-p(2)+2*q0+q(2) 2^2*(p(1)-p(3))+2*(q(1)+q(3)) 3^2*(p(2)-
p(4))+3*(q(2)+q(4)) 4^2*(p(3)-p(5))+4*(q(3)+q(5)) 5^2*(p(4)-p(6))+5*(q(4)+q(6))
6^2*(p(5)-p(7))+6*(q(5)+q(7)) 7^2*(p(6)-p(8))+7*(q(6)+q(8)) 8^2*(p(7)-
p(9))+8*(q(7)+q(9)) -2*q(1) -1^3; ...
    2^2*(p(1)-p(3))+2*(q(1)+q(3)) 4^2*(2*p0-p(4))+4*(2*q0+q(4)) 6^2*(p(1)-
p(5))+6*(q(1)+q(5)) 8^2*(p(2)-p(6))+8*(q(2)+q(6)) 10^2*(p(3)-p(7))+10*(q(3)+q(7))
12^2*(p(4)-p(8))+12*(q(4)+q(8)) 14^2*(p(5)-p(9))+14*(q(5)+q(9)) 16^2*(p(6)-
p(10))+16*(q(6)+q(10)) -4*q(2) 2^3;...
    3^2*(p(2)-p(4))+3*(q(2)+q(4)) 6^2*(p(1)-p(5))+6*(q(1)+q(5)) 9^2*(2*p0-
p(6))+9*(2*q0+q(6)) 12^2*(p(1)-p(7))+12*(q(1)+q(7)) 15^2*(p(2)-
p(8))+15*(q(2)+q(8)) 18^2*(p(3)-p(9))+18*(q(3)+q(9)) 21^2*(p(4)-
p(10))+21*(q(4)+q(10)) 24^2*(p(5)-p(11))+24*(q(5)+q(11)) -6*q(3) -3^3;...
    4^2*(p(3)-p(5))+4*(q(3)+q(5)) 8^2*(p(2)-p(6))+8*(q(2)+q(6)) 12^2*(p(1)-
p(7))+12*(q(1)+q(7)) 16^2*(2*p0-p(8))+16*(2*q0+q(8)) 20^2*(p(1)-
p(9))+20*(q(1)+q(9)) 24^2*(p(2)-p(10))+24*(q(2)+q(10)) 28^2*(p(3)-
p(11))+28*(q(3)+q(11)) 32^2*(p(4)-p(12))+32*(q(4)+q(12)) -8*q(4) 4^3;...
    5^2*(p(4)-p(6))+5*(q(4)+q(6)) 10^2*(p(3)-p(7))+10*(q(3)+q(7)) 15^2*(p(2)-
p(8))+15*(q(2)+q(8)) 20^2*(p(1)-p(9))+20*(q(1)+q(9)) 25^2*(2*p0-
p(10))+25*(2*q0+q(10)) 30^2*(p(1)-p(11))+30*(q(1)+q(11)) 35^2*(p(2)-
p(12))+35*(q(2)+q(12)) 40^2*(p(3)-p(13))+40*(q(3)+q(13)) -10*q(5) -5^3;...
    6^2*(p(5)-p(7))+6*(q(5)+q(7)) 12^2*(p(4)-p(8))+12*(q(4)+q(8)) 18^2*(p(3)-
p(9))+18*(q(3)+q(9)) 24^2*(p(2)-p(10))+24*(q(2)+q(10)) 30^2*(p(1)-
p(11))+30*(q(1)+q(11)) 36^2*(2*p0-p(12))+36*(2*q0+q(12)) 42^2*(p(1)-
p(13))+42*(q(1)+q(13)) 48^2*(p(2)-p(14))+48*(q(2)+q(14)) -12*q(6) 6^3;...
    7^2*(p(6)-p(8))+7*(q(6)+q(8)) 14^2*(p(5)-p(9))+14*(q(5)+q(9)) 21^2*(p(4)-
p(10))+21*(q(4)+q(10)) 28^2*(p(3)-p(11))+28*(q(3)+q(11)) 35^2*(p(2)-
p(12))+35*(q(2)+q(12)) 42^2*(p(1)-p(13))+42*(q(1)+q(13)) 49^2*(2*p0-
p(14))+49*(2*q0+q(14)) 56^2*(p(1)-p(15))+56*(q(1)+q(15)) -14*q(7) -7^3;
    8^2*(p(7)-p(9))+8*(q(7)+q(9)) 16^2*(p(6)-p(10))+16*(q(6)+q(10)) 24^2*(p(5)-
p(11))+24*(q(5)+q(11)) 32^2*(p(4)-p(12))+32*(q(4)+q(12)) 40^2*(p(3)-
p(13))+40*(q(3)+q(13)) 48^2*(p(2)-p(14))+48*(q(2)+q(14)) 56^2*(p(1)-
p(15))+56*(q(1)+q(15)) 64^2*(2*p0-p(16))+64*(2*q0+q(16)) -16*q(8) 8^3;
    -2*q(1) -4*q(2) -6*q(3) -8*q(4) -10*q(5) -12*q(6) -14*q(7) -16*q(8) 4*q0 0;
    -1^3 2^3 -3^3 4^3 -5^3 6^3 -7^3 8^3 0 0 ]

B= [1 0 0 0 0 0 0 0 -2 0;...
```

```
    0 1 0 0 0 0 0 0  1 0;...
    0 0 1 0 0 0 0 0 -2/3 0;...
    0 0 0 1 0 0 0 0 1/2 0;...
    0 0 0 0 1 0 0 0 -2/5 0;...
    0 0 0 0 0 1 0 0 1/3 0;...
    0 0 0 0 0 0 1 0 -2/7 0;...
    0 0 0 0 0 0 0 1 1/4 0;...
    -2 1 -2/3 1/2 -2/5 1/3 -2/7 1/4 2*pi^2/3 0;...
    0 0 0 0 0 0 0 0 0 0]


A1=inv(A)*B


latroots=eig(A1)
I=eye(10,10)
om1= (I/(2.*latroots(2,1)*r0))^(1/2)
om2= (I/(2.*latroots(3,1)*r0))^(1/2)
om3= (I/(2.*latroots(4,1)*r0))^(1/2)


I2=eye

ll=1

%wyn1=(I2*(2*om1^2*r0)^-1)\A1
%wyn1a=(A*transpose(a))\(2*om1^2*r0*B*transpose(a))
wyn1=A\B
%wyn3=A\(2*om3^2*r0*B)
[phi, lambda] = eig(A1)
[lambda, idx] = sort(diag(lambda),'descend');
lambda=(1./(2.*lambda*r0)).^(1/2)


for k=1:7
y =@(x) phi(9,k)*x

n=8
syms x
for i = 1:n

        y =@(x) y(x) + (phi(i,k).*sin(i*x))

end

norm=max(abs(y(0:pi)))
phin=phi./norm

yn =@(x) phin(9,k)*x
for i = 1:n

        yn =@(x) yn(x) + (phin(i,k).*sin(i*x))

end

%yn(x) = y(x) / max(abs(y(0:pi)));
```

```
% Wykresy drgań własnych
figure
hold on;
xlabel('Radial position x')
ylabel('Relative displacement y')
ll=ll+1
if k==2
ll=1
end
title(['Mode shape - ',num2str(double(lambda(ll,1))),' Hz'])
fplot(@(x) yn(x/pi), [0 pi], 'b-', 'LineWidth', 1.5);

yn3=yn(x);
if k==1
yn1=cell(8,1);
end

yn1{k}=yn3;
%hold on;
%xlabel('Radial position x')
%ylabel('Relative displacement')
%fplot(@(x) y(x), [0 pi], 'r-', 'LineWidth', 1.5);

syms  r psi xx

hold off;
yn2=subs(yn(x),x,(pi*r/R))

m3=subs(mx,xx,x)


coe=int(yn2^2*m2,r,0,R);



%yn2=subs(yn(x),x,(pi*r/R))



g(k,1)=int(dF*yn2,r,0,R)/coe



    xxx=diff(yn(x),x,1)^2
    yyy=double(int((m2*yn2.^2),r,0,R))
   coealf(k,1)=double(int(m3*x.*int(xxx,x,0,x),x,0,1)./yyy) %%% check
lamnr(ll,1)=double((lambda(ll,1)^2-coealf(k,1)*om^2)^(1/2))
%A(n,k)=(lambda(n,1)*(ga(n,k)^2+gb(n,k)^2))/()


end
exitFLAG=0
n=1
while ~exitFLAG
if n< 3          % find collective loop
    exitFLAG=0
else

    exitFLAG=1
```

```
end

ga(1,n)=2/pi*int(g(2,1)*cos((2*n)*psi),psi,0,pi)
gb(1,n)=2/pi*int(g(2,1)*sin((2*n)*psi),psi,0,pi)
ga(2,n)=2/pi*int(g(3,1)*cos((2*n)*psi),psi,0,pi)
gb(2,n)=2/pi*int(g(3,1)*sin((2*n)*psi),psi,0,pi)
ga(3,n)=2/pi*int(g(4,1)*cos((2*n)*psi),psi,0,pi)
gb(3,n)=2/pi*int(g(4,1)*sin((2*n)*psi),psi,0,pi)

n=n+1
end

g0(1,1)=1/pi*int(g(2,1),0,2*pi)
g0(2,1)=1/pi*int(g(3,1),0,2*pi)
g0(3,1)=1/pi*int(g(4,1),0,2*pi)
damp=1/(0.79*R)*int(ro*c*r*a/(m2*2),r,0,R)


for n=1:3
    for k=1:3
 Ain(n,k)=double((lamnr(n,1)*(ga(n,k)^2+gb(n,k)^2)^(1/2))/(((lambda(n,1^2)-
k^2*om^2)^2+k^2*damp^2*om^4)^(1/2)))
 Ai0(n,1)=double(lamnr(n,1)*g0(n,1)/lambda(n,1))
 psiin(n,k)=double(atan(k*damp*om^2/(lambda(n,1)-k^2*om^2)))
 phiin(n,k)=double(atan(gb(n,k)/ga(n,k)))
    end

end

for n=1:3
Mix(n,1)=m2.*yn1{n+1}.*(Ai0(n,1)+Ain(n,1).*cos(psi-psiin(n,1)-
phiin(n,1))+Ain(n,2).*cos(2.*psi-psiin(n,2)-phiin(n,2))+Ain(n,3).*cos(3.*psi-
psiin(n,3)-phiin(n,3)))

Mx(n,1)=int(Mix(n,1),x,0,pi)

end

M(psi)=Mx(1,1)+Mx(2,1)+Mx(3,1)
dM=Mix(1,1)+Mix(2,1)+Mix(3,1)



figure
%tiledlayout(2,4)
hold on
for n=1:8
dMx2(x)=subs(dM,psi,2*pi*n/8)
dMx(r)=subs(dMx2,x,(pi*r/R))
%nexttile
fplot(@(x) dMx(x), [0 R], 'LineWidth',
1.5,'DisplayName',[num2str(360*n/8),char(176)]);

%title(['Bending moment for - ',num2str(360*n/8),char(176),' azimuth position'])

end
xlabel('Radial position x')
ylabel('Bending moment [Nm]')
title(['Bending moment for azimuth position'])
```

```
legend('Location','northwest')
hold off
dM=subs(dM,x,pi*r/R)
moment(x)=int(dM,psi,0,2*pi)
moment180(x)=subs(dM,psi,pi)
moment360(x)=subs(dM,psi,2*pi)
for n=1:16

    moment2(n,1)=double(subs(moment,r,R*n/16))
    moment3(n,1)=double(subs(moment180,r,R*n/16))
    moment4(n,1)=double(subs(moment360,r,R*n/16))
end
writematrix(moment2, 'moment.txt')
writematrix(moment3, 'moment180.txt')
writematrix(moment4, 'moment360.txt')
figure
hold on;
xlabel('Azimuth')
ylabel('Bending moment')
title(['Bending moment'])
fplot(@(x) moment(x), [0 pi], 'b-', 'LineWidth', 1.5);
```

B2. Kody źródłowe GRIP

Program C – parametryczny model jednołopatowej symulacja CFD

```
ENTITY/PT0(6001),PT1(200),PT2(100),PT3(100),PT4(100),SPL1(20),SPL2(20),$
SPL3(20),SPL4(20),SPLC(3),LN(20),LN1(20),SSRF(5),SOL(5),BLD(5),PLN,CYL(2)
STRING/FNAM(50)
NUMBER/x1,y1,x2,y2,R(8),NUM,MAT(12),A(3),B(3),R0,C0,R1,cf,rf,xm,fi(6),dfi,z$

DELETE/ALL

C0=0.44
R0=7.75
R1=0.21
xm=0
z=4

PARAM/'ENTER DATA','C=',C0,'R=',R0,RSP1
BCK10:
PARAM/'Enter blade begining position','R1=',R1,RSP1

$$ Radius polonymal $$
R(7)=-184.82
R(6)=641.23
R(5)=-912.87
R(4)=683.5
R(3)=-284.18
R(2)=62.234
R(1)=-4.6044
```

```
PARAM/'Enter polynomial coefficients',$
'r^6',R(7),'r^5',R(6),'r^4',R(5),$
'r^3',R(4),'r^2',R(3),'r',R(2),'X',R(1),RSP1

$$ Pitch polonymal $$
fi(4)=0
fi(3)=0
fi(2)=-11.814
fi(1)=8.2364
PARAM/'Enter polynomial coefficients',$
'fi^3',fi(4),'fi^2',fi(3),'fi',fi(2),'X',fi(1),RSP1


BCK20:

FNAM='G:\praca doktorska\artykuly\23015.txt'

M=16
dr=(1-R1)/M
K=0

L10:

N=0
FETCH/TXT,1,FNAM
RESET/1

L20:
N=N+1
READ/1,LINNO,N*10,IFEND,L30:,x1,y1,x2,y2

$$ current radius $$
cr=(K*dr)+R1

$$ delta chord $$
dc=R(7)*cr**6+R(6)*cr**5+R(5)*cr**4+R(4)*cr**3+R(3)*cr**2+R(2)*cr+R(1)

PRINT/USING,'Wartość wyliczona dc=#@@@@.@@',dc
PRINT/USING,'Wartość wyliczona cr=#@@@@.@@',cr

IFTHEN/K>(M/2)
IF/dc<1, xm=(C0*(1-dc))/2
ENDIF

PT0(N)=POINT/x1*C0*dc+xm,y1*C0*dc,cr*R0
PT1(N)=POINT/x2*C0*dc+xm,y2*C0*dc,cr*R0
```

```
JUMP/L20:


L30:
$$ PT3(K+1)=POINT/x1*C0*dc+xm,y1*C0*dc,cr*R0


$$ Airfoil geometry
SPL3(K+1)=SPLINE/PT0(1..N-1) $$ upper surface
SPL4(K+1)=SPLINE/PT1(1..N-1) $$ lower surface
$$ LN1(K+1)=LINE/PT0(N-1),PT1(N-1)

dfi=fi(4)*cr+fi(3)*cr+fi(2)*cr+fi(1)

PRINT/USING,'value dc=#@@@@.@@',dc
PRINT/USING,'Wartość wyliczona cr=#@@@@.@@',cr
PRINT/USING,'Wartość wyliczona dfi=#@@@@.@@',dfi

MAT=MATRIX/XYROT,-dfi
SPL1(K+1)=TRANSF/MAT,SPL3(K+1)
SPL2(K+1)=TRANSF/MAT,SPL4(K+1)
$$ LN(K+1)=TRANSF/MAT,LN1(K+1)

PT2(K+1)=POINT/ENDOF,XSMALL,SPL1(K+1)
PT3(K+1)=POINT/ENDOF,XLARGE,SPL1(K+1)
PT4(K+1)=POINT/ENDOF,XLARGE,SPL2(K+1)
LN(K+1)=SPLINE/PT3(K+1),PT4(K+1)

DELETE/PT0,PT1,SPL3,SPL4,LN1

IFTHEN/K<M
K=K+1
JUMP/L10:
ELSE
JUMP/L40:
ENDIF

L40:
A=&POINT(PT3(1))
B=&POINT(PT4(1))

SPLC(1)=SPLINE/PT2(1..K+1)
SPLC(2)=SPLINE/PT3(1..K+1)
SPLC(3)=SPLINE/PT4(1..K+1)


SSRF(1)=BSURF/MESH,SPLC(1..2),WITH,SPL1(1..K+1),TYPE,3,TOLER,.01,.01
SSRF(2)=BSURF/MESH,SPLC(1),SPLC(3),WITH,SPL2(1..K+1),TYPE,3,TOLER,.01,.01
```

```
SSRF(3) = RLDSRF/SPLC(2),,SPLC(3)

SSRF(4) =RLDSRF/SPL1(1),,SPL2(1)
SSRF(5) =RLDSRF/SPL1(K+1),,SPL2(K+1)
BLD(1)=SEW/SSRF(1..5)


DELETE/PT2,PT3,PT4,LN,SPLC

PT2(1)=POINT/4*R0-1,0,R1*R0
PT2(2)=POINT/4*R0-1,2*R0,R1*R0
PT2(3)=POINT/-R0/2-1,2*R0,R1*R0
PT2(4)=POINT/-R0/2-2*R0-1,0,R1*R0
PT2(5)=POINT/-R0/2-1,0,R1*R0
LN(1)=LINE/PT2(4),PT2(1)
LN(2)=LINE/PT2(1..2)
LN(3)=LINE/PT2(2..3)
LN(4)=CIRCLE/CENTER,PT2(5),RADIUS,2*R0,START,90,END,180
CYL(1)=SOLREV/LN(1..4),ORIGIN,0,0,R1*R0,ATANGL,180,AXIS,1,0,0
CYL(2)= SUBTRA/CYL(1),WITH,BLD(1),CNT,c
HALT
```

Program D – parametryczny model n-łopatowej symulacja CFD

```
ENTITY/PT0(6001),PT1(200),PT2(100),PT3(100),PT4(100),SPL1(20),SPL2(20),$
SPL3(20),SPL4(20),SPLC(3),LN(20),LN1(20),SSRF(5),SOL(5),BLD(8),PLN,$
DISK(6),LN2(5),DOM(10),CYL(10),CENT
STRING/FNAM(50)
NUMBER/x1,y1,x2,y2,R(8),NUM,MAT(12),MAT2(12),A(3),B(3),R0,C0,R1,cf,rf,xm,fi(6),$
dfi,z,c,A1,B1,a0,MAT3(12),D(3),E(3),Frad

DELETE/ALL

C0=0.44
R0=7.75
R1=0.21
xm=0
z=4
pitch=5
A1=0
B1=0
BCK10:
PARAM/'ENTER DATA','C=',C0,'R=',R0,'b=',z,RSP1
a0=7

PARAM/'Enter blade begining position','R1=',R1,RSP1


PARAM/'ENTER ROTOR TRIM ANGLES','Pitch=',pitch,'A1=',A1,'B1=',B1,'a0=',a0,RSP1
```

```
PARAM/'Enter blade begining position','R1=',R1,RSP1


C0=C0*1000
R0=R0*1000


$$ Radius polonymal $$
R(7)=-184.82
R(6)=641.23
R(5)=-912.87
R(4)=683.5
R(3)=-284.18
R(2)=62.234
R(1)=-4.6044

PARAM/'Enter polynomial coefficients',$
'r^6',R(7),'r^5',R(6),'r^4',R(5),$
'r^3',R(4),'r^2',R(3),'r',R(2),'X',R(1),RSP1

$$ Pitch polonymal $$
fi(4)=0
fi(3)=0
fi(2)=-11.814
fi(1)=8.2364
PARAM/'Enter polynomial coefficients',$
'fi^3',fi(4),'fi^2',fi(3),'fi',fi(2),'X',fi(1),RSP1


BCK20:

FNAM='g:\praca doktorska\artykuly\23015.txt'

M=16
dr=(1-R1)/M
K=0

L10:

N=0
FETCH/TXT,1,FNAM
RESET/1

L20:
N=N+1
READ/1,LINNO,N*10,IFEND,L30:,x1,y1,x2,y2

$$ current radius $$
```

```
cr=(K*dr)+R1

$$ delta chord $$
dc=R(7)*cr**6+R(6)*cr**5+R(5)*cr**4+R(4)*cr**3+R(3)*cr**2+R(2)*cr+R(1)

PRINT/USING,'Wartość wyliczona dc=#@@@@.@@',dc
PRINT/USING,'Wartość wyliczona cr=#@@@@.@@',cr

IFTHEN/K>(M/2)
IF/dc<1, xm=(C0*(1-dc))/2
ENDIF

PT0(N)=POINT/x1*C0*dc+xm,y1*C0*dc,cr*R0
PT1(N)=POINT/x2*C0*dc+xm,y2*C0*dc,cr*R0

$$ IF/N==1, PT2(K+1)=POINT/x1*C0*dc+xm,y1*C0*dc,cr*R0


JUMP/L20:


L30:
$$ PT3(K+1)=POINT/x1*C0*dc+xm,y1*C0*dc,cr*R0


$$ Airfoil geometry
SPL3(K+1)=SPLINE/PT0(1..N-1) $$ upper surface
SPL4(K+1)=SPLINE/PT1(1..N-1) $$ lower surface
$$ LN1(K+1)=LINE/PT0(N-1),PT1(N-1)

dfi=fi(4)*cr+fi(3)*cr+fi(2)*cr+fi(1)

PRINT/USING,'value dc=#@@@@.@@',dc
PRINT/USING,'Wartość wyliczona cr=#@@@@.@@',cr
PRINT/USING,'Wartość wyliczona dfi=#@@@@.@@',dfi

MAT=MATRIX/XYROT,-dfi
SPL1(K+1)=TRANSF/MAT,SPL3(K+1)
SPL2(K+1)=TRANSF/MAT,SPL4(K+1)
$$ LN(K+1)=TRANSF/MAT,LN1(K+1)

PT2(K+1)=POINT/ENDOF,XSMALL,SPL1(K+1)
PT3(K+1)=POINT/ENDOF,XLARGE,SPL1(K+1)
PT4(K+1)=POINT/ENDOF,XLARGE,SPL2(K+1)
$LN(K+1)=SPLINE/PT3(K+1),PT4(K+1)

D=&POINT(PT3(K+1))
E=&POINT(PT4(K+1))
Frad=ABSF((D(2)-E(2))/2)
CENT=POINT/D(1)+Frad/2,(D(2)+E(2))/2,D(3)
```

```
LN(K+1)= CIRCLE/PT3(K+1),CENT,PT4(K+1)
CRVTRM/LN(K+1),REF,PT4(K+1),FIRST,SPL1(K+1),$
STATUS,STAT,IFERR,ER1:
CRVTRM/LN(K+1),REF,PT3(K+1),FIRST,SPL2(K+1),$
STATUS,STAT,IFERR,ER1:
$LN(K+1)=FILLET/SPL2(K+1),SPL1(K+1),CENTER,CENT,RADIUS,FRAD,NOTRIM


ER1:


A=&POINT(PT2(1))
B=&POINT(PT4(1))


DELETE/PT0,PT1,SPL3,SPL4,LN1

IFTHEN/K<M
K=K+1
JUMP/L10:
ELSE
JUMP/L40:
ENDIF

L40:

SPLC(1)=SPLINE/PT2(1..K+1)
SPLC(2)=SPLINE/PT3(1..K+1)
SPLC(3)=SPLINE/PT4(1..K+1)



SSRF(1)=BSURF/MESH,SPLC(1..2),WITH,SPL1(1..K+1),TYPE,3,TOLER,.01,.01
SSRF(2)=BSURF/MESH,SPLC(1),SPLC(3),WITH,SPL2(1..K+1),TYPE,3,TOLER,.01,.01

SSRF(3) =BSURF/MESH,SPLC(2..3),WITH,LN(1..K+1),TYPE,3,TOLER,.01,.01
SSRF(4) =AUTOSF/SPL1(1),LN(1),SPL2(1)
SSRF(5) =AUTOSF/SPL1(K+1),LN(K+1),SPL2(K+1)
BLD(8)=SEW/SSRF(1..5)


DOM(8)= SOLCYL/ORIGIN,(A(1)+B(1))/2-C0/2,(A(2)+B(2))/2,-400+(A(3)+B(3))/2,$
HEIGHT,1.2*R0,DIAMTR,3*C0,AXIS,0,0,1

MAT=MATRIX/TRANSL,-C0/2,0,0
BLD(1)=TRANSF/MAT,BLD(8)
MAT=MATRIX/XYROT,-pitch
BLD(2)=TRANSF/MAT,BLD(1)
DOM(9)=TRANSF/MAT,DOM(8)
$$CYL(9)=TRANSF/MAT,CYL(8)
```

```
DOM(9)= SUBTRA/DOM(9),WITH,BLD(2),CNT,c

DELETE/BLD(8),DOM(8),CYL(8)


DELETE/PT2,PT3,PT4,LN,SPLC


$$ blade multiplication

ang=360/z

z0=1
B10:

MAT=MATRIX/ZXROT,z0*ang

MAT2=MATRIX/XYROT,-(-A1*COSF(90+z0*ang)-B1*SINF(90+z0*ang))
MAT3=MATRIX/YZROT,-a0

DOM(8)=TRANSF/MAT2,DOM(9)
DOM(7)=TRANSF/MAT3,DOM(8)
DOM(z0+1)=TRANSF/MAT,DOM(7)
DELETE/DOM(7..8)
IFTHEN/z0<z-1
z0=z0+1
JUMP/B10:
ELSE
JUMP/B20:
ENDIF


B20:
MAT2=MATRIX/XYROT,-(-A1*COSF(90*ang)-B1*SINF(90*ang))

DOM(8)=TRANSF/MAT2,DOM(9)
$$CYL(8)=TRANSF/MAT2,CYL(9)
DOM(1)=TRANSF/MAT3,DOM(8)
DELETE/DOM(8..9),CYL(8..9)



CANCEL:
CHOOSE/'Choose flight conditions',$
        'Hover',$
        'Forward flight',$
        DEFLT,1,RSP
JUMP/B20:,CANCEL:,,,HOVER:,FFLIGHT:,RSP

HOVER:
```

```
DISK(2)= SOLCYL/ORIGIN,0,-0.5*(10*R0),0,HEIGHT,10*R0,DIAMTR,20*R0,$
AXIS,0,1,0
JUMP/NEXT:

FFLIGHT:
DISK(2)= SOLBLK/ORIGIN,-0.4*16*R0,-0.5*(8*R0),-0.5*(8*R0),SIZE,16*R0,8*R0,8*R0
$$DISK(3)= SUBTRA/DISK(2),WITH,DISK(1),CNT,c $$ enclosure
JUMP/NEXT:

NEXT:

DISK(4)= SOLCYL/ORIGIN,0,-0.25*(9*C0),0,HEIGHT,9*C0,DIAMTR,1.5*R0*2,$
AXIS,0,1,0

DELETE/BLD

HALT
```

Program E – parametryczny model strukturalny

```
ENTITY/PT0(6001),PT1(200),PT2(100),PT3(100),PT4(100),SPL1(20),SPL2(20),$
SPL3(20),SPL4(20),SPLC(6),LN(20),LN1(20),SSRF(10),SOL(5),BLD(8),PLN(20),$
LN2(5), OFSPL1(20),OFSPL2(20),PT(100),PT5(100),PT6(100),SPR,SEC(100),BND(20),$
CENT,PTS1(200),PTS2(100),PTS3(100),PTS4(100),LNS1(200),LNS2(100),LNS3(100),$
LNS4(100),PTS5(200),PTS6(100),PTS7(100),PTS8(100),LNS5(10),SPAR(8),$
PTS9(100),PTS10(100),BND2(20),PLAN

STRING/FNAM(50)
NUMBER/x1,y1,x2,y2,R(8),NUM,MAT(12),MAT2(12),A(3),B(3),R0,C0,R1,cf,rf,xm,fi(6),$
dfi,z,c,A1,B1,STAT,w,h,wyn(42),wyn2(32),wyn3(32),ctrl(20),D(3),E(3),Frad,DIST,$
wall,moment(20),hgh,width(20),height(20),str,Ix,F(3),G(3),CHECK(20),SF,XC1(50),$
XC2(50),YC1(50),YC2(50)

DELETE/ALL

C0=0.44
R0=7.75
R1=0.21
xm=0
z=4
pitch=5
A1=0
B1=0
BCK10:
PARAM/'ENTER DATA','C=',C0,'R=',R0,'b=',z,RSP1
SF=1.3

PARAM/'Enter blade begining position','R1=',R1,RSP1
PARAM/'Enter safety factor','SF=',SF,RSP1
```

```
C0=C0*1000
R0=R0*1000


$$ Radius polonymal $$
R(7)=-184.82
R(6)=641.23
R(5)=-912.87
R(4)=683.5
R(3)=-284.18
R(2)=62.234
R(1)=-4.6044

PARAM/'Enter polynomial coefficients',$
'r^6',R(7),'r^5',R(6),'r^4',R(5),$
'r^3',R(4),'r^2',R(3),'r',R(2),'X',R(1),RSP1

$$ Pitch polonymal $$
fi(4)=0
fi(3)=0
fi(2)=-11.814
fi(1)=8.2364
PARAM/'Enter polynomial coefficients',$
'fi^3',fi(4),'fi^2',fi(3),'fi',fi(2),'X',fi(1),RSP1
M=16

i=0
LOOP:
IFTHEN/i<M
width(i+1)=30
height(i+1)=1
ctrl(i+1)=-4
i=i+1
JUMP/LOOP:
ELSE
ENDIF
wall=-28
OPT1:
$$wall=wall-0.1
FNAM='g:\praca doktorska\artykuly\202303\moment.txt'



dr=(1-R1)/M

K=0
LAB10:

N=0
```

```
FETCH/TXT,1,FNAM
RESET/1

LAB20:
N=N+1
READ/1,LINNO,N*10,IFEND,LAB30:,moment(N)

JUMP/LAB20:

LAB30:


BCK20:

FNAM='g:\praca doktorska\artykuly\23015.txt'



L10:

xm=0
N=0
FETCH/TXT,1,FNAM
RESET/1

L20:
N=N+1
READ/1,LINNO,N*10,IFEND,L30:,x1,y1,x2,y2

$$ current radius $$
cr=(K*dr)+R1

$$ delta chord $$
dc=R(7)*cr**6+R(6)*cr**5+R(5)*cr**4+R(4)*cr**3+R(3)*cr**2+R(2)*cr+R(1)
XC1(N)=x1
XC2(N)=x2
YC1(N)=y1
YC2(N)=y2

IFTHEN/K>(M/2)
IF/dc<1, xm=(C0*(1-dc))/2

ENDIF


PT0(N)=POINT/x1*C0*dc+xm,y1*C0*dc,cr*R0
PT1(N)=POINT/x2*C0*dc+xm,y2*C0*dc,cr*R0

$$ IF/N==1, PT2(K+1)=POINT/x1*C0*dc+xm,y1*C0*dc,cr*R0
```

```
JUMP/L20:


L30:
$$ PT3(K+1)=POINT/x1*C0*dc+xm,y1*C0*dc,cr*R0


A=&POINT(PT0(1))
B=&POINT(PT1(1))

w=C0*dc/3.5 $$+width
h=C0*dc/20 $$+height


$$ Airfoil geometry
SPL3(K+1)=SPLINE/PT0(1..N-1) $$ upper surface
SPL4(K+1)=SPLINE/PT1(1..N-1) $$ lower surface

dfi=fi(4)*cr+fi(3)*cr+fi(2)*cr+fi(1)



MAT=MATRIX/XYROT,-dfi
SPL1(K+1)=TRANSF/MAT,SPL3(K+1)
SPL2(K+1)=TRANSF/MAT,SPL4(K+1)


$$$$$$$$$$$SPAR $$$$$$$$$$



PT2(K+1)=POINT/ENDOF,XSMALL,SPL1(K+1)
PT3(K+1)=POINT/ENDOF,XLARGE,SPL1(K+1)
PT4(K+1)=POINT/ENDOF,XLARGE,SPL2(K+1)
$LN(K+1)=SPLINE/PT3(K+1),PT4(K+1)

D=&POINT(PT3(K+1))
E=&POINT(PT4(K+1))
Frad=ABSF((D(2)-E(2))/2)
CENT=POINT/D(1)+Frad/2,(D(2)+E(2))/2,D(3)
LN(K+1)= CIRCLE/PT3(K+1),CENT,PT4(K+1)
CRVTRM/LN(K+1),REF,PT4(K+1),FIRST,SPL1(K+1),$
STATUS,STAT,IFERR,ER1:
CRVTRM/LN(K+1),REF,PT3(K+1),FIRST,SPL2(K+1),$
STATUS,STAT,IFERR,ER1:


$$$$$$$  OFFSET
PT(K+1)=POINT/C0/2,0,cr*R0
```

```
TH=1
OFSPL1(K+1)=OFFCRV/SPL1(K+1),TH,PT(K+1)
OFSPL2(K+1)=OFFCRV/SPL2(K+1),TH,PT(K+1)


CRVTRM/OFSPL1(K+1),REF,PT3(K+1),FIRST,OFSPL2(K+1),$
INT,PT3(K+1),STATUS,STAT,IFERR,ER1:
CRVTRM/OFSPL1(K+1),REF,PT2(K+1),FIRST,OFSPL2(K+1),$
INT,PT2(K+1),STATUS,STAT,IFERR,ER1:



LNS1(K+1)=OFFCRV/SPL1(K+1),TH+2+height(K+1),PT(K+1)
LNS3(K+1)=OFFCRV/SPL2(K+1),TH+2+height(K+1),PT(K+1)

CRVTRM/LNS1(K+1),REF,PT3(K+1),FIRST,LNS3(K+1),$
INT,PT3(K+1),STATUS,STAT,IFERR,ER1:
CRVTRM/LNS1(K+1),REF,PT2(K+1),FIRST,LNS3(K+1),$
INT,PT2(K+1),STATUS,STAT,IFERR,ER1:



PLAN=PLANE/YZPLAN,C0/3-width(K+1)

CRVTRM/LNS1(K+1),REF,PT3(K+1),FIRST,PLAN,$
INT,PT3(K+1),STATUS,STAT,IFERR,ER1:
CRVTRM/LNS3(K+1),REF,PT3(K+1),FIRST,PLAN,$
INT,PT3(K+1),STATUS,STAT,IFERR,ER1:

PTS4(K+1)=POINT/ENDOF,XSMALL,LNS3(K+1)
PTS5(K+1)=POINT/ENDOF,XLARGE,LNS1(K+1)
PTS6(K+1)=POINT/ENDOF,XLARGE,LNS3(K+1)

LNS4(K+1)=LINE/PTS5(K+1),PTS6(K+1)
DELETE/PLAN
ER1:
$$$$$$$$$$$$
PT5(K+1)=POINT/ENDOF,XSMALL,OFSPL1(K+1)
PT6(K+1)=POINT/ENDOF,XLARGE,OFSPL1(K+1)

A=&POINT(PT2(1))
B=&POINT(PT4(1))


DELETE/PT0,PT1,SPL3,SPL4,LN1,PT

IFTHEN/K<M
K=K+1
JUMP/L10:
ELSE
```

```
JUMP/L40:
ENDIF

L40:

LNS5(1)=SPLINE/PTS5(1..K)
LNS5(2)=SPLINE/PTS4(1..K)
LNS5(3)=SPLINE/PTS6(1..K)
$$LNS5(4)=SPLINE/PTS4(1..K)



SPLC(1)=SPLINE/PT2(1..K+1)
SPLC(2)=SPLINE/PT3(1..K+1)
SPLC(3)=SPLINE/PT4(1..K+1)
SPLC(4)=SPLINE/PT5(1..K+1)
SPLC(5)=SPLINE/PT6(1..K+1)


SSRF(1)=BSURF/MESH,SPLC(1..2),WITH,SPL1(1..K+1),TYPE,3,TOLER,.01,.01
SSRF(2)=BSURF/MESH,SPLC(1),SPLC(3),WITH,SPL2(1..K+1),TYPE,3,TOLER,.01,.01

SSRF(3) =BSURF/MESH,SPLC(2..3),WITH,LN(1..K+1),TYPE,3,TOLER,.01,.01
SSRF(4) =AUTOSF/SPL1(1),LN(1),SPL2(1)
SSRF(5) =AUTOSF/SPL1(K+1),LN(K+1),SPL2(K+1)
SSRF(6)=BSURF/MESH,SPLC(4..5),WITH,OFSPL1(1..K+1),TYPE,3,TOLER,.01,.01
SSRF(7)=BSURF/MESH,SPLC(4..5),WITH,OFSPL2(1..K+1),TYPE,3,TOLER,.01,.01
SSRF(8) =AUTOSF/OFSPL1(1),OFSPL2(1)
SSRF(9) =AUTOSF/OFSPL1(K+1),OFSPL2(K+1)
BLD(8)=SEW/SSRF(1..5)

DELETE/LN,PT2,PT3,PT4,SPLC,LN,PTS1,PTS2,PTS3,PTS4,PTS5,PTS6

SPAR(2)=BSURF/MESH,LNS5(1..2),WITH,LNS1(1..K),TYPE,3,TOLER,.01,.01
SPAR(3)=BSURF/MESH,LNS5(2..3),WITH,LNS3(1..K),TYPE,3,TOLER,.01,.01
SPAR(4)=BSURF/MESH,LNS5(3),LNS5(1),WITH,LNS4(1..K),TYPE,3,TOLER,.01,.01
$$SPAR(5)=BSURF/MESH,LNS5(4),LNS5(1),WITH,LNS4(1..K),TYPE,3,TOLER,.01,.01
SPAR(5)=AUTOSF/LNS1(1),LNS3(1),LNS4(1)
SPAR(6)=AUTOSF/LNS1(K),LNS3(K),LNS4(K)
SPAR(8)=SEW/SPAR(2..6)

BLD(7)=SEW/SSRF(6..9)
MAT=MATRIX/TRANSL,0,0,0
BLD(5)=TRANSF/MAT,BLD(7)
SPAR(1)=TRANSF/MAT,SPAR(8)

BLD(6)= SUBTRA/BLD(8),WITH,BLD(7),CNT,c $$ enclosure
&COLOR(BLD(6))=100

DELETE/LN,PT2,PT3,PT4,PT5,PT6,SPLC
```

```
PLN(1)=PLANE/YZPLAN,C0/3+wall
BLD(1..2)= SPLIT/BLD(5),WITH,PLN(1)

PLN(2)=PLANE/XYPLAN,A(3)+1
SEC(1..3)= SECT/BLD(1),WITH,PLN(2)
BND(1)=BOUND/SEC(1..3)
BND(2)=BOUND/LNS1(1),LNS3(1),LNS4(1)
ANLSIS/TWOD,BND(1),MMETER,wyn2
ANLSIS/TWOD,BND(2),MMETER,wyn3




PRINT/'--------Spar Cross section analysis-----------'
PRINT/USING,'Cross section area Fdz=#@@@@@@.@@ [mm^2]',wyn2(2)-wyn3(2)
PRINT/USING,'Moment of Intertia Idz=#@@@@@@@.@@ [mm^4]',wyn2(9)-wyn3(9)
PRINT/USING,' center of mass:  X=#@@@@@@@@@@@@@.@@@ mm',wyn2(3)
PRINT/USING,'                  Y=#@@@@@@@@@@@@@.@@@ mm',wyn2(4)
PRINT/USING,' center of mass:  X=#@@@@@@@@@@@@@.@@@ mm',wyn3(3)
PRINT/USING,'                  Y=#@@@@@@@@@@@@@.@@@ mm',wyn3(4)
PRINT/USING,' Principal axis:  X=#@@@@@@@@@@@@@.@@@ mm',wyn2(17)
PRINT/USING,'                  Y=#@@@@@@@@@@@@@.@@@ mm',wyn2(18)
PRINT/USING,' Principal axis:  X=#@@@@@@@@@@@@@.@@@ mm',wyn3(17)
PRINT/USING,'                  Y=#@@@@@@@@@@@@@.@@@ mm',wyn3(18)
DIST=0
N=0
K=3*(N+1)
PLAN_CREATE:
K=3*(N+1)
DIST=0
IF/N==M,DIST=5
IF/N==0,DIST=-1
PLN(N+1)=PLANE/XYPLAN,A(3)+(R0-R1*R0)*N/M-DIST
SEC(K-2..K)= SECT/BLD(1),WITH,PLN(N+1),CNT,c
BND(N+1)=BOUND/SEC(K-2..K)
BND2(N+1)=BOUND/LNS1(N+1),LNS3(N+1),LNS4(N+1)
ANLSIS/TWOD,BND(N+1),MMETER,wyn2
ANLSIS/TWOD,BND2(N+1),MMETER,wyn3


IFTHEN/N+1<M
N=N+1
JUMP/PLAN_CREATE:
ELSE
JUMP/END_PLAN:
```

```
ENDIF

END_PLAN:

str=800
N=0

hgh=(0.15*C0)/2
K=7
OPT2:
IFTHEN/K<M
$$IFTHEN/CHECK(M)==1
$$JUMP/OPT_END:
        IFTHEN/CHECK(K+1)==0
        JUMP/FRWD:
        ELSE
        K=K+1
        JUMP/OPT2:
        ENDIF
ELSE
JUMP/OPT_END:
ENDIF

FRWD:
IFTHEN/N<M

        IFTHEN/CHECK(N+1)==0
        ANLSIS/TWOD,BND(N+1),MMETER,wyn2
        ANLSIS/TWOD,BND2(N+1),MMETER,wyn3
        Ix=wyn2(9)-wyn3(9)
        tens=ABSF(moment(N+1)*1000*hgh/Ix)
        PRINT/USING,'Section nr #@@',N+1
        PRINT/USING,'Moment is  M=#@@@@@@@.@@ [Pa]',moment(N+1)
        PRINT/USING,'Cross section area Fdz=#@@@@@@.@@ [mm^2]',wyn2(2)-
wyn3(2)
        PRINT/USING,'Moment of Intertia Idz=#@@@@@@@.@@ [mm^4]',wyn2(9)-
wyn3(9)
        PRINT/USING,'Stress is  sig1=#@@@@@@@@.@@ [MPa]',tens

                IFTHEN/ABSF(SF*tens-str)>0.08*str

                        IFTHEN/str-SF*tens>0

                        $$IFTHEN/N+1>=7
                        $$IF/(str-SF*tens)>0.2*str,height(N+1)=height(N+1)-0.5
                        $$IF/(str-SF*tens)<=0.2*str,height(N+1)=height(N+1)-0.1
                                IFTHEN/ABSF(width(N+1))<=wall-4
                                IF/ABSF(str-SF*tens)>0.2*str,width(N+1)=width(N+1)-2
                                IF/ABSF(str-SF*tens)<=0.2*str,width(N+1)=width(N+1)-1
                                ELSE
```

```
                    JUMP/RED:
                    ENDIF
                $$ENDIF
                $$IFTHEN/N+1<7
                $$height(N+1)=height(N+1)-0.1

                $$ENDIF
                ELSE

                IF/ABSF(str-SF*tens)>0.2*str,height(N+1)=height(N+1)+1
                IF/ABSF(str-SF*tens)<=0.2*str,height(N+1)=height(N+1)+0.1
                IF/ABSF(str-SF*tens)>0.2*str,width(N+1)=width(N+1)+10
                IF/ABSF(str-SF*tens)<=0.2*str,width(N+1)=width(N+1)+1



                ENDIF

            N=N+1
            JUMP/FRWD:
            ELSE
            RED:
            CHECK(N+1)=1
            N=N+1
            JUMP/FRWD:
            ENDIF
        ELSE
            ANLSIS/TWOD,BND(N+1),MMETER,wyn2
        ANLSIS/TWOD,BND2(N+1),MMETER,wyn3
        Ix=wyn2(9)-wyn3(9)
        tens=ABSF(moment(N+1)*1000*hgh/Ix)
        PRINT/USING,'Section nr #@@',N+1
        PRINT/USING,'Moment is  M=#@@@@@@@.@@ MPa]',moment(N+1)
        PRINT/USING,'Cross section area Fdz=#@@@@@@.@@ [mm^2]',wyn2(2)-
wyn3(2)
        PRINT/USING,'Moment of Intertia Idz=#@@@@@@@.@@ [mm^4]',wyn2(9)-
wyn3(9)
        PRINT/USING,'Stress is  sig=#@@@@@@@@.@@ [MPa]',tens
        N=N+1
        JUMP/FRWD:
        ENDIF
ELSE
DELETE/BLD,SPAR,SPLC,SEC,BND,BND2,LNS5,PLN
$$MESSG/' End of iteration'
JUMP/OPT1:
ENDIF
ANLSIS/TWOD,BND(M),MMETER,wyn2
        ANLSIS/TWOD,BND2(M),MMETER,wyn3
        Ix=wyn2(9)-wyn3(9)
        tens=ABSF(moment(M)*1000*hgh/Ix)
```

```
        PRINT/USING,'Section nr #@@',M
        PRINT/USING,'Moment is  M=#@@@@@@@.@@ [Pa]',moment(N+1)
        PRINT/USING,'Cross section area Fdz=#@@@@@@.@@ [mm^2]',wyn2(2)-
wyn3(2)
        PRINT/USING,'Moment of Intertia Idz=#@@@@@@@.@@ [mm^4]',wyn2(9)-
wyn3(9)
        PRINT/USING,'Stress is  sig1=#@@@@@@@@.@@ [MPa]',tens

OPT_END:
MAT=MATRIX/TRANSL,0,0,0
BLD(3)=TRANSF/MAT,SPAR(8)
SPR=SUBTRA/BLD(1),WITH,SPAR(8),CNT,c

&DUNIT=1
&SDUNIT=3
&SDENS(SPR)=1.8   $$g/cm^3
&SDENS(BLD(6))=1.8
&SDENS(BLD(2))=0.08   $$g/cm^3
&SDENS(BLD(3))=0.08   $$g/cm^3
ANLSIS/SOLID,SPR,BLD(2),BLD(6),BLD(3),GCM,wyn

PRINT/'----------  Blade mass analysis ------------'
PRINT/USING,' volume:  #@@@@@@@@@@@@@@@.@@@ cm^3',wyn(2)
PRINT/USING,' mass:    #@@@@@@@@@@@@@.@ g',wyn(3)
PRINT/USING,' center of mass:  X=#@@@@@.@@@ mm',wyn(4)*10
PRINT/USING,'                  Y=#@@@@@.@@@ mm',wyn(5)*10
PRINT/USING,'                  Z=#@@@@@.@@@ mm',wyn(6)*10


HALT
```